UNIVERSITY OF SOUTHAMPTON

FACULTY OF NATURAL AND ENVIRONMENTAL SCIENCES

School of Chemistry

Characterisation of the Stringent Response and Polyphosphate Biosynthesis in the Intracellular Pathogens *Burkholderia pseudomallei*, *Francisella tularensis* and *Yersinia pestis*.

by

Amber Louise Murch

Thesis for the degree of Doctor of Philosophy

September 2016

Abstract

The paucity of novel antibiotics to treat intracellular pathogens has become a matter of intense concern for the scientific community. Similarly, innate, emerging and even engineered antibiotic resistance is of disquiet for pathogens of concern including those of interest in biodefence. Therefore there is a significant need to identify novel classes of antibiotics.

Under conditions of nutrient limitation, bacteria initiate the stringent response, co-ordinated by the signalling nucleotides guanosine tetra- and penta-phosphate, collectively termed (p)ppGpp. During starvation, (p)ppGpp accumulates and coordinates diverse transcriptional alterations. (p)ppGpp levels are controlled by two enzymes, RelA and SpoT, which are a monofunctional (p)ppGpp synthetase and a bifunctional (p)ppGpp synthetase/hydrolase, respectively.

Inorganic polyphosphate, a global regulatory molecule, has also been linked to the stringent response. Levels of polyphosphate are controlled by a polyphosphate kinase (PPK) and an exopolyphosphatase (PPX). Mutation of the genes *relA* and *spoT* results not only in abrogation of (p)ppGpp production, but also results in lower levels of polyphosphate accumulation. However, the interaction of the stringent response with the polyphosphate regulon is not yet clearly understood.

The aim of this project is to inactivate the key genes involved in (p)ppGpp and polyphosphate metabolism in intracellular pathogens of interest to defence. The characterisation of these mutants *in vitro* and *in vivo* and the analysis of the global stringent response regulon are discussed in this thesis.

Contents

List of Figures

List of Tables

Declaration of Authorship

I, Amber Louise Murch declare that this thesis and the work presented in it are my own and has been generated by me as the result of my own original research:

Characterisation of the Stringent Response and Polyphosphate Biosynthesis in the Intracellular Pathogens *Burkholderia pseudomallei*, *Francisella tularensis* and *Yersinia pestis*.

I confirm that:

1. This work was done wholly or mainly while in candidature for a research degree at this University;

2. Where any part of this thesis has previously been submitted for a degree or any other qualification at this University or any other institution, this has been clearly stated;

3. Where I have consulted the published work of others, this is always clearly attributed;

4. Where I have quoted from the work of others, the source is always given. With the exception of such quotations, this thesis is entirely my own work;

5. I have acknowledged all main sources of help;

6. Where the thesis is based on work done by myself jointly with others, I have made clear exactly what was done by others and what I have contributed myself;

7. Parts of this work have been published as:

Batten Laura E, Parnell Alice E, Wells Neil J, Murch Amber L, Oyston PCF, Roach Peter L. 2016. Biochemical and structural characterization of polyphosphate kinase 2 from the intracellular pathogen *Francisella tularensis*. Bioscience Reports **36**.

Signed: .....

Date: .....

Acknowledgements

I would like to thank my supervisor Petra Oyston for her excellent technical support and guidance throughout my PhD studies. Her outstanding technical expertise and constructive feedback have helped me strive to achieve to the best of my abilities. I would like to thank my supervisor Peter Roach for his resounding encouragement and critique. His enthusiasm and attention to detail throughout my PhD studies has been second to none. I would like to thank both Petra and Peter for the opportunity to work on such an exciting and rewarding project.

Many thanks also go to the Microbiology Group at Dstl for providing a welcoming, productive and supportive working environment. Particular thanks to any members of the group who have helped me with practical or technical advice over the past four years. Thanks to Mark Richards for his dedication, support and guidance as my high containment microbiology trainer and mentor. Thanks also go to Petra Oyston, Diane Williamson and Andrew Scott for their high containment laboratory support. Thank you to Donna Ford for her mutant making skills during the final year of this project and Richard Thomas for proof reading this thesis. I would also like to acknowledge Konrad Paszkiewicz and the generous support from Exeter Sequencing Service and Computational core facilities at the University of Exeter for RNA sequencing experiments. I also acknowledge Paul Skipp at the University of Southampton for completing the proteomics experiment for this project and Laura Craddock at Dstl for her assistance with transcriptomics data analysis.

This PhD would not have been possible without the love and support from my wonderful family and friends with particular thanks to my Mum, Dad and Sister.

Last but by no means least special and heartfelt thanks go to my Fiancé Jacob, for his unwavering support and encouragement without which I would not have had the confidence to complete this PhD.

This thesis is dedicated to the memory of my Grandparents

John & Jean and Bob & Daphne

Abbreviations

B. anthracis – Bacillus anthracis

B. mallei – Burkholderia mallei

B. pseudomallei – Burkholderia pseudomallei

C. jejuni – Campylobacter jejuni

C. burnetii – Coxiella burnetii

E. coli – Escherichia coli

F. novicida – Francisella novicida

F. tularensis – Francisella tularensis

M. tuberculosis – Mycobacterium tuberculosis

P. aeruginosa - Pseudomonas aeruginosa

S. enterica - Salmonella enterica

Y. pestis – Yersinia pestis

ACDP – Advisory Committee for Dangerous Pathogens

ACP – Acyl carrier protein

AMP – Adenosine monophosphate

ANOVA – Analysis of variance

ATP – Adenosine triphosphate

BAB – Blood agar base

BCGA – Blood cysteine glucose agar

BLAST – Basic local alignment search tool

BWA – Biological warfare agents

BTWC – Biological and Toxin Weapons Convention

$CaCl_2$ – Calcium chloride

CAS – Chrome Azurol S

CASAVA - Consensus assessment of sequence and variance

$CHCl_3$ - Chloroform

CDC – Centres for Disease Control and Prevention

CDM – Chamberlain's defined medium

cDNA – Complementary deoxyribonucleic acid

CFU – Colony forming unit

DESeq – Differential Expression Sequence

DNA – Deoxyribonucleic acid

gDNA – Genomic deoxyribonucleic acid

ssDNA – Single stranded deoxyribonucleic acid

dsDNA – Double stranded deoxyribonucleic acid

DSTL – Defence Science and Technology Laboratory

DTT – Dithiothreitol

EDTA - Ethylenediaminetetraacetic acid

$FeCl_3$ – Iron chloride hexahydrate

FPI – *Francisella* Pathogenicity Island

g – Gram

GC – Guanine Cytosine

GCS - Glycine cleavage system

GDP – Guanosine diphosphate

GTP – Guanosine triphosphate

HCl – Hydrochloric acid

HDTMA - Hexadecyltrimethylammonium bromide

H_2O_2 – Hydrogen peroxide

HPLC-MS – High performance Liquid Chromatography Mass Spectrometry

HTSeq – High throughput sequencing

KH_2PO_4 – Potassium phosphate monobasic

L - Litre

µL - Microlitre

LB – Luria Bertini

LPS – Lipopolysaccharide

LVS – Live Vaccine Strain

MIC – Minimum inhibitory concentration

µg - Microgram

mg – Milligram

mL – Millilitre

MLD – Median lethal dose

MLN – Mediastinal lymph node

MM9 - Minimal Media 9

NaCl – Sodium chloride

NaN_3 – Sodium azide

NaOH – Sodium hydroxide

ng - Nano gram

NH_4Cl – Ammonium chloride

dNTP – Deoxyribonucelotide triphosphate

O_2^- – Superoxide

OD – Optical density

OH – Hydroxyl radical

ORF – Open reading frame

PA - Phenylacetic acid

PBP – Penicillin binding protein

PBS – Phosphate buffered saline

PCR – Polymerase chain reaction

pg – Pico gram

pgm – Pigmentation locus

PIPES - piperazine-N,N'-bis(2-ethanesulfonic acid

ppGpp – Guanosine 3', 5' bisphosphate

pppGpp – Guanosine 5'- triphosphate 3'diphosphate

PPi – Pyrophosphate

PTP – Pico titre plate

RSH – rel/spo homologue

rpm – Revolutions per minute

RNA – Ribonucleic acid

RNAP – Ribonucleic acid polymerase

RNA-seq – RNA sequencing

mRNA – Messenger ribonucleic acid

rRNA – Ribosomal ribonucleic acid

tRNA – Transfer ribonucleic acid

RND - Resistance-nodulation-division

ROS – Reactive oxygen species

RTA - Real Time Analysis

RT-PCR – Reverse transcriptase polymerase chain reaction

SBS – Sequencing by synthesis

SDS - Sodium dodecyl sulfate

SNP – Single nucleotide polymorphism

SOD – Superoxide dismutase

TTSS – Type three secretion system

TSSS – Type six secretion system

1. Introduction

1.1. Biological Warfare Agents Throughout History

The use of infectious diseases in warfare has been observed throughout history. Examples of microorganisms being used as biological warfare agents (BWA) in a malicious manner date back to the Middle Ages, when military leaders recognised that infectious disease victims, such as those who succumbed to the Black Death, could be used as weapons against an enemy (1). The plague was also misused in the mid-14th Century, where Tartar forces in the Ukraine catapulted plague-infected bodies into the Genoese colony of Kaffa (2). Biological warfare has not been limited to bacteria, as British forces distributed smallpox-contaminated blankets to North American Indians in the late 18th Century (3). Between World War I and World War II, many nations including the UK, the USA and Japan had active biological weapons programmes, developing weapons and munitions. The USA had potentially one of the largest active BWA weaponisation and stockpiling programmes between 1943 and 1969 including agents such as *Bacillus anthracis*, *Francisella tularensis* and *Coxiella burnetii* (4). Another example is provided by the events during the summer of 1942 when the UK used Gruinard Island as a site for conducting *B. anthracis* aerosolisation trials. However, it was eventually recognised that the use of such weapons should be prohibited and the implementation of the Biological and Toxin Weapons Convention (BTWC) in 1975 resulted in the renunciation of biological warfare by 140 nations world-wide, including the UK which is a designated depositary state for the BTWC (5). The BTWC was the first multilateral disarmament treaty banning an entire category of weapons, and to date has 173 States Parties. In addition to this international treaty, in 1999 the United States Congress tasked the Centres for Disease Control and Prevention (CDC) and world-leading experts to establish a defined classification list of BWA (6). This list classified biological agents into categories A, B and C based on the agents severity of disease, dissemination potential and mechanism and public perception of the organism (7). However, it was the anthrax attacks on the Unites States in 2001 that reignited concern of the genuine and potentially deadly threat posed by bioterrorism (6). Lessons learned from these events throughout history have necessitated research into understanding the mechanisms of pathogenesis of BWA and the impact on human health and global security. Consequently, the development of therapies, preventative countermeasures and detection systems are currently of high priority for many nations. Since the establishment of the aforementioned BWA classification list, defence organisations around the world, have engaged in active research

programmes to develop medical countermeasures for the treatment and prevention of infections caused by high priority agents that are listed on the A and B lists.

1.2. Intracellular Pathogens

Of particular importance to impact on human health are the intracellular pathogens. Moreover, the majority of BWA are intracellular pathogens. These organisms have evolved sophisticated and effective mechanisms to evade the human immune system and cause severe and often fatal infections, thereby surviving and proliferating inside mammalian cells (8). Intracellular microbial pathogens have developed diverse mechanisms to survive or even prevent hostile environmental conditions, particularly those encountered after phagocytosis in the macrophage phagosome (9, 10). Some bacteria such as *Yersinia* species are able to prevent phagocytosis in the first place and avoid such stressful environmental conditions, whereas others can escape the phagosome, such as *Francisella* and *Burkholderia* species (11-13). Three intracellular pathogens that are also considered BWA and classified as tier one biological select agents are *Burkholderia pseudomallei*, *F. tularensis* and *Yersinia pestis*, which have been selected as the microorganisms of focus for the work presented herein. These three organisms were selected due to the availability of established genetic tools to generate deletion mutants, and previous researching suggesting that the stringent response and polyphosphate biosynthetic pathways might make appropriate targets for the development of novel antimicrobial therapies to treat melioidosis, tularaemia and plague (14-16).

1.2.1. *Burkholderia pseudomallei*

B. pseudomallei is a highly motile, Gram negative facultative intracellular bacterium, existing primarily as a soil dwelling saprophyte, but also an intracellular pathogen and is the causative agent of the human disease melioidosis (17). Melioidosis is a major cause of disease in certain parts of the tropics and is endemic in areas such as South East Asia and Australia as shown in figure 1, where the bacterium can be frequently isolated from soil and surface waters (18-21).

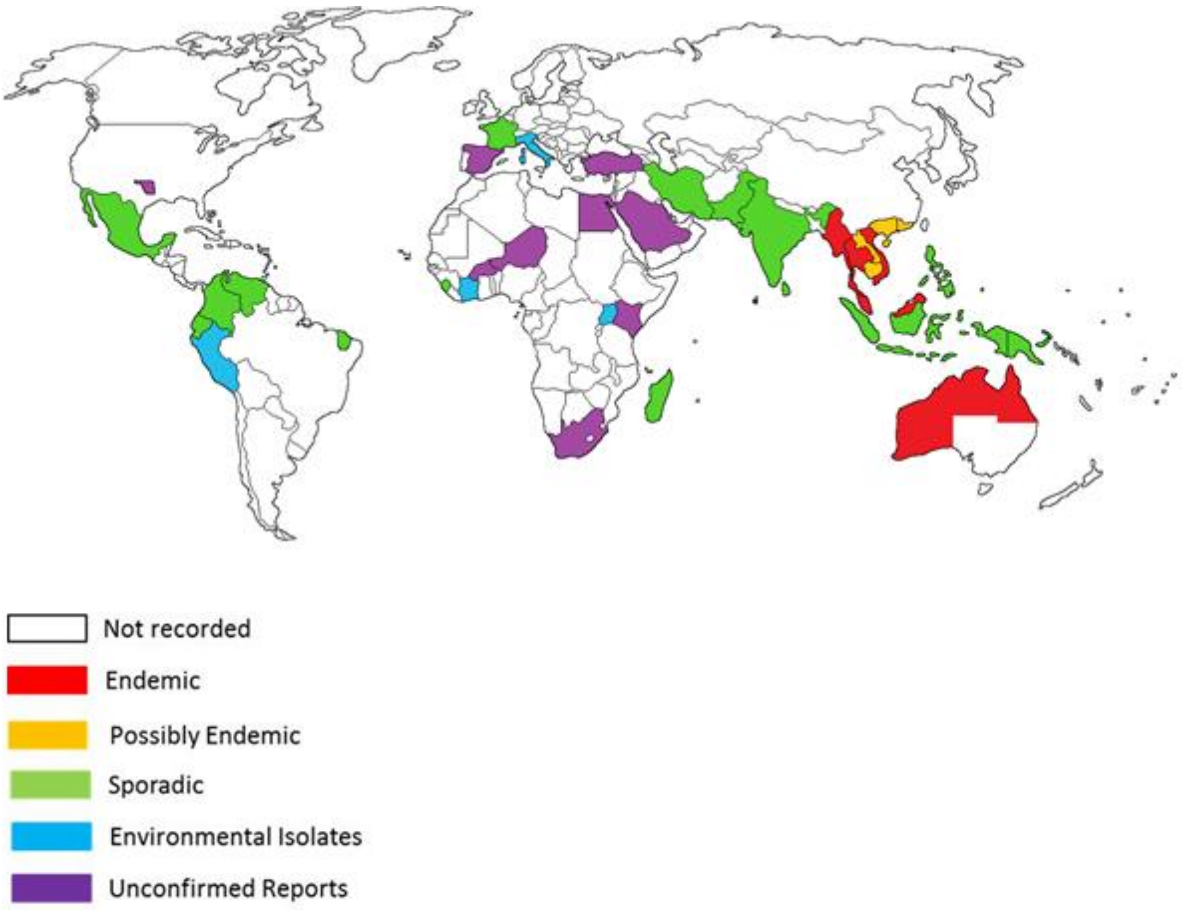

Figure 1. Global distribution of melioidosis indicating areas in which the disease is endemic, potentially endemic but not confirmed, where sporadic occurrences have been detected, areas where the organism has been isolated from the environment or areas where there have been suspected but unconfirmed cases. Figure adapted from Cheng *et al* and Limmathurotsakul *et al* (22, 23).

Most cases of the disease are thought to occur via contamination of minor cuts or abrasions with environmental organisms, or via inhalation of aerosols generated from contaminated water or soil (24). Clinical manifestations of the disease are extremely variable, with the acute form of the illness ranging from non-specific flu-like symptoms to fulminant septicaemia with abscesses in multiple organs (20). Severe pneumonia and septicaemia with high mortality are the most common forms of melioidosis in Thailand and northern Australia (20). However, chronic infection is also a possibility, with incubation periods lasting up to 26 years, with

relapse often coinciding with concurrent disease or injury (25, 26). Unlike the other two microorganisms discussed in this work, *B. pseudomallei* is a flagellated, intracellular pathogen (25, 26). The flagella are believed to play a key role in the ability of the bacterium to disseminate from the site of localised infection to almost any other organ of the body via the bloodstream (27). The flagellin protein, FliC, has been demonstrated to be involved in motility and virulence (27). In addition to its flagella *B. pseudomallei* also produces a plethora of virulence determinants including several secreted virulence factors such as lecithinase, lipase, haemolysin and a water-soluble siderophore for iron acquisition from the infected host (59). In addition to secreted antigens, cell-associated antigens have also been identified in *B. pseudomallei* including exopolysaccharides and lipopolysaccharides which help protect the bacterium from host defences such as phagocyte-mediated killing (28, 29). It has been found that *B. pseudomallei* contains four operons that encode capsular polysaccharide (CPS) (30). The CPS I operon encodes the well characterised mannoheptose capsule -3)-2-O-acetyl-6-deoxy-beta-D-manno-heptopyranose-(1- which has been shown to be an essential virulence determinant in *B. pseudomallei* (30, 31). The roles of CPS II and IV in *B. pseudomallei* virulence remain to be elucidated, whereas CPS III has been found not to have an essential role in the virulence of *B. pseudomallei* (30). Until recent advancements in DNA sequencing and molecular biology, little had been understood about the molecular mechanisms contributing to the pathogenicity, survival, virulence and antimicrobial resistance of *B. pseudomallei*. The elucidation of the full genome sequence of this microorganism has facilitated further studies into its virulence mechanisms and regulation thereof. The *B. pseudomallei* strain K96243 genome comprises two circular chromosomes of 4.07 Mb and 3.17 Mb, both of which have high GC contents (17). Horizontal gene transfer has contributed significantly to the evolution of *B. pseudomallei*, with genes on both chromosomes showing similarity to mobile genetic elements such as insertion sequences, bacteriophages and plasmids (17, 32, 33). Additionally, genetic heterogeneity in *B. pseudomallei* enables the bacterium to survive in the environment as well as the mammalian host. This has been demonstrated by the discovery of multiple *B. pseudomallei* ribotypes characterised by variation in rRNA loci among geographically and environmentally distinct bacterial isolates (34).

A closely related tier one select agent is *Burkholderia mallei* which is the causative agent of glanders. *B. mallei* can also cause a severe infection in humans, particularly when acquired via the aerosol route of infection although this is a rare occurrence as *B. mallei* more commonly

infects equine animals. There has been research to suggest that *B. mallei* is in fact a genetic equine-adapted clone of *B. pseudomallei* as analysis by multi locus sequence typing revealed *B. mallei* to have an identical allelic profile to that of *B. pseudomallei* (35). Despite the organisms' common ancestry *B. mallei* has a significantly reduced genome in comparison to *B. pseudomallei* and consequently lacks the ability to survive effectively outside of a mammalian host (36). More recent detailed genetic analyses have identified regions of genetic diversity between the two organisms, meaning it is now possible to distinguish between them at the genetic level using targeted PCR assays (37-41). The life cycles of the pathogens differ. *B. pseudomallei* is an opportunistic pathogen that will not only infect immunocompromised and sometimes healthy individuals but also survive for prolonged periods in moist soil environments (36). *B. mallei* on the other hand is an obligate pathogen due to its reduced genome requiring a host in which to proliferate and has not been found to survive in the environment (36).

Antibiotic therapies exist for the treatment of melioidosis. However, even with antibiotic treatment mortality rates for the acute form of the disease can be up to 50 % (42). A particular challenge for antibiotic treatment of melioidosis is the innate antimicrobial resistance of the bacterium (43-45). Resistance has also been known to emerge during treatment of melioidosis, to drugs such as chloramphenicol and ceftazidime (figures 2 and 3) (46).

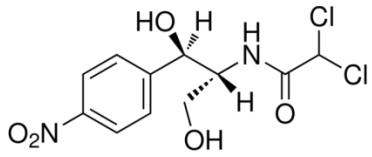

Figure 2. Chemical structure of chloramphenicol.

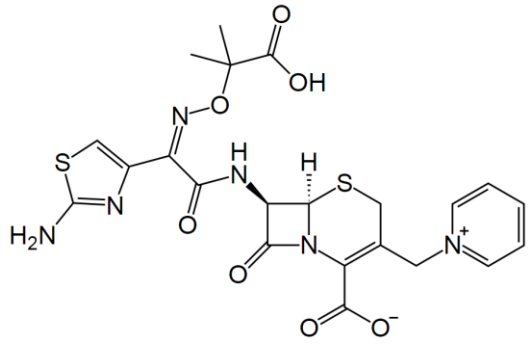

Figure 3. Chemical structure of ceftazidime.

Such resistant strains were found to be fully virulent and showed resistance to other antimicrobials (46). The key mechanism giving rise to broad spectrum antibiotic resistant *B. pseudomallei* is efflux. *B. pseudomallei* possesses efflux pumps from the resistance-nodulation-cell division (RND) family which play a pivotal role in the bacterium's intrinsic antibiotic resistance (45). Genome sequencing revealed strain K96243 to encode at least 10 putative RND pumps, the majority of which remain to be characterised (47). The operon *bpeR-bpeAB-oprB* in *B. pseudomallei* which encodes an RND-family efflux pump resides on chromosome 1 and comprises a three-component antimicrobial efflux system, which is the key efflux pump conferring multidrug resistance (figure 4) (46-48). This system comprises a repressor of TetR family (BpeR), a periplasmic linker protein (BpeA), an inner membrane protein (BpeB) and an outer membrane protein (OprB) (46, 48). It is also known that at least one other *B. pseudomallei* efflux system, AmrAB-OprA, exists that contributes to resistance to the aminoglycosides and macrolides (46, 47, 49).

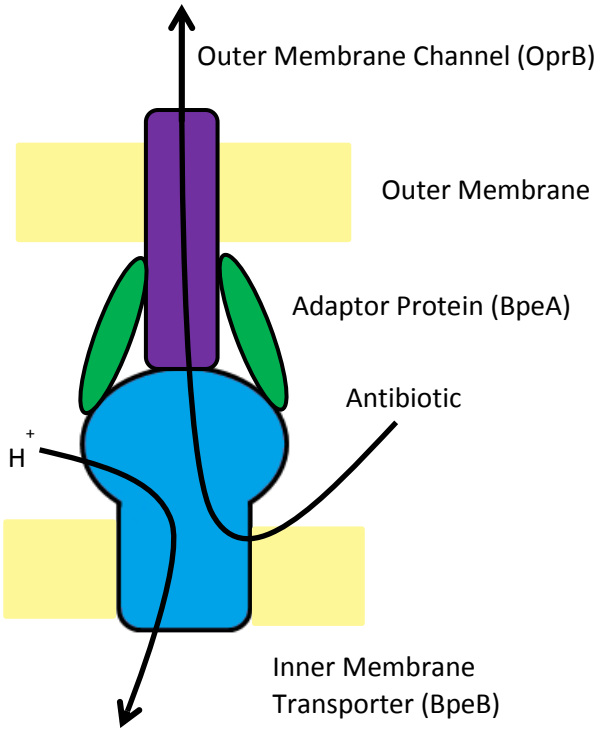

Figure 4. RND-type periporter antibiotic efflux pump found in *B. pseudomallei*. Figure adapted from Yamaguchi *et al* (50).

In addition to efflux, *B. pseudomallei* down regulates expression of porins as an alternative mechanism to increase antibiotic resistance. Porins are molecules that create water-filled channels through which compounds such as antibiotics can diffuse. Altered expression affects antibiotic accumulation inside the bacterial cell resulting in intracellular levels of antibiotic not being sufficient to effectively damage the bacterium (51). As porins are a classical approach used by bacteria to mediate antibiotic resistance, they have been well characterised in terms of biochemical, functional, genetic, immunochemical and structural properties across many species including *Escherichia coli* and *Salmonella enterica,* which both encode OmpC and OmpF porins (52-55). These porins in *E. coli* confer β-lactam resistance and in *S. enterica* they are involved in cephalosporin, chloramphenicol and imipenem resistance. Porins have been less well characterised in *B. pseudomallei* and it is currently unclear how many porins are encoded in the *B. pseudomallei* genome. However, there have been studies into the specific mechanism by which antibiotics are transported through the major outer membrane porin, Omp38 of *B. pseudomallei* (56). Topology prediction and molecular modelling suggested that Omp38 of *B. pseudomallei* has a typical membrane porin β-barrel structure (51). In addition, antibiotic

translocation through the Omp38 porin was assessed and revealed that various classes of antibiotics including β-lactams, cephalosporins, fluoroquinolones and carbapenems were all translocated through the porin effectively, providing experimental evidence for multi-drug resistance that has been observed in *B. pseudomallei* (56).

Considering the complexities associated with antibiotic resistance, latent infection and the high virulence of *B. pseudomallei* infection, intravenous and aggressive combined antibiotic treatment is required over prolonged periods of time to manage the disease. In addition there is still no licenced vaccine for prophylaxis against melioidosis, despite various vaccine candidates being developed. Several vaccine candidates have demonstrated some degree of immunogenic protection against melioidosis infection in rodent models of infection but there has been no vaccine candidate able to provide sterilizing immunity (57, 58). Other issues associated with the development of safe and effective *B. pseudomallei* vaccines surround the complexities of the host-pathogen interactions (57). A particular challenge is the facultative pathogenic nature of *B. pseudomallei* which means the bacterium can invade non-phagocytic cells which enables evasion of the humoral immune response (59, 60). Host immune system evasion and ineffective clearance of infection even in the presence of IgG immunoglobulins means novel antimicrobials or small molecule inhibitors to enhance the efficacy of currently available antibiotics (adjuvants) are needed for the successful treatment of melioidosis, in the interest of public health in endemic areas and for biodefence (61-63).

1.2.2. *Francisella tularensis*

F. tularensis is a highly virulent, non-motile intracellular bacterium and the aetiological agent of tularaemia (6, 64, 65). This Gram negative zoonotic bacterium is able to infect a wide range of mammalian hosts, including humans (66). There are three subspecies of *F. tularensis* currently accepted: subspecies *tularensis* (type A) is found exclusively in North America (67), the less virulent subspecies *holarctica* (type B) is found in North America and Eurasia (67), and the relatively avirulent subspecies *mediasiatica* is found in central Asia, as shown in figure 5 (67). A proposed fourth subspecies *novicida* currently remains a separate species despite its genetic similarities to sub-species *tularensis* (66). A live vaccine strain (LVS) of a type B biovar has previously been used to protect against laboratory acquired tularaemia. However, due to the variability in protection levels and unknown mechanisms of protection, *F. tularensis* LVS has never reached licensure, leaving a capability gap for an effective prophylaxis in addition to effective treatments.

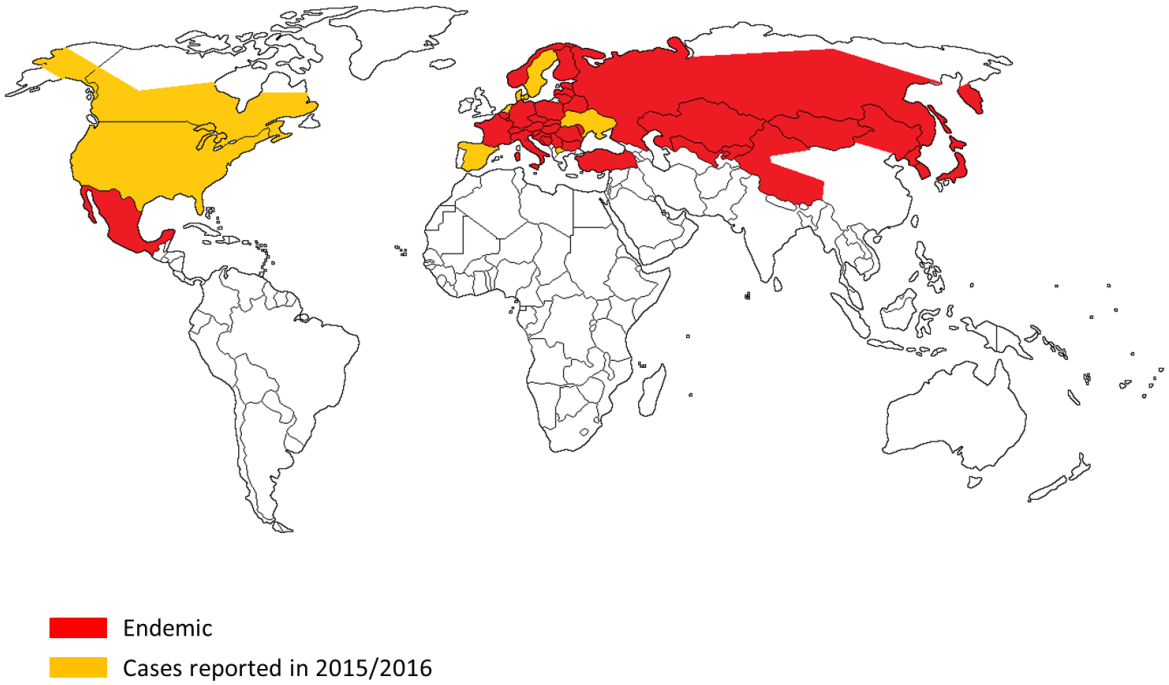

Figure 5. The geographical distribution of tularaemia is indicated in red and orange. Figure adapted from WHO guidelines on tularaemia. The data were compiled from publications in the medical literature between 1952–2006 as published by de Carvalho *et al* (68, 69).

The clinical manifestations of tularaemia depend on the route of infection. When infection occurs through skin abrasions or oral mucous membranes, the result is usually a conspicuous enlarged tender node. When *F. tularensis* is inhaled, the pneumonic form of the infection will manifest as deep lymph-node enlargement, specifically the mediastinal lymph node (MLN) and present systemically with the patient suffering from high fever (70, 71). Clear respiratory symptoms may not be apparent however other symptoms such as malaise, chills, delirium and cough can be life threatening if infection is caused by the highly virulent sub-species *tularensis* (64, 72). Although historically the mortality rate of tularaemia infection was greater than 50% of cases, this has now been reduced to less than 2% in the Unites States due to declining case numbers and modern antibiotic regimens (64, 73). Despite this dramatic reduction in mortality rate, there remain issues surrounding the treatment of tularaemia. In previous years the drug of choice for treatment of tularaemia was streptomycin, however this antibiotic causes toxic side effects including vestibular dysfunction (74, 75). This has led to alternative treatment options being sought including gentamicin, tetracycline and ciprofloxacin (74, 76-78). Although ciprofloxacin has successfully been used to treat tularaemia outbreaks in Spain (77) and Turkey (79), animal studies suggest the efficacy of ciprofloxacin against the highly virulent type A biovar strain SCHU S4 is dependent on timely antibiotic administration and must be within 24 hours of exposure, which in human disease outbreaks is less likely to be possible (80).

F. tularensis is both a physically and genetically small microorganism, comprising a single circular chromosomal genome of only 1.89 Mb and no virulence plasmids (81, 82). Despite this, *F. tularensis* has an extremely low infectious dose of as few as 10 – 50 bacteria required to cause infection in a human (81, 83). The ability of the bacterium to invade and multiply within immune cells in the mammalian host is at the core of *F. tularensis* pathogenesis. Following uptake the bacterium resides temporarily within phagosomes, but then escapes to replicate in the cytoplasm, all the while evading the host immune system (84). However, the molecular mechanisms controlling these processes are yet to be fully understood. Although, many virulence genes have been identified following whole genome sequencing of *F. tularensis* strains, there remain many knowledge gaps regarding the molecular pathogenesis of *F. tularensis* (84). A major contributor to the pathogen's ability to infect and cause disease, particularly phagosomal escape and replication within the macrophage cytosol, is the

Francisella Pathogenicity Island (FPI) which encodes a putative type VI secretion system (schematic shown in figure 6) and has been studied in great detail over the years (84).

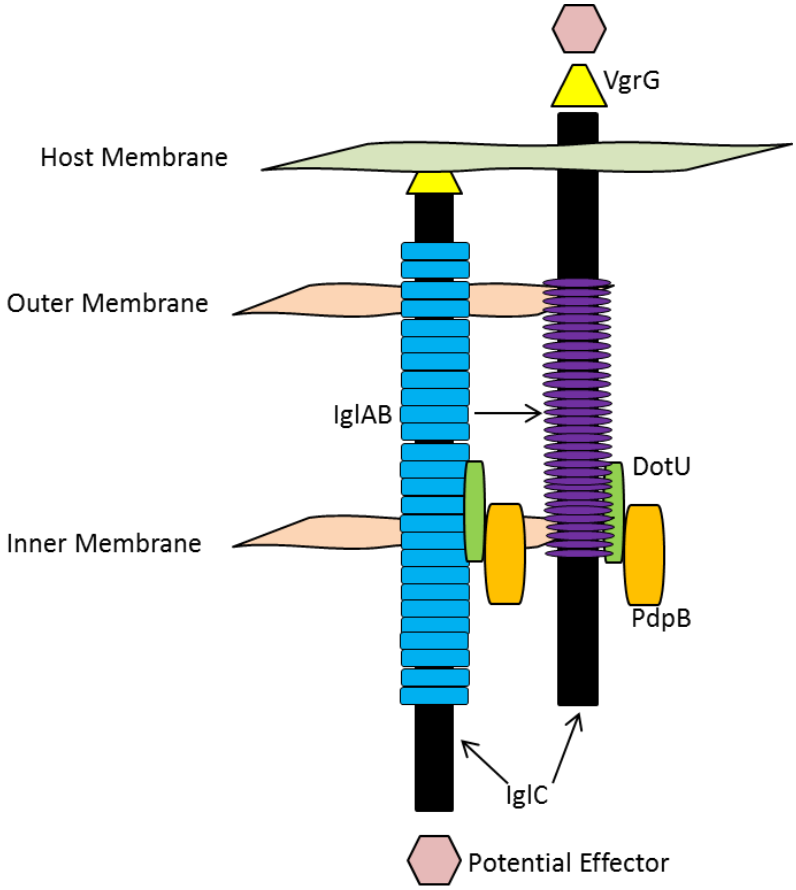

Figure 6. Schematic adapted from the model proposed by Bruin *et al* (85) of the FPI-encoded type VI secretion apparatus. IglAB form a tube-like complex that spans the inner and outer bacterial membranes. The inner tube structure is proposed to comprise IglC and as the IglAB tube contracts the IglC inner tube is driven through the host cell membrane. Penetration of the host membrane is facilitated by VrgG. DotU and PdpB interact with the tube structure at the bacterial inner membrane interface. Effector proteins that are hypothesised to be delivered via the type VI secretion system are depicted but remain uncharacterised (85).

The ability of *F. tularensis* to replicate intracellularly also contributes to its high virulence as this is a process that enables the bacterium to evade and inhibit the innate and adaptive host immune response (71). FPI regulation has been recently linked to the stringent response, which is discussed in more detail later in section 1.5.8, but remains poorly understood (86). In

fact, generally little is still understood about how *F. tularensis* regulates gene expression in different niches, with few regulatory proteins being identified during whole genome annotation (30). The paucity of regulatory systems identified could be viewed as surprising due to the diversity of cells types that *F. tularensis* is able to infect, including mammalian immune cells and amoebae (87), and the fact that the bacterium can survive both intracellularly and extracellularly (30). However, recent studies have gone some way to shed light on the regulation of *Francisella* virulence. Cuthbert *et al* have paid particular attention to the macrophage growth locus protein A (MglA) and the stringent starvation protein (SspA), which have been found to play key roles in regulating the essential virulence genes residing on the FPI (88). Structural studies have shown that MglA and SspA form a heterodimer complex (shown in figure 7) which is required for active RNA polymerase (RNAP) recruitment via direct binding to the RNAP and binding of transcriptional regulators PigR and OmrA to then activate transcription from specific virulence promoters (88).

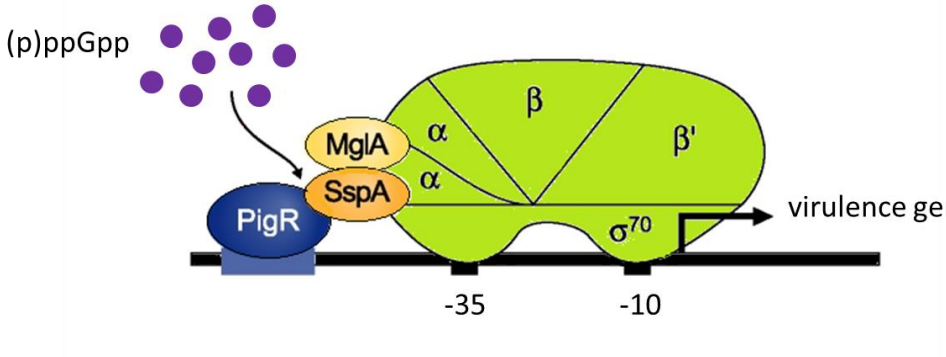

Figure 7. Model adapted from Charity *et al* (86) showing interaction between PigR and the MglA-SspA complex that associates with RNAP which in turn activates virulence gene expression in *F. tularensis* (86).

Bacteria need to be able to sense and respond to environmental stimuli to survive in a diverse range of environments. *F. tularensis* expresses different genes when isolated from broth culture compared to isolates from inside macrophages (89). Significant changes in gene expression from bacteria isolated from infected macrophages over a time course, where 658 genes were differentially expressed, in an infection stage-dependent manner (90). Horzempa

et al (91) compared the global gene expression profiles of *F. tularensis* LVS cultivated in defined medium at 26 °C (environmental temperature) versus 37 °C (mammalian body temperature) (91). It was found that 11% of genes were differentially expressed, and of those genes, 40% that displayed increased expression levels at 37 °C were known to be involved in intracellular growth and/or virulence (91). Lenco *et al* conducted proteomic analysis of *F. tularensis* SCHU S4 and *F. tularensis* LVS and concluded that FPI proteins were more abundant during stationary phase of growth and at 25 °C compared to 42 °C (92). This study supported the temperature-dependent transcriptional alterations in *F. tularensis* discussed by Horzempa *et al* (91). These studies indicate that despite the fact few regulatory mechanisms have been identified, *F. tularensis* undergoes significant genetic regulation to survive and adapt to different environmental niches, and therefore further studies are required to elucidate these regulatory systems.

Due to the high virulence, low infectious dose and the ease with which *F. tularensis* can be disseminated and infect via the aerosol route, the US CDC has categorised this microorganism as category A select agent. Despite the lack of natural resistance to antibiotics used for clinical therapy there are still many issues associated with tularaemia therapy including antibiotic toxicity, disease relapse despite treatment with antibiotics and poor antibiotic efficacy against the highly pathogenic type A biovar (80, 93-95). In addition to the lack of a safe and effective vaccine, there is the potential for engineered antibiotic resistance which means there is a global requirement for more effective treatment options for tularaemia.

1.2.3. *Yersinia pestis*

Y. pestis is a Gram negative, non-motile, non-spore forming coccobacillus and the causative agent of the infectious disease plague (105,106). This facultative anaerobe has been responsible for three world wide human pandemics; the Justinian plague during the sixth to eighth centuries, the Black Death during the fourteenth to nineteenth centuries and the current plague originating from the nineteenth century to the present day (worldwide cases of the current plague pandemic are shown in figure 8) (96). Plague has three clinical manifestations, bubonic, pneumonic and septicaemic. As a zoonotic disease, *Y. pestis* has reservoirs throughout the world involving insect and rodent hosts (96). *Y. pestis* strains have traditionally been classified into biovars; *antiqua*, *mediavalis* and *orientalis* and a recently accepted fourth biovar *microtus*, based on their ability to utilise glycerol, reduce nitrate, and their geographical origin (16,154,159).

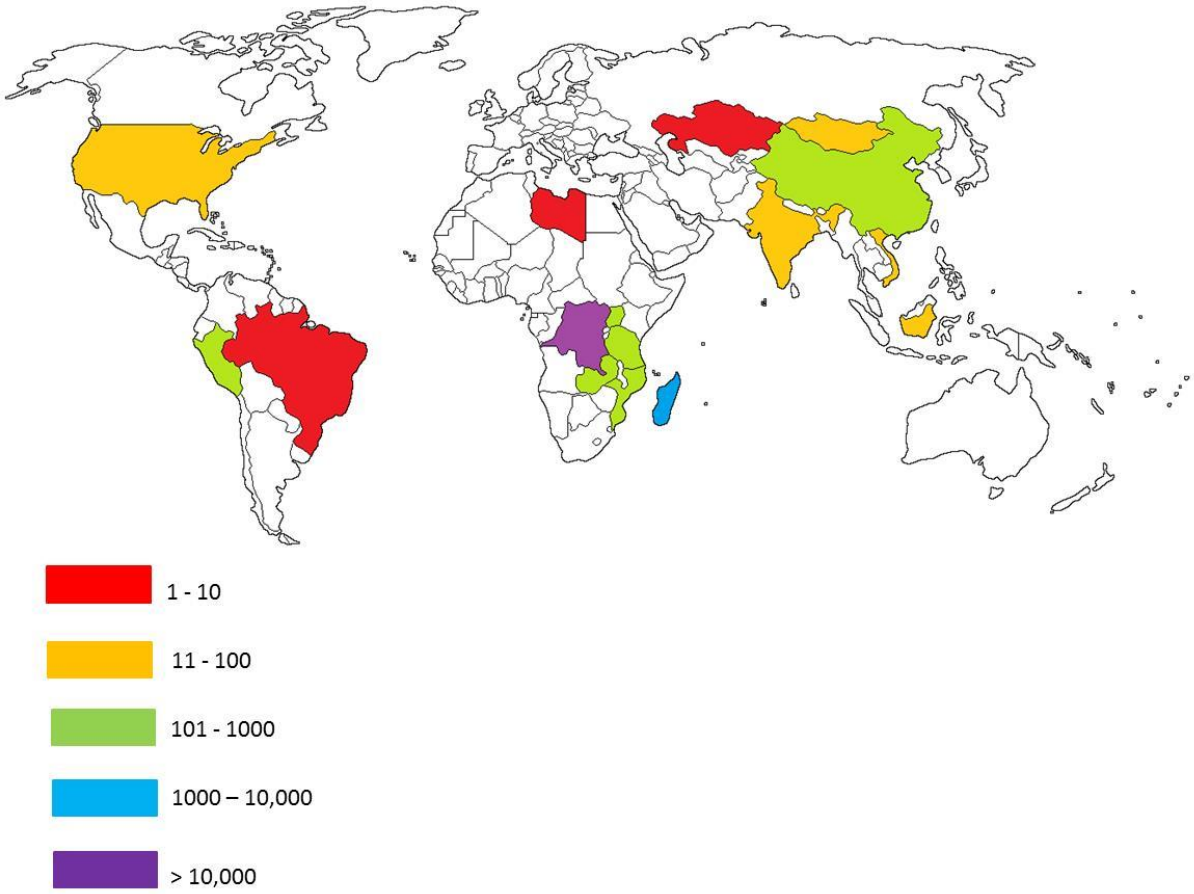

Figure 8. Distribution of worldwide plague cases reported by countries 2000 - 2009. Figure adapted from CDC *Y. pestis* datasheet. Data obtained from WHO.

It was previously thought that the three main biovars could be correlated with the three pandemics mentioned above (16). However recent genomic analysis and single nucleotide polymorphism (SNP) identification has demonstrated that this is incorrect (97): Biovar *orientalis* has been proven to be the closest relative of all three strains responsible for the pandemics (97). Biovar *mediavalis* has been shown never to have been associated with a pandemic, and biovar *antiqua* was demonstrated to have not been associated with the Japanese pandemic with which it has historically been accredited (97). The whole genome sequences of several strains of *Y. pestis* have been elucidated in recent years, providing insight into virulence and survival mechanisms of this pathogen (98-103). The *Y. pestis* genome includes a chromosome and three plasmids which are essential to pathogenicity and virulence (96). The virulence plasmid pCD1 encodes a type III secretion system (TTSS), which injects host cells with cytotoxins and effector proteins that inhibit phagocytosis of the bacterium and the host's innate immunity (104). The V antigen encoded on the pCD1 plasmid inhibits the generation of proinflammatory cytokines, thus subverting the mammalian host immune defences (105). The pCD1 plasmid is conserved in other pathogenic *Yersinia* species, *Yersinia enterocolitica* and *Yersinia pseudotuberculosis* (96). However, *Y. pestis* has additionally two unique plasmids termed pPCP1, which encodes pesticin, coagulase and plasminogen activator genes required for tissue invasion, and pMT1, which encodes the murine toxin required for survival in the intermediate flea host (96). Due to *Y. pestis* existing in the oriental rat flea, *Xenopsylla cheopis* and mammalian hosts, the bacterium must adapt to surviving in different temperature environments. *Y. pestis* will proliferate at both 26-28 °C in *X. cheopis* and at 37 °C in the human host (106). *Y. pestis* displays different nutritional requirements at these two temperatures, with 37 °C signalling the intracellular niche which demands more complex nutritional requirements due to the complex stresses present in this environment (105, 107). Research has also found that growth of the bacterium at different temperatures results in global changes in gene expression, for example temperature shift to mammalian body temperature, 37 °C triggers expression of virulence genes including the TTSS, residing on pCD1 (105). In contrast, at 26 °C which is the temperature if the insect feeding on an animal, virulence gene expression is down regulated (105). These findings demonstrate that temperature is an important environmental cue that triggers appropriate gene expression changes to enable *Y. pestis* to adapt to the niche in which it resides.

Antibiotic regimens used for treatment or prophylaxis of plague include the historically preferred antibiotic streptomycin, and alternatives such as gentamicin, ciprofloxacin, tetracycline or doxycycline (96). It is unusual for patients to be treated for the full course of ten days with streptomycin due the toxicity of the antibiotic (96). For this reason, it is often preferable to treat with a newer class of antimicrobial, such as the fluoroquinolone, ciprofloxacin. Alarmingly, *Y. pestis* is also acquiring antibiotic resistance and the first multi drug resistant strain was isolated in 1995, and initiated a significant international public health and biodefence concern (108). Consequently, novel therapies are required for the treatment of plague.

1.3. Antibiotics and Antibiotic Resistance

1.3.1. Antibiotics

Antimicrobials have significantly contributed to the control of infectious diseases that were once the leading cause of morbidity and mortality throughout human history (109). The first antibiotic was discovered in the early 20th century by Paul Ehrlich, who discovered Salvarsan after a large scale-screening programme of 5000 compounds in mice, which is used to treat syphilis (110, 111). This screening approach remained the basis of subsequent antibiotic discovery strategies, which identified, for example, sulphonamides (109, 112, 113). In 1928, Alexander Fleming made the iconic discovery of penicillin, eventually leading to the mass production and distribution of penicillin in 1945 (114). Following this discovery caution was raised about the potential of antibiotic resistance if penicillin was used at sub-optimal concentrations or for a too short time course (109). Antibiotic resistance has now become a global issue at the forefront of clinical practice, biomedical and biochemical research and has resulted in the UK among other nations, commissioning reviews into the crisis to build an international consensus on the global nature of the antibiotic resistance issue and convince other nations and international bodies to work together to solve this problem (115).

Antibiotics fall into two distinct categories: natural products derived from a biological source or synthetic compound prepared by a chemical route. Today, at least 17 different classes of antibiotic have been produced (some of which are described in table 1). However, there is a limited variety of mechanisms of actions for these antibiotics (116-118). There are four main targets for currently available antibiotics activity as shown in figure 9; (i) cell wall biosynthesis, (ii) protein biosynthesis, (iii) DNA and RNA biosynthesis and (iv) folate biosynthesis. Antibiotics that inhibit cell wall biosynthesis include the penicillins and cephalosporins and are collectively termed β-lactams. Antibiotics that inhibit protein biosynthesis include the aminoglycosides and tetracyclines, which target the 16S rRNA and 30S subunits of the bacterial ribosome, whereas chloramphenicol and macrolides target the 23S and 50S subunits (119-121). Antibiotics targeting protein biosynthesis block various stages of protein synthesis from initiation and elongation to termination (118). DNA and RNA synthesis is an essential process for all living organisms, and therefore make a desirable target for antibiotics. The quinolones are a class of antibiotics that target DNA gyrase in Gram negative bacteria and result in DNA fragmentation during DNA replication (122). Rifampicin, an isolate from *Amycolatopsis*

mediterranea disrupts protein synthesis by inhibiting RNA Polymerase (RNAP) (123). Other targets include folic acid metabolism, a target of the sulphonamides, and cell membrane biosynthesis, a target of the polymyxins, which increase the permeability of cell membranes leading to leakage of cellular components, increased uptake of the antibiotic itself and eventually cell death (124).

Mechanism of Action	Classes of Antibiotics	Chemical Structure of Antibiotics Discussed in This Study
Inhibition of cell wall biosynthesis: Inactivates a transpeptidase, an enzyme involved in peptidoglycan synthesis., known as penicillin binding proteins (PBPs) **(125)**.	β-lactams; glycopeptides; cyclic lipoproteins	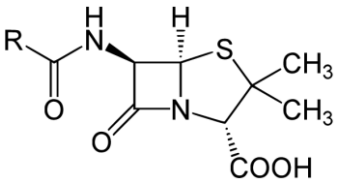 Chemical structure of penicillin (β-lactam)
Inhibition of protein synthesis: Streptomycin and gentamicin irreversibly bind the 16S rRNA of the 30S subunit of the bacterial ribosome, interfering with the binding of formyl-methionyl-tRNA to the 30S subunit. This leads to codon misreading, inhibition of protein synthesis and ultimately cell death **(126, 127)**.	Aminoglycosides; tetracyclines; oxalidonones; streptogramins; ketolides; macrolides; lincosamides	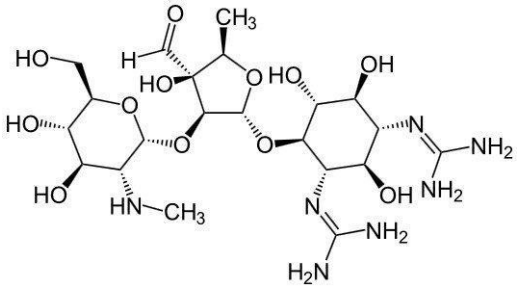 Chemical structure of streptomycin 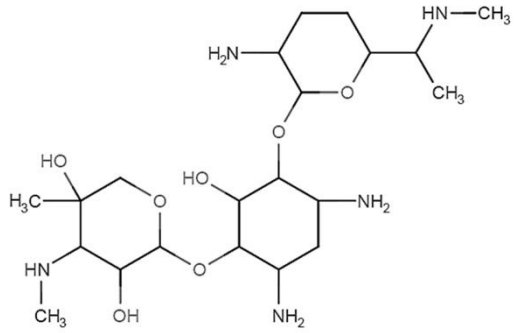 Chemical structure of gentamicin

Tetracycline and doxycycline inhibit protein synthesis by blocking the attachment of charged aminoacyl-tRNA to the ribosomal A site. They also bind the 30S subunit which prevents introduction of new amino acids to the nascent peptide chain. Tetracycline activity is usually reversible after withdrawal of the antibiotic **(128, 129)**.		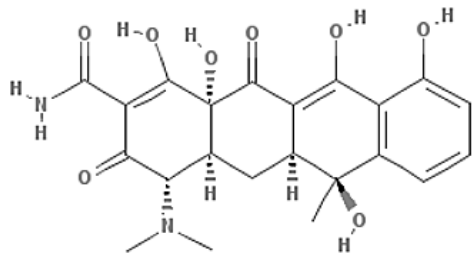 Chemical structure of tetracycline 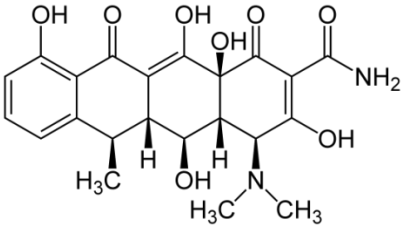 Chemical structure of doxycycline
Inhibition of DNA synthesis: Ciprofloxacin inhibits DNA gyrase, and a type II topoisomerase, (topoisomerase IV) which is necessary to separate bacterial DNA, thereby inhibiting cell division **(130)**.	Fluoroquinolones	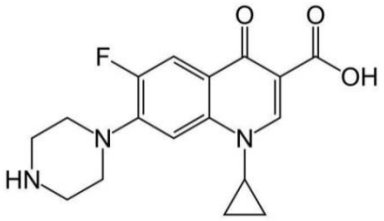 Chemical structure of ciprofloxacin
Inhibition of RNA synthesis: Rifampicin allosterically binds the β subunit of RNAP and blocks the formation of phosphodiester bonds, preventing RNA extension **(90)**.	Rifampicin	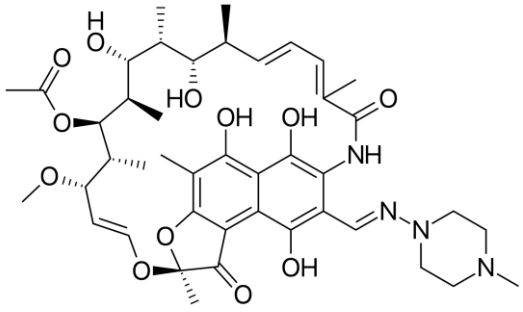 Chemical structure of rifampicin

Competitive inhibition of folic acid synthesis: Trimethoprim binds to dihydrofolate reductase and inhibits the reduction of dihydrofolic acid to tetrahydrofolic acid (THF) **(131)**. THF is an essential precursor in the thymidine synthesis pathway and disruption of this pathway inhibits bacterial DNA synthesis **(131, 132)**.	Sulfonamides; trimethoprim	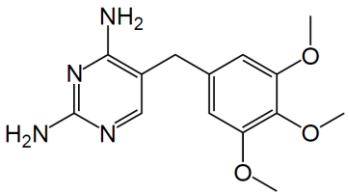 Chemical structure of trimethoprim
Membrane disorganising agents: Polymyxin B alters the bacterial outer membrane permeability by binding a negatively charged site in the lipopolysaccharide layer resulting in a destabilized outer membrane **(133, 134)**. This dissolves the fatty acid portion of the cytoplasmic membrane and disrupts membrane integrity leading to leakage of cellular molecules and inhibition of cellular respiration **(133, 134)**.	Polymyxins	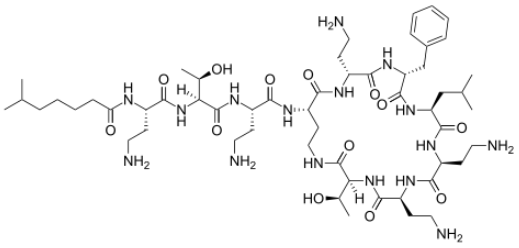 Chemical structure of polymyxin B

Table 1. Table showing antibiotics of different classes relevant to this work and the associated mechanism of action and chemical strictures.

In recent years there has been a distinct paucity of novel antibiotics reaching licensure, which has left the medical community with a worrying lack of therapies to treat the most challenging outbreaks of resistant or persistent bacteria (135). This innovation gap has been, in part due to the lengthy and costly processes involved in taking a novel antibiotic from discovery through development, to mass production and distribution, with average time frames approximately 12 years (117, 136). In addition antibiotic development is not an attractive field of research for pharmaceutical companies, as the income stream associated with antibiotic discovery and manufacture is poor, in comparison to drugs that can be taken on a life-long scale, such as statins. This being said, the advent of rapid genome sequencing combined with transcriptomic and proteomic analysis has resulted in the ability to tailor antibiotic development at a functional level, specifically focussing on essential and anti-virulence targets (109). Greater understanding of host-pathogen interactions has also enabled the development of host-targeted antimicrobials, exploiting components of human innate immunity (137-140).

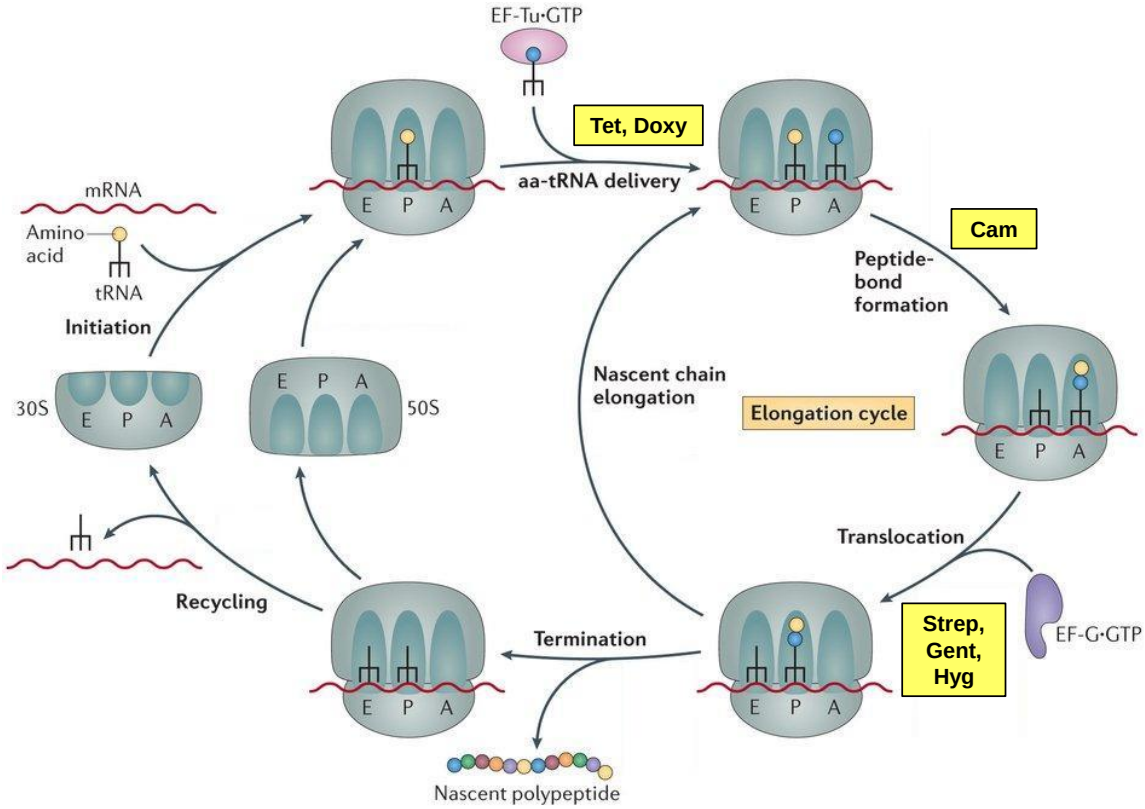

Figure 9. Antibiotic target sites during bacterial protein synthesis. Initiation of protein synthesis involves the formation of a 70S ribosome (composed of a 30S and 50S subunit) with the initiator tRNA and start codon of the mRNA positioned at the P site. The elongation cycle involves the delivery of the aminoacylated-tRNA to the A site on the ribosome by elongation factor EF-Tu. This is inhibited by streptomycin, gentamicin and the tetracyclines and the attachment of acylated tRNA is blocked by tetracycline and doxycycline. Peptide bond formation between the A- and P-site is inhibited by chloramphenicol (141). Abbreviations used; Tet – tetracycline, Doxy – doxycycline, Cam – chloramphenicol, Strep – streptomycin, Gent – gentamicin, Hyg – hygromycin.

1.4. Antibiotic Resistance and Persistence

Antibiotic resistance is a naturally occurring phenomenon, for example the ancient enzymes β-lactamases originated more than two billion years ago (142, 143). However, the spread of modern day antibiotic resistance has been driven by certain practices in the clinic. Such practices include, excessive, inappropriate and over-utilisation of antibiotics and short term use, use of antibiotics in agriculture, lack of use of preventative infection control measures such as hand washing and isolation of patients with infections has contributed to the spread of resistant bacteria and, increased use of invasive surgical procedures and use of prosthetic medical devices, which provide suitable environments for biofilm formation of resistant bacteria, which are notoriously difficult to treat (116).

Antibiotic resistance can arise naturally; it can be acquired or of concern to the defence community, be deliberately selected for or engineered. Bacteria have three main mechanisms of antibiotic resistance; (i) prevention of antibiotic accumulation by reducing uptake or increasing efflux (144), (ii) inactivation of the antibiotic by enzymatic hydrolysis or modification such as acyltransfer, phosphorylation or glycosylation (145), (iii) alteration of the antibiotic target by mutation (125). Bacteria are able to prevent the accumulation of antibiotics in the cell by either decreasing influx or increasing efflux of antibiotics across the cell membrane (118). For example *E. coli* encodes tetracycline resistance across four plasmids pRP1, pR222, pR144, and pRAI to decrease the accumulation of intracellular tetracycline in an energy-dependent manner attributed to increased efflux (146). Efflux has also been identified as a key mechanism for the acquired resistance of *Burkholderia cepacia* complex bacteria against fluoroquinolones (147). *B. pseudomallei* alone encodes at least 10 efflux pumps of the resistance-nodulation-division (RND) family, that confer resistance to a multitude of antibiotics (46, 47, 49). Two of the RND efflux systems in *B. pseudomallei* have been well characterised, AmrAB-OprA from the sequenced strain 1026b, and BpeAB-OprB from strain KHW (47). Both systems share responsibility for the efflux of common substrates, including macrolides, and more recently demonstrated, fluoroquinolones (47). It is established that antibiotics enter bacterial cells via outer membrane protein (Omp) channels, referred to as porins (46). A number of bacteria have been found to demonstrate limited cellular drug uptake through genetically modified Omp channels (51, 56). For example, the porin Omp38, as discussed previously in section 1.2.1, has acquired substitutions at various amino acid residues which

affects drug translocation through the porin and contributes to drug resistance of the highly virulent *B. pseudomallei* (56). Efflux resistance mechanisms have been less well characterised in *Y. pestis*, although tetracycline resistance was found to be mediated by efflux in a strain isolated from Madagascar (148, 149). The high mortality rates associated with multiple drug resistant bacteria is of major concern for the medical community and, amongst other concerns, has provoked urgency for the development of novel antimicrobial therapies.

One of the most common mechanisms that bacteria employ to resist naturally derived antibiotic activity involves the enzymatic inactivation of antibiotics by hydrolysis or modification such as acyltransfer, phosphorylation or glycosylation (118, 144, 145, 150). Target modification is a key factor in penicillin resistance, resulting in structural modifications of PBPs leading to lower binding affinity of penicillin (151, 152). In contrast to resistance mechanisms for naturally derived antibiotics, enzymatic hydrolysis or modification of synthetic antibiotics has not yet been found (125). However, the acquisition of novel genes to alter antibiotic binding targets, such as the bacterial ribosome, has been observed in erythromycin resistance (153).

Strategies for the control and prevention of antibiotic resistance include the development of novel antimicrobials, exploiting the plethora of genomic, transcriptomic and proteomic information now widely available (154, 155). This has enabled the screening of targeted novel classes of antimicrobials such as those inhibiting: fatty acid biosynthesis (156, 157), efflux pumps, DNA replication (GyrB subunit inhibitor) (158), and signalling networks (118, 159). Regardless of the abundance of powerful identification and screening tools currently available, the majority of new agents that have reached clinical application since 2000, have been derivatives of known antibiotic classes (160). As yet it is unclear, and perhaps too soon to determine the impact that genomic, transcriptomic, proteomic and metabolomic information has had on progress within the field. Despite advancements in antimicrobial research, control and prevention of resistance must take on a multi-factorial approach, with surveillance and rigorous control of infectious diseases taking a priority. Similarly, the prudent use of antibiotics should be encouraged amongst medical professionals (161). Finally, tighter regulation of the sale of antibiotics in developing countries is required; however this will only be possible with education about the consequences of antibiotic resistance (117, 150).

1.4.1. Bacterial Persistence

Bacterial persistence is a significant challenge for physicians, and is a known cause of chronic infections such as *Pseudomonas aeruginosa* infection in cystic fibrosis patients, that are extremely difficult to treat (162-164). Bacterial persistence was discovered by Joseph Bigger in 1944 following experiments investigating how bacteria respond to killing by penicillin, wherein cultures of *Staphylococcus* could not be completely killed by antibiotic treatment (165). The rare (10^{-5} – 10^{-6} bacterial cells), so-called 'persister cells' were found to be genetically identical to the rest of the population but displayed a decreased sensitivity to antibiotics (166). However, subsequent bacterial generations derived from persister cells showed levels of antibiotic sensitivity identical to that of their ancestors, demonstrating persistence was not a heritable phenotype (162). This spontaneous and reversible switching from a 'normal' antibiotic sensitive phenotype to a 'persistent' antibiotic tolerant phenotype appears to be of a stochastic nature and cells are referred to as type II persister cells (167). In contrast, type I persisters are cells that exhibit a very slow exit from stationary phase, and the number of persister cells is dependent on the number of cells that pass through stationary phase, i.e. not stochastic (167, 168). Persistence has been shown to be a highly conserved phenomenon, and has been observed in every antibiotic-sensitive bacterium studied to date (169). The persistent phenotype protects bacteria from killing by not only penicillin, as first demonstrated by Bigger, but varied and multiple antibiotics, simultaneously (170).

Bacterial persistence has recently been linked to the stringent response, specifically the (p)ppGpp biosynthetic pathway and the polyphosphate biosynthetic pathway, which is discussed later in this introduction in section 1.5.9. Additionally, bacterial sensitivity to antibiotics has also been implicated in the stringent response (171). Both antibiotic resistance and persistence in relation to the stringent response will be discussed in detail later.

1.5. The Stringent Response

1.5.1. The Stringent Response Pathway

In order to survive and replicate in their environmental niche bacteria must monitor and adapt to changing conditions by modifying their stress tolerance and nutrient utilisation pathways in response to local cues (172). During times of nutrient limitation bacteria are able to rapidly reallocate their cellular resources, by down regulating processes such as nucleic acid and protein synthesis, and up regulating processes such as essential amino acid production and protein degradation (173). The synchronised sequence of events in response to amino acid and fatty acid starvation is known as the stringent response (173, 174). The bacterial stringent response involves sensing nutrient depletion in the surrounding environment and subsequent adaptation to limited amino acids and fatty acids (174). The stringent response results in a dramatic alteration of global transcription profiles and is coordinated by the signalling nucleotides, guanosine tetraphosphate (ppGpp) and guanosine pentaphosphate (pppGpp), collectively termed (p)ppGpp (174), which accumulate under starvation conditions (175, 176). Transcriptional modifications are brought about by direct binding of (p)ppGpp to various binding targets, such as RNA polymerase and sigma factors (177). In *E. coli*, via an interaction between (p)ppGpp and RNA polymerase, rRNA operons are directly repressed and amino acid biosynthetic operons are directly activated (178). Ultimately the stringent response gives rise to adaptive gene expression changes before nutrient levels are too limited to enable bacteria to survive long term during stationary phase of growth. This has been demonstrated *in vitro* in the organism *F. novicida*, in which a Δ*relA*/*spoT* mutant displayed higher bacterial counts during exponential phase of growth, but then died rapidly upon entry to stationary phase due to an inability to adapt to environmental cues via the stringent response (15).

Intracellular concentrations of (p)ppGpp in bacteria are regulated by two related enzymes: RelA and SpoT. RelA is a monofunctional (p)ppGpp synthetase and SpoT is a bifunctional (p)ppGpp synthetase/hydrolase (175). RelA and SpoT have been shown to have activity in a range of bacteria including *E. coli*, *Pseudomonas aeruginosa*, *Y. pestis* and *F. tularensis* (15, 16, 175). It has been demonstrated that the RelA-dependent stringent response is induced specifically by amino acid starvation and the SpoT-dependent response is induced by limitation of fatty acids and other nutrient sources, including carbon starvation (179), phosphate starvation (180) and iron starvation (173, 180). Both enzymes synthesise (p)ppGpp from

guanosine diphosphate (GDP) or guanosine triphosphate (GTP) and adenosine triphosphate (ATP), as shown in figure 9 . SpoT also catalyses the degradation of (p)ppGpp when it is not required into GDP and pyroposphate (PPi) and pppGpp to GTP and PPi, to prevent uncontrolled, lethal accumulation of (p)ppGpp (173, 174). Unabated accumulation of (p)ppGpp disrupts cell cycle control (174), therefore a degradation mechanism is essential for bacterial survival and growth. Mutagenesis studies have found that it is possible to generate strains defective in RelA and RelA/SpoT, but inactivation of *spoT* alone is a lethal mutation, as without the (p)ppGpp degradation activity of SpoT an unabated accumulation of (p)ppGpp eventually leads to cell cycle disruption and cell death (181). Consequently the RelA-dependent stringent response has been well characterised in bacteria (16, 182-184), and the specific mechanism by which RelA senses amino acid starvation has been elucidated, and has been shown to involve ribosomal stalling due to entry of an uncharged tRNA entering the ribosome, thus preventing further translation and triggering synthesis of (p)ppGpp (figure 10) (185). Figure 10 shows an actively translating ribosome stalling upon entry of an uncharged, highly distorted tRNA, to the ribosomal A site, which signals RelA to bind to ribosome, in turn catalysing the synthesis of (p)ppGpp (182). The highly distorted conformation of the uncharged tRNA allows the simultaneous binding of the tRNA to the ribosomal A site and RelA (184). RelA can then transfer, or 'hop' from this ribosome to another stalled ribosome (182, 184). Due to the challenges associated with gene inactivation studies, the SpoT-dependent response is less well understood. However, some studies have characterised the domain structure and function of SpoT and demonstrated that this protein comprises two separate catalytic sites in its N-terminal domain accounting for the (p)ppGpp-synthesis and -degradation activities of the enzyme (186). These separate catalytic sites, however, share a central bundle of α-helices that enable allosteric transition between two conformational states, suggesting that regulation of the two active sites is linked (186). Other studies have also shed some light on the molecular mechanism of the SpoT-dependent stringent response, specifically linking its activity to that of the acyl carrier protein (ACP). ACP is a small protein which acts as a cofactor in fatty acid and lipid metabolism (187). Battesti *et al* (187) proposed a hypothesis that the ACP could act as a switch for SpoT activity and a fatty acid starvation response (187). Battesti *et al* (188) then went on to confirm that this interaction observed between SpoT and ACP was specific to those bacteria that possess separate RelA and SpoT proteins, the gamma- and beta-proteobacteria, as opposed to those bacteria that encode a single rel/spo homologue (RSH) protein (188). It was found that ACP interacts with the C-terminal domain of SpoT, as SpoT

mutants unable to interact with ACP were also unable to respond to SpoT-specific starvation (188).

Whilst the majority of studies on the role of (p)ppGpp have been conducted in *E. coli,* studies have also been conducted in other bacteria including *B. pseudomallei*, *Y. pestis* and *F. tularensis* presented herein (15, 16, 181). The (p)ppGpp-mediated stringent response previously has not been well characterized in members of the betaproteobacteria, however Muller *et al* (181) have recently conducted studies into the role of the stringent response enzymes RelA and SpoT in *B. pseudomallei* strain K96243 (181). It was found that inactivation of both *relA* and *spoT* resulted in attenuation in a macrophage, *Galleria mellonella* and murine model of infection (181). The K96243 double Δ*relA*/*spoT* mutant also provided partial protective immunity in a murine model of infection against virulent wild type *B. pseudomallei* K96243, indicating a key role for these enzymes in the virulence of *B. pseudomallei* and their potential as antibiotic targets (181).

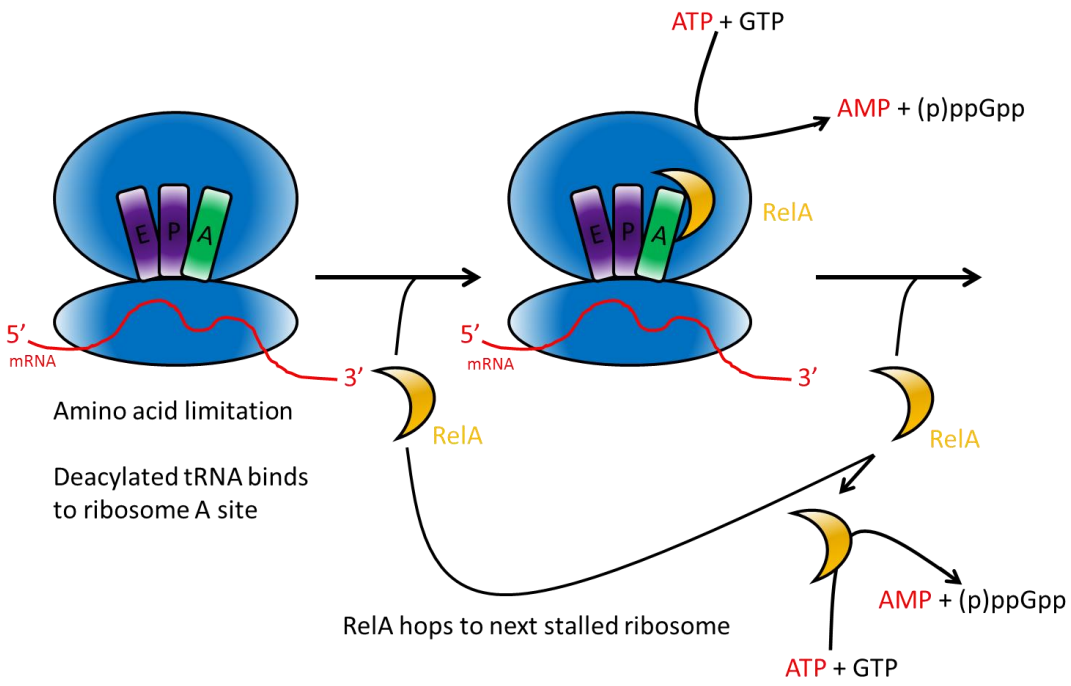

Figure 10. Ribosome-dependent synthesis of ppGpp by RelA. RelA catalyses conversion of ATP and GTP to AMP and (p)ppGpp. Schematic for RelA recognition of ribosomes stalled by deacylated tRNA and production of (p)ppGpp (189).

Sun *et al* (16) investigated the role of (p)ppGpp in bacterial growth, protein synthesis, gene expression and virulence of *Y. pestis* in response to amino acid or carbon starvation (16). A double *relA*/*spoT* deletion mutant was created and was unable to synthesise (p)ppGpp in response to nutritional starvation. Other novel observed phenotypes included reduced growth rate and autoaggregation at 26°C (16). The double *relA*/*spoT* mutant also provided protective immunity in mice following a sub-cutaneous challenge of virulent *Y*. pestis (16).

Work conducted previously has investigated the role of RelA in *Francisella* virulence and intracellular survival. The inactivation of the *relA* gene in *F. novicida* resulted in a mutant that was unable to produce (p)ppGpp under amino acid starvation conditions (15). The *relA* mutant also displayed delayed entry into stationary phase of growth and increased biofilm formation, which could be linked to the delay in entering stationary phase (15). When tested in a murine model of tularaemia, the mutant was attenuated, and induced protective immunity to the virulent wild type organism. This demonstrated the importance of (p)ppGpp as an intracellular signalling molecule for pathogenesis of *F. novicida* (15). To date, however there has been no assessment of how amino acid starvation and the stringent response affect global gene expression in *F. tularensis*.

An experimental model of the stringent response can be chemically induced in a controlled way *in vitro* and thus permits analysis of the interplay between regulatory mechanisms. Previous studies have shown the amino acid analogue L-serine hydroxamate to inhibit protein synthesis, thus simulating amino acid starvation conditions and triggering the stringent response (figure 11) (190). Serine hydroxamate is a competitive inhibitor of seryl transfer ribonucleic acid (tRNA) synthetase (190). L-serine hydroxamate competes with L-serine, thus excluding the amino acid substrate from the enzyme leading to depletion of seryl-tRNA as charging of serine tRNA is prevented (190, 191). As amino acid starvation conditions results in an increase in the ratio of uncharged tRNA to charged tRNA for the depleted amino acid, the bacterial ribosome stalls; this in turn activating ribosome associated RelA which is a sensor of the charging state of tRNA, and subsequent synthesis of (p)ppGpp (184). Thus, artificially induced depletion of charged tRNA by serine hydroxamate triggers the stringent response and enables bacterial gene expression studies under active stringent response conditions without the need to starve bacterial cultures *in vitro*. This approach facilitates sampling for studies of

this nature and accurately stimulates bacteria to accumulate (p)ppGpp much the same as upon entry to stationary phase of growth (192). However, limitations include the fact that amino acid starvation is perhaps not the sole trigger for the stringent response *in vivo*, and the gene expression profiles of bacteria *in vivo* may reflect this more complex environment (89). As such, the use of artificial stringent response activation gives an indication of *in vivo* gene expression not a perfect representation of bacteria in this environment.

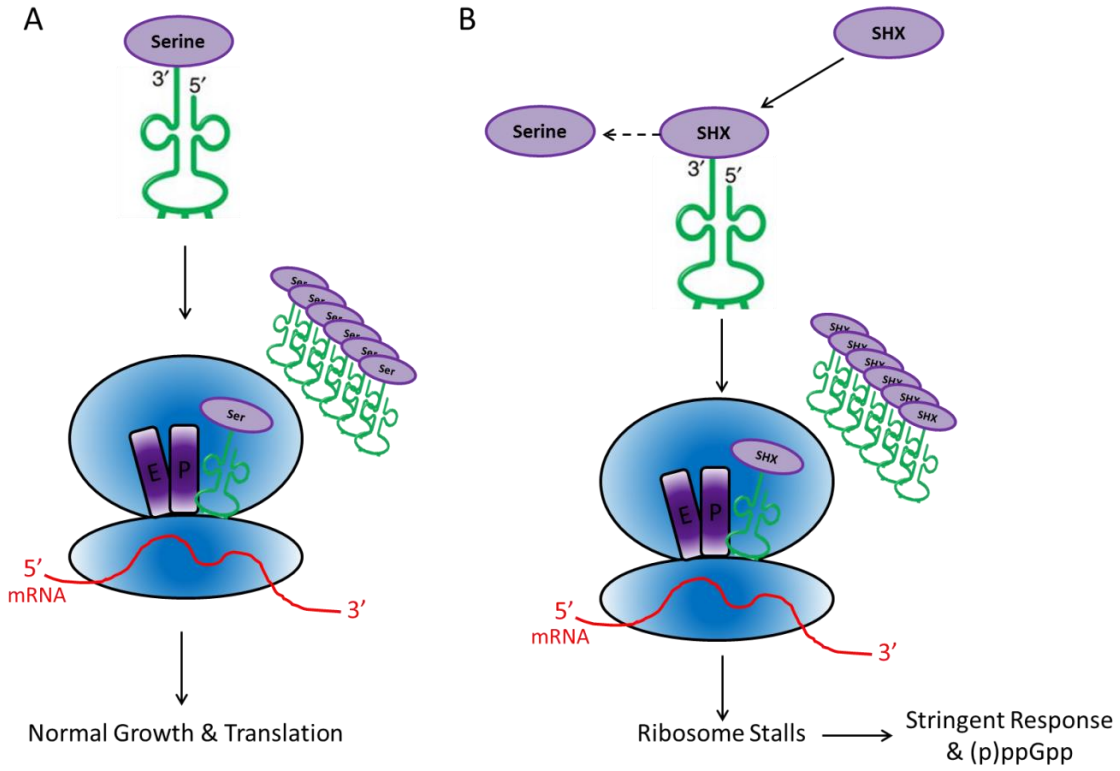

Figure 11. Schematic A shows normal charging of tRNA with serine (Ser) under normal growth conditions. Schematic B shows the addition of serine hydroxamate (SHX) which out competes serine and prevents charging of tRNA, whereupon an uncharged tRNA enters the A site of the bacterial ribosome and causes the ribosome to stall translation, giving rise to the relA-dependent stringent response and subsequent production of (p)ppGpp (190, 191).

1.5.2. The Stringent Response and Environmental Stress Tolerance

Although the bacterial stringent response is primarily linked to nutrient starvation conditions, specifically, amino acid and fatty acid limitation, more detailed studies of the stringent response have revealed correlation with a wide range of adaptive responses to other environmental stresses (193, 194). Such stresses include exposure to reactive oxygen species (ROS), antibiotics, salinity, heat and carbon starvation. Some of the key stress responses that have been found to be linked to the stringent response are discussed below.

ROS can take the form superoxide (O_2^-), a charged molecule unable to penetrate membranes which causes exogenous oxidative stress (193, 195). Hydrogen peroxide (H_2O_2) in contrast, is an uncharged molecule that can pass easily through membranes, and so causes endogenous oxidative stress (193, 196, 197). A third form of free radical that bacteria encounter is hydroxyl radical ($^{\cdot}OH$), which is a by-product of the macrophage immune response (198). Therefore, bacteria require mechanisms to enable survival against these molecules. As a first line of defence against oxygen toxicity, bacteria have evolved superoxide dismutases (SODs), highly conserved enzymes which convert O_2^- into H_2O_2, which is then broken down into water and oxygen by catalases (199, 200).

SODs are classified according to the metal ion cofactor required for activity, to date four types have been identified in bacteria; copper-zinc (Cu/Zn-SOD), manganese (Mn-SOD), iron (Fe-SOD) and nickel (Ni-SOD) (200, 201). SODs have been well characterised in *E. coli*, which possesses three types: a Fe-SOD encoded by the constitutive gene *sodB* which provides continuous low level protection from intracellular oxidative stress (202), a Mn-SOD encoded by the inducible gene *sodA* which provides superior protection than *sodB* against DNA damage during oxidative stress encountered upon entry to stationary phase (200, 202), and a Cu/Zn-SOD encoded by *sodC* protects the cell periplasm and membrane from exogenous O_2^- (24).

Catalases, the enzymatic scavengers of H_2O_2 are encoded by the genes *katA* and *katB* in many bacteria (63). It has been previously established that KatA dominates bacterial defences against endogenous H_2O_2 and is required for survival *in vivo* (64,74).

Khakimova *et al* (203) recently showed that inactivation of both of the stringent response genes, *relA* and *spoT*, decreased the activity of superoxide dismutase and catalases in *P. aeruginosa*, resulting in a strain that was more susceptible to oxidative stress than the wild type organism (203). Complementation of the genes restored oxidative stress tolerance to wild type levels (203). After the addition of serine hydroxamate during the exponential phase of growth, catalase levels increased in wild type *P. aeruginosa*, but did not increase in the Δ*relA/spoT* mutant strain, indicating (p)ppGpp signalling is required for increased expression of catalases (203). This study also investigated the contribution of the sigma factor RpoS as an intermediate regulator of catalase activity, which was demonstrated by decreased catalase activity in both stringent response and RpoS mutant strains (203).

As the stringent response has been found to give rise to increased bacterial survival during nutritional stress and oxidative stress, it has also been investigated whether the stringent response also confers tolerance to other forms of stress including antibiotic treatment. For example, research has shown that amino acid starvation and subsequent induction of the stringent response is linked to transient tolerance of the antibiotics ofloxacin and ampicillin in *E. coli* (42). Additionally, a phenotypic study into *Campylobacter jejuni* demonstrated the stringent response gene *spoT* is required for rifampicin resistance and survival in oxygen rich conditions (194). This result reflects the interactions of (p)ppGpp, RNA polymerase (RNAP) and rifampicin, whereby ppGpp exerts stringent control by binding RNAP at the same site (β subunit) at which rifampicin (structure shown in table 1) binds, thus preventing the antibiotic from working (194). A Δ*spoT* mutant showed a significantly decreased resistance to rifampicin, highlighting the interaction of ppGpp, RNAP and the antibiotic (194). Inactivation of the stringent response genes, *relA* and *spoT* in *P. aeruginosa* also dramatically decreased the tolerance of nutritionally starved cells to various classes of antibiotics, including gentamicin (table 1) and ofloxacin (figure 12), an aminoglycoside and fluoroquinolone respectively (171). This led to a hypothesis that, many bactericidal antibiotics induce the production of ROS, and thus kill by the common mechanism of oxidative damage (66,98,148). To counter this the stringent response coordinates bacterial oxidative stress defence mechanisms (171). However debate is now surrounding this theory of antibiotic killing (193), so further investigation into the contribution of the stringent response to antibiotic tolerance is required (193, 204).

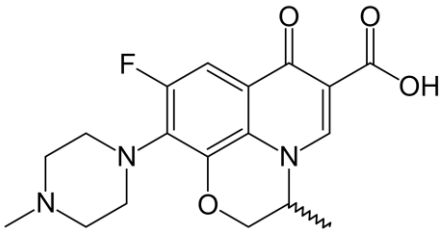

Figure 12. Chemical structure of the fluoroquinolone, ofloxacin.

Stringent control has also been observed under conditions of carbohydrate starvation (205). Glucose-starved exponentially growing *E. coli* demonstrated resistance to a rapid up-shift in temperature, from 37°C to 57°C compared to un-starved bacteria (206). Although glucose starvation is not a direct inducer of the *relA/spoT* mediated stringent response, it has been linked to increased (p)ppGpp production during starvation conditions (207). In addition to amino acid starvation and fatty acid starvation the stringent response has been found to be induced by carbon starvation conditions leading to an accumulation of the signalling nucleotide (p)ppGpp (208), which in turn coordinates global gene expression changes to enable survival until favourable conditions are restored. Finally, a study into the role of RelA in *Enterococcus faecalis* demonstrated that bacterial strains lacking RelA displayed reduced growth in the presence of NaCl (209), indicating RelA induces a response that aids survival in highly saline conditions. Work preceding this study supported this finding that the stringent response genes also have a role during saline stress. Yamada *et al* (210) investigated the role of bacterial homologues of plant RelA and SpoT and found that expression of these genes in *E. coli* enabled bacterial growth in the presence of NaCl and sorbitol, simulating salt stress and osmotic stress respectively (210).

The fact that multiple sources of stress including oxidative, carbohydrate and carbon all lead to an increase in (p)ppGpp production in bacteria suggests that the stringent response is a truly global stress response enabling bacteria to response to a complex variety of stresses that bacteria encounter *in vivo* or *in vitro* when numerous nutrient sources become depleted and bacteria enter a much more competitive environment for survival.

1.5.3. Interaction of the Stringent Response and the Polyphosphate Regulon

Regulatory systems such as the stringent response rarely stand alone in their metabolic activities, and often form a hierarchy of control with overlapping regulons to create a network of biochemical pathways. One such example of overlapping metabolic pathways is that of the stringent response, i.e. (p)ppGpp metabolism, with inorganic polyphosphate metabolism (211-213). Coordination of these pathways to enable bacterial survival in unfavourable conditions requires complex regulation, which is now beginning to come to light with augmenting research into the (p)ppGpp signalling and polyphosphate involvement in stress responses.

1.5.4. Inorganic Polyphosphate Metabolism

Inorganic polyphosphate (figure 13) has been linked to both the stringent response and bacterial virulence. Inorganic polyphosphate is a linear molecule of phosphate residues linked by phosphoanhydride bonds, in bacteria, ranging from tens to at least hundreds of residues in length depending on the cellular location and the metabolic state of the cell (214). Polyphosphate accumulates in some bacteria as metachromatic granules and has numerous and varied biological functions (215, 216). Inorganic polyphosphate can serve as an energy source, and a phosphorylating agent for alcohols, sugars, proteins and nucleosides. It can also activate the precursors for the metabolism of fatty acids, phospholipids, polypeptides and nucleic acids (214, 215, 217). Polyphosphate is also involved in activating the Lon protease complex which degrades ribosomal proteins to provide a pool of amino acids for the synthesis of new proteins (191, 218).

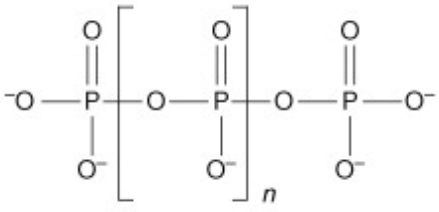

Figure 13. Linear polyphosphate structure (218, 219).

1.5.5. Polyphosphate Metabolic Genes - PPK and PPX

Levels of polyphosphate in bacterial cells are regulated by polyphosphate kinase 1 (PPK1), polyphosphate kinase 2 (PPK2) or polyphosphate kinase 3 (PPK3), and an exopolyphosphatase encoded by PPX (220, 221). PPK 1 has been well characterised in *E. coli* and favours the synthesis of polyphosphate (222-224). PPK2 has also been studied in *E. coli* but is structurally distinct from PPK1 and can perform either the synthesis of polyphosphate or the catalysis of GTP or ATP from polyphosphate (222, 223, 225). PPX is associated with the degradation of polyphosphate chains to free phosphate (Pi) residues (226). The polyphosphate metabolic genes have been annotated in many bacteria including *P. aeruginosa* and the three pathogens of focus in the work presented herein; *B. pseudomallei*; *F. tularensis* and *Y. pestis* (227, 228). *P. aeruginosa and B. pseudomallei* have been found to encode both PPK1 and PPK2 (229), whereas *F. tularensis* encodes a single PPK2 and *Y. pestis* encodes a single PPK1 (26, 103, 220, 229, 230). Biochemical, structural and functional studies have also been carried out in *F. tularensis* to elucidate the role of PPK in virulence (14, 230). Richards *et al* (14) found that mutation of *Francisella ppK* caused defects for intracellular growth in macrophages and attenuation in mice, supporting a key role for the putative polyphosphate kinase in virulence (14). Inactivation of the gene annotated as FTN1472/FTT1564 resulted in the abolishment of polyphosphate production in *F. novicida*. This confirmed FTN1472/FTT1564 as encoding a polyphosphate kinase, and the locus was thus re-designated *ppK* (14).

1.5.6. Coordination of (p)ppGpp and Polyphosphate Accumulation

Inorganic polyphosphate is accumulated along with (p)ppGpp during nutrient starvation conditions (218). (p)ppGpp inhibits PPX (25) as shown in figure 14, which leads to an accumulation of polyphosphate, which in turn increases the turnover of ribosomal proteins providing a pool of amino acids needed for the synthesis of new proteins required during the adaptation process (25,26). Stringent response mutants which have diminished levels of (p)ppGpp also harbour lower levels of polyphosphate, suggesting polyphosphate plays a key role in stress survival.

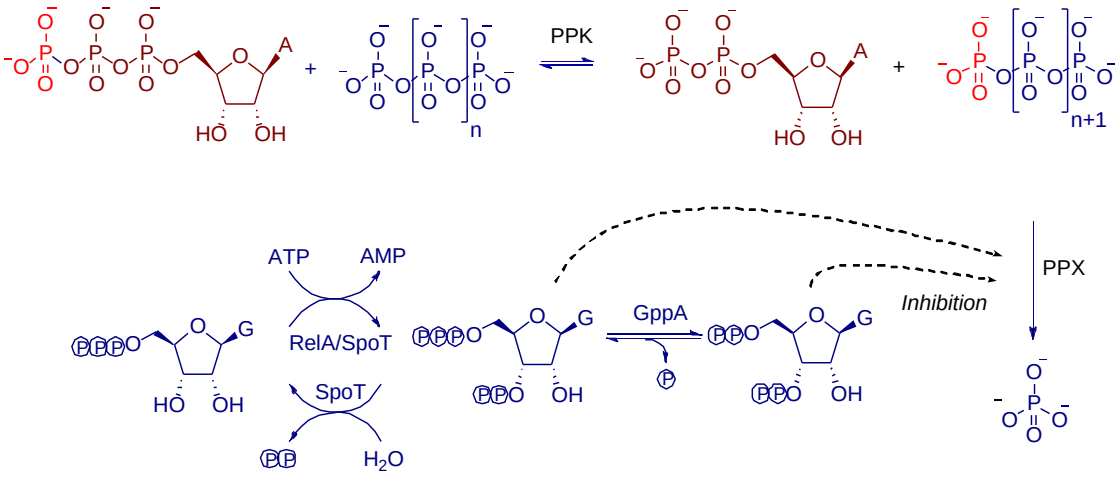

Figure 14. Interaction of (p)ppGpp biosynthesis with polyphosphate metabolism. PPK catalyses the reversible synthesis of polyphosphate from the terminal phosphate from ATP (231). PPX catalyses the degradation of polyphosphate into free Pi residues (232, 233). GppA, an exopolyphosphatase catalyses the conversion of pppGpp to ppGpp (232, 234). RelA catalyses the synthesis of (p)ppGpp from ATP and GTP or GDP (235-237). SpoT catalyses both the synthesis of (p)ppGpp from ATP and GTP or GDP and the degradation of ppGpp to GDP and PPi and pppGpp to GTP and PPi (238).

1.5.7. The Stringent Response and Virulence Gene Expression

It has now been established through gene expression studies that *in vitro* cultured bacteria during stationary phase of growth are much more representative of bacteria during the infection process than bacteria in the exponential growth phase (105). It has also been found that bacterial virulence gene expression is associated with starvation conditions and the stringent response. This is likely due to the host-associated intracellular niche providing a more competitive environment for survival and demanding complex nutritional requirements for pathogens (239). It has been reported in numerous bacteria that the stringent response is required for virulence-related phenotypes, such as biofilm formation and intracellular survival (194, 240-242). Bacterial mutants lacking stringent response genes have also displayed a failure to produce virulence factors (243, 244). For example, in the pathogen *Vibrio cholerae* increased levels of (p)ppGpp also results in induction of virulence genes (245). The associateion of the stringent response and virulence gene expression has also been observed in other organisms such as *F. tularensis*, as discussed in section 1.2.2, where Charity *et al*

proposed a model of ppGpp interaction with RNAP and a MglA/SspA protein complex to give rise to *Francisella* virulence gene expression (239).

1.5.8. The Stringent Response and the *Francisella* Pathogenicity Island

The association of virulence gene expression with nutrient starvation has been found to be true for the intracellular pathogen *F. tularensis*, where starvation causes a significant up-regulation of virulence genes residing on the FPI (86). The 30 Kb FPI encodes 11 genes that comprise a Type VI secretion system, pictured below and discussed in section 1.2.2 (figure 15) has been shown to be essential for survival and growth within host macrophages (246, 247). More recent studies have also shown that several genes encoded on the FPI are directly regulated by MglA, a regulatory protein that activates FPI gene transcription and has also been implicated in the response of *Francisella* to starvation conditions and oxidative stress (248). For example, the intracellular growth locus protein IglC is induced during intracellular infection of macrophages and is directly regulated by MglA (249). MglA is also homologous to *E. coli* stringent starvation protein SspA, which is also a transcription factor (250). However, *F. tularensis* has an additional separate SspA homologue and it is thought that *Francisella* MglA and SspA interact and bind RNAP to regulate FPI gene expression during stress (239).

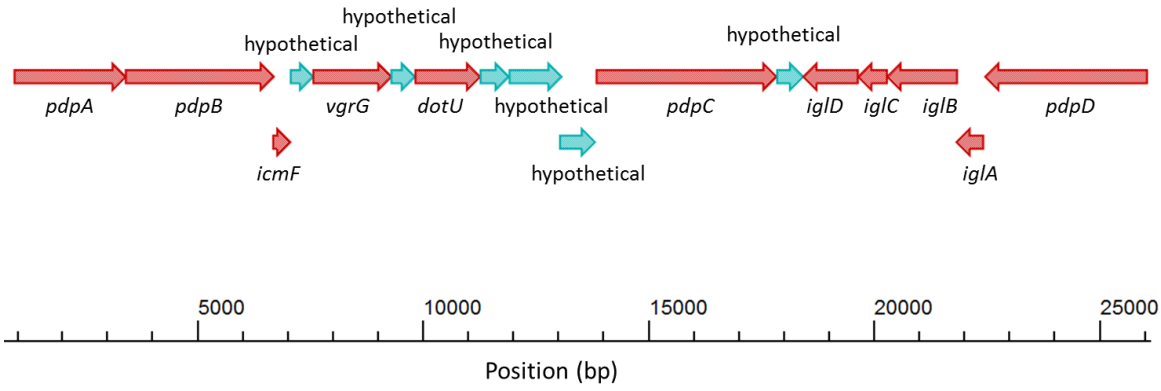

Figure 15. Gene arrangement of the FPI which encodes a putative TSSS (as shown in figure 6) (247).

1.5.9. The Stringent Response and Bacterial Persistence

As discussed previously in section 1.4, bacterial mechanisms for survival in changing environmental conditions include genetically mediated adaptations such as sporulation, phase variation and adaptive mutation resulting in antibiotic resistance. Conversely, adaptation to environmental change can be epigenetic, for example persistence, which gives rise to phenotypically distinct, but genetically identical subpopulations of tolerant bacteria (165).

Bacterial persistence has recently been linked to the stringent response and toxin-antitoxin (TA) systems in bacteria (figure 16). To study persistence and its molecular mechanisms of action, *hi*gh *p*ersister (*hip*) mutants have been previously generated in *E. coli* and have demonstrated that type II persister cells pre-exist as stochastic subpopulations within bacterial communities (167, 251). More detailed analyses of *E. coli hip* mutants revealed a genetic locus, termed *hipA,* to be a key component of the persister phenotype (167, 169, 251, 252). HipA encodes the toxin component of a TA system, of which there are several in most bacteria (166, 253). TA systems generally consists of a stable toxin, which inhibits essential cellular processes such as translation, via mRNA degradation, and a less stable antitoxin, usually in the form of a protein or RNA which counters the action of the toxin under normal growth conditions (166, 253). Although the function and effects of TA loci are numerous and diverse, they have now been demonstrated to play a key role in bacterial persistence, inducing this non-growing state (169, 252, 254). Studies into the molecular mechanism of TA loci and persistence have revealed links to other cellular process and molecules that impact this phenomenon. One such process that has been implicated in TA activation is the activity of the Lon protease, which has been shown to degrade the antitoxin component of the TA system, giving rise to toxin activation and subsequent growth inhibition for example via mRNA degradation (169, 252).

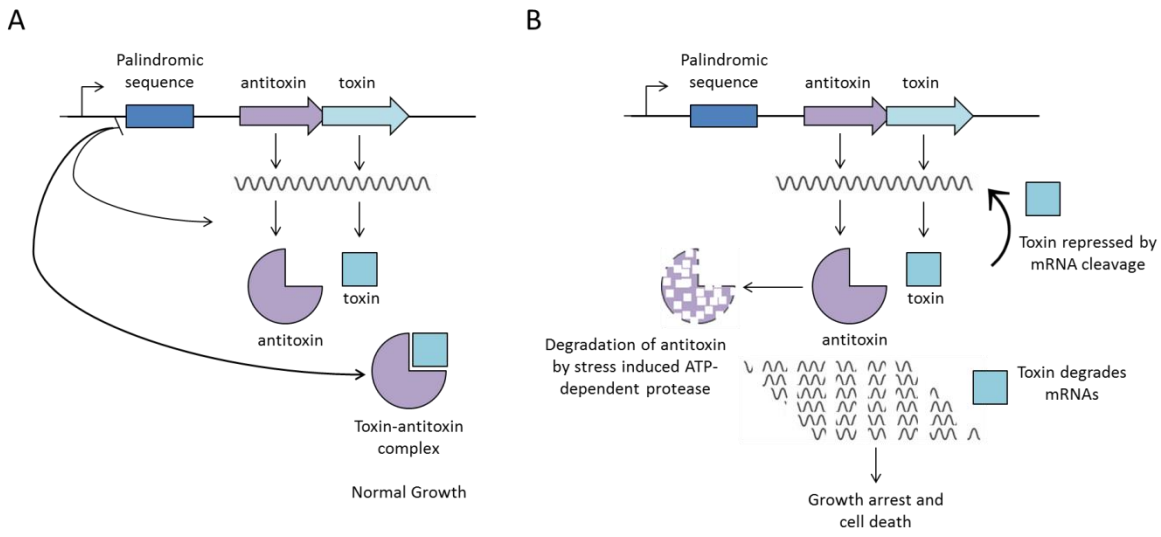

Figure 16. Figure adapted from Yamaguchi *et al* (255). Schematic A shows the toxin and antitoxin being synthesised from the same promoter under normal growth conditions, wherein the toxin is in complex with the antitoxin and therefore cannot bring about toxin effects to the cell. Schematic B shows the antitoxin being degraded under conditions of stress and subsequent toxin activity that leads to bacterial cell growth arrest and eventually bacterial cell death (255).

The Lon protease has been recently implicated in the stringent response (256). Lon, as mentioned in section 1.5.4, is an enzyme that is directly activated by polyphosphate, a ubiquitous molecule previously shown to be essential for virulence in many bacteria and a molecule that accumulates along with (p)ppGpp under amino acid starvation conditions (173, 256). Persistence is triggered by a cascade of biochemical steps ultimately leading to Lon activation. The cascade is initiated by nutrient limitation activating RelA and resulting in the accumulation of (p)ppGpp. Following this (p)ppGpp inhibits PPX, thus reducing polyphosphate hydrolysis and resulting in a an accumulation of polyphosphate (218). This in turn interacts directly with Lon, activating the proteolysis of the antitoxin. As a result there is an accumulation of free active toxin, which functions as an mRNase degrading mRNA and leading to the persister phenotype. This hierarchical control over TA systems and persistence has recently been proposed as a working model (figure 17) by Germain *et al* (169).

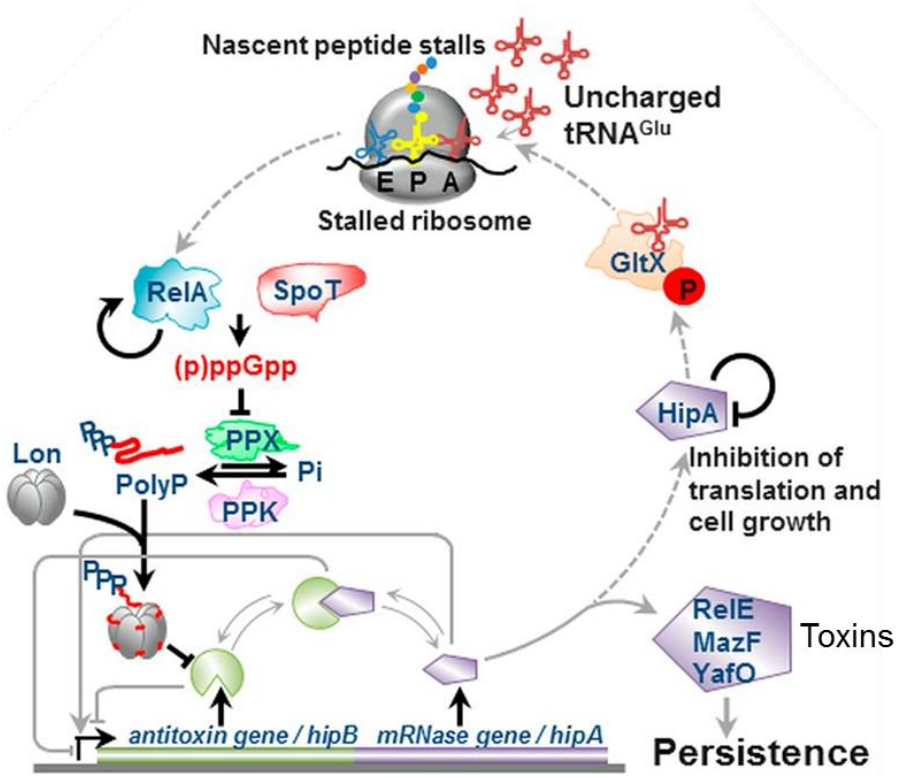

Figure 17. Figure adapted from Germain *et al* (169) Free HipA phosphorylates GltX, the resulting inhibition of Glu-tRNA^{Glu} increases uncharged tRNA^{Glu} loading at the A site of the ribosome and triggers RelA-dependent (p)ppGpp production. (p)ppGpp competitively inhibits PPX. In turn, polyphosphate is synthesized by PPK and stimulates Lon to degrade antitoxins, activating mRNases that inhibit translation and cell growth and induce persistence. The arrow emerging from RelA and pointing back to RelA indicates a positive feedback loop in which (p)ppGpp activates further (p)ppGpp synthesis. RelE, MazF and YafO are examples toxin components of TA systems present in *E.coli*. (183).

1.6. Investigating Stringent Control on a Global Scale

It is important to characterise the global stringent response as the effects are widespread within bacterial cells and as yet are still poorly understood or even known about at all. Therefore global gene expression profiling enables targeted analysis to provide a more complete picture of this complex stress response. To investigate the regulatory networks involved in the stringent response and polyphosphate metabolism, and their interaction with other genetic elements of the bacterial genome, global gene expression profiles can be elucidated. Until recent years microarray was the preferred technique for evaluating whole genome expression patterns (257). However, limitations associated with this technique, such as the requirement for *a priori* knowledge of the genome sequence under interrogation and the time and costs involved, have led to its gradual replacement by high throughput sequencing technologies (258). High-throughput sequencing, also termed next generation sequencing, offers significantly greater resolution, no prerequisite for known genome sequences and the ability to analyse multiple samples in a massively parallel fashion. Thus, a next generation sequencing technique for the analysis of transcriptomes, termed RNA-seq has been selected for our experiments.

Next generation sequencing has revolutionised the field of biology in recent years. With costs continuing to fall and data output increasing at a rate exceeding Moor's law, this technology is becoming increasingly routine in biology laboratories around the world. From the publication of the human genome first being sequenced in its entirety at a cost of US$3 billion in 2000, DNA sequencing has progressed significantly and beyond experts' predictions (259). As sequencing platforms become more sophisticated, increasing throughput and streamlining data analysis, the race is now on to achieve the US$1000 human genome (260).

Currently, the sequencing market remains a competitive one. The leading companies continue to push one another to increase throughput, lower costs, simplify protocols, reduce run times and provide computational solutions for the vast volumes of data generated that laboratory workers can exploit with limited bioinformatic training. For example, the human genome project ran for 10 years, utilising a plethora of sequencers to generate the 2.91 billion base pair (bp) consensus sequence (259). Nowadays, the Illumina HiSeq2000 instrument can generate 600 billion bp of data in a single run taking 11 days (261).

The current platforms exploit different sequencing chemistries and therefore provide different advantages depending on the desired application. The Roche 454 GS FLX+ and the GS Junior Sequencers use pyrosequencing (summarised in figure 18), otherwise known as sequencing by synthesis. This chemistry uses a luciferin/luciferase based enzyme cascade to emit a light signal following base incorporation to a complementary strand of DNA. The reactions are performed on a pico titre plate (PTP), which contains millions of wells in which bead based micro-reactors display the DNA template fragments. This technology has the advantage of long read lengths of up to 600 bp (the longest offered by a non-real-time sequencer), meaning these platforms are well suited to *de novo* sequencing to generate a single scaffold reference sequence. Long read lengths are also advantageous for phylogenetic microbial profiling using amplicon sequencing of genetic markers such as 16S rRNA.

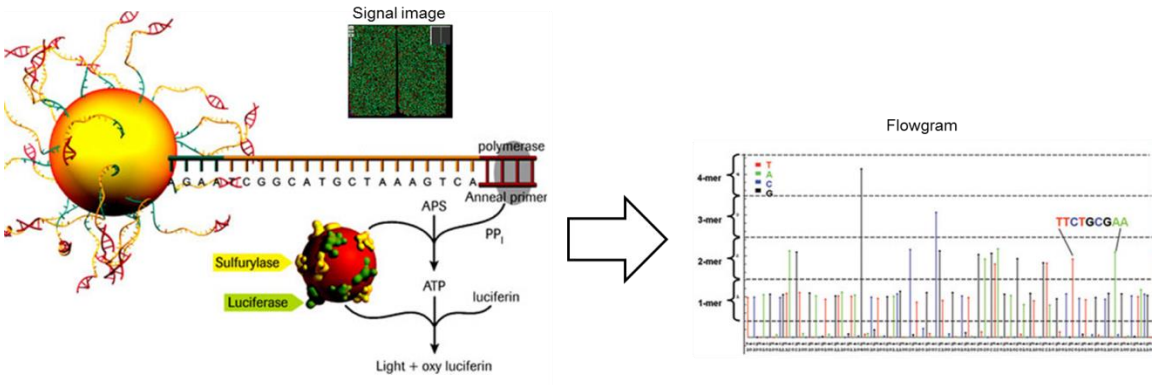

Figure 18. 454 sequencing by synthesis showing millions of copies of clonal fragments of genomic DNA captured on a bead. Light signal intensity of each nucleotide incorporation event at each well position to is used to determine the sequence of all the DNA reads in parallel. Light signals are processed to provide a flowgram which can then be analysed by bioinformatic software.

The Illumina platforms (The HiSeq2500 and the MiSeq) utilise reversible terminator technology (summarised in figure 19). Reversible terminator technology is also based on sequencing by synthesis, where a fluorescently labelled terminator is imaged as each nucleotide is incorporated into the growing DNA strand. After incorporation, the terminator is cleaved to allow addition of the next nucleotide. Although the read lengths generated by the Illumina platforms are shorter, the data output far exceeds any other Next Generation sequencing platform on the current market. As such, these platforms, particularly the HiSeq2000, are particularly well suited to draft *de novo* sequencing of multiple strains for comparative analysis. Re-sequencing and transcriptomics are also techniques appropriate for these platforms.

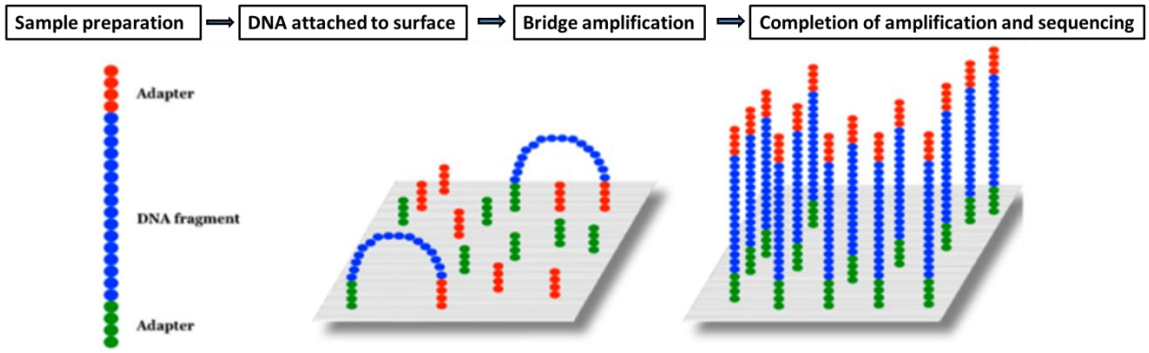

Figure 19. Sequencing by synthesis (SBS) clustering technology developed by Illumina which uses bridge DNA amplification combined with fluorescently labelled nucleotides to provide a signal upon incorporation into the synthesised DNA strand.

The Ion Torrent Personal Genome Machine is a semi-conductor chip based system that detects the release of a proton and the associated pH change, when a nucleotide is incorporated into a complementary strand of DNA. The data output of this technology is limited to the size of the chip used on the instrument, delivering 10 Mb from an Ion 314 chip which contains 1 million wells, to 1 Gb from an Ion 318 chip which contains 11 million wells. SOLiD Sequencing, in a similar fashion to 454, Illumina and IonTorrent uses fluorescently labelled nucleotides to detect the ligation of complementary di-bases to a template DNA library. This technology is prized for its sequencing accuracy, and ability to accurately sequence homopolymers, where

platforms like the Roche 454 sequencer fail. However, the short read lengths pose drawbacks for certain applications such as metagenomics. Finally, the Pacific Biosciences PacBio RS differs considerably being a single molecule sequencer, referred to as single molecule real time sequencing (SMRT). SMRT sequencing exploits the natural ability of DNA polymerase to synthesise complementary DNA (cDNA). Again, the pool of DNA bases is fluorescently labelled and the emission spectrum of a DNA base being incorporated into the growing strand as DNA is extended is compared to a nucleotide not being incorporated. This signal is detected as the incorporation event occurs to generate real time sequence data. Although this technology offers extraordinarily long read lengths, far surpassing other platforms on the current market, and quick run times without amplification bias, the platform has suffered with high error rates. It also has an extremely large physical footprint, unsuitable for most biology laboratories.

1.6.1. Whole Genome Transcriptional Analysis by RNA-Sequencing

As mentioned above, the research application area for which a next generation sequencer is best suited differs depending on the chemistry it employs and the associated experimental advantages. A field of next generation sequencing that has begun to rapidly expand in very recent years is RNA sequencing (RNA-seq). RNA-seq exploits next generation sequencing to sequence cDNA synthesised from isolated RNA to map and quantify genetic transcripts (262). RNA-seq offers many advantages over current transcript profiling techniques. For example, microarrays are reliant upon prior knowledge of transcript sequences to which test samples can be matched, whereas RNA-seq can generate *de novo* sequences that were previously unpredicted (262). Transcriptomics can provide a novel and detailed means of understanding immune regulation (263, 264), host-pathogen interactions (265-267) and non-coding micro RNAs (miRNAs) (268) involved in the post transcriptional regulation of mRNA (269, 270). In depth analysis of gene expression could provide the novel insights required for the development of medical countermeasures for infectious diseases.

1.7. Exploiting the Stringent Response for Novel Antibiotic Targets

Despite progress that has been made in recent years in the discovery and development of novel antimicrobial therapies, current treatments for plague, tularaemia and melioidosis all have limitations. In addition, the drive towards broad spectrum therapies is increasing; as such extremely widely distributed metabolic pathways and their constituent genes among organisms of interest are preferred targets. Considering the diversity of adaptive mechanisms that are called into play by bacteria when exposed to environmental stresses particularly during the infection process, understanding the interactions between these regulatory systems and their coordinating molecules, such as (p)ppGpp, can form the basis of novel antimicrobial targets. At the start of this project it was envisaged that the key proteins involved in the stringent response (RelA and SpoT) and polyphosphate metabolism (PPK and PPX) might make suitable targets for antimicrobial inhibitors. The stringent response and polyphosphate biosynthetic pathways were selected as novel targets for inhibitor development for several reasons: polyphosphate and (p)ppGpp production are conserved pathways among many bacterial species including the pathogens in this work; the effects of these pathways are widespread therefore it is less likely that resistance would emerge to an inhibitor targeting polyphosphate or (p)ppGpp production; These pathways do not have homologs in humans which makes them druggable targets; the genes involved in polyphosphate and (p)ppGpp biosynthesis are not essential on their own and would not give rise to a selection pressure leading to resistance, however they do comprise an essential process for bacterial survival and virulence; finally, these targets could increase sensitivity to antibiotics meaning a small molecule inhibitor could be used an antibiotic adjuvant.

Our objective was to evaluate these pathways for their role in intracellular pathogen survival and virulence and characterise the metabolic pathways that regulate the stringent response and polyphosphate metabolism. These genes will be inactivated using methods to avoid polar effects and the impact of the genetic deletion characterised in three serious human pathogens *Y. pestis, F. tularensis* and *B. pseudomallei*. These organisms will also be used as the model organisms for analysis of the stringent response regulon, and will be subjected to chemically induced amino acid starvation and subsequent whole genome transcriptional analysis by RNA-seq to characterise global gene expression profiles under active stringent response conditions. Stringent response regulated genes may also provide novel targets themselves as specific targets for each organism. As these metabolic pathways are essential to permit these bacterial

BWA to adapt to their intracellular phase of infection, they are anticipated to validate targets for inhibitors that function as effective antibiotics or antibiotic adjuvants.

2. *Yersinia pestis* Mutants

2.1. Introduction

There have been relatively few studies into the stress responses in *Yersinia* species. To date, the only study specifically investigating the stringent response in *Y. pestis* strain KIM5^{+} has been conducted by Sun *et al* (16), whereas more generic stress response studies have focussed on *Y. enterocolitica* (271-273). Therefore, further research is required to better understand the stringent response in the highly pathogenic *Y. pestis* strain GB and the work presented in this thesis contributes to this understanding.

As discussed previously in section 1.5.1, Sun *et al* (16) investigated the role of (p)ppGpp in *Y. pestis* and constructed a Δ*relA*/*spoT* deletion mutant which was found to be unable to synthesise (p)ppGpp in response to nutritional starvation. Other novel observed phenotypes included reduced growth rate and autoaggregation at 26°C (16). The double *relA*/*spoT* mutant also induced protective immunity in mice following a sub-cutaneous challenge of virulent *Y. pestis*, suggesting this mutant could be a promising vaccine candidate to provide protection again plague infection (16). However, it is unlikely that a live attenuated vaccine will reach licensure when a subunit vaccine is available (274-276), as adverse reaction to a subunit vaccine is much less likely (277).

Considering complexities associated with regulation of the stringent response in bacteria, a study by Kakoschke *et al* (272) has gone some way to shedding light on the regulatory mechanisms at play during adaptation to changes in environmental conditions in the enteropathogen *Y. enterocolitica* (272). This study focussed on the conserved RNA chaperone Hfq, which has previously been linked to the stringent response, specifically the RelA-dependent response to amino acid starvation (278), by constructing mutants defective for *hfq* (272). It was found that mutants defective for *hfq* displayed defective lipid metabolism and transport, defective cell redox homeostasis, defective mRNA translation and defective ATP synthesis, and were more sensitive to other environmental stresses such as oxidative stress and pH (272). Further studied elucidating the relationship between Hfq and the stringent response included Argaman *et al* (278) who revealed that RelA, a key enzyme in the stringent

response, stimulates Hfq multimerization to enhance sRNA binding (278). It was hypothesised that the RelA-Hfq interaction is a mechanism aimed at controlling translation of newly synthesized incoming mRNAs (278). Other studies have also been carried out in *Y. pestis* and have shown Hfq to be important for *Y. pestis* virulence and stress responses (279-283). For example, Geng *et al* (279) used *in vitro* growth assays to demonstrate that Hfq is required for resistance to H_2O_2, heat and antibiotic stress and contributed to growth under nutrient limiting conditions in *Y. pestis* strain KIM (279). It was reported that an *hfq* deletion mutant showed growth repression of 40 % upon exposure to heat or oxidative stress, the mutant also showed repressed growth in the presence of polymyxin B and when cultured in minimal media (279). These results indicate that Hfq has an important role in stress survival, which suggests that Hfq could also have an essential role in the infection process as the mammalian intracellular niche also subjects bacteria to stresses of this nature. This hypothesis has been evidenced by Bai *et al* (280) who observed limited growth of *hfq* mutants in *Y. pestis* strains KIM and CO92 at 37 °C compared to the wild type strains, suggesting Hfq is essential for plague infection of mammalian hosts (280). This effect appeared to be specific to *Y. pestis* as the severe growth defect of the *hfq* mutant was not observed in the less virulent *Y. pseudotuberculosis* (280). Another stress resistance mechanism that associates Hfq with the stringent response is the ability of *Y. pestis* to form biofilms, particularly to facilitate transmission from the flea vector to the mammalian host (281). It has been demonstrated that during conditions of nutrient limitation and concurrent active stringent response, bacteria a more likely to form biofilms to enable survival during the stressful condition (284, 285). For example, active stringent response has been implicated in the formation of bacterial biofilms in *E. coli* and *V. cholerae* (241, 286). Furthermore, Hfq and its associated sRNAs have been implicated in biofilm development and virulence phenotypes in uropathogenic *E. coli* (287). Kulesus *et al* (287) reported that an *E. coli hfq* mutant was significantly impaired for colonisation of the bladder and kidneys of CBA/J mice compared to the wild type (287). Moreover, Hfq has been implicated in disease transmission phenotypes in *Y. pestis* evidenced by an *hfq* deletion mutant which was found to be unable to form biofilm blockage of the flea midgut, a process essential for transmission to the mammalian host (282). Gene expression studies in *Shigella flexneri* provide further evidence for the complex interactions between the stringent response pathway and Hfq activity during stress responses. Sharma *et al* (240) found that addition of ppGpp, along with the pleotropic stress response regulatory protein DksA, in an *in vitro* transcription assay resulted in an increase in transcription of *hfq*, indicating that DksA is

required for maximal transcription of hfq during both exponential and stringent response growth conditions (240).

As these examples suggest, Hfq is associated with stringent response and stress resistance adaptations both directly and indirectly. Direct association of Hfq with the stringent response occurs via the action of RelA stimulating Hfq hexamerisation. Indirect association of Hfq with the stringent response occurs via environmental cues giving rise to phenotypes conserved between stringent response mutants and *hfq* mutants.

The aforementioned studies indicate that the stringent response and its associated regulatory mechanisms are appropriate targets to investigate as targets for novel medical countermeasures for the treatment or prevention of the deadly bacterial infection, plague. Therefore, in order to investigate the stringent response and polyphosphate metabolism in the highly virulent intracellular pathogen *Y. pestis,* strain GB, mutagenesis strategies were designed for the inactivation of the key genes involved in the coordination of these pathways. The genes *relA* and *spoT* that synthesise and degrade (p)ppGpp in response to nutrient starvation, and *ppK* and *ppX* which synthesise and degrade intracellular polyphosphate, which also accumulated alongside (p)ppGpp were targeted for mutagenesis.

2.2. *Yersinia pestis* Mutant Creation

2.2.1. Bioinformatic Analysis of PPK and PPX

Protein alignments were first analysed as shown in appendix 8.1 to analyse homology to previously annotated RelA, SpoT, PPK and PPX proteins in other bacteria such as *E. coli*. The *ppK* and *ppX* genes in the *Y. pestis* CO92 genome sequence were identified by BLAST (Basic Local Alignment Search Tool) nucleotide analysis previously during the genome annotation of this reference strain, and are shown below in figure 20 (104). As yet, there is no published genome sequence for *Y. pestis* GB, however this strain is believed to share an extremely high degree of sequence homology with strain CO92, as predicted from previous genetic studies (96). The *ppX* gene (3166073-3167632) is annotated as a putative exopolyphosphatase, and the *ppK* gene (3163999-3166062) as a polyphosphate kinase. The genomic organisation of the region is shown in Figure 20.

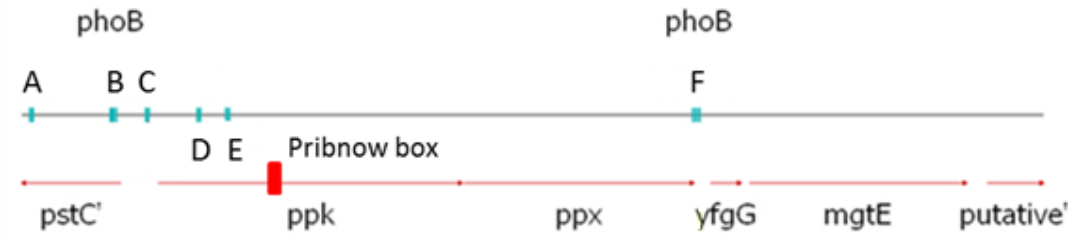

Figure 20. *ppK-ppX* region. Putative promoter regions are indicated in blue as A-F. Promoters labelled above indicate 5' - 3' strand and promoters labelled below indicate 3' - 5' strand. Putative Pribnow box indicated in red.

The *ppK* and *ppX* open reading frames (ORFs) appear to be part of an operon driven by a promoter directly upstream from *ppK*; this promoter is likely to be located in the intergenic space or at the proximal end of the *pstC* gene running on the complementary strand. There was a predicted Pribnow box located approximately 300 bp inside the *ppK* gene. This is a strongly predicted promoter matching the classical consensus TATAAT (third promoter on coding strand running in the 5'-3' direction as shown in figure 20). To maintain these regulatory elements it was considered that it might be necessary to retain the 5' 300 bp and

delete the remaining 1713 bp of the *ppK* gene. Although this would allow production of a truncated protein of approximately 117 amino acids, it was unlikely to result in a biologically active protein and still produce the desired outcome of an inactivation of *ppK*. In the intergenic region between the divergently transcribed *pstC* and *ppK* genes, one putative promoter was identified. However, this was on the complementary strand and likely to control expression of *pstC*. The nearest promoter which was on the coding strand was located at the beginning of the *pstC* gene (promoter B on coding strand running in the 5'-3' direction as shown in figure 20) that could be in control of *ppK* expression.

When designing a method for the generation of a deletion mutant lacking the *ppX* ORF, care was taken to avoid disruption of expression of the downstream *yfgG* gene which encodes a hypothetical protein. Analysis of putative promoters of *yfgG* was therefore also undertaken. This analysis revealed a -10 sequence close to the stop codon of *ppX* with the sequence TAATAAAAT. This indicated that the -35 sequence extended into the end of the *ppX* ORF. It was therefore decided that when creating either the *ppX* single or *ppK/ppX* double mutant a small 3' part of *ppX* was left in place to ensure the promoter potentially regulating transcription of *yfgG* (and potentially *mgtE* which encodes a putative divalent cation transport protein) was not disrupted through removal of regulatory elements.

Two regions were identified with predicted PhoB binding sequences. This transcription factor binds to control expression of a range of genes under phosphate-limiting conditions. Diminished expression of *ppK* was observed in *phoB* mutants of organisms such as such as *E. coli*, *Klebsiella aerogenes* and *Streptomyces lividans* (45,61,112). Our bioinformatic analysis indicated that similarly polyphosphate metabolism may be regulated by PhoB in *Y. pestis* due to the presence of PhoB binding sites flanking the polyphosphate biosynthesis operon. As such, consideration was also taken when designing mutants to maintain PhoB binding sites as well as promotor regions.

When considering a *ppK/ppX* double mutant, a single construct was considered as the genes were directly adjacent. By deleting the two ORFs simultaneously, care was taken during primer design not to disrupt putative regulatory regions of the adjacent *yfgG* gene. Similarly, a marked mutant approach should be acceptable for the generation of the polyphosphate genes isogenic

mutants as no promoter sequences were predicted within the coding regions of *ppK* or *ppX*. However, expression of *ppX* must be confirmed in the *ppK* mutant to ensure there were no polar effects as a result of mutagenesis.

2.2.2. Bioinformatic Analysis of RelA and SpoT

The *relA* gene in the *Y. pestis* CO92 genome sequence was identified by BLAST nucleotide analysis during the genome annotation (105). The genomic organisation of the region is shown in figure 21.

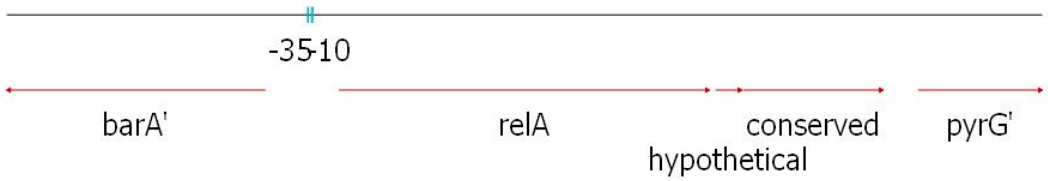

Figure 21. The *relA* region. Putative promoter regions are indicated: ¯10 and ¯35 are putative promoter sequences on 5'-3' strand.

The *spoT* gene in the *Y. pestis* CO92 genome sequence had also been identified by BLAST nucleotide analysis during the genome annotation (105). The genomic organisation of the region is shown below in figure 22.

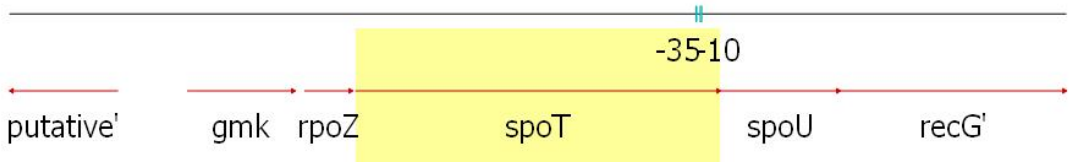

Figure 22. The *spoT* region. Putative promoter regions are indicated: ¯10 and ¯35 are putative promoter sequences on 5'-3' strand.

As discussed in section 1.5 inactivating *spoT* as a single mutation is often lethal as it leads to an unabated accumulation of (p)ppGpp which eventually results in cell death, an unmarked, in-frame deletion is the only option to create a double *relA*/*spoT* mutant . To facilitate this process, the unmarked *relA* mutant was used as the genetic background to subsequently generate the double *relA*/*spoT* mutant.

2.2.3. Mutagenesis Methods – *Y. pestis*

Historically, mutants in *Y. pestis* have been created using isogenic allelic replacement (288-290). To create unmarked mutants, the suicide vector pDM4 (291) was used to deliver deletion inserts to *Y. pestis* GB by conjugation, which then replaced the gene of interest by homologous recombination (291). However, due to the low recombination efficiency of *Y. pestis*, the Lambda (λ) Red Recombinase mutagenesis method (outlined in the schematic in figure 23) was employed to generate marked mutants (292). To create marked mutants λ Red Recombinase mutagenesis using plasmid pAJD434 was used to replace target genes with an antibiotic resistance marker utilizing a plasmid-driven recombination system (271, 292). The λ Red Recombinase mutagenesis method involved amplifying a kanamycin antibiotic resistance cassette (Kan^R) with oligonucleotide primers that contained regions of sequence homology to the flanking regions of the gene being targeted for deletion (293). For example PK1 and PK2 in figure 24, PX1 and PX2 in figure 25, PKX1 and PKX2 in figure 26 and R1 and R2 in figure 27 (primer sequences are listed in appendix 8.2). This PCR product was then directly transformed into *Y. pestis* GB by electroporation. The recipient *Y. pestis* strain contained a previously transformed plasmid, pAJD434 which encoded the λ red operon genes for stimulating homologous recombination (figure 24). The primary advantage of the λ Red Recombinase mutagenesis method was its speed. However, the major drawback was the creation of marked mutants. The incorporation of a selectable marker such as an antibiotic resistance cassette increased the risk of polar effects on the expression of genes adjacent to the target gene. Therefore, it was important to confirm expression of adjacent genes. The λ Red Recombinase mutagenesis method was used to generate the deletion mutants for *ppK*, *ppX* a double *ppK*/*ppX* and *relA* (as shown in figures 25, 26, 27 and 28 respectively). The λ red recombination method involved the use of the Bacteriophage λ red operon, encoded on a plasmid (figure 24) to facilitate integration of recombinant DNA by stimulating homologous recombination. The red operon consists of three genes; γ β and exonuclease (exo). The gene products are Gam, Beta and exo respectively. Gam inhibits the host RecBCD exonuclease V so

that Bet and Exo can gain access to DNA ends to promote recombination. After Gam protein has inhibited exonuclease V activity of the RecBCD system, exonuclease binds to dsDNA ends, progressively leaving 3' single stranded DNA (ssDNA) overhangs. Beta then binds to the ssDNA and mediates invasion of ssDNA into unbroken homologous duplex. RecF is essential for formation of the recombination complex (RecA stabilises the complex of Bet, DNA and RecF) (294). RuvAB helicase-driven branch migration results in Holliday junction formation (295, 296). This is resolved by a RuvC-Holliday junction endonuclease into a recombinant molecule (124).

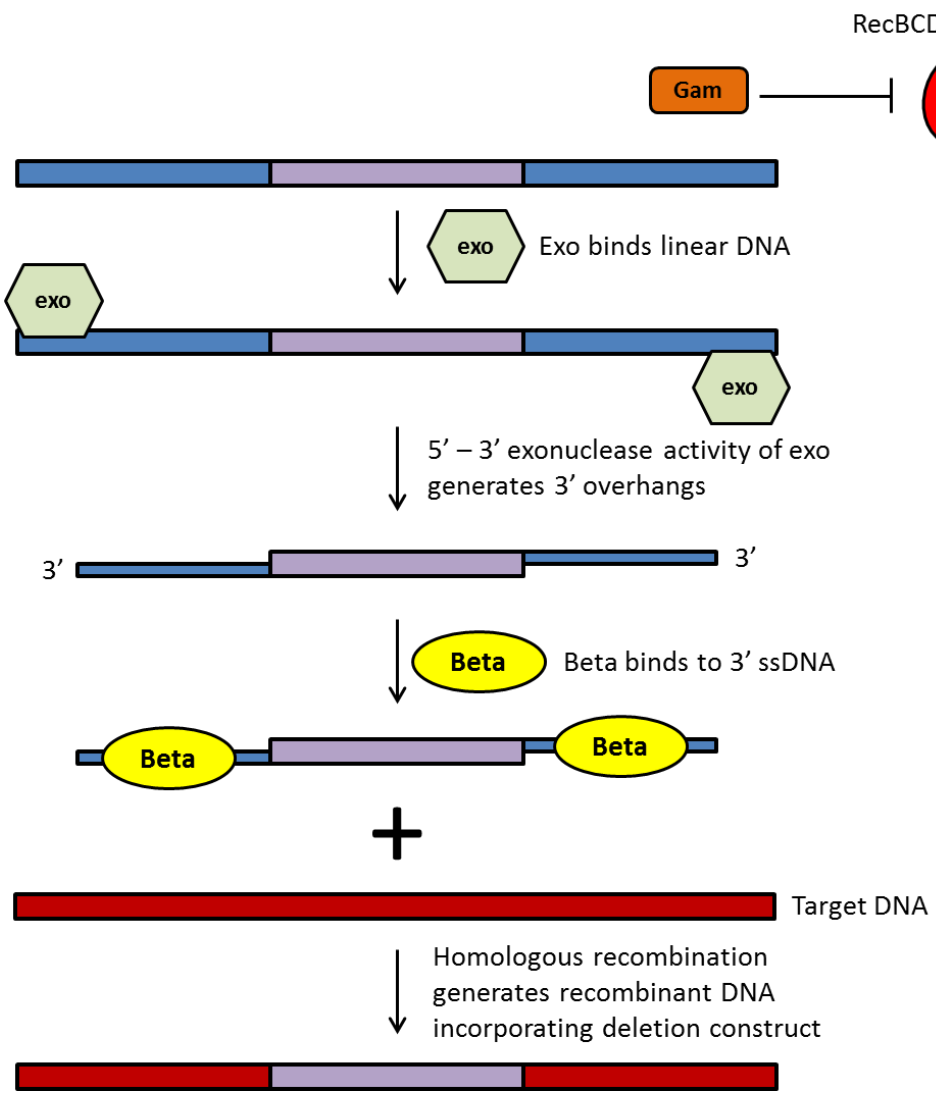

Figure 23. Figure showing λ Red Recombinase operon recombination adapted from Sharan *et al* (297). Exo has a 5'- to 3'-dsDNA exonuclease activity, which can generate 3'-overhangs on linear DNA. Beta binds the single-stranded DNA (3'-overhangs), promotes ss-annealing and generates recombinant DNA. Gam, which prevents RecBCD nuclease from degrading double-stranded linear DNA fragments, is also required for dsDNA recombineering (297).

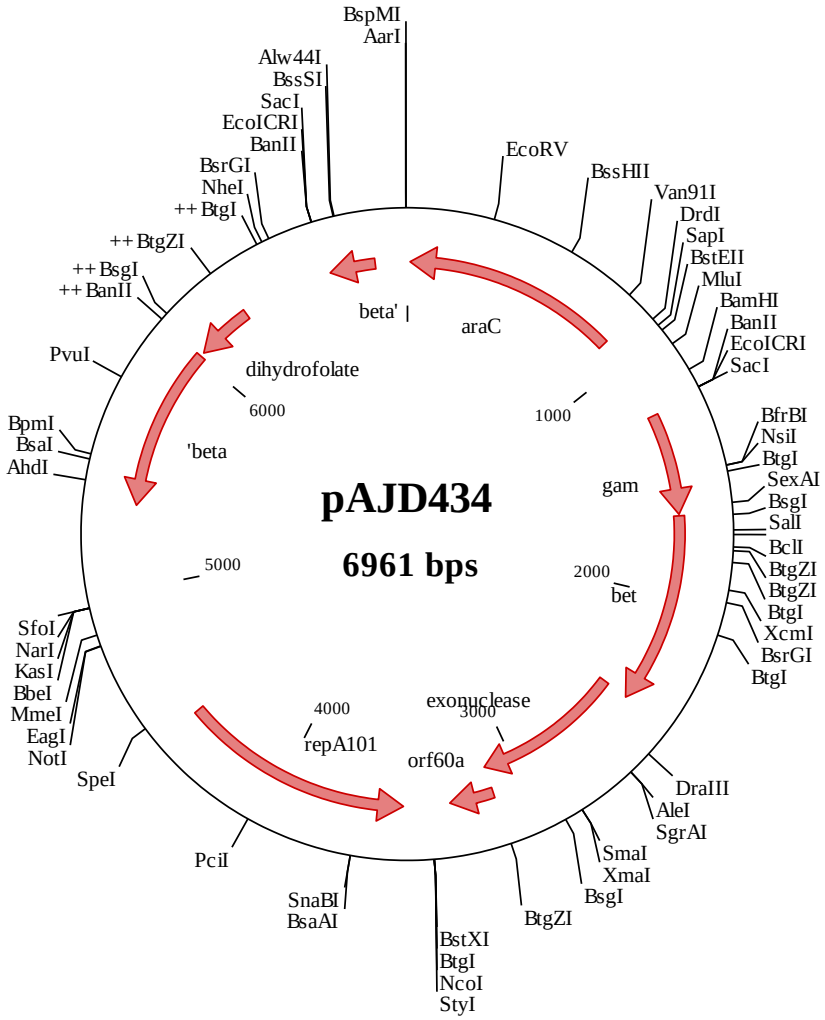

Figure 24. λ Red Recombinase plasmid pAJD434, encoding the Red Recombinase operon from bacteriophage λ. Expression of this operon stimulates homologous recombination required for insertion of the deletion construct into the genome of *Y. pestis*.

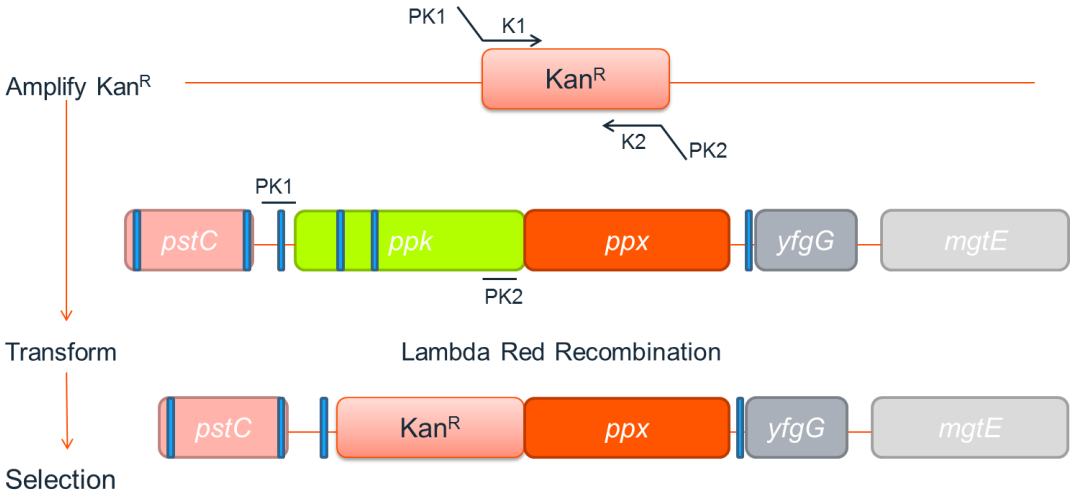

Figure 25. Mutagenesis schematic for the deletion of *ppK* from the genome of *Y. pestis*. PK1 and PK2 indicate the *ppk*-specific primer binding sites. K1 and K2 indicate the Kan^R cassette-specific primer binding sites.

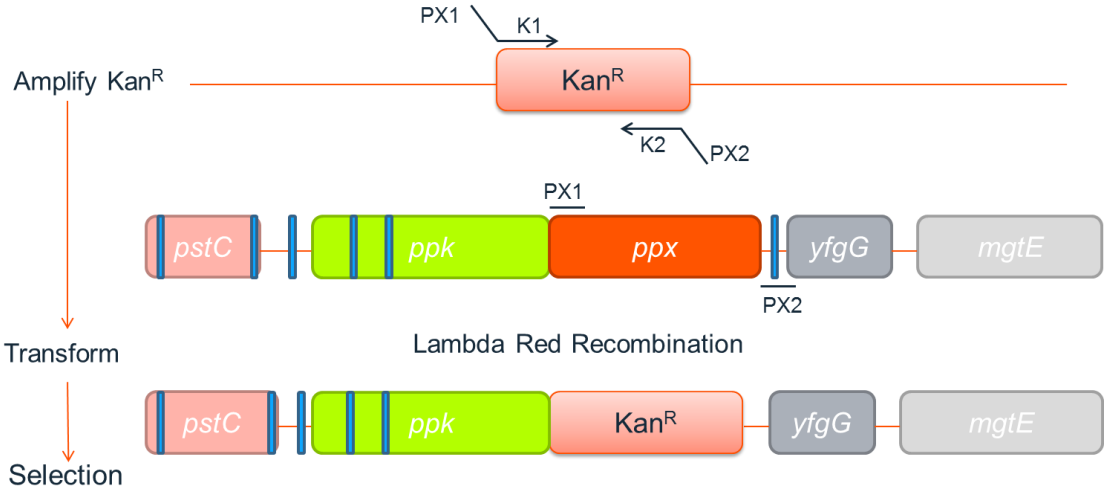

Figure 26. Mutagenesis schematic for the deletion of *ppX* from the genome of *Y. pestis*. PX1 and PX2 indicate the *ppx*-specific primer binding sites. K1 and K2 indicate the Kan^R cassette-specific primer binding sites.

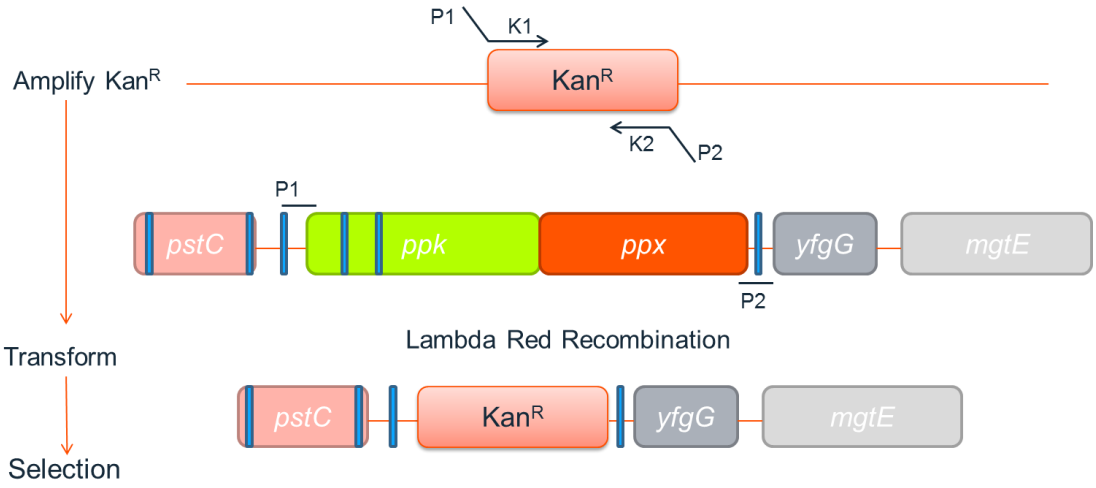

Figure 27. Mutagenesis schematic for the deletion of *ppK* and *ppX* from the genome of *Y. pestis*. P1 indicates the *ppk*-specific primer binding site and P2 indicates the *ppx*-specific primer binding sites. K1 and K2 indicate the Kan^R cassette-specific primer binding sites.

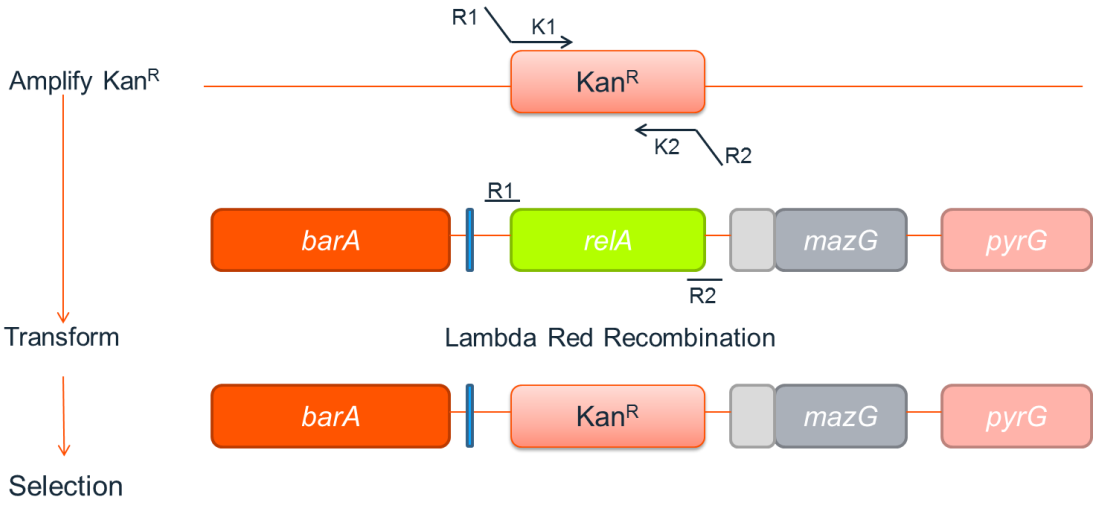

Figure 28. Mutagenesis schematic for the deletion of *relA* from the genome of *Y. pestis*. R1 and R2 indicate the *relA*-specific primer binding sites. K1 and K2 indicate the Kan^R cassette-specific primer binding sites.

2.2.4. Mutant Verification by Polymerase Chain Reaction

The Kan^R from a plasmid designated pK2 (289) was amplified by PCR using primer sets ppk_ppX_F/ppX_R and ppX_single_F /ppX_R (primer sequences are listed in appendix 8.2). The PCR product was then purified using the Qiagen PCR purification kit according to the manufacturer's instructions and then transformed by electroporation (detailed in method section 7.4) into *Y. pestis* GB containing the λ Red Recombinase encoding plasmid pAJD434 (shown in figure 24). Transformed cells were plated onto Blood Agar Base (BAB) plates containing hemin and supplemented with 50 µg/mL kanamycin to select for the Kan^R. Colonies that grew in the presence of kanamycin were analysed by PCR using primers Kan Forward/Kan Reverse (Appendix 8.2) to confirm the presence of the Kan^R (Figures 29 and 30).

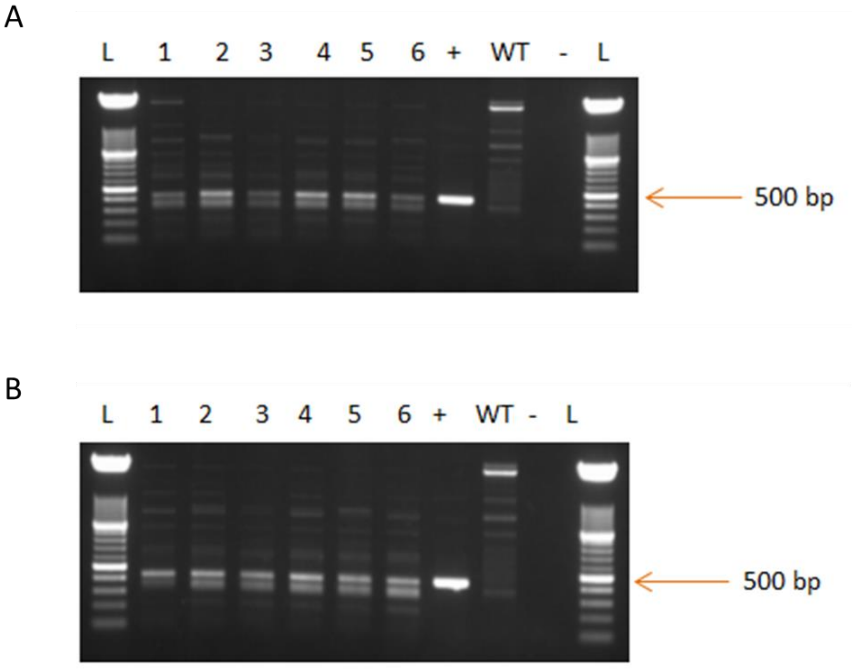

Figure 29. Amplification of Kan^R from kanamycin resistant clones of the *ppK* (A) and *ppX* (B) mutants. The 500 bp fragment size is indicated with an arrow, as the expected PCR product size. L indicates molecular weight marker XIV (Roche Diagnostics).

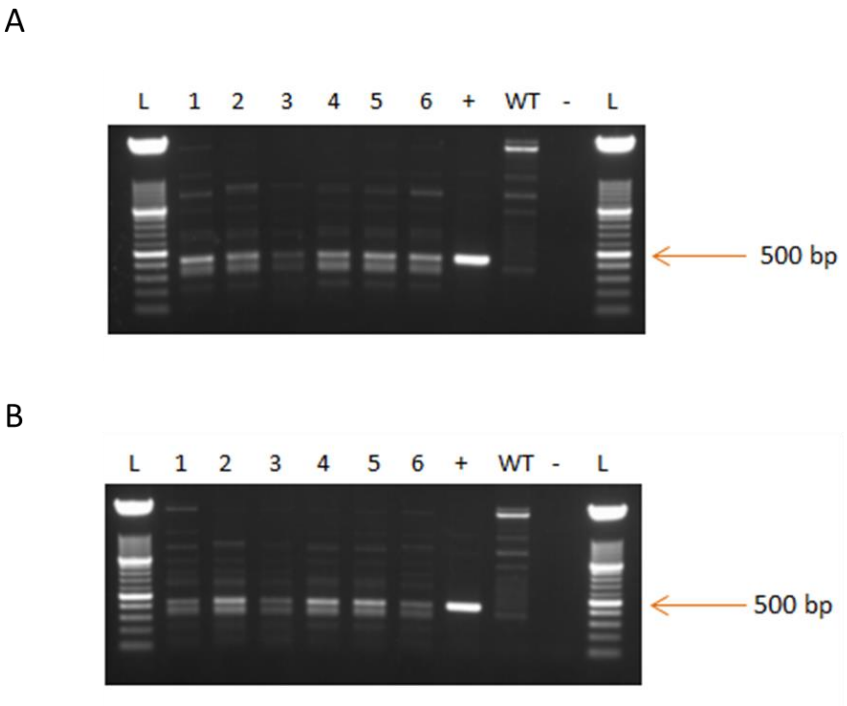

Figure 30. Amplification of Kan^R from resistant clones of the *relA* (A) and *ppK/ppX* (B) *Y. pestis* mutants. The 500 bp fragment size is indicated with an arrow, as the expected PCR product size. L indicates molecular weight marker XIV (Roche Diagnostics).

Although a double band was visible at 500 bp, it was decided that further optimisation was not necessary to obtain a single band, as clear bands of the correct size were observed across all clones analysed.

Following curing of the temperature sensitive plasmid pAJD434 by growth of mutant strains at 37 °C in the presence of calcium chloride ($CaCl_2$) to prevent loss of the virulence plasmid pCD1, verification of the presence of this plasmid was confirmed by PCR targeting the *lcrV* gene encoded on pCD1 (primer sequences are listed in appendix 8.2) (298). All mutant strains tested positive for the presence of *lcrV*, indicating that pCD1 was still present in these organisms (figures 31 and 32). Sensitivity to the antibiotic trimethoprim was then assessed to ensure that pAJD434 had been successfully cured from the strains. Strains that showed sensitivity to trimethoprim showed that the plasmid pAJD434 had successfully been cured.

During the PCR analysis of the *lcrV* virulence gene a high degree is miss-priming occurred resulting in multiple bands present in figures 31 and 32. This was due limited DNA being present in the samples as this reaction was carried out using a crude DNA extraction method and colony PCR (colony PCR method detailed in section 7.3). However, due to the correct band size being observed with a high degree of clarity in nearly all the clones and pressing time constraints, further PCR optimisation was not carried out.

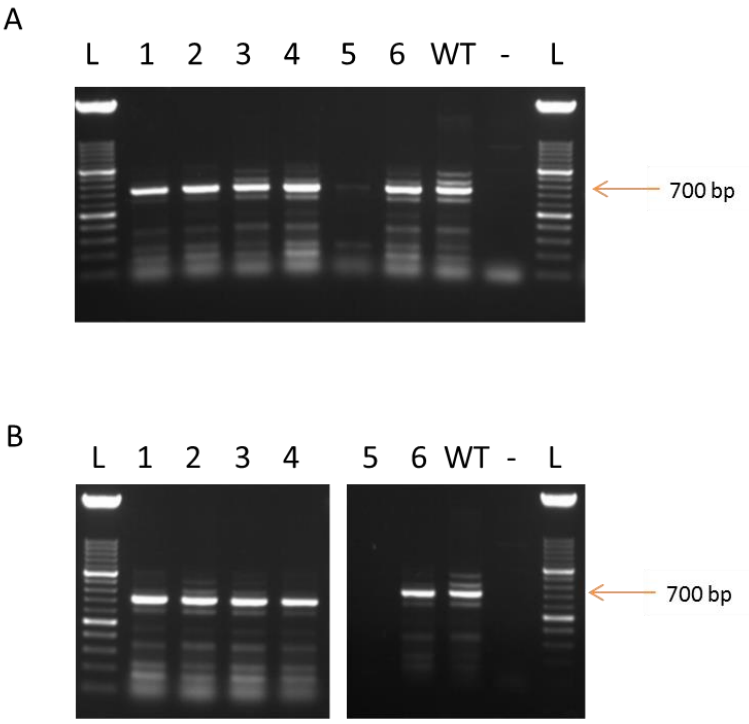

Figure 31. Amplification of the *lcrV* virulence gene for Δ*ppK* (A) and Δ*ppX* (B) *Y. pestis* mutants. The 700 bp fragment size is indicated with an arrow, as the expected PCR product size. L indicates molecular weight marker XIV (Roche Diagnostics).

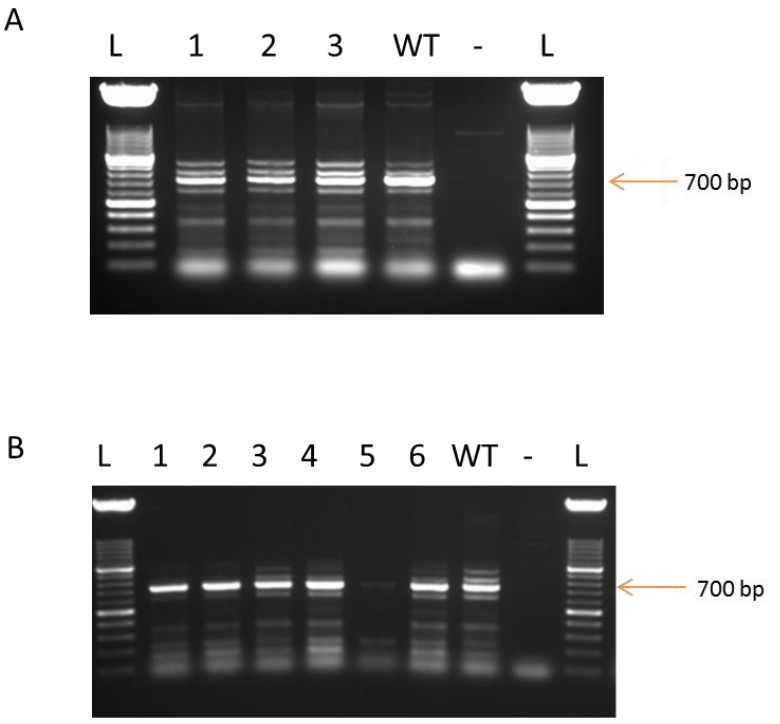

Figure 32. Amplification of *lcrV* for Δ*relA* (A) and Δ*ppK/ppX* (B) *Y. pestis* mutants. The 700 bp fragment size is indicated with an arrow, as the expected PCR product size. L indicates molecular weight marker XIV (Roche Diagnostics).

2.2.5. Mutant Verification by Gram's staining

Gram's staining was carried out on mutants and wild type strains to confirm *Y. pestis* GB cell morphology after mutagenesis. All strains were deemed to have characteristic *Y. pestis* bipolar staining and cell morphology similar to that of wild type.

2.2.6. Mutant Verification by Pigmentation Locus Analysis

Mutant strains were assessed for the presence of the pigmentation locus, *pgm* which results in a pigmented phenotype (Pgm+) in wild type *Y. pestis* strains. Pgm+ refers to the ability of *Y. pestis* cells to absorb exogenous hemin or Congo Red, giving a distinct appearance on solid media (299). The *pgm* locus is prone to genetic rearrangement and it is therefore important to ensure strains that have undergone mutagenesis maintain this region of the genome (300). If the *pgm* locus is lost from the genome this is indicative of deletion of the High-Pathogenicity Island (HPI) and a concurrent loss of virulence (300). Congo Red binding has been reported to be associated with virulence in other organisms such as *Shigella flexneri* and *E. coli,* specifically the invasion of mammalian cells which is a key characteristic of *Y. pestis* pathogenesis (301-303).

Mutants were streaked onto Congo Red agar and incubated for 24-48 hours at 28°C. All mutant strains formed pigmented colonies that matched the phenotype observed on wild type streak plates confirming that the pigmentation locus had not been disrupted during the mutant making process.

2.2.7. Targeted Isogenic Allelic Replacement Mutagenesis – *relA*

To subsequently create a *Y. pestis* GB double gene deletion mutant with inactivated *relA* and *spoT*, an in-frame isogenic allelic replacement mutant was required to create Δ*relA* background without an antibiotic resistance marker, in which to also inactivate *spoT*. A synthetic deletion construct was commercially sourced for the creation of the unmarked Δ*relA* mutant, the gene sequence for which is shown in appendix 8.3.

The Δ*relA* deletion construct was excised from the cloning vector pUC57 by overnight digest with the restriction enzyme *Bgl*II (figure 33). The suicide vector pDM4 was also digested overnight with *Bgl*II to linearise the plasmid and to ensure compatible ends for ligation of the insert into the suicide vector were present. Restriction digests were analysed on an agarose gel to visualise the digested insert, and linearised pDM4 (figure 34). The Δ*relA* insert was expected to produce a band of 2100 bp and pDM4 was predicted to produce a band of 7107 bp and (figures 33 and 34). The appropriate bands were excised from the gel, purified using a Qiagen gel extraction purification kit according to the manufacturer's instructions and separated on an agarose gel to ensure DNA quality, quantity and correct sizes.

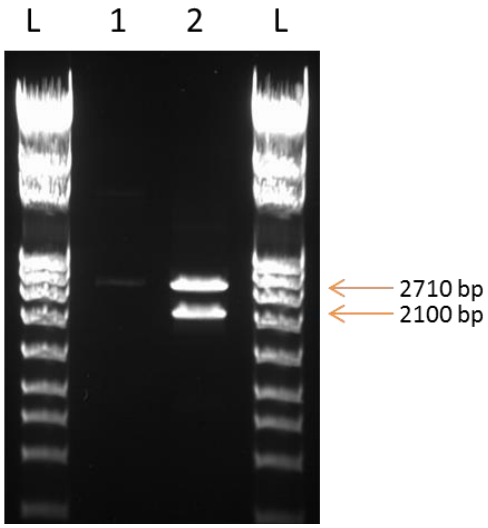

Figure 33. Gel image of (1) uncut pUC57 and (2) *Bgl*II digested pUC57, showing the Δ*relA* insert at 2100 bp and linearised pUC57 at 2710 bp. L indicates molecular weight marker IV (Roche Diagnostics).

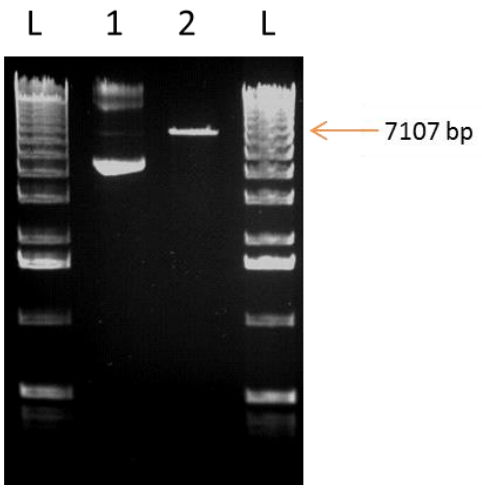

Figure 34. Gel image of (1) uncut pDM4 and (2) linear *Bgl*II digested pDM4 at 7107 bp. L indicates molecular weight marker X (Roche Diagnostics).

Linearised pDM4 was treated with shrimp alkaline phosphatase (SAP) to prevent re-circularisation of the suicide vector. The Δ*relA* insert was then ligated into pDM4 in an overnight ligation reaction at 16°C. Control ligations were also set up with non- SAP treated pDM4 with no insert and SAP-treated pDM4 with no insert to ensure the suicide vector had not re-ligated. L indicates molecular weight marker X (Roche Diagnostics).

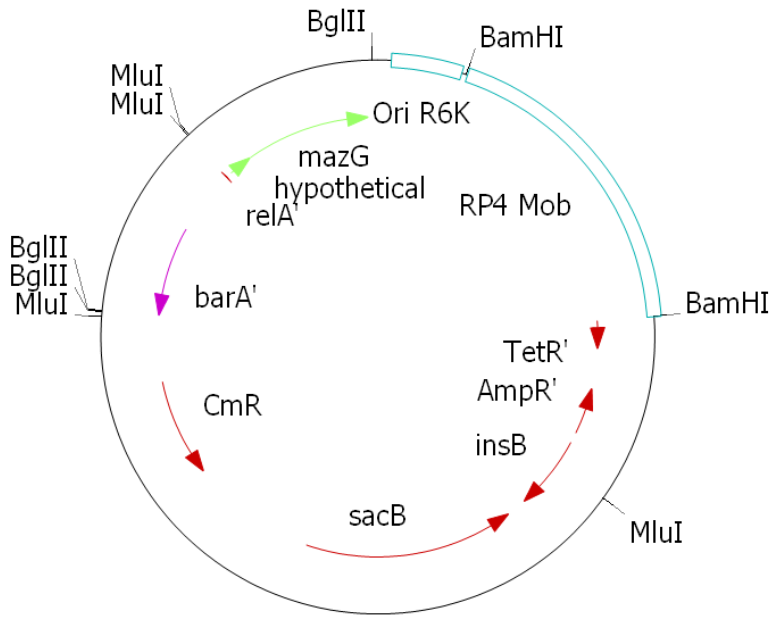

Figure 35. Circular pDM4 map showing *Bgl*II restriction sites used for cloning the flanking regions of *relA*. Plasmid size including Δ*relA* insert was 7107 bp.

Ligations were analysed by electrophoresis on an agarose gel to check the predicted ligation of 9207 bp was present (figure 36). Figure 36 shows a visible band at the upper limit of molecular weight marker X (Roche Diagnostics) which is too large to accurately determine the size of. However, due to the absence of the smaller bands of unligated insert and vector the gel indicated a successful ligation. Following confirmation of successful ligation, reactions were desalted in preparation for electroporation on a nitrocellulose disc floating on distilled water to allow salts to diffuse out.

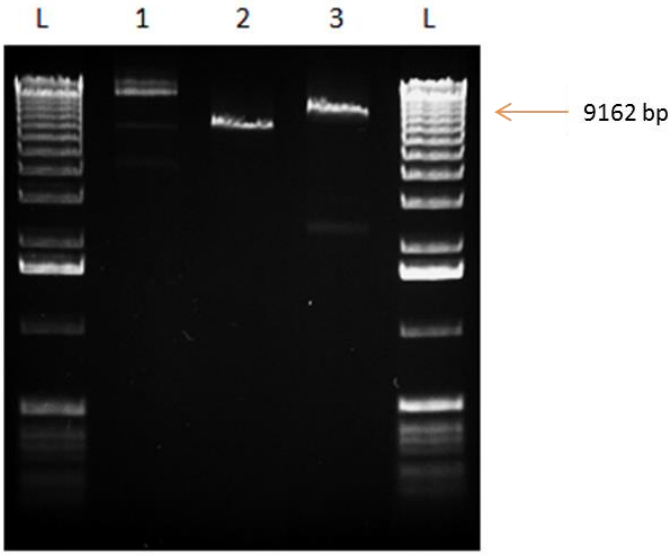

Figure 36. Gel image showing (1) ligation control 1 (re-circularised pDM4), (2) ligation control 2 (dephosphorylated pDM4/no insert (3) and the test ligation (dephosphorylated pDM4 + Δ*relA* insert). The molecular weight marker size (9162 bp) that was closest to the predicted ligation of 9207 bp is labelled as such. L indicates molecular weight marker X (Roche Diagnostics).

De-salted ligation products, including controls, were electroporated into *E. coli* DH5α λ *pir* electro-competent cells. Electroporated cells were allowed to recover for 1.5 hours prior to being plated onto selective LB (Luria-Burtani) agar plates supplemented with 50 μg/ml chloramphenicol. An *E. coli* DH5α cell control was also prepared to ensure the antibiotic was working. Colonies that grew on the electroporation plates after 48 hours were sub-cultured onto LB agar chloramphenicol grid plates and incubated for a further 24-48 hours. A single colony from these plates was then used to inoculate an overnight culture for subsequent freezer stocks to be made and plasmid DNA extraction using the Qiagen plasmid miniprep spin kit, according to the manufacturer's instructions. Presence of the insert/vector ligation in *E. coli* DH5α was then confirmed by PCR as shown in figure 37 using the previously designed LFF and RFR primer pair (listed in appendix 8.2). The suicide vector containing clone 1.3 of the deletion construct was then electroporated into *E. coli* S17 λ *pir* cells in preparation for conjugation into *Y. pestis* GB. *E. coli* S17 λ *pir* was selected as an appropriate strain to use for conjugation as this strain encodes chromosomally integrated broad host range conjugal transfer functions from the self-transmissible IncPα plasmid RP4 (304). Plasmid RP4 is known for its extremely broad host range and its stability in all Gram-negative bacteria (305).

Furthermore, the RP4 transfer system can mediate DNA transmission by conjugation to a variety of different organisms, making it suitable for *Y. pestis*/*E. coli* matings (306). Therefore *E. coli* S17 λ *pir* can function as an appropriate donor strain during the bioparental mating process without the requirement for a helper strain (307).

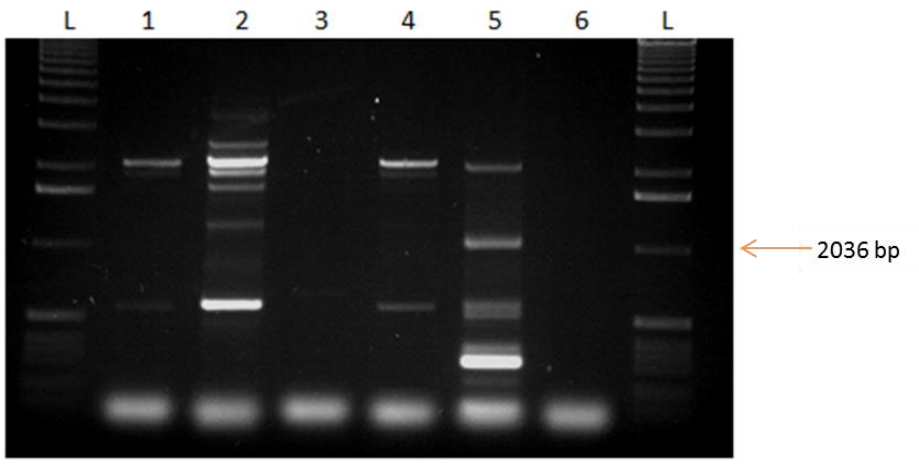

Figure 37. PCR of plasmid DNA isolated from colonies that grew following electroporation using the LFF and RFR primer pair which should produce a PCR product of 2100 bp. (1) Clone 1.2. (2) Clone 1.3. (3) Clone 6.4. (4) Clone 6.5. (5) Positive control. (6) Negative control.

2.3. *Yersinia pestis* Marked Mutant Characterisation *in Vitro*

Following confirmation of the mutants' creation and successful confirmation that the *lcrV* and *pgm* loci were intact, *in vitro* characterisation of these mutants were carried out to discern phenotypes attributed to the mutations.

2.3.1. Analyis of Growth Kinetics

Growth of mutants (Δ*ppK*, Δ*ppX* Δ*ppK/ppX* and *ΔrelA*) was compared to that of the wild type, *Y. pestis* GB, in a 96 well plate format over the course of 20 hours. In short, 50 mL cultures of BAB broth supplemented with 50 µg/mL kanamycin were inoculated to an OD_{600} of 1.5 and incubated at 28°C overnight. Cultures were checked for growth demonstrated by an increase in OD_{600} to approximately 2.0. Fresh media supplemented with 50 µg/mL kanamycin was then inoculated with the overnight culture to an OD_{600} of exactly 0.06. Starter cultures of 200 µL were transferred to a 96 well plate sealed with a gas permeable membrane in technical replicates of 6 and incubated at 28°C with shaking in the MultiSkan™ FC microplate photometer. Optical density readings were taken every 15 minutes for 20 hours. Growth curves were plotted from the data generated as shown in figures 39, 40, 41 and 42.

The *Y. pestis* Δ*ppK* mutant displayed similar growth kinetics *in vitro* compared to wild type *Y. pestis* GB (figure 38). A slower exponential growth phase was observed and cultures reached a lower final optical density compared to the wild type. The difference in growth was below the $P < 0.005$ threshold so was statistically significant, however in comparison to Δ*ppX* and Δ*ppK/ppX* was minor. The *Y. pestis* Δ*ppX* mutant displayed slightly slower growth kinetics *in vitro* compared to wild type *Y. pestis* GB (figure 39). The data was analysed by one way ANOVA (analysis of variance) test and cultures reached a statistically significantly ($P < 0.0001$) lower optical density compared to the wild type. The *Y. pestis* double Δ*ppK/ppX* mutant displayed a statistically significant ($P < 0.0001$) growth defect compared to wild type *Y. pestis* GB (figure 40). Cultures reached the same end point optical density, however, exponential phase of growth was slower and entry into stationary phase of growth was delayed. The *Y. pestis* Δ*relA* mutant displayed similar growth kinetics *in vitro* compared to wild type *Y. pestis* GB (figure 41). A slightly slower exponential growth phase was observed and cultures reached a slightly lower optical density compared to the wild type. However, this was not statistically significant ($P = 0.0321$) therefore no growth defect was reported.

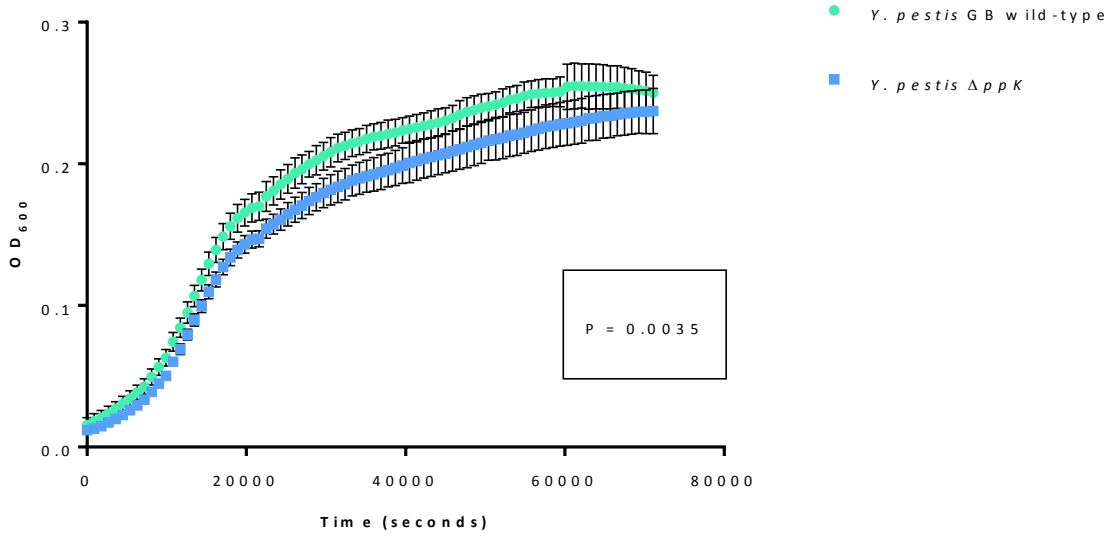

Figure 38. Growth curve showing the *Y. pestis* Δ*ppK* mutant growth kinetics *in vitro* compared to wild type *Y. pestis* GB. Each data point represents combined results from 3 biological replicates in which 6 technical replicates were analysed. Error bars are shown for each data point.

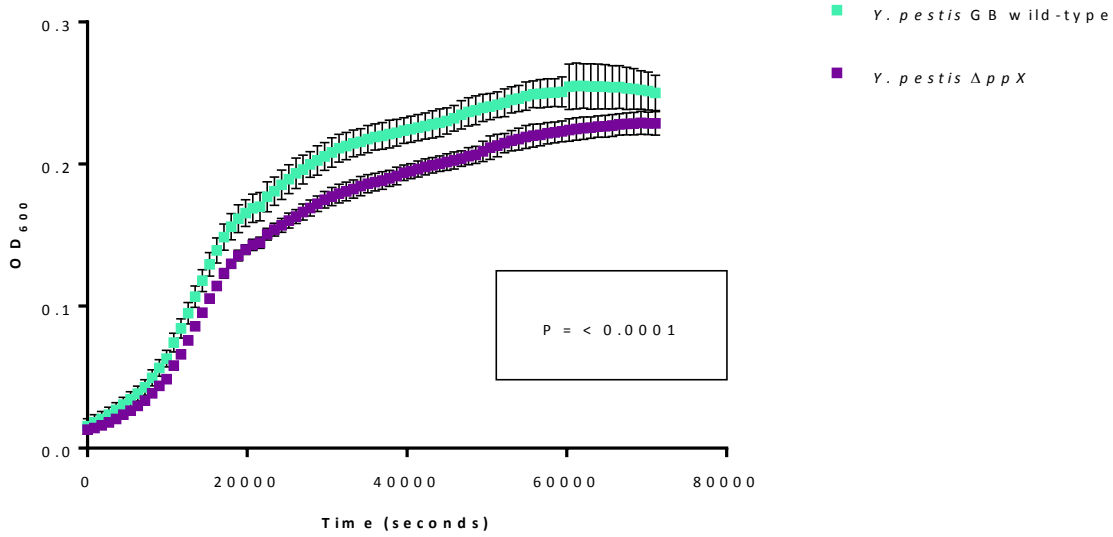

Figure 39. Growth curve showing the *Y. pestis* Δ*ppX* mutant growth kinetics *in vitro* compared to wild type *Y. pestis* GB. Each data point represents combined results from 3 biological replicates in which 6 technical replicates were analysed. Error bars are shown for each data point.

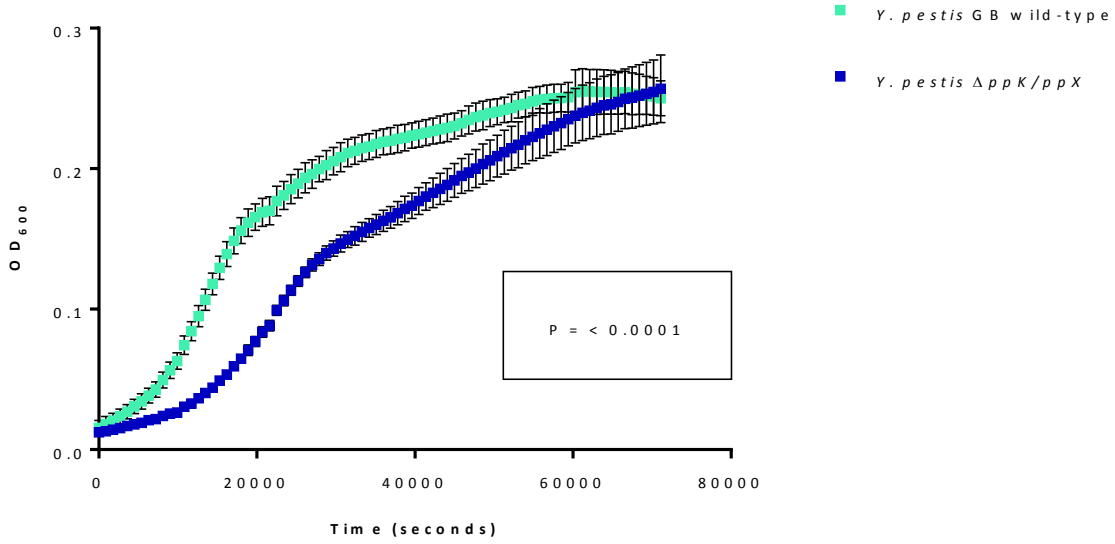

Figure 40. Growth curve showing the *Y. pestis* double Δ*ppK/ppX* mutant growth kinetics *in vitro* compared to wild type *Y. pestis* GB. Each data point represents combined results from 3 biological replicates in which 6 technical replicates were analysed. Error bars are shown for each data point.

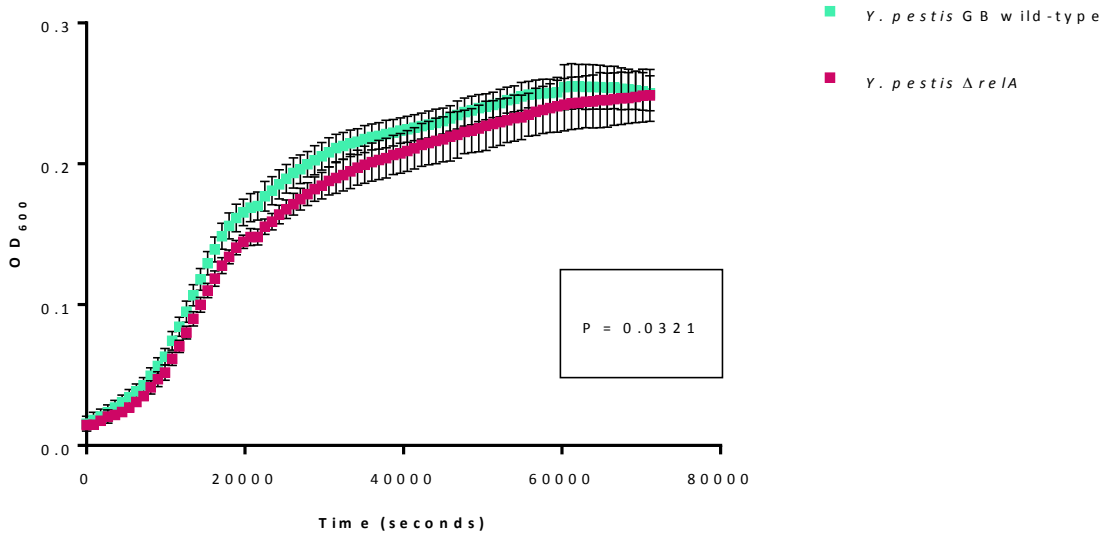

Figure 41. Growth curve showing the *Y. pestis* Δ*relA* mutant growth kinetics *in vitro* compared to wild type *Y. pestis* GB. Each data point represents combined results from 3 biological replicates in which 6 technical replicates were analysed. Error bars are shown for each data point.

The Δ*ppK,* Δ*ppX* and Δ*ppK/ppX* mutants showed a statistically significant growth defect compared to the wild type strain. The double Δ*ppK/ppX* mutant showed the most pronounced growth defect. The Δ*ppK* and the Δ*ppX* mutants displayed similar patterns of growth, only reaching slightly lower final optical densities compared to the wild type. The Δ*relA* mutant displayed growth similar to that of the wild type and therefore did not have a statistically significant growth defect.

Growth of the marked mutant strains was conducted in media supplemented with the appropriate antibiotic (kanamycin), and media with no supplements. Statistically and as expected, there were no differences observed in the growth of mutants in media with or without antibiotic supplementation (data not shown).

2.3.2. Intracellular Phosphate Quantification

As previously discussed in section 1.5 the stringent response biosynthetic pathway is directly linked, via the inhibitory action of (p)ppGpp on PPX, to the inorganic polyphosphate biosynthetic pathway (174, 219). In brief, as (p)ppGpp levels increase in response to stress, polyphosphate levels simultaneously increase due to (p)ppGpp inhibiting the exopolyphosphatase PPX, meaning PPK synthesises polyphosphate without a mechanism to degrade the polyphosphate (174, 215). Inactivation of the polyphosphate biosynthetic pathway in other bacterial species affects the levels of intracellular polyphosphate, as demonstrated in the intracellular bacterium *F. tularensis,* in which a putative polyphosphate kinase was inactivated and resulted in decreased levels of intracellular polyphosphate being detected when assayed by malachite green spectrophotometric test (14).

To assess the ability of the *Y. pestis* mutants to generate intracellular polyphosphate the phosphate content of *Y. pestis* GB and the Δ*ppK*, Δ*ppX*, Δ*ppK*/*ppX* and Δ*relA* mutants was quantified using a malachite green phosphate quantification kit as outlined in the schematic in figure 42 (method described in section 7.7). Polyphosphate is a linear polymer of phosphate residues, found in bacterial, fungal, plant and animal cells and has been specifically linked to the stringent response in bacteria as shown in figures 13 and 14, section 1.5 (214). Intracellular phosphate was quantified using the malachite green phosphate assay kit

(BioAssay Systems) according to the manufacturer's instructions. The malachite green assay provided a non-radioactivity based method for quantification intracellular polyphosphate in the *Y. pestis* mutant strains in comparison to wild type GB. The malachite green assay is based on quantification of the green complex formed between malachite green, molybdate and free orthophosphate as shown in figure 42 (308). The rapid colour formation from the reaction was measured using a spectrophotometer at 600 nm. During optimisation of the polyphosphate quantification assay it was found that the dense bacterial cell suspension (1 g) that the method suggested could easily saturate the assay, therefore 0.5 g cell suspension was used. Additionally, 0.75 g was used to remove nucleoside phosphates such as AMP, by adsorption (309). A standard curve was initially generated to enable accurate phosphate quantification (figure 43).

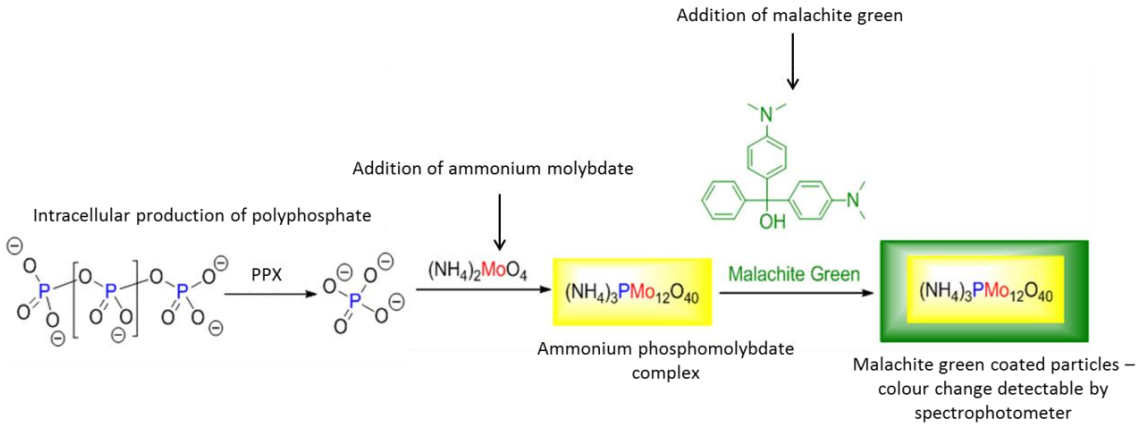

Figure 42. Mechanism of action of malachite green spectrophotometric assay for the detection and quantification of polyphosphate (310-312). The exopolyphosphatase PPX hydrolyses intracellular polyphosphate chains into free phosphate residues. Upon addition of ammonium molybdate reagent an ammonium phosphomolybdate complex is formed to which malachite green binds and gives rise to a detectable and quantifiable colour change.

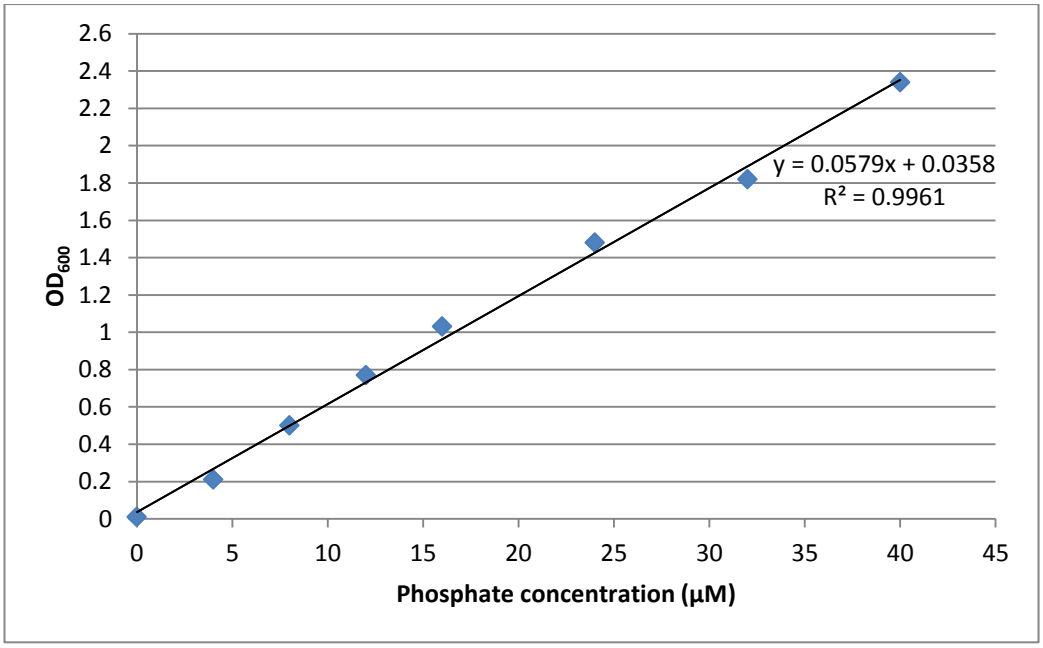

Figure 43. Standard curve generated using the malachite green phosphate quantification kit for subsequent quantification of *Y. pestis* phosphate extracts.

The conversion of polyphosphate to free phosphate by hydrolysis at 100 °C of acid soluble extracts obtained from the supernatant from activated charcoal-bacterial cell suspensions resulted in a significant difference between pre- and post-hydrolysis measurements of phosphate concentrations for the wild type strain and the Δ*ppX* and Δ*relA* mutants ($P < 0.05$). This indicated that these organisms produced intracellular polyphosphate similar to that of the wild type (figure 44). Significantly lower total phosphate concentrations were recorded for the Δ*ppK and* Δ*ppK/ppX* mutants, and there was no significant difference between the pre- and post-hydrolysis phosphate concentrations for these mutants ($P < 0.05$), indicating that polyphosphate production had been significantly impaired by inactivation of *ppK* (figure 44).

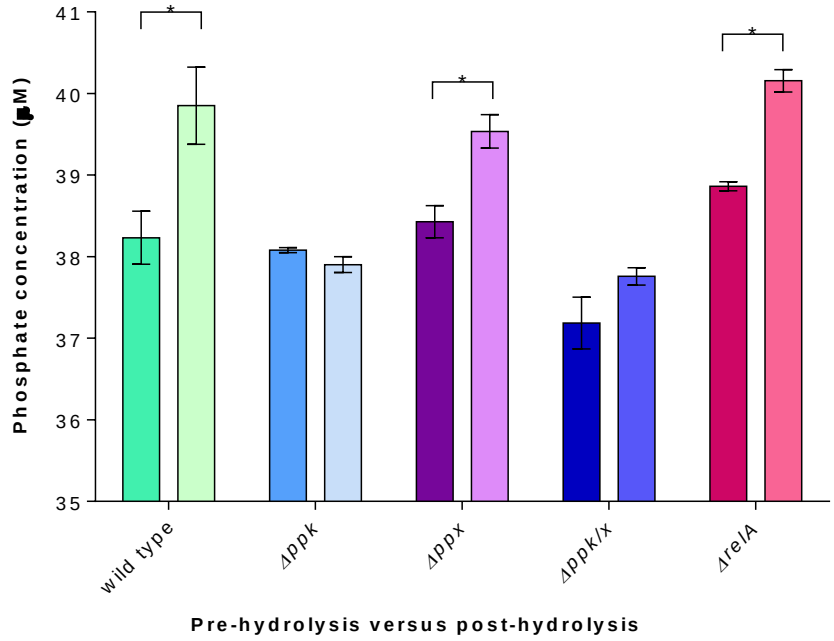

Figure 44. Phosphate concentration measured for *Y. pestis* mutants and GB wild type comparing pre- and post-hydrolysis phosphate concentrations as quantification by spectrophotometric measurement. Statistical significance is indicated by *. * $P \leq 0.05$.

Pre-hydrolysis phosphate concentrations were subtracted to account for background phosphate levels including other sources of phosphate such as ATP and AMP. The difference between hydrolysed phosphate concentrations between the *Y. pestis* mutants and the wild type were then compared. The Δ*ppK and* Δ*ppK/ppX* mutants showed a significant lack of polyphosphate production, compared to that of the wild type *Y. pestis* GB ($P < 0.05$) following an unpaired t-test with Welch's correction to assume unequal variances between samples (figure 45).

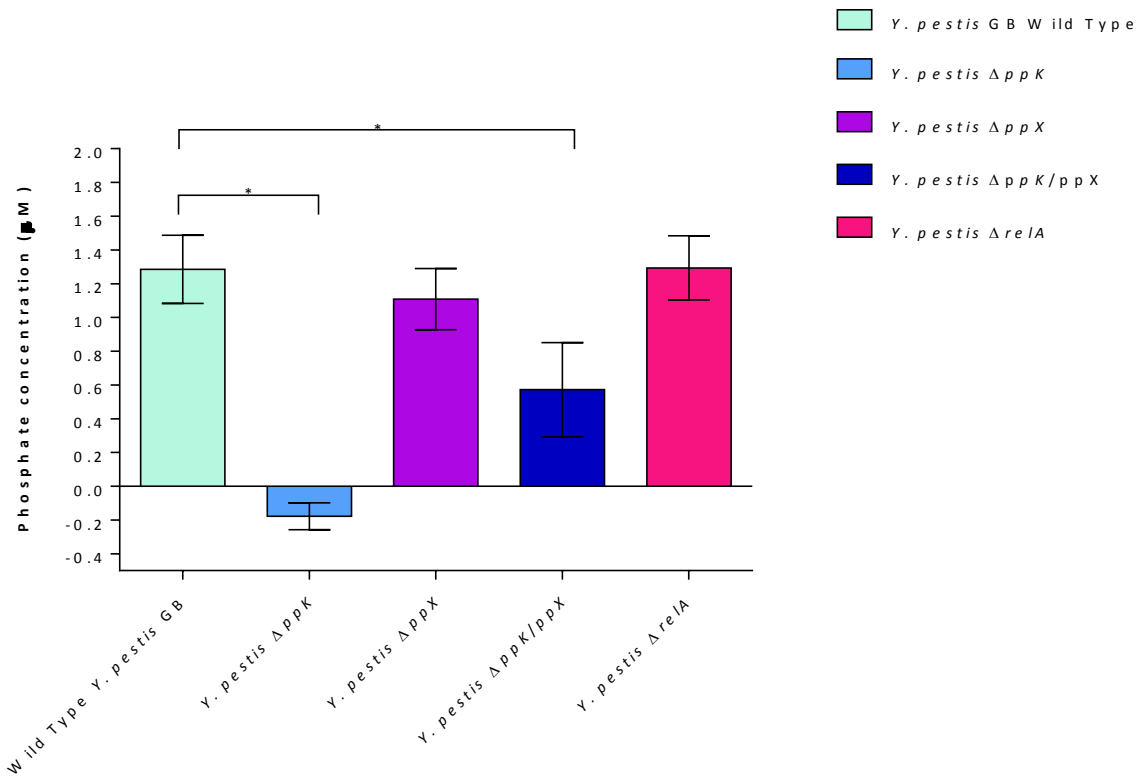

Figure 45. Phosphate concentrations measured from *Y. pestis* mutants and GB wild type following removal of background phosphate signal. Statistical significance is indicated by *. * P ≤ 0.05.

Inactivation of the polyphosphate kinase gene, *ppk*, significantly reduced the ability of the bacterium to synthesise intracellular polyphosphate, as did simultaneous inactivation of *ppK* and the exopolyphosphatase gene *ppX*. Inactivation of *ppX* as a single deletion had no effect on the cell's ability to synthesise intracellular polyphosphate, as proven by phosphate concentrations being measured that were similar to the wild type strain. Inactivation of the (p)ppGpp synthetase gene *relA* also had no impact on the cell's ability to generate intracellular polyphosphate. One might expect the Δ*ppX* mutant to accumulate more polyphosphate than the wild type due to the lack of a polyphosphate degradation mechanism, however this was not observed as polyphosphate levels in the Δ*ppX* mutant strain were only slightly lower than those observed for the wild type GB strain. This is likely due to the pyrophosphatase, GppA compensating for the exopolyphosphatase activity in the absence of PPX and degrading polyphosphate chains into free phosphate residues. This observation was also made by

Wrench *et al* who reported a *F. novicida* Δ*ppX* mutant that showed similar levels of intracellular polyphosphate concentrations to wild type *F. novicida* (313).

2.3.3. Environmental Stress Sensitivity Assays – Antibiotics

Bacteria that experience environmental stress and initiate the stringent response in reaction to such conditions, often also display altered tolerances to other stressors or antimicrobial compounds such as antibiotics (171). Amino acid starvation and subsequent induction of the stringent response was linked to a transient tolerance to the antibiotics ofloxacin and ampicillin in *E. coli* (314). It has also been found that inactivation of the (p)ppGpp biosynthesis genes *relA* and *spoT* gave rise to a dramatically decreased tolerance to treatment with various classes of antibiotics including gentamicin and ofloxacin, an aminoglycoside and fluoroquinolone respectively, in *P. aeruginosa* (171). Furthermore it has been found that *ppk1* and *ppk2* mutants in *P. aeruginosa* demonstrated increased susceptibility to different types of antibiotics including ciprofloxacin, chloramphenicol and rifampicin (315). It was therefore hypothesised that the *Y. pestis* deletion mutants; Δ*ppK*, Δ*ppX*, Δ*ppK*/*ppX* and Δ*relA* might also be sensitised to some antibiotics. To test this it was decided that antibiotics from diverse classes would be used in disc diffusion assays to avoid target-specific effects. The antibiotics and their mechanisms of action are listed in table 1 in section 1.3. The antibiotics also comprised current treatment options for plague infection for clinical relevance. Antibiotics selected for disc diffusion assays included the following: the aminoglycosides streptomycin, gentamicin and hygromycin; streptomycin is an aminoglycoside antibiotic that inhibits protein synthesis in Gram-positive and Gram-negative bacteria (table 2). Streptomycin binds to 16S rRNA and interferes with formyl-methionine-tRNA (fmet tRNA) binding to the 30S ribosomal subunit (126). This in turn leads to codon misreading and inhibition of protein synthesis eventually causing cell death (316). Gentamicin, is also an aminoglycoside antibiotic that works by a different action, irreversibly binding the A site of the 30S subunit of the bacterial ribosome, interrupting protein translocation (317) (table 2). Aminoglycoside binding stabilizes the tRNA–mRNA interaction in the A site by decreasing tRNA dissociation rates, which in turn interferes with proofreading steps that leads to codon misreading (318). Hygromycin inhibits polypeptide synthesis by binding the tRNA-ribosomal acceptor site, stabilising the complex and preventing translocation (119).

Tetracyclines are also protein synthesis inhibitors, inhibiting the binding of charged aminoacyl-tRNA to the mRNA-ribosome complex by binding to the 30S ribosomal subunit in the mRNA translation complex (119, 319). The destabilisation of the ribosomal/mRNA complex prevents amino acids being synthesised (320). Tetracycline (table 2) inhibits cell growth by inhibiting translation (319). The antibiotic binds to the 30S ribosomal subunit and prevents the amino-acyl tRNA from binding to the A site of the ribosome (319). Doxycycline, is also a tetracycline antibiotic and functions in the same way as tetracycline, inhibiting protein translation (320). However, doxycycline has enhanced lipophilic properties compared to the original tetracycline (321), making it more easily transmissible across cell membranes, and cell uptake of the antibiotic is improved, thus increasing bioavailability (319). Doxycycline is also more chemically stable than other tetracyclines (322) (table 2).

The fluoroquinolone ciprofloxacin was also selected for its wide spectrum activity against the microorganisms discussed in this work. Ciprofloxacin is a second-generation fluoroquinolone antibiotic and a broad-spectrum antibiotic active against Gram-positive and Gram-negative bacteria (shown in table 2) (130, 323). Liposome-encapsulated ciprofloxacin is currently the antibiotic of choice for the treatment of tularaemia (93). Ciprofloxacin functions by inhibiting the A subunit of DNA gyrase, a type II topoisomerase, and topoisomerase IV enzymes, which are essential bacterial ATP-dependent enzymes to separate bacterial DNA during replication. By binding the A subunit of DNA gyrase, the DNA-enzyme complex is stabilised, blocking DNA replication and thereby inhibiting cell division (323, 324).

Polymyxin B was used in this study to demonstrate the broad effects that disruption of the stringent response and associated polyphosphate biosynthesis has on bacteria. The mechanisms of action of polymyxin B are different to all other antibiotics used in this study; additionally it is widely used for the treatment of Gram negative bacterial infections (table 2). Polymyxin B is an antibiotic isolated from strains of the Gram positive bacterium *Bacillus polymyxa* (133). Although polymyxin B is bactericidal to Gram negative bacteria, it has no activity against Gram positive bacterial infections. The key mechanism of action of polymyxin B is mediated by interation of the antibitoic with the lipopolysaccharide (LPS) of the outer membrane of Gram negaitive bacteria (325). Specifically, the polycationic cyclopeptide ring binds the outer membrane and displaces calcium and magnesium bridges that stablilse the LPS

(325). The displacement of these ions leads to disruption of the outer membrane. The fatty acid side chain of polymyxin B also interacts with the LPS, enhancing uptake of the antibiotic into the bacterial cell (134). These processes culminate in increased permeability of the outer membrane permiting passage of polymyxin, amongst other molecules, into the bacterial cell, and leakage of cellular contents out of the cell which eventually leads to bacterial cell death (325).

Antibiotics used in the mutant characterisation work presented here were selected to encompass a variety of mechanisms of action (as shown in figure 1 in section 1.3), and for their effective activity against *B. pseudomallei*, *F. tularensis* and *Y. pestis*. In short, streptomycin was selected for inclusion in the *Y. pestis* and *F. tularensis* assays as this antibiotic is one of the first lines of defence against *Y. pestis* infection and also has efficacy against *F. tularensis*. Gentamycin was selected as an alternative aminoglycoside antibiotic to streptomycin, which targets an alternative binding site on the bacterial ribosome to interrupt protein synthesis. Ciprofloxacin was included in the *F. tularensis* assays, being the antibiotic of choice for the treatment of tularaemia. The tetracyclines, tetracycline and doxycycline were selected based on their mechanism of action being different to that of the aminoglycosides and ciprofloxacin. B lactams were not selected due to *F. tularensis* and *Y. pestis* being highly resistant to these antibiotics. The evaluation of the antibiotic susceptibility of *F. tularensis* and *B. pseudomallei* mutants is discussed in sections 3.3.1 and 4.3.1 respectively.

When our marked *Y. pestis* mutants were tested for antibiotic sensitivity (example plate shown in figure 46) it was found that a statistically significantly larger zone of inhibition was observed around lawns of the Δ*ppK,* Δ*ppX,* Δ*ppK/ppX* and Δ*relA,* mutants (5.875 mm P = 0.0120, 6.25 mm P = 0.0059, 7.125 mm P = 0.0142 and 6.0 mm P = 0.0017 respectively) compared to the wild-type bacterium (4.5 mm) (Figure 47, and summarised in table 2).

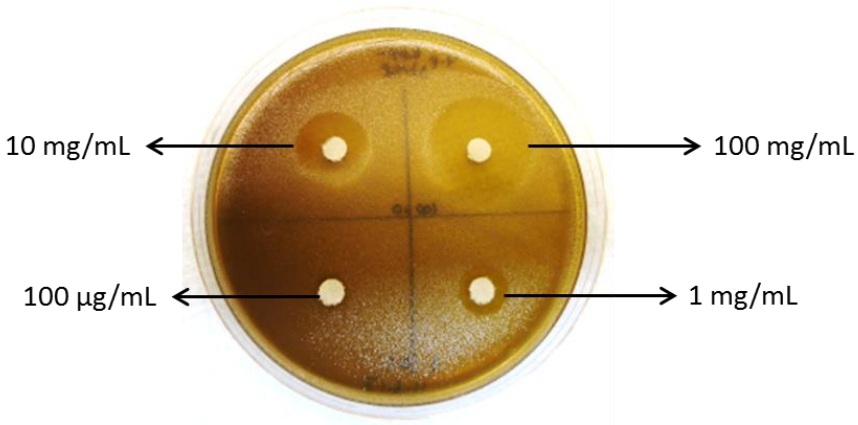

Figure 46. Example of disc diffusion assay showing 4 different concentrations of antibiotic and zones of bacterial growth inhibition surrounding antibiotic discs.

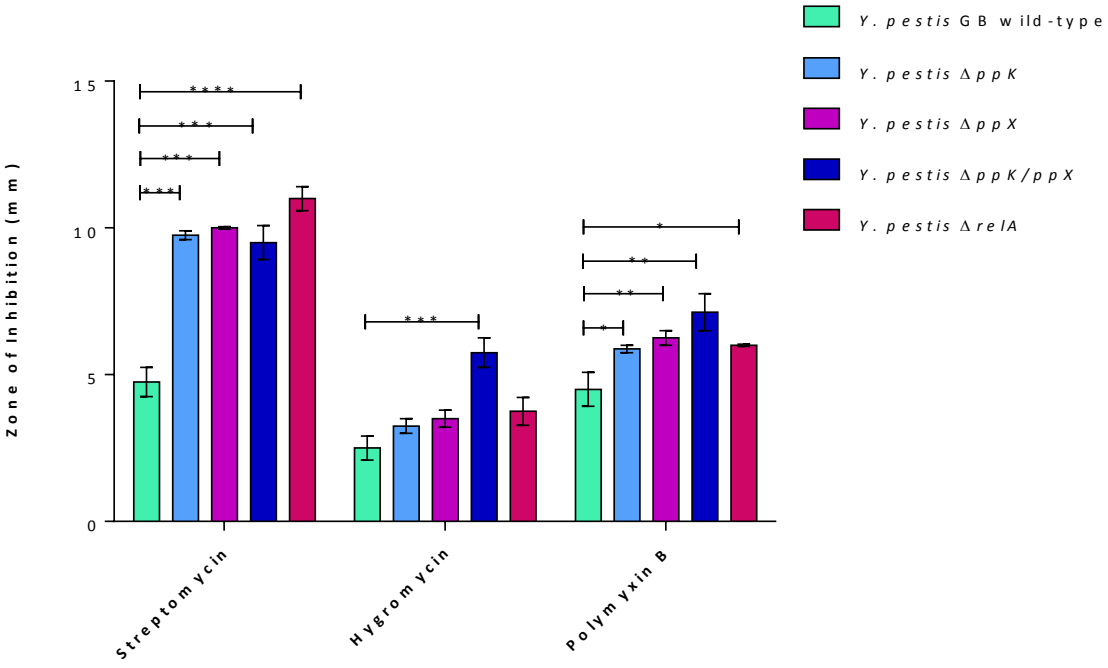

Figure 47. Graph showing the zones of inhibition measured surrounding antibiotic impregnated discs in lawns of *Y. pestis* GB wild type and mutant strains. Graph plotted shows mean with standard deviation from data combined from four technical replicates and three biological replicates. Statistical significance is indicated by *. * $P \leq 0.05$, ** $P \leq 0.01$, *** $P \leq 0.001$, **** $P \leq 0.0001$.

Antibiotic	**Mode of Action**	**Mutant/strain**	**Statistical significance (compared to wild type)**
Streptomycin	Protein synthesis - initiation	*Y. pestis* Δ*ppk*	***
		Y. pestis Δ*ppX*	***
		Y. pestis Δ*ppk/ppX*	***
		Y. pestis Δ*relA*	****
Gentamicin	Protein synthesis - initiation	*Y. pestis* Δ*ppk*	*
		Y. pestis Δ*ppX*	*
		Y. pestis Δ*ppk/ppX*	*
		Y. pestis Δ*relA*	*
Polymyxin B	Cell membrane destabilisation	*Y. pestis* Δ*ppk*	*
		Y. pestis Δ*ppX*	**
		Y. pestis Δ*ppk/ppX*	**
		Y. pestis Δ*relA*	*
Hygromycin	Protein synthesis - translocation	*Y. pestis* Δ*ppk*	-
		Y. pestis Δ*ppX*	-
		Y. pestis Δ*ppk/ppX*	***
		Y. pestis Δ*relA*	-
Ciprofloxacin	DNA gyrase	*Y. pestis* Δ*ppk*	*
		Y. pestis Δ*ppX*	*
		Y. pestis Δ*ppk/ppX*	*
		Y. pestis Δ*relA*	*

Table 2. Summary of results for environmental stress assays based on the size of zones of bacterial growth inhibition measured surrounding discs impregnated with the various antibiotics listed in the first column. Statistical significance is indicated by *. * $P \leq 0.05$, ** $P \leq 0.01$, *** $P \leq 0.001$, **** $P \leq 0.0001$.

2.3.4. Environmental Stress Sensitivity Assays – Oxidative Stress

The stringent response has been linked to bacterial susceptibility to environmental stresses. One such stress is that posed by the generation of ROS in the form of H_2O_2 or O_2^-, either endogenously by metabolic reactions as part of the bacterial life cycle or exogenous presence in the extracellular environment (326, 327). The spontaneous oxidation of pyrogallol (1,2,3-trihydroxybenzene) generates O_2^- which can be used as a means of artificially inducing exogenous oxidative stress (328). As such, pyrogallol disc sensitivity assays were used to assess inhibition of growth of wild-type and mutant strains by exogenous superoxide anions. A significantly smaller zone of inhibition was observed around the discs in the lawn of the Δ*relA,* Δ*ppK,* Δ*ppX and* Δ*ppK/ppX* mutants (7.5 mm P = 0.0001, 4 mm P = 0.0001, 4 mm P <0.0001 and 9.5 mm P = 0.0027 respectively) compared to wild-type bacteria (11.5 mm) (Figure 48) showing increased tolerance.

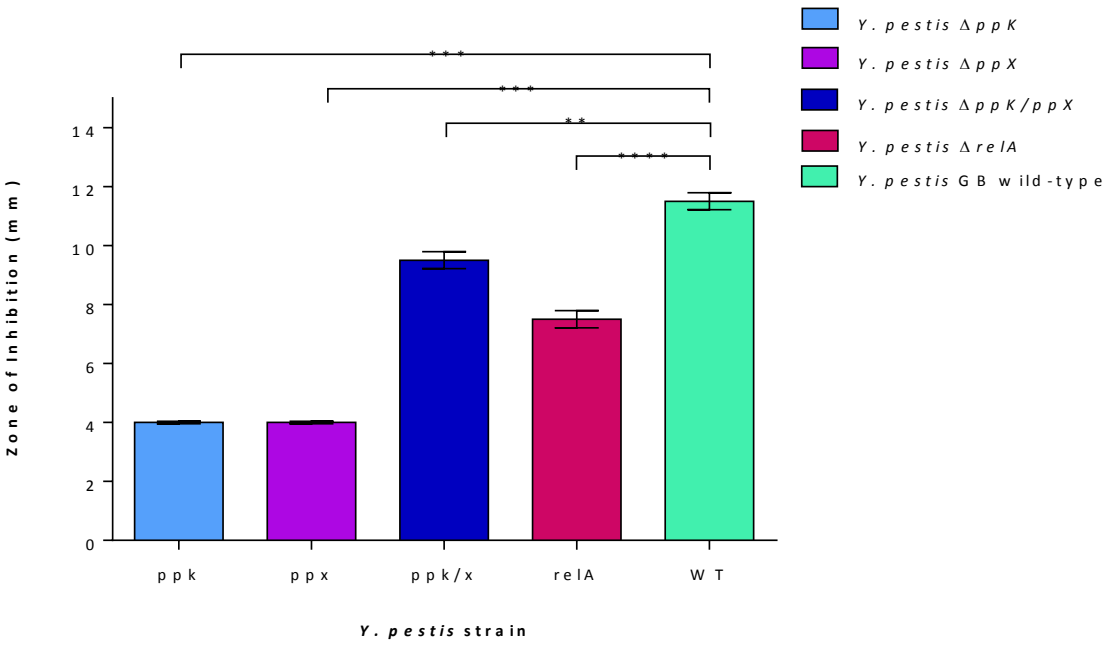

Figure 48. Zones of inhibition measured surrounding sterile discs impregnated 1000 mM pyrogallol. Graph presented plots the mean with standard error from combined data from four technical replicates and three biological replicates for *Y. pestis* GB and *Y. pestis* mutant strains. Statistical significance compared to wild type GB is indicated by *. ** P ≤ 0.01, *** P ≤ 0.001, **** P ≤ 0.0001.

All mutants tested had a statistically significantly smaller zone of inhibition surrounding the 1000 mM pyrogallol discs. This indicates that disruption of polyphosphate metabolism and the stringent response results in increased tolerance of exogenous oxidative stress. It is unclear as to the exact biochemical processes at play that have given rise to this increased tolerance. However, disruption of these key biosynthetic pathways could be leading to a de-repression of genes involved in responding to exogenous oxidative stress, such as the expression of SODs (199, 201, 329). As discussed in the introduction, section 1.5, bacterial regulatory systems often overlap forming complex and global regulatory systems to enable bacterial survival in different environmental niches. This is evident for the regulation of the bacterial oxidative stress response genes *sodA* and *sodB*, *katA* and *katB* which work together to protect bacteria from oxidative stress (330). For example *sodA* is negatively regulated by two global regulators, ArcA which is an aerobic respiration control regulator, and Fur which is a ferric iron uptake regulator and represses expression of *sodA* in an iron-dependent manner (331, 332). Conversely, *sodB* is positively regulated by Fur, which has been demonstrated by *sodB* expression studies which detected eight times higher protein product levels for wild type *E. coli* compared to a Δ*fur* mutant (333). OxyR has been demonstrated to play a key role in the regulation of bacterial the catalases *katA* and *katB* (334, 335). An *oxyR1* mutant of *Pseudomonas putida* which overexpresses oxidative stress genes, was shown to induce expression of katA and katB and give rise to increased enzyme activity of both enzymes (336).

To determine sensitivity of the mutant *Y. pestis* strains to endogenous oxidative stress, a similar disc diffusion experiment was carried out using sodium azide (NaN_3), a known inhibitor of aerobic respiration. A significantly larger zone of inhibition was observed in the lawn of the Δ*relA,* mutant (18.5 mm P = 0.0005) compared to wild-type bacteria (9.5 mm) (Figure 49). The Δ*ppK,* Δ*ppX and* Δ*ppK/ppX* mutants showed no statistically significant difference in the diameter of the zone of inhibition compared to the wild-type organism.

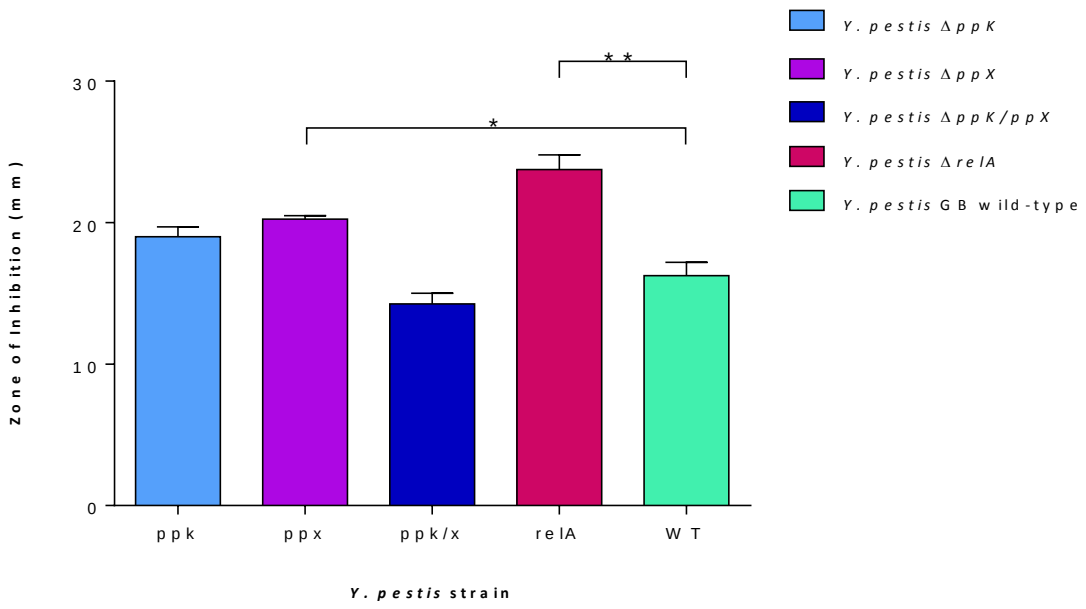

Figure 49. Zones of inhibition measured surrounding sterile discs impregnated with 100 mM NaN_3. Graph presented plots the mean with standard error from combined data from four technical replicates and three biological replicates for *Y. pestis* GB and *Y. pestis* mutant strains. Statistical significance compared to wild type GB is indicated by *. * $P \leq 0.05$, ** $P \leq 0.01$.

In contrast to the pyrogallol results presented above, the Δ*relA* and Δ*ppX* mutants appear to be more sensitive to NaN_3, an inducer of endogenous oxidative stress and a disruptor of aerobic respiration. This implies that the regulatory mechanisms involved in how bacteria respond to exogenous and endogenous oxidative stress conditions vary. The increased sensitivity to endogenous ROS seen here concurs with previous studies that have found that an active stringent response confers increased resistance to intracellular oxidative stress in *E. coli* and *Salmonella typhimurium* (327).

2.3.5. Persister Assay

Bacterial mechanisms for survival in changing environmental conditions include genetically regulated adaptations such as sporulation (337), phase variation (338) and adaptive mutation resulting in resistance (339, 340). Conversely, adaptation to environmental change can be epigenetic, such as persistence, giving rise to phenotypically distinct, but genetically identical subpopulations of tolerant bacteria (169, 253). As discussed in section 1.4.1, bacterial

persistence was discovered by Joseph Bigger in 1944 following experiments investigating how bacteria respond to killing by penicillin, whereby cultures of *Staphylococcus* could not be completely killed by this antibiotic treatment (165). The rare (only 1 in 10^5 – 10^6 bacterial cells), so-called 'persister cells' were found to be genetically identical to the rest of the population but displayed a decreased sensitivity to antibiotics (166). However, subsequent bacterial generations derived from persister cells showed restored levels of antibiotic sensitivity identical to that of their ancestors, demonstrating persistence was not a heritable phenotype (163). This spontaneous and reversible switching from a 'normal' antibiotic sensitive phenotype to a 'persistent' antibiotic tolerant phenotype appears to be of a stochastic nature (167). Two different types of persister cell have been discovered and characterised in *E. coli*. Type I persister cells are generated during stationary phase and remain in a non-growing phase once the culture is transferred to fresh medium (341). Type II persister cells accumulate independently of passage through stationary phase and exhibit a very slow exit from stationary phase (167, 168, 251). Persistence has been shown to be a highly conserved phenomenon, and has been observed in nearly every bacterium studied to date (169). Additionally, the persistent phenotype protects bacteria from killing by not only penicillin, as first demonstrated by Bigger, but varied and multiple antibiotics, simultaneously (170).

To study persistence, *hi*gh *p*ersister (*hip*) mutants have been previously generated in *E. coli* and have demonstrated that type II persister cells present as pre-existing stochastic subpopulations within bacterial communities (167, 251). More detailed analyses of *E. coli hip* mutants revealed a genetic locus, termed *hipA,* to be a key component of the persister phenotype (167, 169, 251, 252). HipA is the toxin component of a toxin-antitoxin (TA) system, of which there are several in most bacteria (166, 253). TA systems generally consists of a stable toxin, which inhibits essential cellular processes such as translation, via mRNA degradation, and a less stable antitoxin, usually in the form of a protein or RNA which counters the action of the toxin under normal growth conditions (166, 253). Although the function and effects of TA loci are numerous and diverse, they have now been demonstrated to play a key role in bacterial persistence, as shown in figure 16 (169, 252, 254, 342). Studies into the molecular mechanism of TA loci and persistence have revealed links to other cellular process and molecules that impact this phenomenon reviewed by Gerdes and Maisonneuve (342). One such process that has been implicated in TA activation is the activity of the Lon protease (shown in figure 17).

Lon has been shown to degrade the antitoxin component of the TA system, giving rise to toxin activation and subsequent growth inhibition via mRNA degradation, this cascade effect is detailed in figures 54, 55, 56 and 57 (169, 252) and Lon protease is directly activated by polyphosphate (174, 256). Previous research has demonstrated that RelA-derived (p)ppGpp inhibits the exopolyphosphatase PPX, which degrades polyphosphate chains into free phosphate residues, resulting in more polyphosphate being present in the cell due to the activity of PPK, a polyphosphate synthetase (218). This increase in polyphosphate results in increased Lon activation and downstream antitoxin inhibition, which in turn leads to toxin activation (169). This hierarchical control over TA systems and persistence has recently been proposed as a working model (figure 17) by Germain *et al* (169).

To investigate the effects of inactivation of the genes involved in the stringent response (*relA* and *spoT*) and polyphosphate biosynthesis (*ppK* and *ppX*), previously shown to have growth, virulence and polyphosphate deficiencies and increased sensitivity to antibiotics, persister assays were then conducted with *Y. pestis* GB deletion mutants. Building on previous results from antibiotic disc diffusion experiments which showed that stringent response and polyphosphate metabolism deficient mutants were more sensitive to killing by various classes of antibiotics, the effects on persister cell formation were investigated in *Y. pestis* Δ*ppK* and Δ*relA* mutants using appropriate antibiotics.

The antibiotics selected for testing with the persister assays were gentamicin and ciprofloxacin. Gentamicin, an aminoglycoside and part of the same class of antibiotics as streptomycin, which has traditionally been an antibiotic of choice for the treatment of plague, was selected as it was expected to give rise to less spontaneous resistance than streptomycin due to the transfer of streptomycin resistance occurring at a higher frequency than that of gentamicin resistance (148, 149). Ciprofloxacin was also selected to test in the persister assays, as this would also serve as a more current antibiotic therapy for the treatment of plague. Ciprofloxacin was also an antibiotic that resulted in a statistically significant difference when tested in the antibiotic disc diffusion assays.

Initially *Y. pestis* GB cultures were treated with gentamicin at 2 µg/mL, which was representative of the Minimum Inhibitory Concentration 90% (MIC90) (figure 50), and then at

1 µg/mL, which was representative of the MIC50 (figure 51). Treatment with 2 µg/mL gentamicin, appeared to kill the bacteria too quickly to capture the level of persistence over the three hour time course, as no viable counts were obtained after the 30 minutes time point (figure 50). This initial experiment did not reveal any statistically significant differences between the strains tested. Therefore, the assay was repeated using gentamicin treatment at the MIC50 (1 µg/mL). This enabled enumeration of colony forming units (CFU) for the *Y. pestis* strains tested at all of the time points throughout the experiment (figure 51). As predicted, the Δ*ppK* mutant displayed a statistically significantly decrease in persistence compared to wild type *Y. pestis* GB.

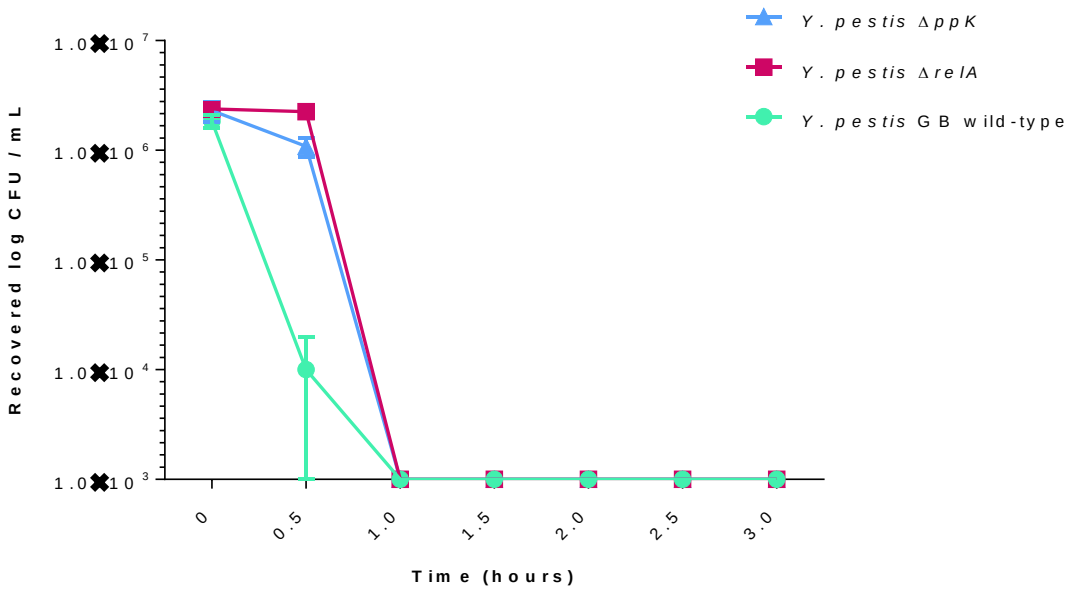

Figure 50. Early optimisation results for the persister assay. Graph showing the number of bacteria recovered following treatment with 2 µg/mL gentamicin over a time course of three hours. Data points represent the average from two biological replicates and six technical replicates. Two-way ANOVA revealed no statistical differences between the *Y. pestis* strains.

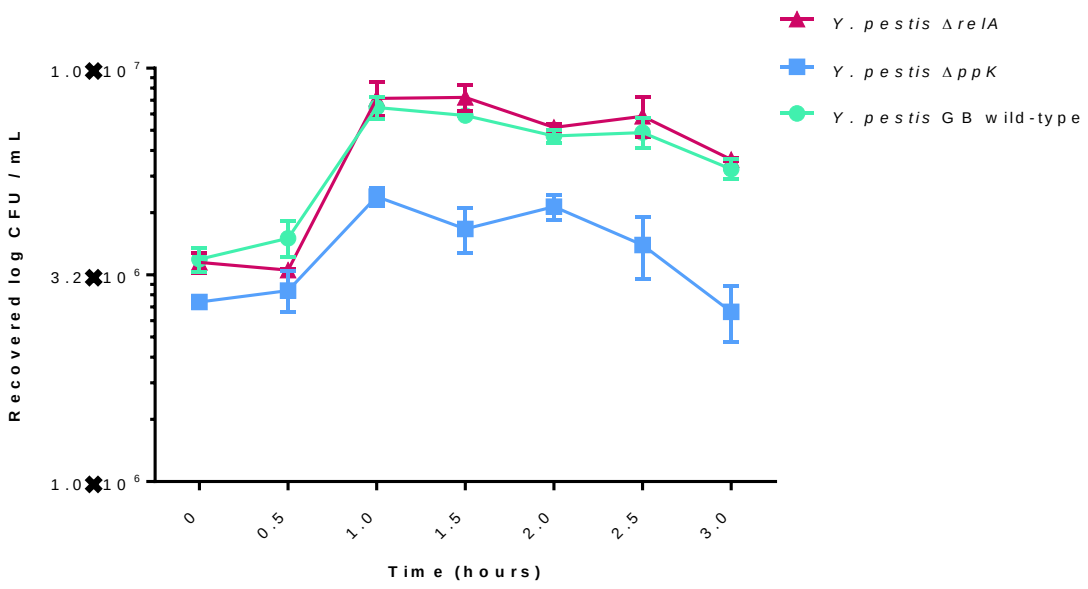

Figure 51. Subsequent iteration of optimised persister assay method. Number of bacteria recovered following treatment with 1 µg/mL gentamicin over a time course of three hours. Data points represent the average from two biological replicates and six technical replicates. Two-way ANOVA with Bonferroni's correction for multiple comparisons at the 95% confidence interval revealed a statistically significant difference between *Y. pestis* GB wild type and *Y. pestis* Δ*ppK* ($P < 0.01$).

For comparison, persister assays with ciprofloxacin were also carried out and the number of bacteria was enumerated from *Y. pestis* GB strains treated with ciprofloxacin, initially at 1.0 µg/mL, which was representative of 10x the MIC50 (figure 52) and then with 2.0 µg/mL which was representative of 10x the MIC90 (Figure 53). The latter experiment revealed a statistically significant difference between *Y. pestis* GB wild type and the Δ*relA* mutant at the 2.5 hour time point ($P \leq 0.01$).

All results for antibiotic sensitivity disc diffusion assays and persister assays are summarised in table 3 to indicate if the mutants' sensitivity to antibiotics increased or decreased in comparison to *Y. pestis* GB wild type.

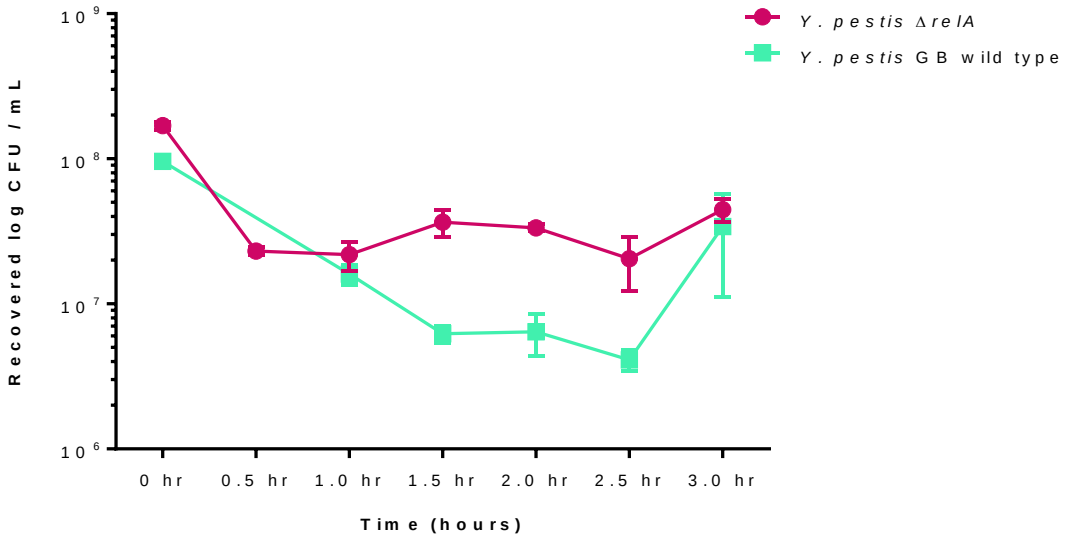

Figure 52. Number of bacteria recovered following treatment with 1.0 µg/mL ciprofloxacin over a time course of three hours. Data points represent the average from three biological replicates and nine technical replicates. Two-way ANOVA with Bonferroni's correction for multiple comparisons at the 95% confidence interval revealed a statistically significant difference between *Y. pestis* GB wild type and *Y. pestis* Δ*relA* ($P < 0.01$).

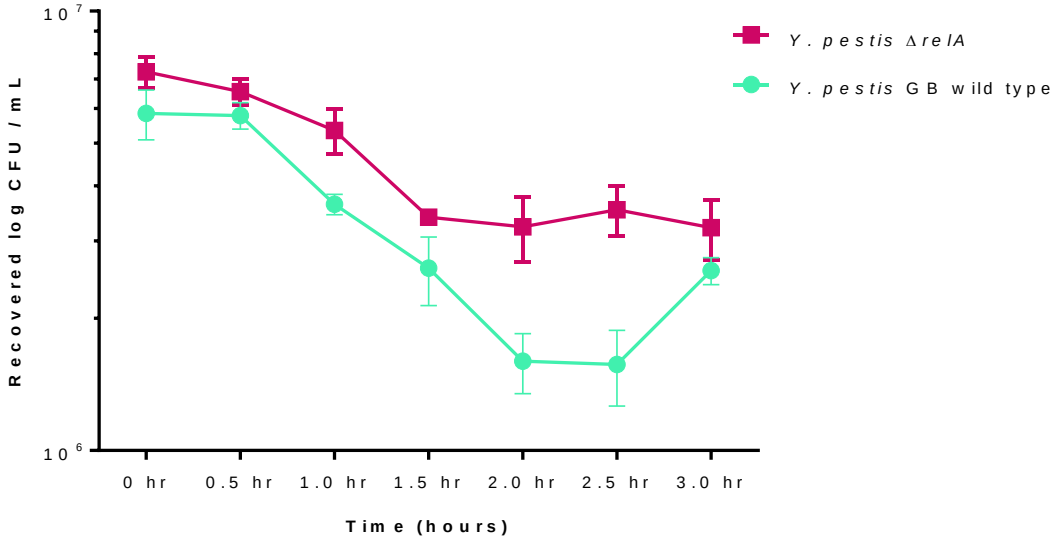

Figure 53. Number of bacteria recovered following treatment with 2.0 µg/mL ciprofloxacin over a time course of three hours. Data points represent the average from three biological replicates and nine technical replicates. Two-way ANOVA with Bonferroni's correction for multiple comparisons at the 95% confidence interval revealed a statistically significant difference between *Y. pestis* GB wild type and *Y. pestis* Δ*relA* ($P < 0.01$).

Bacterial Strain	**Disc diffusion antibiotic sensitivity, increase (↑) or decrease (↓)**	**Persister assay antibiotic sensitivity, increase (↑) or decrease (↓)**	**Oxidative stress sensitivity increase (↑) or decrease (↓)**
Y. pestis Δ*ppK*	↑	↓	↓
Y. pestis Δ*ppX*	↑	↑	↓
Y. pestis Δ*ppK/ppX*	↑	NT	↓
Y. pestis Δ*relA*	↑	NT	↓

Table 3. Table summarising antibiotic disc diffusion assays, persister assays and oxidative stress assays. An increase in sensitivity to stress is indicated by ↑ and a decrease in sensitivity is indicated by ↓. NT indicates not tested.

2.4. *Yersinia pestis* Mutant Characterisation *In Vivo*

2.4.1. Non-Mammalian Model of Infection – *Galleria mellonella*

The use of non-mammalian models of infection for investigating human pathogens has increased over recent years. These models allow virulence assessments to be made without the use of mammals and are cheaper and easier to use (343-346). Non-mammalian insect or insect larvae models of infection have been one approach investigated in recent years due to their ability to survive at 37 °C, the temperature at which many human pathogen virulence factors are expressed (347). Another major advantage of using an insect larvae model of infection is the similarity of their immune cells, termed haemocytes to mammalian phagocytic cells (348, 349). In addition, the immune system of insects such as the wax moth *Galleria mellonella* shares a high degree of structural and functional homology to mammalian innate immune systems (348). The humoral immune response in insects consists of melaninisation where by melanin accumulates in the hemolymph causing a colour change in the larvae from creamy white to a dark brown (350). The humoral immune response in insects also consists of hemolymph clotting and the production of a large range of antimicrobial peptides (349, 351). As such, *G. mellonella* has been shown to be susceptible to infection with bacterial pathogens such as *F. tularensis* (351), *Burkholderia mallei* (352) and *Y. pseudotuberculosis* (347). It has also been observed that fully virulent *Y. pestis* appears to be less virulent than *Y. enterocolitica* but still results in death of *G. mellonella* and the bacteria will replicate in haemocytes (353), which can provide an alternative intracellular viability assay to macrophage infectivity assays (347, 354, 355).

To assess the *Y. pestis* mutants for intracellular growth, groups of 5 *G. mellonella* larvae in their 6th stage of larval development were challenged in the right foremost leg with $1X10^6$ bacteria. Groups included wild type *Y. pestis* GB, the mutant strains Δ*ppK*, Δ*ppX*, Δ*relA* and Δ*ppk*/*ppX*, a PBS injection control and a non-injection control group. After 24 hours incubation at 37 °C each larva was drained of haemolymph, and bacterial load was enumerated by plating out serially diluted haemolymph onto BAB-hemin plates. Plates were then incubated for 48 hours at 28 °C and single CFU enumerated.

After 24 hours incubation at 37 °C approximately 1x10^5 CFU were recovered from the larvae haemolymph for the Δ*ppK,* Δ*relA* mutants and the wild type *Y. pestis* GB. As a significant growth defect was observed for the Δ*ppX* and Δ*ppK*/*ppX* mutants *in vitro*, a similar phenotype was anticipated to be apparent in the *G. mellonella* study. 1x10^4 CFU were recovered from the larvae haemolymph for the Δ*ppX* and Δ*ppK/ppX* mutants, significantly lower than the other strains (P < 0.005) (figure 54).

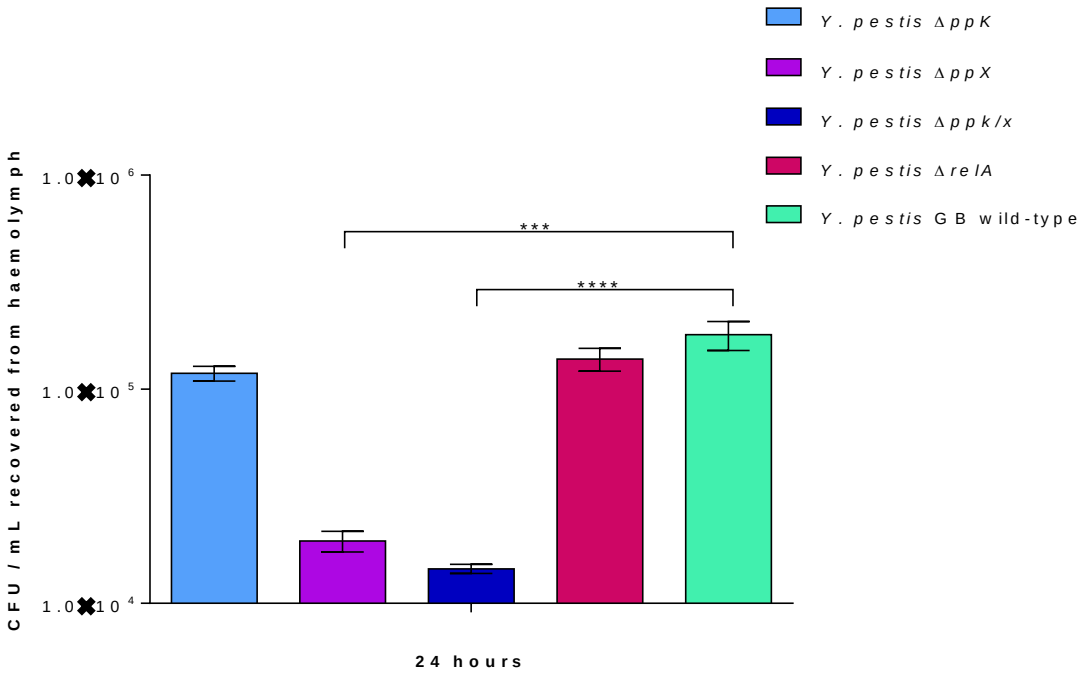

Figure 54. CFU recovered from *G. mellonella* haemolymph at 24 hours post challenge with 1x10^6 CFU *Y. pestis* strains. Graphs shows means and standard error plotted from three replicates. Statistical significance compared to wild type GB is indicated by *. *** P ≤ 0.001, **** P ≤ 0.0001.

Therefore, a second *G. mellonella* study was carried out focusing on the Δ*ppX* and Δ*ppK*/*ppX* mutants with an increased incubation time post challenge from 24 hours to 28 hours at 37 °C (figure 55).

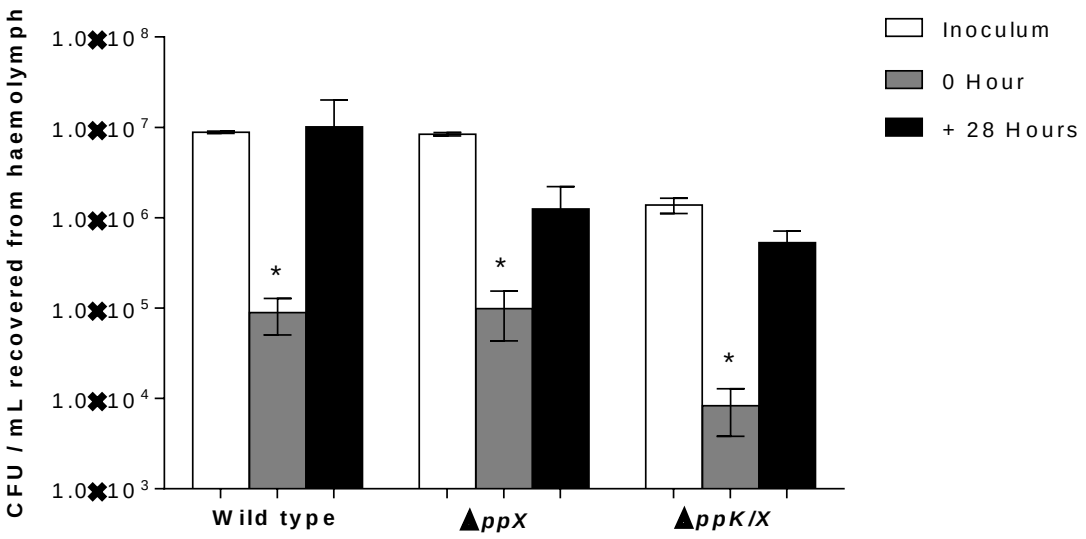

Figure 55. CFU / mL recovered from *G. mellonella* haemolymph at 0 hour and 28 hours post challenge plotted alongside initial inoculum viable count data. Graphs shows means and standard error plotted from three replicates. Statistical significance between 0 hours and +28 hours is indicated by *. * $P \leq 0.05$.

Both mutant strains significantly replicated in the larvae haemocytes ($P = 0.0002$) and none of the larvae used in this study succumbed to the *Y. pestis* infection for any strain. However the larvae from all groups did start to show signs of melaninisation around the challenge injection site. Melaninisation was most prominent in the wild-type group. This *G. mellonella* study indicates that following innoculation, bacterial load is significantly decreased in the early stages of infection, and then the wild type strain recovers well and grows to significantly higher titres. Whereas the Δ*ppX* and Δ*ppK*/*ppX* mutants did not recover as well and reached lower bacterial loads following 28 hours of incubation. It is also evident that an incubation time of at least 28 hours is required for bacterial growth in haemocytes, as recovered CFU at 24 hours was less than the challenge dose for all *Y. pestis* strains.

2.4.2. Mammalian Model of Infection – Murine

The *Y. pestis* mutants were tested for attenuation in a murine model of infection. The median lethal dose (MLD) for a subcutaneous challenge of *Y. pestis* in a murine model of infection is 1 CFU (356). Therefore it was decided to challenge with 100 CFU and $1x10^4$ CFU to ensure that a

lethal infection would be observed for the wild type strain. Each mutant and the wild type GB were delivered in a sub-cutaneous challenge retrospectively determined at the following doses as shown below in table 4;

Bacterial Strain	**Low Dose (CFU)**	**High Dose (CFU)**
Y. pestis Δ*ppK*	269	2.696×10^4
Y. pestis Δ*ppX*	246	2.466×10^4
Y. pestis Δ*ppK/ppX*	103	1.033×10^4
Y. pestis Δ*relA*	242	2.423×10^4
Y. pestis GB wild-type	116	1.163×10^4

Table 4. Challenge doses based on viable counts of *Y. pestis* mutant attenuation study.

Following sub-cutaneous challenge each group of mice were monitored for 14 days. The single mutants (Δ*ppK,* Δ*ppX* and Δ*relA)*, showed no attenuation throughout the study, and mice died at similar rates to the wild type bacterium (figures 56 and 57). However, the double Δ*ppK/ppX* resulted in no deaths in either group throughout the duration of the study, demonstrating attenuation (figures 56 and 57).

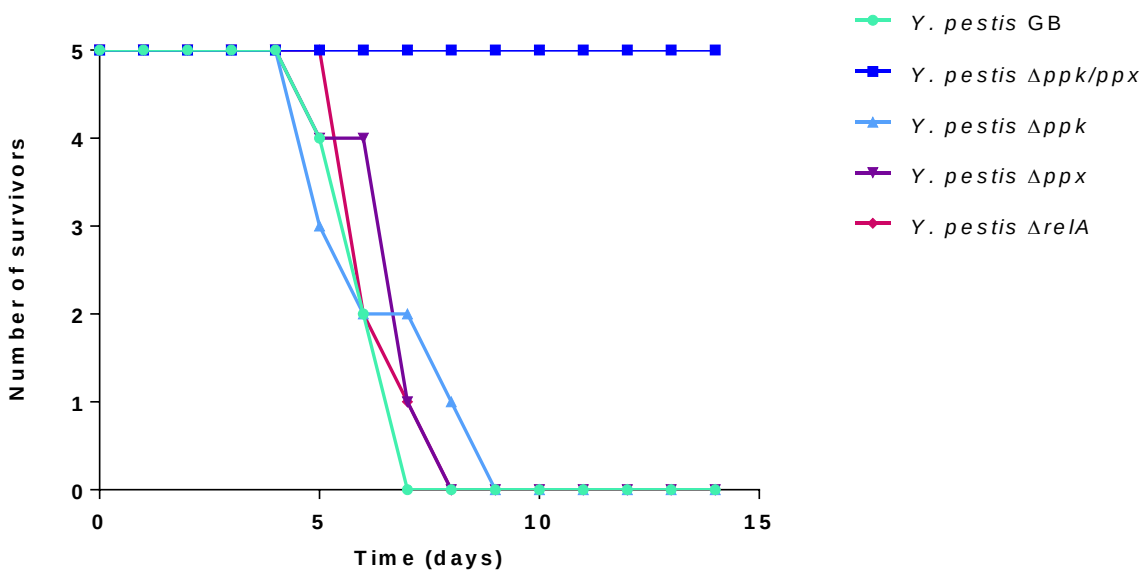

Figure 56. Graph showing number of murine survivors over a 14 day time course following sub-cutaneous challenge with ~100 CFU *Y. pestis*.

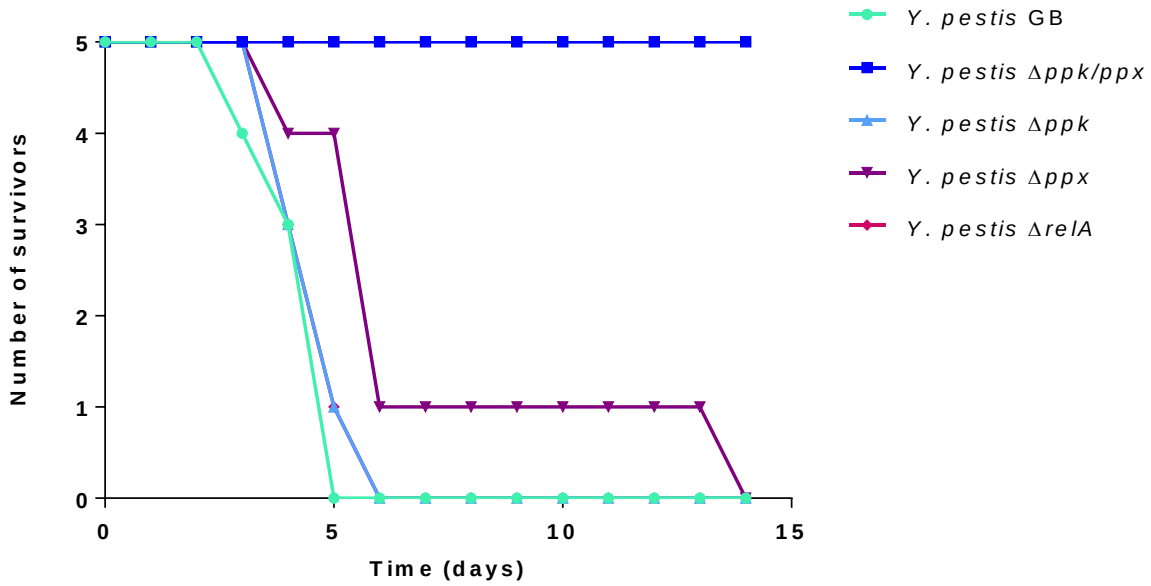

Figure 57. Graph showing number of murine survivors over a 14 day time course following sub-cutaneous challenge with ~1 x 10^4 CFU *Y. pestis*.

Although not a stistically siginificant result the Δ*ppX* mutant appeared to show a slight delay to death in comparison to the other strains in the murine attenuation study. This could be indicative of compromised fitness that has been observed in previous experiments *in vitro* and *in vivo*.

Two Δ*relA Y. pestis* mutants (one marked with an antibiotic selectable marker and one unmarked to avoid polar effects) were also tested for attenuation in a murine model of infection. Each mutant and the wild type were delivered by sub-cutaneous challenge with retrospective determination of dose given (table 5).

Bacterial Strain	**Low Dose (CFU)**	**High Dose (CFU)**
Y. pestis Δ*relA* marked (M)	77	$7.7x10^3$
Y. pestis Δ*relA* unmarked (-)	98	$9.8x10^3$
Y. pestis GB wild type	94	$9.4x10^3$

Table 5. Challenge doses based on viable counts of *Y. pestis* mutants. +

Following sub-cutaneous challenge mice were monitored for 14 days (figure 58). The single mutants (Δ*ppK,* Δ*ppX* and Δ*relA*) showed no attenuation throughout the study, and mice died at similar rates to those challenged with the wild type bacteria, except for the Δ*relA* marked mutant for which there was one survivor at both challenge dose groups at the end of the study (table 5). The reason for these survivors is unclear as the single *relA* mutation is not expected to impact virulence in *Y. pestis* and the previous challenge shown in figures 56 and 57 showed the Δ*relA* mutant resulting in no survivors at challenge doses of 100 and $1x10^4$ CFU.

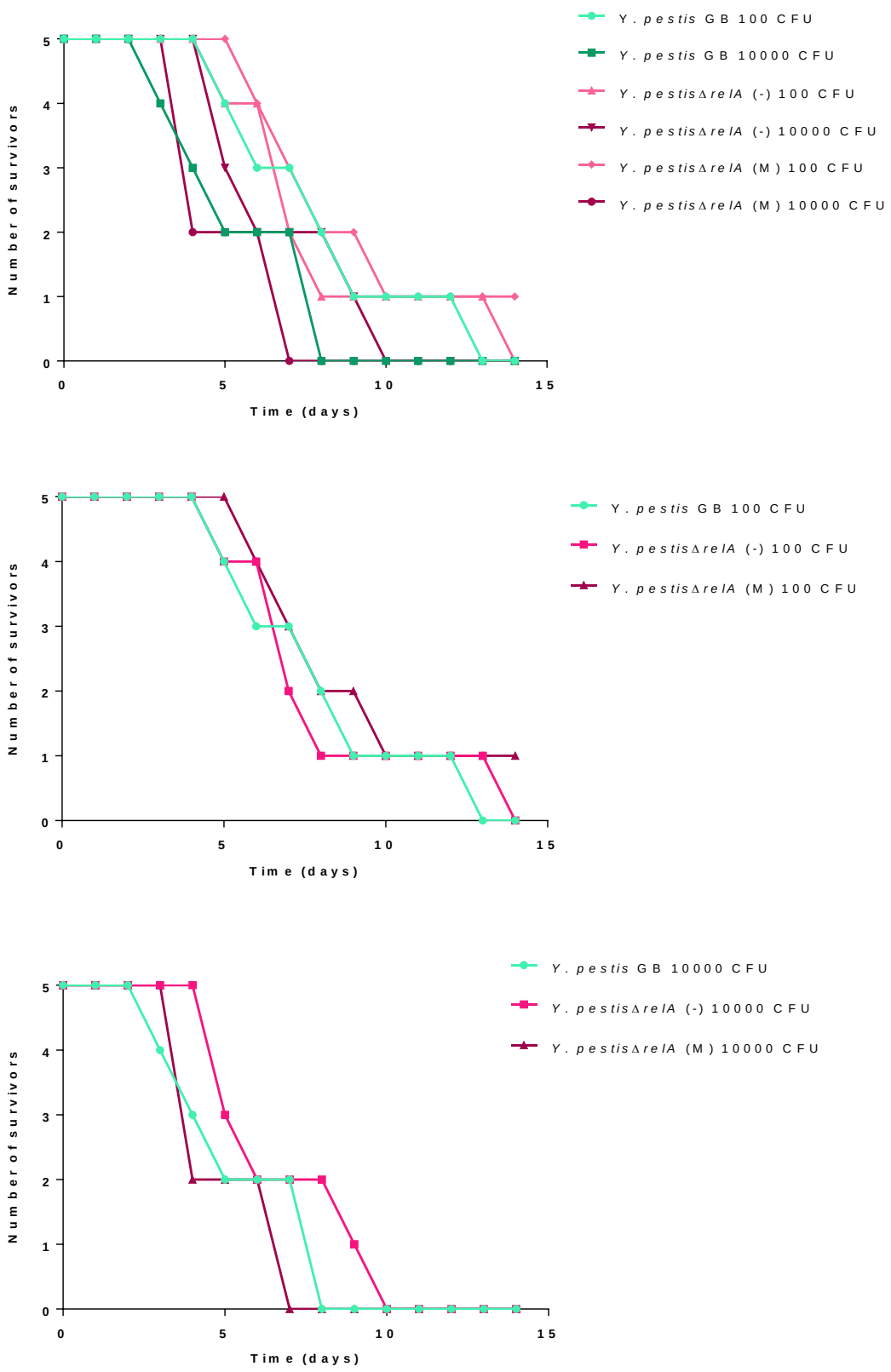

Figure 58. Number of murine survivors over a 14 day time course following sub-cutaneous challenge with 100-10000 CFU *Y. pestis*. (-) refers to the unmarked mutant, and (M) refers to the antibiotic resistant marked mutant generated by lambda red recombinase mutagenesis.

There were no statistically significant differences determined for the survival of mice challenged with the mutant strains in this study (summarised in table 6), which correlates with the previous mouse study results for the Δ*relA* mutant as shown previously in figures 56 and 57.

Bacterial Strain	**Dose (CFU)**	**Number survivors at 14 days**	**Mean time to death (days)**
Y. pestis Δ*relA* (marked)	77	1	8
Y. pestis Δ*relA* (marked)	$7.7x10^3$	1	4
Y. pestis Δ*relA* (unmarked)	98	0	7
Y. pestis Δ*relA* (unmarked)	$9.8x10^3$	0	5
Y. pestis GB wild type	94	0	8
Y. pestis GB wild type	$9.4x10^3$	0	4

Table 6. Summary of number of murine survivors at the end of the study and the associated mean time to death for each group.

2.5. *Yersinia pestis* Mutant Complementation

To confirm the phenotypes that have been observed for the previously generated *Y. pestis* mutants, it is necessary to express an intact copy of the deleted gene in the mutant background and test for a restoration of wild type phenotype. As a priority the double Δ*ppk/ppX Y. pestis* mutant was selected for complementation, as this was the mutant that displayed the most prominent phenotypes including a growth defect, attenuation in a murine model of infection, increased susceptibility to antibiotics and an inhibited ability to generate intracellular polyphosphate as shown in section 2.3.

To initially complement the *ppk* deletion in the double Δ*ppk/ppX* mutant, PCR primers (listed in table 23, Appendix 8.2) were used to amplify the gene including its natural promoter upstream from *ppk* (figure 59). It is not possible to use the same approach to complement the single *ppX* gene as it appears both *ppk* and *ppX* are driven from a single promoter upstream from *ppk*. For this reason the P_{BAD} promoter encoded on pBAD33 (357), was used as an alternative promoter. The *ppk* PCR product (figures 60 and 61) was digested with *Xba*I and *Hind*III and ligated into the backbone derived from pBAD33 digested with matching enzymes (figures 62 and 64). The *ppk* PCR was digested with *Xba*I and *Hind*III and ligated into the backbone derived from pBAD33 digested with matching enzymes using T4 DNA ligase (figure 63).

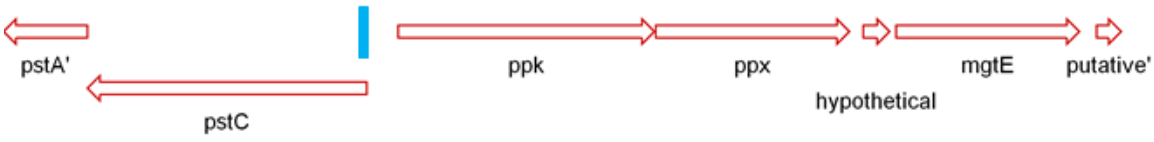

Figure 59. Genetic region showing the *ppk*/*ppX* operon and adjacent genes in the *Y. pestis* CO92 genome. The blue bar indicates the location of promoter sequence for the polyphosphate metabolism operon.

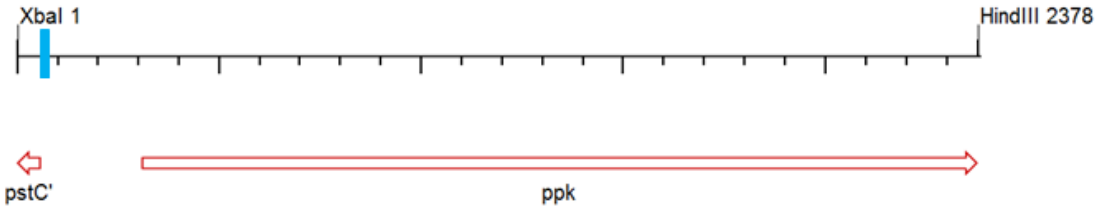

Figure 60. PCR product of *Y. pestis* wild type *ppk* gene and associated promoter region (blue bar). PCR product comprises a 2378 bp DNA fragment with *Xba*I and *Hind*III restriction sites at the 5' and 3' ends respectively.

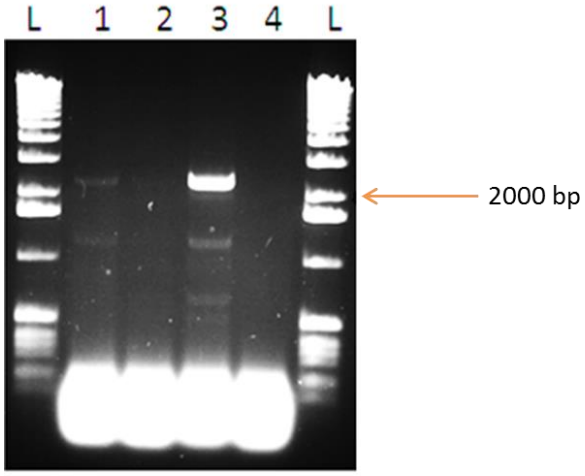

Figure 61. PCR amplification of the *ppk* gene from *Y. pestis* GB genomic DNA. Lane 1 - replicate 1 (faint band present), lane 2 - replicate 2 (no band present), lane 3 - replicate 3 (band present), lane 4 - negative control. L - molecular weight marker X (Roche Diagnostics). Arrow indicates 2000 bp on marker. The desired band size for the PCR product from the *ppk* gene amplification is a 2378 bp.

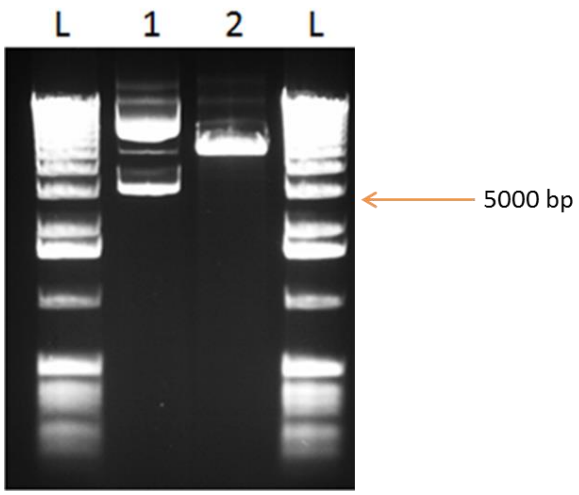

Figure 62. Digest of pBAD33 with *Xba*I and *Hind*III. Lane 1 – undigested pBAD33 showing supercoiled plasmid. Lane 2 –pBAD33 linearised by digestion with *Xba*I and *Hind*III. L – molecular weight marker X (Roche Diagnostics). Arrow indicates 5000 bp on the molecular weight marker. Linearised pBAD33 is 5352 bp.

The plasmid pBAD33 uses an arabinose operon promoter (P_{BAD}) and a regulatory gene, *araC* to either positively or negatively regulate gene expression in the presence or absence of arabinose (357) (figure 63). In the presence of arabinose, transcription from the pBAD promoter is switched on, and subsequent encoded genes will also be expressed given the presence of their natural promoter sequence.

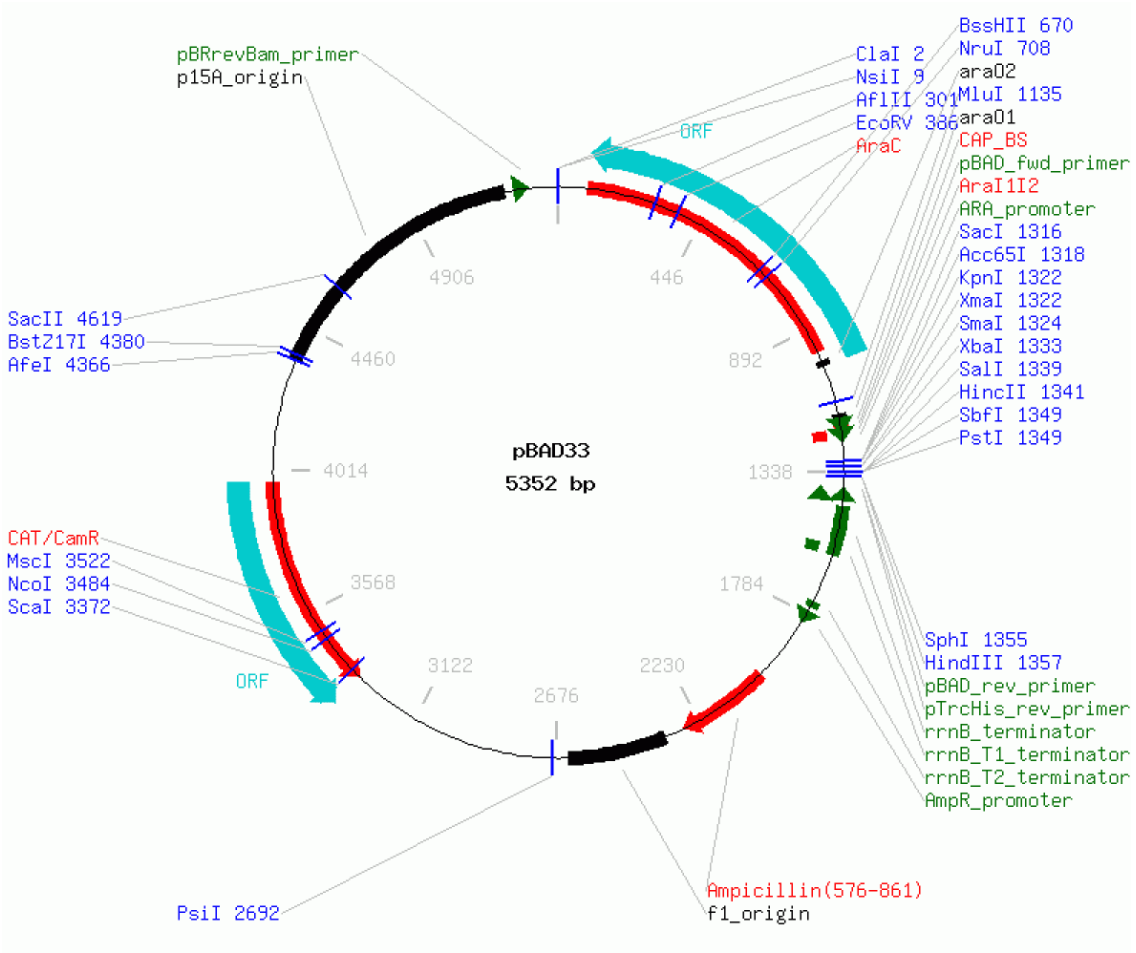

Figure 63. Map of pBAD33, showing antibiotic resistance cassettes for chloramphenicol and ampicillin, the P_{BAD} *araC* promoter and the multiple cloning site.

Ligation of the *ppk* gene product into the pBAD33 plasmid was unsuccessful as there is visible unligated insert present on the gel (Figure 64), and the desired band size of 7730 bp was not visible. This cloning process was inefficient and required further optimisation, which was not possible on this project.

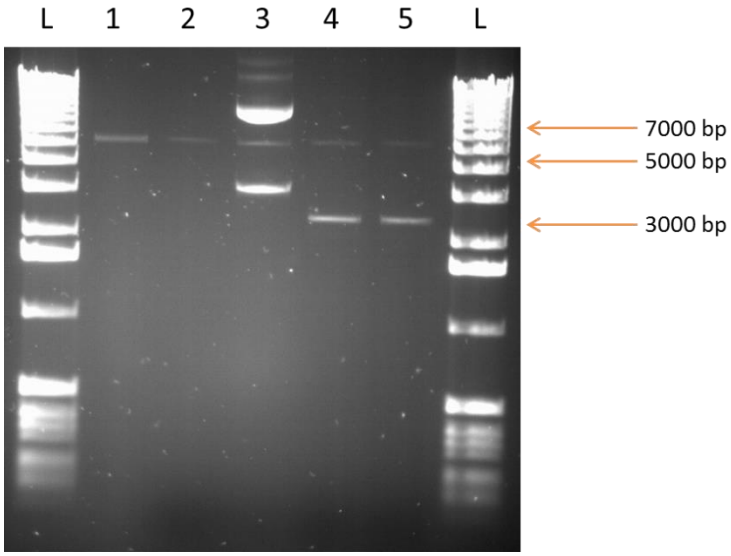

Figure 64. Ligation of *ppk* insert into pBAD33 vector. Lane 1 – Digested pBAD33 (*Xba*I/*Hind*III), Lane 2 – no insert/digested plasmid control. Lane 3 – undigested pBAD33. Lane 4 – test ligation 1. Lane 5 – test ligation 2. L – Molecular weight marker X (Roche Diagnostics).

2.6. Discussion and Conclusions *Y. pestis* mutants

The following mutants have been generated during this project: *Y. pestis* Δ*ppK; Y. pestis* Δ*ppX; Y. pestis* Δ*ppK*/*ppX* and *Y. pestis* Δ*relA* (lambda red recombinase marked mutant and isogenic unmarked mutant). A mutant that was not generated in this study but would add value to future work was a double *relA*/*spoT* mutant and the complemented single mutants.

Due to the interaction of the stringent response and polyphosphate biosynthesis, it was expected that disruption of the polyphosphate pathway would impact the ability of *Y. pestis* to respond to nutrient limitation during a standard growth curve. No *in vitro* growth defects were observed for the Δ*ppK* and Δ*relA* mutants. However, a statistically significant growth defect was observed for the Δ*ppK*/*ppX* and Δ*ppX* mutants. Of these, the most pronounced growth defect was observed for the Δ*ppK*/*ppX* double mutant, which showed significantly less growth during exponential phase and a delayed entry into stationary phase compared to the single *Y. pestis* mutants and the wild type GB. It was hypothesised that the double mutant may show more pronounced phenotypes compared to wild type, as abolition of an entire metabolic pathway was likely to disrupt polyphosphate production, particularly at late exponential stage of growth when the stringent response is initiated. It was also hypothesised that the single mutants may disrupt the fine tuning of the biological stress response process at the regulatory level but perhaps not significantly impact bacterial growth and or virulence.

To first evaluate the direct effect on the polyphosphate biosynthetic pathway intracellular phosphate quantification using a malachite green spectrophotometric assay was carried out on the *Y. pestis* mutants; Δ*ppK,* Δ*ppX,* Δ*ppK*/*ppX* and Δ*relA*. Considering the relative functions of the enzymes that had been inactivated in these mutants, the phosphate quantification assay revealed predicted effects on the ability of *Y. pestis* to synthesise intracellular polyphosphate. The wild type strain, the Δ*ppX* mutant and the Δ*relA* mutant all revealed similar high levels of intracellular polyphosphate, whereas the Δ*ppK* and Δ*ppK*/*ppX* mutants showed a statistically significant drop in intracellular polyphosphate levels compared to the other strains. This result supports our hypothesis as one would expect *Y. pestis* to retain the ability to synthesise polyphosphate in the absence of PPX or RelA. In the case of PPX the ability to degrade polyphosphate would be disrupted but not the ability to synthesise (211, 232). Concurrently, the Δ*ppX* mutant was also predicted to produce much higher levels of polyphosphate due to

the absence of a polyphosphate degradation mechanism. This expected increase in polyphosphate was not observed in the quantification assay. This is likely to be due to an alternative exopolyphosphatase compensating for the lack of PPX, and the enzyme with a predicted exopolyphosphatase activity which is required for the conversion of pppGpp to ppGpp is GppA and is likely to be carrying out this role. In the case of RelA, the polyphosphate biosynthetic pathways might remain intact, and the stringent response pathway would be compensated for by the bifunctional activity of SpoT (169, 252).

Previous studies have also linked the stringent response to bacterial antibiotic sensitivity, whereby an active stringent response triggers a broad spectrum increase in tolerance to antibiotic treatment (171). Antibiotic disc diffusion assays conducted herein revealed an increase in sensitivity to various classes of antibiotics when *Y. pestis* mutants defective for polyphosphate and stringent response genes were tested. Specifically, Δ*ppK,* Δ*ppK*/*ppX* and Δ*relA* mutants showed increased sensitivity to streptomycin and polymyxin B suggesting that these genes could have potential as novel antibiotic targets or adjuvants to current therapies.

To further investigate the effect of mutation of polyphosphate- and stringent response-associated genes other sources of stress were used in disc diffusion assays, starting with oxidative stressors. It is also interesting to consider the recently proposed mechanism of antibiotic killing of bacteria which states that, besides through specific drug-target interactions, antibiotics kill bacteria by a common mechanism involving production of ROS (358, 359), although this has been hotly debated (204, 360-362). Kohanski *et al* (359) first identified this common mechanism which involved the production of hydroxyl radicals by which all bactericidal antibiotics could induce cell death (359). Despite the ongoing debate it is likely that ROS production contributes to antibiotic-mediated killing (358). However, the extent to which ROS contribute to bacterial cell death depends on the specific environmental conditions present (361, 362). Hence, differences in experimental procedures could be the cause of the conflicting results reported in literature (358). Therefore, to test oxidative stress sensitivity in the *Y. pestis* mutants, disc diffusion assays were carried out using pyrogallol which produces the ROS superoxide and NaN_3 a reducing agent and a known inhibitor of aerobic respiration. Interestingly, all *Y. pestis* mutants defective for components of the stringent response or polyphosphate production were more tolerant to pyrogallol, whereas the Δ*relA*

mutant was more sensitive to NaN_3. These results do not correlate well with results of previous research in other bacteria (193, 206, 209, 248); in fact the opposite effect was observed in this study when the *Y. pestis* mutants were challenged with pyrogallol. The molecular mechanisms at play here are unclear, however the stringent response and associated polyphosphate biosynthetic pathway are renowned for their complexity and diversity of downstream effects, so it is possible that pyrogallol stress in this example, where the stringent response is not completely abolished, merely knocked down, is triggering a de-repression of proteins such as the superoxide dismutases and catalases, thus mitigating a challenge with ROS. These results also indicate that polyphosphate biosynthesis does not play a key role in the ability of *Y. pestis* to respond to the bacteriostatic action of NaN_3(a source of exogenous oxidative stress), whereas the stringent response genes are perhaps more important.

In addition to characterisation of the mutant strains sensitivity to antibiotics and oxidative stress, in light of recent research proposing a cascade of biochemical steps controlling bacterial persistence involving (p)ppGpp, polyphosphate and bacterial toxin-antitoxin systems (169, 342, 363, 364), persister assays were carried out for a number of *Y. pestis* mutants. Considering the hierarchical control over bacterial persistence involving RelA, (p)ppGpp, polyphosphate and Lon, one might expect the following results from deletion mutants at the following loci:

- Δ*ppK* - decreased persistence (more sensitive to antibiotics) (figure 65)
- Δ*ppX* - increased persistence (less sensitive to antibiotics) (figure 66)
- Δ*ppK/ppX* - decreased persistence (more sensitive to antibiotics) (figure 67)
- Δ*relA* - increased persistence (less sensitive to antibiotics) (figure 68)

According to the proposed model of bacterial persistence inactivation of PPK should give rise to less persistence, in other terms an increased sensitivity to antibiotic treatment. Whereas, inactivation of RelA should give rise to higher levels of persistence, as per figures 65, 66, 67 and 68. However, when the Δ*ppX* mutant was tested for intracellular polyphosphate production, polyphosphate levels did not increase above background which was predicted to be due to a compensatory exopolyphosphatase mechanism most likely catalysed by GppA.

Therefore an impact on persistence in Δ*ppX* strain is less likely to be detected compared to the other mutant strains.

The persister assay required multifactorial optimisation (optimisation data not shown) including; concentration of antibiotic; culture volume; culture vessel and time of incubation. The concentration of antibiotic used was as close to the MIC as possible, which improved the reliability of the assay. The Δ*relA* mutant assays were more reproducible compared to the Δ*ppK* mutant assay and was therefore selected for further testing with an additional antibiotic, ciprofloxacin. Both assays revealed results that fitted the model of persistence proposed by Maisonneuve *et al* (252) but were different to results obtained from the disc diffusion assays. This result perhaps seemed to be contradictory; however, these assays were testing different phenotypes of bacterial fitness.

Our results presented herein support the model of persistence proposed by Germain *et al* (169), as deletion of PPK results in less polyphosphate being synthesised (as demonstrated by polyphosphate quantification by malachite green assay as discussed in section 2.3.2), less activation of Lon, less degradation of antitoxins and decreased free toxin leading to decreased persistence, thus the cells are more sensitive to killing by antibiotics (figure 17). This result supports that obtained from antibiotic disc diffusion assays that showed the *Y. pestis* Δ*ppK* mutant was more sensitive to various classes of antibiotics including gentamicin. As predicted by the model proposed by Germain *et al* (169), the *Y. pestis* Δ*relA* mutant displayed slightly higher persistence than the wild type strain and much higher persistence than the Δ*ppK* mutant. Again, this supports the model as deletion of RelA, results in decreased (p)ppGpp, ultimately giving rise to more toxin activity, increased persistence and therefore tolerance to antibiotics (figure 17). The predicted outcomes based on interpretation of the model for the *Y. pestis* mutants are also presented in figures 65, 66, 67 and 68. Although this result complements the Germain *et al* (169) model of persistence, this result is contrary to that obtained for the Δ*relA* mutant when assayed by disc diffusion, as the Δ*relA* mutant displayed increased sensitivity to various classes of antibiotics, similarly to the Δ*ppK* mutant. When considered independently, the results for the persister assay and the disc diffusion assay for the Δ*relA* mutant can be explained, however when considered together these results are contradictory. It could be that the disc diffusion assay is not testing the bacteria in the same

growth state as the persister assay, as the disc diffusion assay is based on bacterial growth over the course of up to 48 hours of bacteria grown on solid medium, whereas the persister assay uses bacteria at exponential phase of growth in liquid medium.

Bacterial susceptibility and resistance to antibiotics is a population-wide effect due to genetics, whereas persistence is an epigenetic phenomenon affecting only a very small subset of a bacterial population (168). It is therefore plausible that disruption of the stringent response and polyphosphate pathways will have different effects on bacterial persistence and resistance, as demonstrated in this work. These factors should be considered when designing small molecule inhibitors as potential novel therapies for the treatment of plague, as there is the potential that inhibition of RelA or PPX, for example may lead to more persistent bacteria, and therefore an infection that is harder to treat.

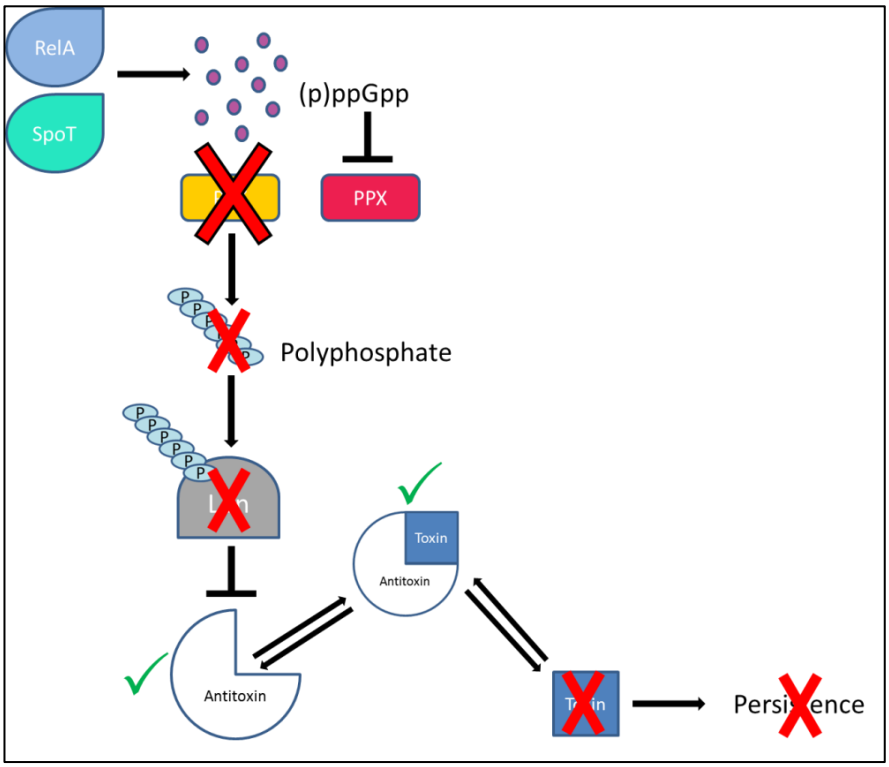

Figure 65. Schematic outlining outcome from persister assay for the *Y. pestis* Δ*ppK* mutant.

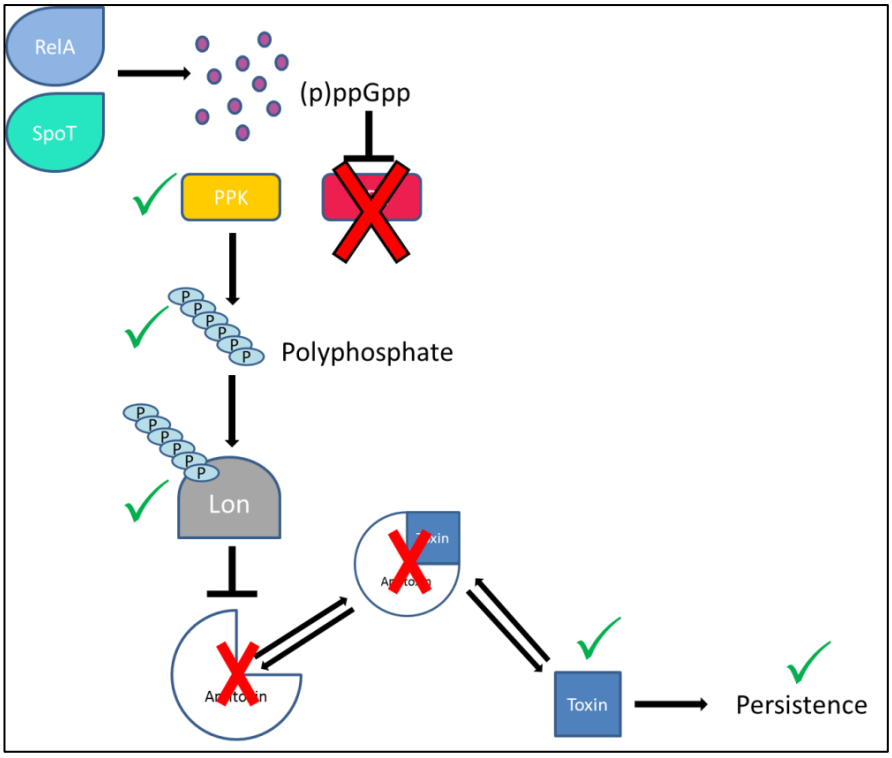

Figure 66. Schematic outlining outcome from persister assay for the *Y. pestis* Δ*ppX* mutant.

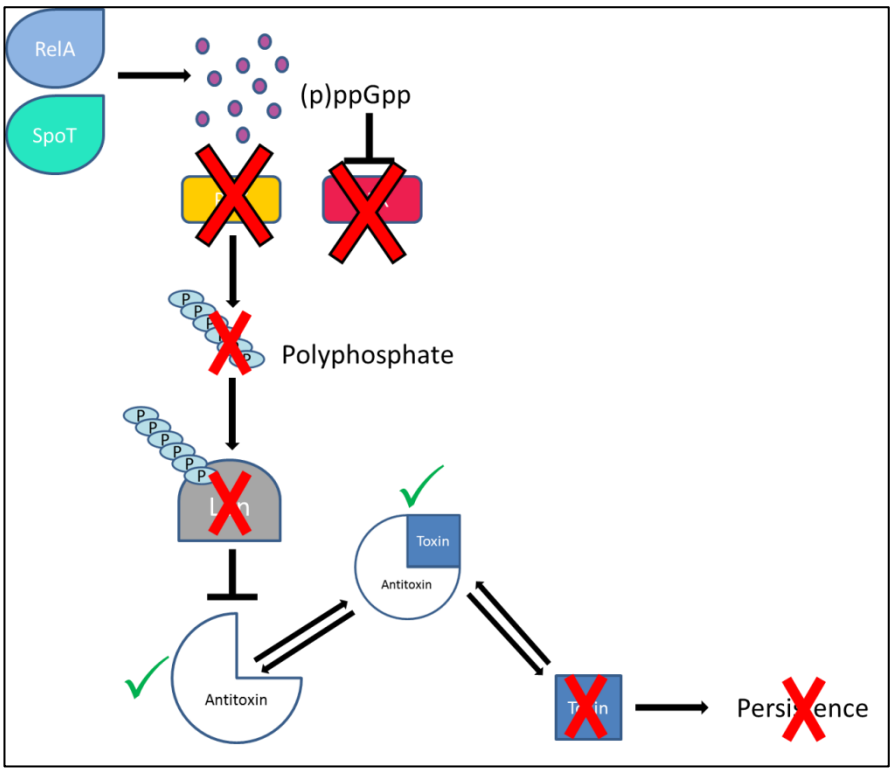

Figure 67. Schematic outlining outcome from persister assay for the *Y. pestis* Δ*ppK*/*ppX* mutant.

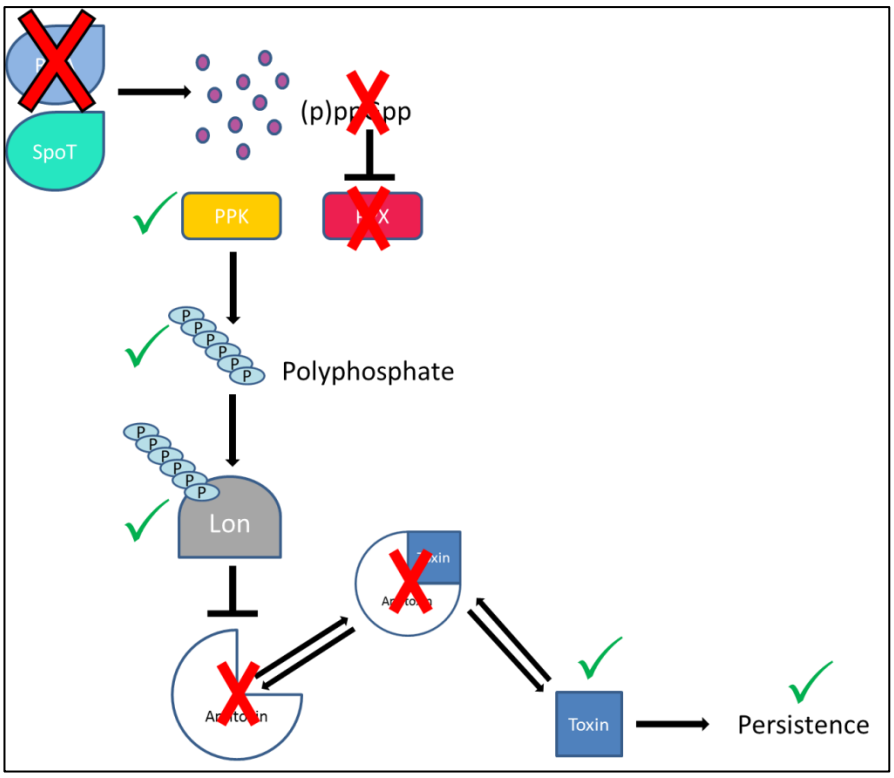

Figure 68. Schematic outlining outcome from persister assay for the *Y. pestis ΔrelA* mutant.

All *Y. pestis* mutants were also tested *in vivo,* starting with a non-mammalian model of infection, *G. mellonella*. Groups of *G. mellonella* were challenged with *Y. pestis* wild type and mutant strains. Haemolymph was then extracted from *G. mellonella* and bacterial load enumerated. Significantly fewer bacteria were recovered from the larvae challenged with the Δ*ppX* and Δ*ppK*/*ppX* mutants compared to the other mutant strains and wild type *Y. pestis*. These mutants also displayed an *in vitro* growth defect, which may have also affected growth *in vivo* rather than a *Galleria*-specific effect. Due to the pronounced growth defect observed for the Δ*ppK*/*ppX* mutant it was expected that attenuation would be apparent when this mutant was tested in a murine model of infection: as hypothesised, the Δ*ppK*/*ppX* mutant was completely attenuated. All other mutants and the wild type retained virulence and mice succumbed to infection within six days. Challenge with the higher dose of the Δ*ppX* mutant resulted in one survivor, although not statistically significant, is perhaps explained by the slight growth defect observed *in vitro*, and the lower recovery from *G. mellonella*, which indicated an impact on fitness.

The Δ*ppK*/*ppX* mutant has consistently showed reduced fitness both *in vitro* and *in vivo*, increased sensitivity to antibiotics and an inability to synthesise adequate levels of intracellular polyphosphate. These data indicate that a future inhibitor should, although technically challenging, aim to target both PPK and PPX to effectively affect intracellular bacterial growth and survival, or effectively enhance current antibiotic action. The Δ*relA* mutant also revealed interesting phenotypes in terms of antibiotic sensitivity, and should also be considered as a future inhibitor target. However, the persister assay results indicate that RelA may not be suitable due to increased persistence being observed from the *Y. pestis* Δ*relA* mutant, therefore further investigation of the global response is required to identify potentially more appropriate targets. The global response will be investigated by whole genome transcriptomic profiling and is presented in chapter 5.

3. *Francisella tularensis* Mutants

3.1. Introduction

There have been many studies into virulence determinants in the intracellular pathogen *F. tularensis* (14, 15, 86, 249, 365-372). The key virulence strategy employed by *F. tularensis* is the FPI, which encodes a putative type six secretion system (figure 6, section 1.2) , and is a duplicated genomic region in the highly virulent subspecies *tularensis* strain SCHU S4 (85, 246, 247, 370, 373-375). Although the key components of the secretion system have been identified and characterised, including the intracellular growth locus proteins IglA, IglB, IglC, and IglD, there have been no conclusive identification of secreted effector proteins (369, 375, 376). Additionally, aside from the FPI, other pathways that have been identified as contributing to *Francisella* virulence include the stringent response pathway and the polyphosphate biosynthetic pathway (14, 15).

The full genome sequence of *F. tularensis* was published in 2005 which identified approximately 2000 genes, however many of the genes are yet to be assigned biological roles (82); consequently some of these could have potential roles in virulence. One such hypothetical protein that was expressed at high levels in macrophages compared to *in vitro* culture that underwent functional characterisation was the putative polyphosphate kinase FTT1564 (14). An isogenic allelic replacement mutant was created, and inactivation of this gene resulted in abolition of polyphosphate production, an intracellular growth defect in macrophages and the mutant was attenuated in a murine model of infection (14).

Work conducted previously has also investigated the role of RelA in *Francisella* virulence and intracellular survival (15). The inactivation of the *relA* gene in *F. novicida* resulted in a mutant that was unable to produce (p)ppGpp under amino acid starvation conditions (15). The *relA* mutant also displayed delayed entry into stationary phase of growth and increased biofilm formation, which could be linked to the delay in entering stationary phase (15). When tested in a murine model of tularaemia, the mutant was attenuated, and induced protective immunity to the virulent wild type organism (15). This demonstrated the importance of (p)ppGpp as an intracellular signalling molecule for pathogenesis of *F. novicida* (15).

The stringent response regulatory pathway is hypothesised to interact with the pathway for polyphosphate biosynthesis. Therefore, cloning strategies were designed to investigate the role of the polyphosphate metabolism genes in *F. tularensis* SCHU S4. Previous work had already constructed deletion mutants for the stringent response and polyphosphate genes, *relA*, *relA*/*spoT* and *ppK*. As such to complete the analysis, a cloning strategy was designed to generate a *ppX* mutant in *F. tularensis* strain SCHU S4 as described in section 3.2. However, this mutant could not be characterised as part of this study as this strain displayed variable growth characteristics following storage at -80 °C and freeze-thawing procedures.

3.2. *Francisella tularensis* Mutant Generation

3.2.1. Bioinformatic Analysis of PPK and PPX

The *ppK* and *ppX* genes in the *F. tularensis* sub-species *tularensis* SCHU S4 genome sequence was identified by BLAST analysis previously during the genome annotation and are shown in figures 69 and 70 (82). Protein alignments were first analysed (as shown in appendix 8.3) to ensure homology to previously annotated PPX proteins in other bacteria such as *E. coli*. Promoter regions that have been predicted in the regions displayed in figure 73 were conserved in the *ppX* mutant strain. Primers to delete the *ppX* gene were designed to generate an in-frame deletion of the *ppX* gene. This is envisaged to eliminate the possibility of polar effects on the expression of adjacent genes such as *trxA1* that rely upon promoter sequences within the region of interest for this mutant.

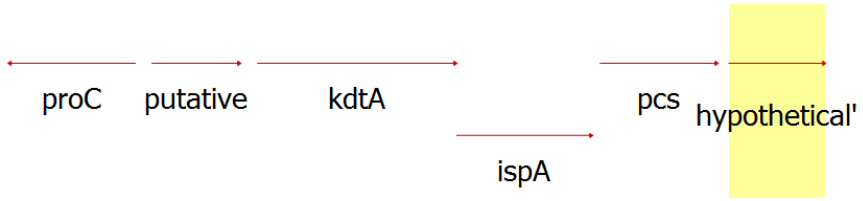

Figure 69. Gene arrangement schematic of the *ppK* (highlighted in yellow) genomic region in *F. tularensis* SCHU S4.

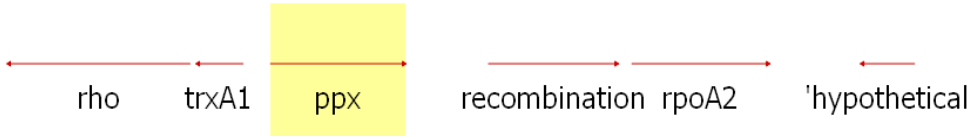

Figure 70. Gene arrangement schematic of the *ppX* (highlighted in yellow) genomic region in *F. tularensis* SCHU S4.

3.2.2. Bioinformatic Analysis of RelA and SpoT

RelA is a monofunctional enzyme that catalyses the synthesis of pppGpp from GTP (guanosine pentaphosphate) and ATP, or ppGpp from GDP (Guanosine tetraphosphate) and ATP (174) and a key enzyme in the stringent response. RelA has also been implicated in bacterial tolerance to other stringencies in addition to nutrient limitation, such as heat stress and antibiotic stress (171, 173). Therefore, it is important to characterise the impact of deletion of *relA* from the *F. tularensis* SCHU S4 genome in terms of virulence and stress tolerance. The genomic arrangements of relA and spoT are depicted in figures 71 and 72.

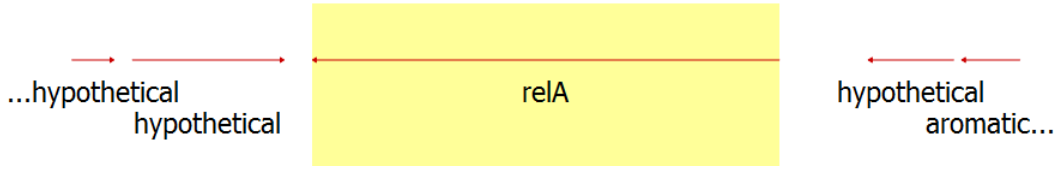

Figure 71. Gene arrangement schematic of the *relA* (highlighted in yellow) genomic region in *F. tularensis* SCHU S4.

SpoT is a bifunctional enzyme that, in addition to synthesising ppGpp from GDP or GTP and ATP, catalyses the hydrolysis ppGpp into GDP and PPi and pppGpp to GTP and PPi (174). Without the activity of SpoT, bacteria cannot degrade RelA-derived ppGpp, and the unabated accumulation of the nucleotide disrupts cell cycle control (174). It has been found that deletion of the *spoT* gene in bacteria is often lethal but deletion of both *relA* and *spoT* can completely abolish the production of (p)ppGpp (173).

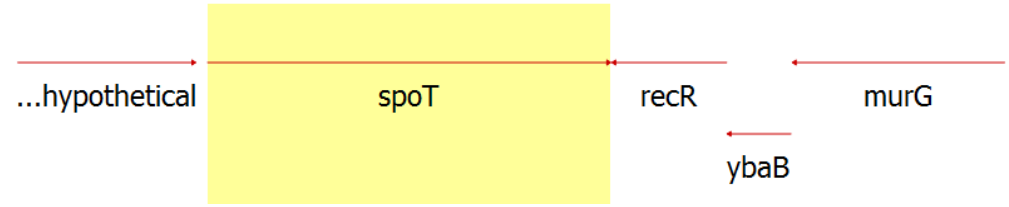

Figure 72. Gene arrangement schematic of the *spoT* (highlighted in yellow) genomic region in *F. tularensis* SCHU S4.

3.2.3. Targeted Isogenic Allelic Replacement Mutagenesis

Primers to delete the *ppX* gene were designed to generate an in-frame, unmarked deletion of the *ppX* gene (Appendix 8.5). Promoter regions that have been predicted in adjacent genomic regions (Figure 73) were conserved in the design of the *ppX* mutant strain to reduce the risk of polar effects on adjacent genes. The cloning strategy for generating the *F. tularensis ppX* mutant is outlined in figure 74. A synthetic insert was generated to incorporate approximately 500 bp upstream and downstream sequences flanking *ppX*. The deletion construct was then cloned into suicide vector pSMP75 (figure 75).

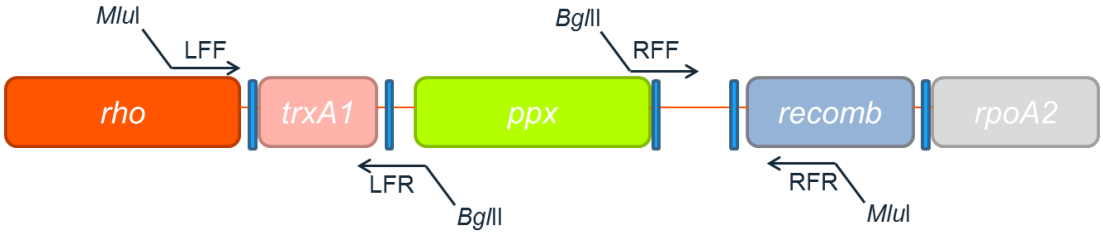

Figure 73. Schematic of the genomic region surrounding target gene, *ppX*, showing predicted promoter regions (blue bars), primer binding sites and the associated restriction sites for each primer. Primer binding sites; Left Flank Forward (LFF) incorporates *Mlu*I restriction enzyme site, Left Flank Reverse (LFR) incorporates *Bgl*II restriction enzyme site, Right Flank Forward (RFF) incorporates B*gl*II restriction enzyme site and Right Flank Reverse (RFR) incorporates *Mlu*I restriction enzyme site.

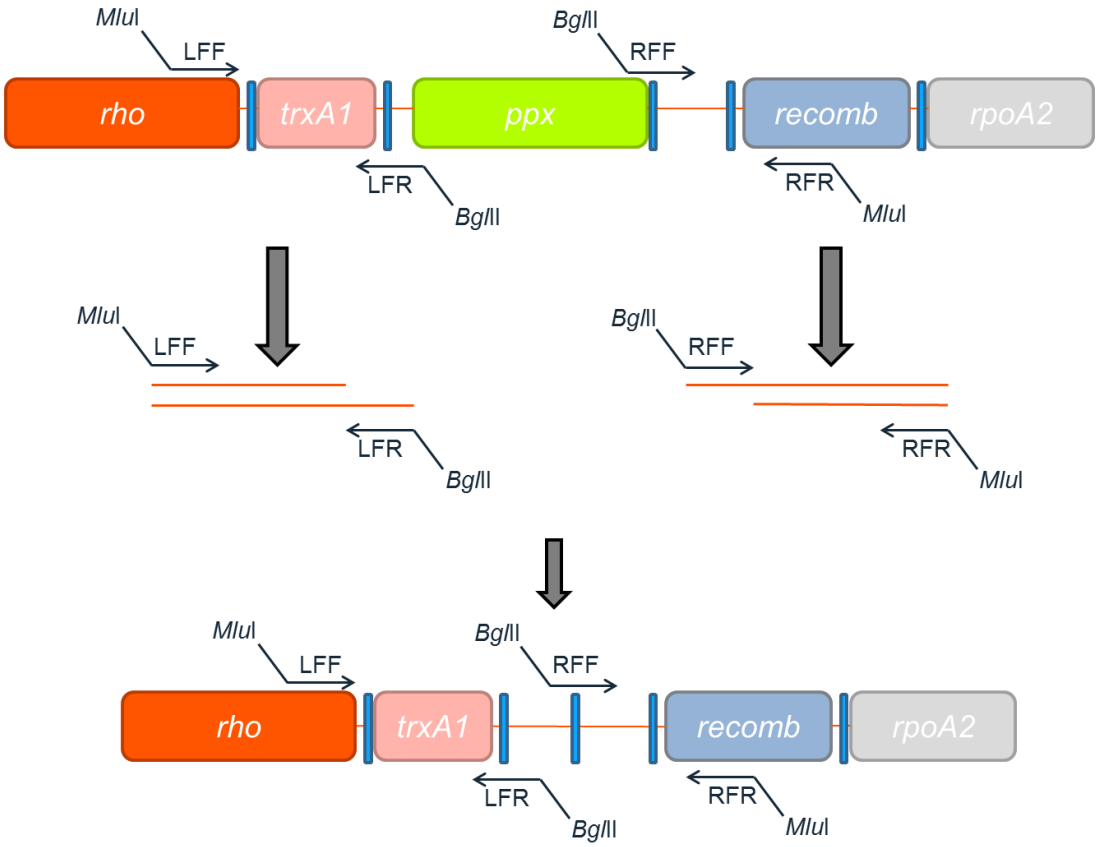

Figure 74. Schematic showing detailed isogenic allelic replacement cloning strategy to delete *ppX* from *F. tularensis* SCHU S4. Predicted promoter sites are indicated in blue and primer binding sites with appropriate restriction enzyme sites incorporated are labelled as; Left Flank Forward (LFF) incorporating *Mlu*I restriction enzyme site, Left Flank Reverse (LFR) incorporating *Bgl*II restriction enzyme site, Right Flank Forward (RFF) incorporating B*gl*II restriction enzyme site and Right Flank Reverse (RFR) incorporating *Mlu*I restriction enzyme site.

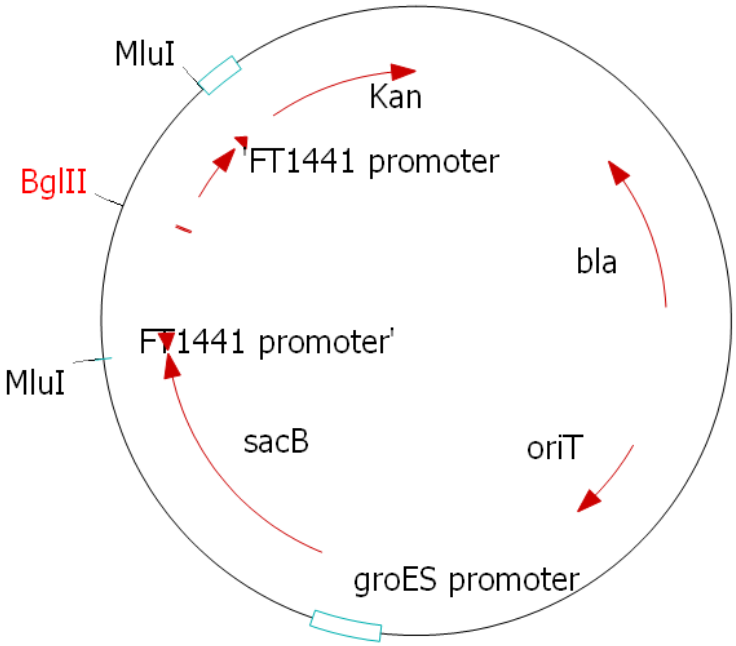

Figure 75. Circular map of suicide vector pSMP75 with the *ppX* deletion construct cloned in at the *Mlu*I restriction enzyme site.

Ligation of the deletion construct into pSMP75 was confirmed by restriction digest using the *Mlu*I restriction enzyme site that had been incorporated into the deletion construct (figure 76).

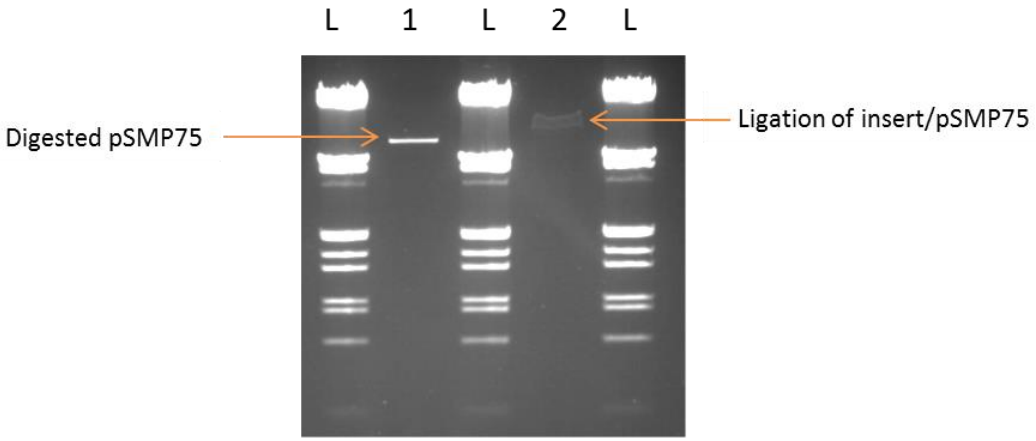

Figure 76. Lane 1 - Digested and dephosphorylated pSMP75. Lane 2 - Ligation of deletion construct into pSMP75. L = Molecular weight marker III (Roche Diagnostics).

Following successful ligation of the deletion construct into pSMP75 (figure 76), the plasmid was transformed into competent *E. coli* JM109 cells. 100 µL of each transformation was plated onto L-agar containing 50 µg/mL kanamycin as pSMP75 confers kanamycin resistance. Successfully grown single colonies (15 in total) were picked onto grid plates and colony PCR was conducted using the LFF and RFR primers (listed in appendix, section 8.5) to check for the presence of the deletion construct (figure 77). Colony PCR directly from the transformant colonies was unsuccessful. Due to the number of colonies present on the plates and the successful transformation control plate, it was decided to carry out DNA isolation and purification. Subsequently PCR analysis was carried out on isolated DNA to confirm the presence of the suicide plasmid containing the deletion construct (figure 78). Colonies were then stored as glycerol freezer stocks.

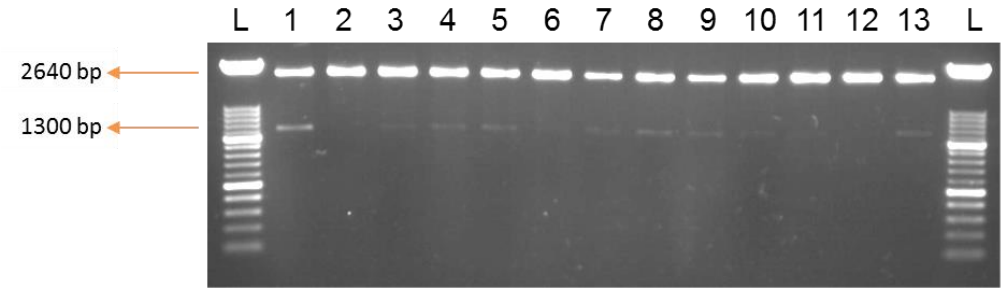

Figure 77. Restriction digests (*Mlu*I) of DNA minipreps of the successful transformant colonies. Bands of the correct size are shown which are present in lanes 1, 3, 4, 5, 7, 8, 9 and 13. L = Molecular weight marker XIV (Roche Diagnostics).

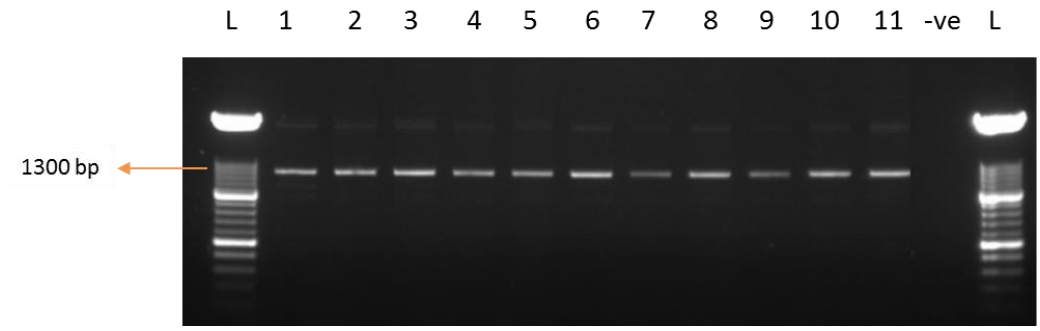

Figure 78. PCR verification of deletion constructs using LFF/RFR primer pair from DNA isolates of successful transformant clones 1-11 showing the expected product size of 1303 bp. L = Molecular weight marker XIV (Roche Diagnostics).

The suicide plasmid pSMP75 encoding the deletion construct is stably maintained in *E. coli* S17 *pir,* however it is unstable in *Francisella*. As such pSMP75 can be used to transfer genetic material into *Francisella* species by conjugation. Conjugations were set up between the donor *E. coli* strain and *F. tularensis* SCHU S4. In short, *E. coli* and *F. tularensis* cells were mixed and spotted onto Thayer Martin agar plates. Bacterial growth was removed and spread onto Thayer Martin agar plates supplemented with polymyxin B to eliminate *E. coli* growth and kanamycin to select for putative *F. tularensis* integrant clones containing pSMP75, which confers kanamycin resistance. Isolated colonies from these plates were then sub-cultured onto Thayer Martin agar plates supplemented with sucrose to select for the crossover event thus confirming excision of pSMP75 from the *F. tularensis* genome. The suicide vector pSMP75 contains the gene *sacB* which encodes levansucrase and can be used as a counter-selectable marker for isogenic allelic replacement mutagenesis. Expression of *sacB* in Gram negative bacteria is lethal in the presence of sucrose. However sucrose selection is used in this procedure to confirm the second crossover event resulting in the loss of the pSMP75 vector from the *F. tularensis* genome, and subsequent incorporation of the deletion region. Therefore culturing bacteria that have been transformed with a plasmid encoding *sacB* on media supplemented with sucrose will only give rise to bacteria that have successfully lost the plasmid. If the plasmid is still incorporated into the genome *sacB* will be expressed and cause lethal toxicity in the presence of sucrose. Allelic replacement was further confirmed by sub-culturing colonies from sucrose-supplemented plates onto kanamycin-supplemented plates to ensure clones were now kanamycin sensitive also. Gram's staining was carried out to ensure isolated colonies from sucrose-supplemented plates were indeed *F. tularensis* and not a

contaminant bacterium as discussed below in section 3.2.5. Colonies were analysed by PCR using the upstream forward and downstream reverse primer pair (appendix 8.5) to confirm the presence of the deletion construct and compare the genomic region size to the wild type organism. PCRs analysed by gel electrophoresis were not conclusive in confirming the incorporation of the Δ*ppX* deletion construct into the *F. tularensis* genome. It was thought the colonies that had been subjected to Gram's staining were potential integrant clones; as such PCR was carried out using a primer pair specific to the kanamycin resistance cassette present on pSMP75 (figure 79).

3.2.4. Mutant Verification by Polymerase Chain Reaction

Following sucrose selection of strains positive for the kanamycin resistance cassette PCR was carried out to determine if mutants had been obtained (figure 79). Although a high degree of miss-priming was observed, the correct band size was clearly visible therefore further optimisation was not carried out. PCR amplification of the genetic region that had been targeted for mutagenesis was expected to give a band size of 1643 bp for the wild type and a band size of 1289 bp for the mutant strains. Lane two in figure 80 below shows a strong band at the desired size for a mutant and no presence of a band at the size of the wild type, indicating that the second crossover event successfully incorporated the deletion cassette to replace the wild type copy of *ppX*.

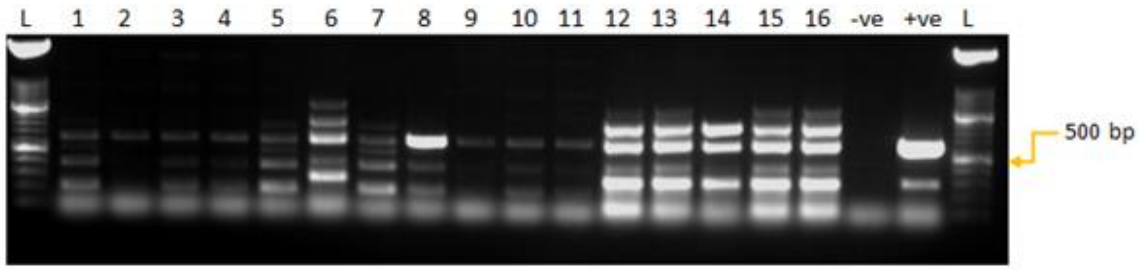

Figure 79. Amplification of the kanamycin resistance gene of pSMP75 for *F. tularensis* Δ*ppX* colonies 1-16 from Thayer Martin/sucrose agar plates. Positive control plasmid DNA of pSMP75. Expected band size of 494 bp. L = molecular weight marker XIV (Roche Diagnostics).

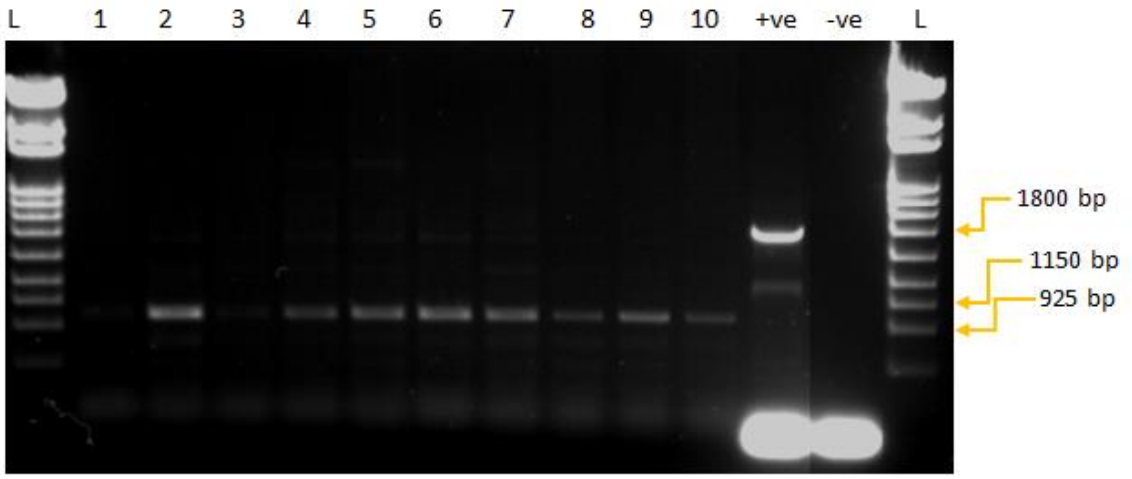

Figure 80. Amplification of *F. tularensis* Δ*ppX* deletion construct from colonies 1-10 from Thayer Martin/sucrose agar plates using LFF and RFR primer pair. Positive control used was *F. tularensis* SCHU S4. The expected band size was 1643 bp for the wild type and 1289 bp for the mutant strains. L = molecular weight marker IV (Roche Diagnostics).

3.2.5. Mutant Verification by Gram's Staining

Gram's staining was carried out on fixed cells from mutants and wild type strains to confirm *F. tularensis* SCHU S4 cell morphology post mutagenesis. All strains we deemed to have characteristic *F. tularensis* cell morphology comparable to that of wild type *F. tularensis* SCHU S4 cells. *F. tularensis* samples were also compared to a control *E. coli* cell slide for reference.

3.3. *F. tularensis* Mutant Characterisation *in Vitro*

3.3.1. Environmental Stress Sensitivity Assays – Antibiotics

Previous research into the stringent response in wild type *E. coli*, *Staphylococcus aureus* and *P. aeruginosa* has reported induction of prolonged antibiotic tolerance by nutrient depletion, particularly amino acids (171, 203, 314, 377). In addition to this finding Nguyen *et al* (171), found that inactivation of the stringent response genes *relA* and *spoT* gave rise to improved antibiotic efficiency in murine infections with *P. aeruginosa* and reduced the emergence of resistant mutants (171). These combined beneficial effects in response to starvation indicates that targeting these adaptations to enhance the activity of existing antimicrobials is a promising approach to mitigate the public health crisis caused by the scarcity of new antibiotics (171) and antibiotic resistance.

To investigate the effect of inactivation of *relA*, *spoT* and the polyphosphate metabolism gene, *ppK* on antibiotic sensitivity of *F. tularensis*, disc diffusion experiments were carried out. Antibiotic discs were selected to cover various mechanisms of action (table 7). Similarly to previous results obtained for the *Y. pestis* mutants, it was observed that *F. tularensis* mutants defective in the stringent response and polyphosphate metabolism were significantly more susceptible to the action of various classes of antibiotics (figure 81).

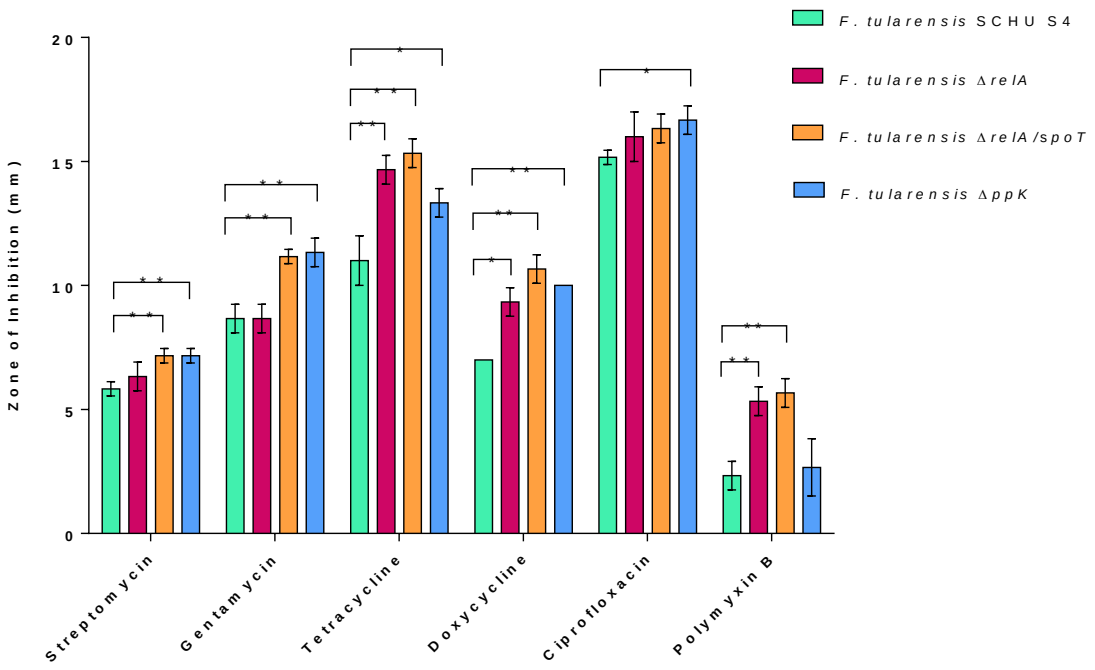

Figure 81. Zones of inhibition measured in lawns of *F. tularensis* SCHU S4 wild type and mutant strains (Δ*relA* Δ*relA/spoT* and Δ*ppk)* surrounding antibiotic discs. Antibiotics used; 10 µg streptomycin, 10 µg gentamycin, 30 µg tetracycline, 30 µg doxycycline, 5 µg ciprofloxacin and 100 µg polymyxin B. Statistical significance determined by unpaired t-test with Welch's correction for unequal variance (* - $P \leq 0.05$, ** - $P \leq 0.01$).

Specifically, *F. tularensis* Δ*relA/spoT* and Δ*ppk* mutants were significantly more sensitive to killing by 10 µg streptomycin (P = 0.0048 and P = 0.0048 respectively) and 10 µg gentamycin (P = 0.0072 and P = 0.0048 respectively) than wild type *F. tularensis* SCHU S4. *F. tularensis* Δ*relA,* Δ*relA/spoT* and Δ*ppk* were all significantly more sensitive to 30 µg tetracycline (P = 0.01, P = 0.0061 and P = 0.0357 respectively) and 30 µg doxycycline (P = 0.0198, P = 0.0082 and P = 0.0028 respectively) than the wild type strain. Only the Δ*ppk F. tularensis* mutant was more susceptible to killing by 5 µg ciprofloxacin (P = 0.0286) than the wild type strain. Ciprofloxacin is the current antibiotic therapy of choice for the treatment of tularaemia, and has very effective antibiotic action against all *F. tularensis* strains; therefore as the Δ*ppk* mutant appeared less fit when grown *in vitro*, this result may not be specific. Polymyxin B was also included as an antibiotic that *F. tularensis* has known resistance to. The Δ*relA* and Δ*relA/spoT* mutants showed a statistically significant increase in susceptibility to killing by 100 µg polymyxin B (P = 0.0031 and P = 0.0021 respectively), whereas the Δ*ppk* mutant showed no difference to the wild type. Although the Δ*relA* and Δ*relA/spoT* mutants showed a significant

difference in their zones of inhibition compared to wild type *F. tularensis*, the zones of inhibition themselves were significantly smaller than for the other antibiotics tested, except for streptomycin (for gentamycin P = 0.0022, for ciprofloxacin P = 0.0003, for tetracycline = P = 0.0003 and for doxycycline P = 0.0044). These results indicate that *F. tularensis* strains defective for the stringent response and polyphosphate metabolism genes are less able to resist killing by various antibiotics, irrespective of the mechanism of action of the antibiotic. These results support findings from previous studies into antibiotic susceptibility of stringent response defective mutants in *P. aeruginosa* (171) and previous results obtained for this project with *Y. pestis* as discussed in section 2.3.3.

Antibiotic	**Mode of Action**	**Mutant/strain**	**Statistical significance**
Streptomycin	Protein synthesis inhibition	*F. tularensis* Δ*relA*	**
		F. tularensis Δ*relA/spot*	-
		F. tularensis Δ*ppk*	**
Gentamicin	Protein synthesis inhibition	*F. tularensis* Δ*relA*	**
		F. tularensis Δ*relA/spot*	-
		F. tularensis Δ*ppk*	**
Tetracycline	Protein synthesis inhibition	*F. tularensis* Δ*relA*	**
		F. tularensis Δ*relA/spot*	**
		F. tularensis Δ*ppk*	*
Doxycycline	Protein synthesis inhibition	*F. tularensis* Δ*relA*	*
		F. tularensis Δ*relA/spot*	**
		F. tularensis Δ*ppk*	**
Ciprofloxacin	Cell division inhibition	*F. tularensis* Δ*relA*	-
		F. tularensis Δ*relA/spot*	-
		F. tularensis Δ*ppk*	*
Polymyxin B	Cell membrane destabilisation	*F. tularensis* Δ*relA*	**
		F. tularensis Δ*relA/spot*	**
		F. tularensis Δ*ppk*	-

Table 7. Table summarising results from antibiotic disc assays for *F. tularensis* mutant strains, showing statistical significance (compared to wild type) of zones of inhibition surrounding discs containing different antibiotics (* - $P \leq 0.05$, ** - $P \leq 0.01$).

3.4. *Francisella tularensis* Mutant Characterisation *in Vivo*

3.4.1. Mammalian Model of Infection – Murine

Previously created *F. tularensis* mutants (14, 15) were tested for virulence in a murine model of infection and compared to the wild type SCHU S4 strain. Each mutant and the wild type were delivered in a sub-cutaneous challenge at the following doses as shown below in table 8;

Bacterial Strain	Low Dose (CFU)	High Dose (CFU)
F. tularensis Δ*relA*	49	490
F. tularensis Δ*relA/spoT*	-	1.2×10^6
F. tularensis SCHU S4 wild type	-	235 or 100

Table 8. Challenge doses based on viable counts of *F. tularensis* mutant attenuation study.

Previously created mutants in *F. tularensis* (14, 15) were tested for virulence in a murine model of infection. Following sub-cutaneous challenge each group of mice were monitored over the course of 14 days. The single mutant (Δ*relA)*, showed no attenuation throughout the study, and mice died at similar rates to the wild type bacterium (figure 82). However, the double Δ*relA*/*spoT* mutant resulted in no deaths throughout the duration of the study, suggesting this mutant was attenuated (figure 83).

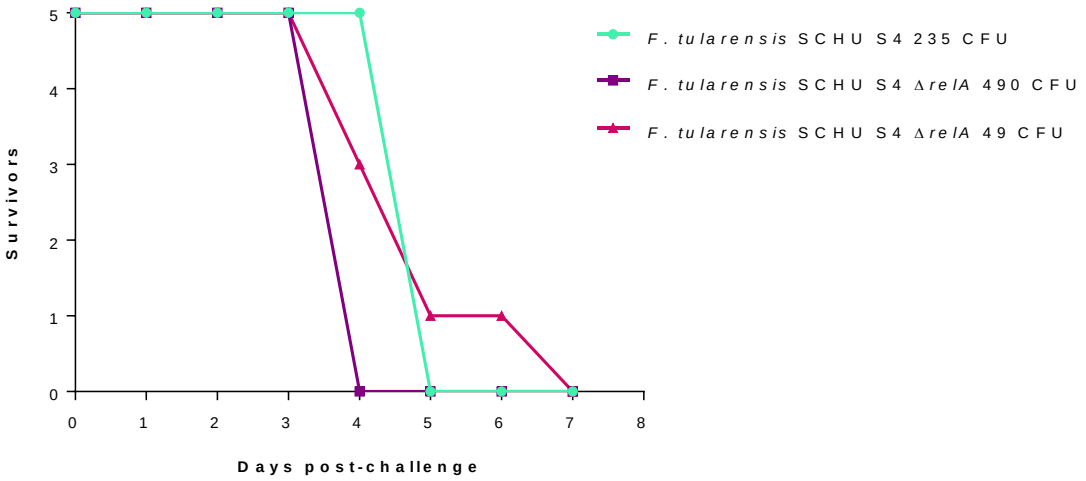

Figure 82. Number of murine survivors over a 7 day time course following sub-cutaneous challenge with 50-500 CFU *F. tualrensis* SCHU S4 wild type or Δ*relA*.

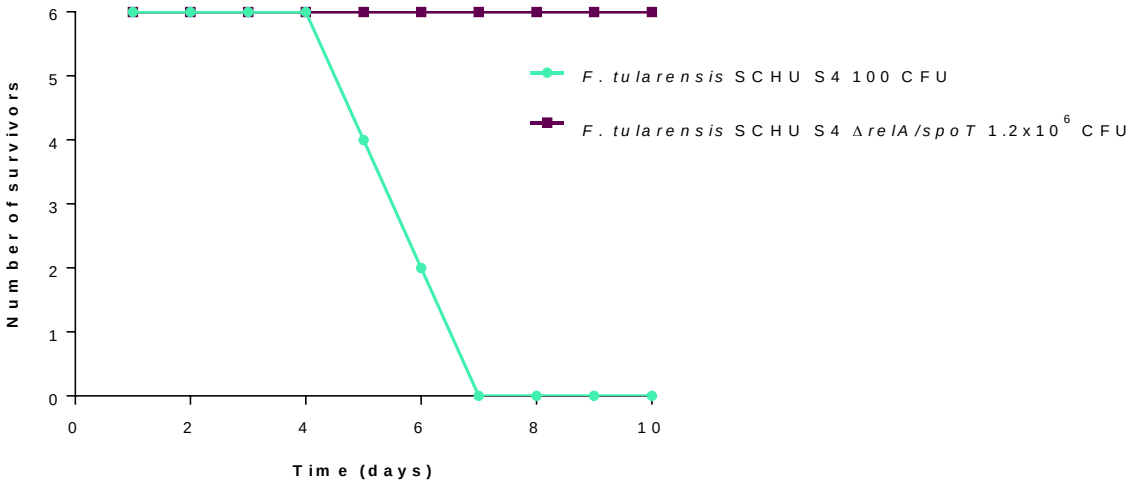

Figure 83. Number of murine survivors over a 10 day time course following sub-cutaneous challenge with 100 - 10^6 CFU *F. tualrensis* SCHU S4 wild type or Δ*relA*/spoT.

As the double Δ*relA*/*spoT* mutant was attenuated in the mouse model, this mutant was tested for immunologic protection against a wild type challenge (figure 84). Surviving animals were challenged with either $1.2X10^6$ or $1.2x10^5$ CFU. As shown below in figure 84, survival of mice immunized with either dose of the Δ*relA*/*spoT* mutant was not significantly increased compared with that of naïve animals. These results demonstrated that vaccination with *F. tularensis* Δ*relA*/*spoT* does not induce protective immunity against wild-type *F. tularensis* SCHU S4 infection *in vivo*. There was one murine survivor in the $1.2X10^6$ challenge dose group indicating that perhaps some immunologic effect was induced by immunisation with the Δ*relA*/*spoT* mutant at the higher dose, however this was not significant and therefore cannot be used as evidence of a protective effect.

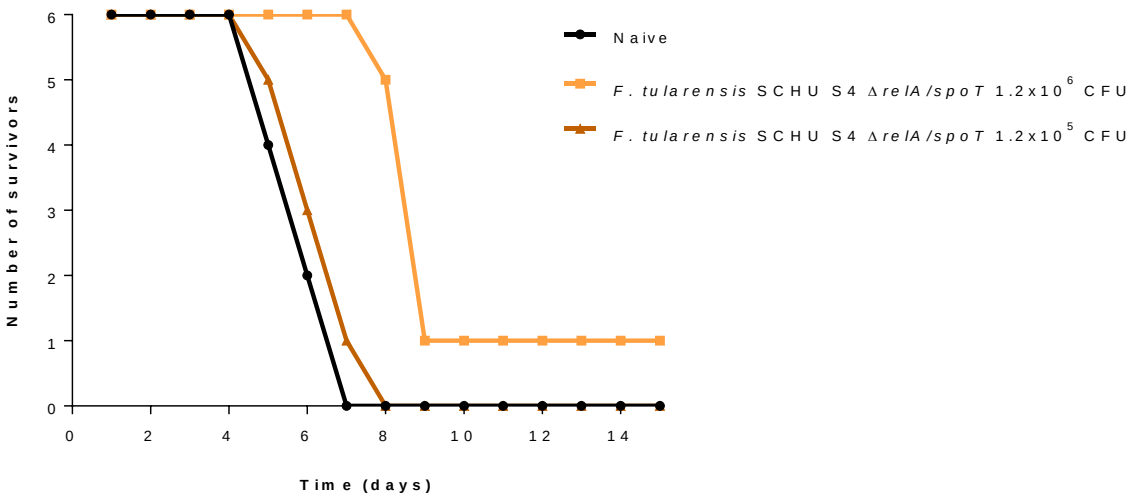

Figure 84. Number of murine survivors over a 14 day time course following sub-cutaneous challenge with 50-500 CFU *F. tualrensis* SCHU S4 wild type.

3.5. Discussion and Conclusions *F. tularensis* Mutants

Previous studies had demonstrated that the Δ*ppK F. tularensis* mutant was defective for intracellular polyphosphate production (14) when tested using a malachite green based spectrophotometric assay (311, 312). We also observed this result when our *Y. pestis* Δ*ppK* and Δ*ppK*/*ppX* mutants were tested using the same assay as discussed in section 2.3.2. These results support findings from experiments with other organisms that found disruption of PPK and PPX impacts the ability of bacteria to effectively control intracellular levels of polyphosphate (14, 313). Given the association of polyphosphate with bacterial virulence (14, 378-381), this also provides evidence for targeting the polyphosphate biosynthesis genes for novel antimicrobial inhibitors.

Previous studies have linked the stringent response to bacterial antibiotic sensitivity (171, 314), indicating that active stringent response triggers a broad spectrum increase in tolerance to antibiotic treatment. Antibiotic disc diffusion assays described herein revealed an increase in sensitivity to various classes of antibiotics when *F. tularensis* mutants defective for polyphosphate and stringent response genes were tested (section 3.3.1). Specifically, Δ*ppK,* Δ*relA* and Δ*relA/spoT* mutants showed increased sensitivity to killing by streptomycin, gentamycin, tetracycline, doxycycline and polymyxin B. As *F. tularensis* is usually resistant to polymyxin B (217, 382, 383), this result emphasises how inactivation of the stringent response and polyphosphate biosynthetic pathways decrease fitness and stress response mechanisms in *F. tularensis*. This result also supports previous hypotheses suggesting the stringent response impacts antibiotic susceptibility (171, 314); and as this work demonstrated that disruption of polyphosphate biosynthesis or the stringent response increases sensitivity to antibiotics, this suggests that these gene targets could have potential as antibiotic adjuvants for enhancement of efficacy of current therapies.

There were no obvious growth defects observed for the Δ*ppK,* Δ*relA* and Δ*relA/spoT* mutants. As previous research suggested links between the stringent response, polyphosphate biosynthesis and virulence (378, 379, 384, 385) it was anticipated that some of these mutants would be attenuated. It was previously found that the *F. tularensis* Δ*ppK* mutant was attenuated in a murine model of infection (14), supporting the links of polyphosphate synthesis to virulence. It was also observed that the Δ*relA/spoT* mutant was attenuated, even

when mice were challenged with 1 x 10^6 CFU, which is a dose 1x10^5 CFU higher than a lethal dose with the wild type strain. The single Δ*relA* mutant was not attenuated and all mice in both the high and low challenge groups succumbed to infection within seven days. Previous studies in the literature have stated that single Δ*relA* mutants in various bacteria including *Y. pestis* have not been attenuated in an animal model of infection (16). This is likely to be due to the fact that the bifunctional protein SpoT is still present in these mutant strains and is compensating for the activity of relA by both synthesising and degrading (p)ppGpp to maintain appropriate levels during stressful conditions.

Overall, the results presented herein provide further evidence that the stringent response biosynthetic pathway and the associated polyphosphate biosynthetic pathway could provide suitable targets for the development of novel medical countermeasures to treat tularaemia, amongst other highly pathogenic bacterial infections also discussed in this thesis. The results obtained for the characterisation of the *F. tularensis* mutants when tested for sensitivity to various classes of antibiotics suggest that these genetic targets could be particularly applicable for the development of antibiotic adjuvants, to enhance the efficacy of current, and limited therapeutic options.

4. *Burkholderia pseudomallei* Mutants

4.1. Introduction

Regulation studies into virulence and stress response mechanisms have revealed the importance of both global and specific response regulators in *B. pseudomallei*. For example, studies conducted by Korbsrisate *et al* and Subsin *et al* have elucidated environmental stress response roles of the sigma factors RpoE and RpoS respectively (21, 386). Korbsrisate *et al* reported that RpoE is important in the adaptation of *B. pseudomallei* to reactive oxygen intermediates as an rpoE deletion mutant was significantly more sensitive to H_2O_2 and menadione (O_2^- generator) (386). Subsin *et al* demonstrated that deletion of the sigma factor RpoS increased *B. pseudomallei* sensitivity to carbon starvation and oxidative stress induced by H_2O_2 and the redox-cycling agent methyl viologen (21). It was also reported that RpoS expression was regulated according to growth phase, as levels of RpoS increased during exponential phase of growth and peaked upon entry to stationary phase (21). Proteomics studies have also revealed that expression of up to 70 proteins are RpoS-dependent according to analysis of *rpoS*$^+$ and *rpoS*$^-$ strains of *B. pseudomallei* (387) indicating that RpoS gives rise to differential gene expression on a global scale. Furthermore, virulence related regulatory mechanisms have been identified in the highly virulent *B. pseudomallei* strain 1909a. For example, BprD a predicted transcriptional regulator which is located in the TTSS is upregulated during infection in mice (388). Additionally, BprC which is a regulator of the T6SS has also been shown to be required for full virulence of *B. pseudomallei* in murine infection models (388).

As discussed more broadly in section 1.5.2, bacteria encode a class of enzymes called catalases to respond to damage caused by oxidative stress, specifically caused by H_2O_2. Loprasert *et al* investigated the regulation of the *katG-dpsA* operon in *B. pseudomallei* and its role in *B. pseudomallei* survival under oxidative stress conditions and found that *katG* (which encodes a catalase-peroxidase gene) and *dpsA* (which encodes a non-specific DNA binding protein) are regulated at the transcriptional level and are upregulated in the presence of oxidants such as H_2O_2 (389).

Until relatively recently however, little has been understood of the stringent response and polyphosphate metabolism in the highly virulent intracellular pathogen *B. pseudomallei* strain K96243. Müller *et al* (181) have recently investigated the role of RelA and SpoT in *B. pseudomallei* virulence and immunity by generating deletion mutants, and characterising these *in vitro* and *in vivo* (93). This research found that a double Δ*relA*/*spoT* mutant displayed a defect in stationary-phase survival and intracellular replication in murine macrophages. Moreover, the mutant was attenuated in both a non-mammalian model of infection *G. mellonella* and in both acute and chronic murine models of melioidosis (181). This group also described the vaccination of mice with the Δ*relA*/*spoT* mutant which resulted in partial protection against infection with wild-type *B. pseudomallei* K96243 (181). As such, (p)ppGpp signalling appears to comprise an essential regulatory component influencing virulence gene expression and adaptation to stress in *B. pseudomallei*. These strains have been obtained as a generous gift from the University of Exeter for further *in vitro* characterisation on this project. In addition, deletion mutants will be generated for the key genes involved in polyphosphate metabolism, *ppK* and *ppX*.

As an intracellular pathogen that is acquiring multiple drug resistance genes (43, 46), that has both public health and defence implications and is currently without a licenced vaccine, *B. pseudomallei* has a requirement to be the focus of research into novel medical countermeasures such as antibiotics and small molecule inhibitors.

4.2. *Burkholderia pseudomallei* Mutant Creation

4.2.1. Bioinformatic Analysis of PPK and PPX

Protein alignments were first analysed as shown in Appendix 8.7 to ensure homology to previously annotated PPK and PPX proteins in other bacteria such as *Pseudomonas aeruginosa*. The *ppK* and *ppX* genes in the *B. pseudomallei* K96243 genome sequence were previously identified by BLAST nucleotide analysis during the genome annotation (17). The PPK shown in figure 85 is a PPK1 (accession number Q63V75), however *B. pseudomallei* K96243 also encodes a PPK2 (accession number Q63KT2) in addition to PPK1, both of which reside at different loci on chromosome 2. It was decided to first target allelic replacement of PPK1 and test the mutant strain for phenotypes as a result of this mutation. If no phenotypes were observed in the PPK1 mutant PPK2 would then be targeted for mutagenesis. Figure 86 below shows the genomic arrangement of *ppX* in *B. pseudomallei*.

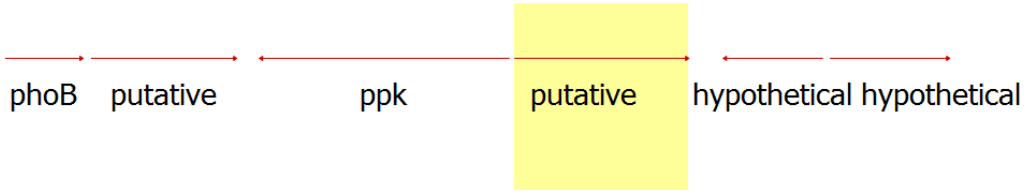

Figure 85. Schematic of the *ppK1* (shown as ppk) and *ppX* genetic region in *B. pseudomallei* K96243. The *ppX* gene is not currently annotated in the *B. pseudomallei* K96243 genome but it is shown as the putative gene highlighted in yellow in this schematic.

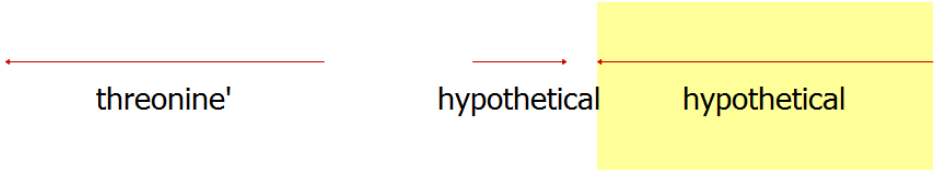

Figure 86. Schematic showing the *ppK2* region in *B. pseudomallei* K96243. PPK2 is currently not annotated in the *B. pseudomallei* K96243 genome but it is shown as the hypothetical gene highlighted in yellow in this schematic. Clear space indicates non-coding region.

4.2.2. Targeted Isogenic Allelic Replacement Mutagenesis

Primer pairs were designed to generate an in-frame unmarked deletion of *ppK*, *ppX* and a double deletion of *ppK*/*ppX* in *B. pseudomallei* K96243 (listed in tables 26, 27 and 28 in appendix section 8.8). A previously established allelic replacement mutagenesis method outlined in Logue *et al* (390), was adopted for the generation of these mutants. Firstly, upstream and downstream DNA sequences, approximately 1 kb in length, flanking the target gene were amplified from *B. pseudomallei* K96243 gDNA using primers listed in appendix 8.8. The protocol then states that the flanking regions should be ligated together and re-amplified using the upstream forward and downstream reverse primers (390). In order to speed up the mutant making process synthetic deletion constructs were commercially sourced (appendix 8.8), for subsequent cloning into the suicide vector pDM4 (figure 87) (291). Unfortunately, these mutant strains were not completed in time to be included in the characterisation experiments in this study.

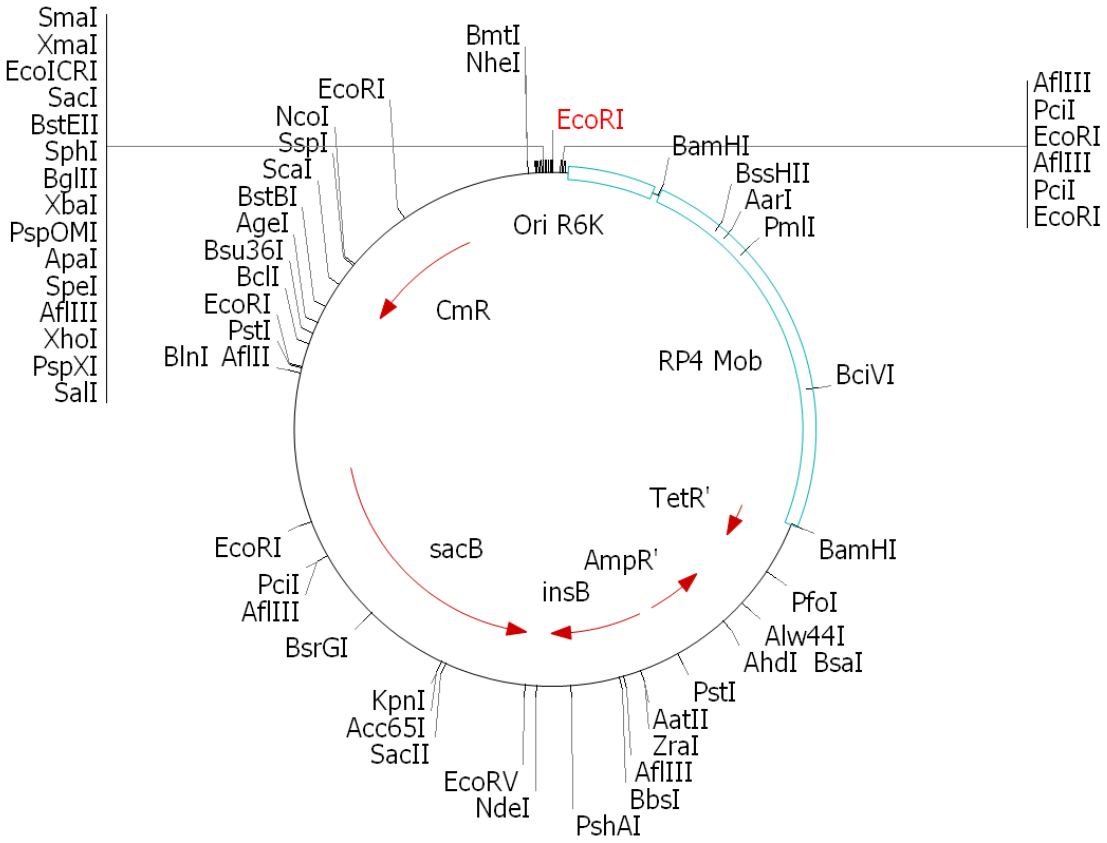

Figure 87. Circular restriction site map of suicide vector pDM4 showing the multiple cloning site, *sacB* (counter-selectable marker), AmpR (ampicillin resistance) and CmR (chloramphenicol resistance).

It was anticipated that the deletion constructs would be then transferred to *B. pseudomallei* by conjugation. However, the cloning of the deletion sequences into the suicide vector pDM4 was unsuccessful despite many optimisation steps and control transformations. Consequently due to time constraints, the decision was made to stop work on the *B. pseudomallei* Δ*ppK* and Δ*ppX* mutant generation.

4.3. *Burkholderia pseudomallei* Characterisation *in Vitro*

4.3.1. Environmental Stress Sensitivity Assays – Antibiotics

To investigate the sensitivity of the *B. pseudomallei* mutants, Δ*relA* and Δ*relA/spoT* (generously gifted by Exeter University) to antibiotics, antibiotic disc assays were carried out (results summarised in table 9).

B. pseudomallei has known resistance to the aminoglycosides so it was expected to see very small, if any zones of inhibition surrounding the discs impregnated with either streptomycin or gentamycin. Both the Δ*relA* and Δ*relA/spoT* mutants showed significantly larger zones of inhibition surrounding discs containing 30 µg tetracycline (compared to the wild type) (P = 0.0240 and P = 0.0049 respectively) and 30 µg doxycycline (P = 0.0054 and P = 0.0013 respectively). No significant differences were observed for treatment with ciprofloxacin (figure 88).

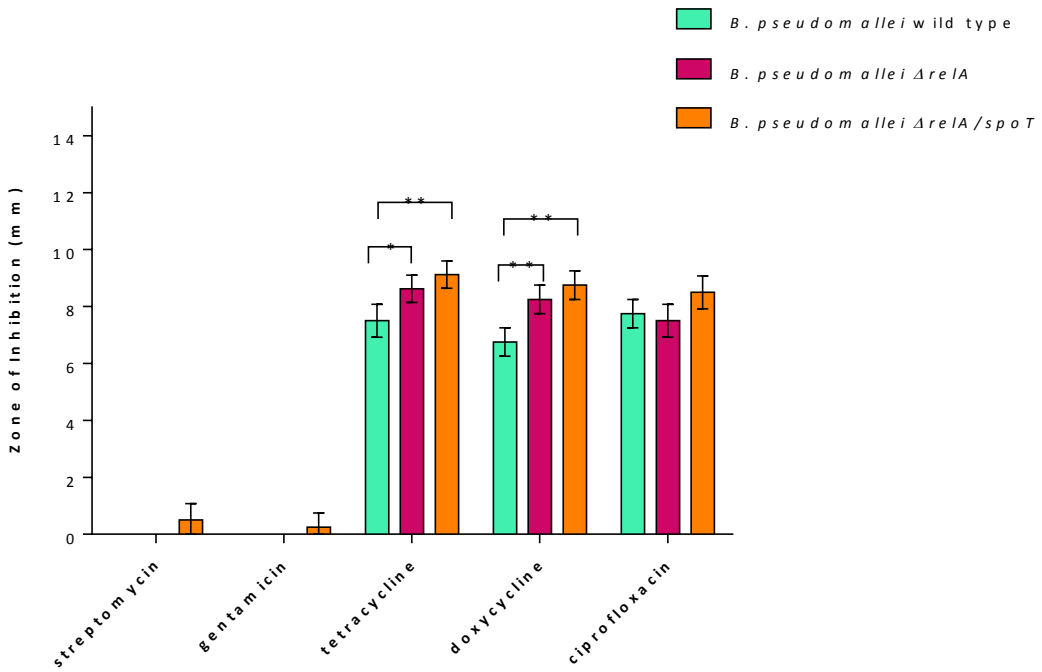

Figure 88. Zones of inhibition measured in lawns of *B. pseudomallei* K96243 wild type and mutant strains (Δ*relA* Δ*relA/spoT*) surrounding antibiotic discs containing: 10 µg streptomycin, 10 µg gentamycin, 30 µg tetracycline, 30 µg doxycycline and 5 µg ciprofloxacin. Statistical significance determined by unpaired t-test with Welch's correction for unequal variance (* - P ≤ 0.05, ** - P ≤ 0.01).

Antibiotic	Mode of Action	Mutant/strain	Statistical significance
Streptomycin	Protein synthesis inhibition	*B. pseudomallei* Δ*relA*	-
		B. pseudomallei Δ*relA/spoT*	-
Gentamycin	Protein synthesis inhibition	*B. pseudomallei* Δ*relA*	-
		B. pseudomallei Δ*relA/spoT*	-
Tetracycline	Protein synthesis inhibition	*B. pseudomallei* Δ*relA*	*
		B. pseudomallei Δ*relA/spoT*	**
Doxycycline	Protein synthesis inhibition	*B. pseudomallei* Δ*relA*	**
		B. pseudomallei Δ*relA/spoT*	**
Ciprofloxacin	Cell division inhibition	*B. pseudomallei* Δ*relA*	-
		B. pseudomallei Δ*relA/spoT*	-

Table 9. Summary of results from antibiotic disc assays for *B. pseudomallei* mutant strains. Statistical significance of zones of inhibition surrounding discs containing different antibiotics compared to wild type *B. pseudomallei* (* - $P \leq 0.05$, ** - $P \leq 0.01$).

4.4. Discussion and Conclusions *B. pseudomallei* Mutants

As described above in chapters 2 and 3, inactivation of genes involved in the stringent response in *Y. pestis*, *F. tularensis* resulted in an increase in sensitivity to various classes of antibiotics of those strains. This phenotype was less apparent in the *B. pseudomallei* mutants; however both *B. pseudomallei* mutants displayed increased sensitivity to the tetracyclines, whereas the same mutants in *Y. pestis* (section 2.3.3) and *F. tularensis* (section 3.3.1) displayed increased sensitivity to many classes of antibiotics. As the *B. pseudomallei* mutants showed attenuation of virulence when tested in a murine model of infection (181) similar to the *F. tularensis* and *Y. pestis* mutants this result was somewhat unexpected. However, *B. pseudomallei* may have further compensatory or stress response mechanisms at play that are yet to be investigated. For example, *B. pseudomallei* has a very effective efflux mechanism which may have provided sufficient activity to resist the action of the antibiotics tested in this study regardless of the mutations in the stringent response pathway.

Although the inactivation of stringent response genes in *B. pseudomallei* K96243 did not result in a generic increases in sensitivity to various antibiotics, targeting the stringent response does result in attenuation in mice (181), which indicates that this pathway could provide appropriate targets for small molecule bacterial inhibitors, vaccines or antibiotic adjuvants.

5. The Stringent Response Regulon Analysis

5.1. Introduction

The stringent response has been associated with bacterial virulence in many species to date including *C. jejuni*, *Mycobacterium tuberculosis, Shigella* and *Salmonella* species (217, 378, 379). Recent studies have now begun to discern a direct link of the bacterial stringent response to virulence gene expression in *F. tularensis*. The key virulence determinant in *F. tularensis* is the well characterised FPI, which encodes genes essential for intra-macrophage growth and virulence (85, 246, 247, 370, 373, 376). To investigate the regulation mechanisms that contribute to FPI gene expression Charity *et al* (239) carried out genetic screens and mutagenesis studies to determine the molecular basis for specific regulatory protein interactions with RNA polymerase, and the downstream effects on FPI gene expression (239). It was found that the transcription factors MglA (macrophage growth locus protein A) and SspA (stringent starvation protein A) form a complex that associates with RNAP to positively control the expression of virulence genes critical for the intra-macrophage growth and survival of *F. tularensis* as described in figure 7, section 1.2 (88, 239, 313, 391). Specifically, the MglA-SspA complex works in concert with a putative DNA-binding protein PigR (designated FevR in other organsims), together with ppGpp, to regulate the expression of target genes including the FPI encoded genes *iglA* and *pdpA* (392). Specifically, ppGpp promotes the interaction between PigR and the RNAP-associated MglA-SspA complex to activate virulence gene expression (239).

The stringent response has been implicated in virulence-associated phenotypes in a number of bacteria including *P. aeruginosa* (393) and *C. jejuni* (194). However, there have been few studies into the stringent response regulation of virulence factors other than those outlined above in *F. tularensis* (86, 239) and research into (p)ppGpp regulation of *Salmonella* virulence genes (243).

Although the aforementioned studies by Charity *et al* (86, 239) and Ramsey *et al* (392) have shed light on the regulation of FPI virulence gene expression and drawn linkages to (p)ppGpp and the stringent response, to date, however there has been no assessment of how amino acid

starvation and the stringent response affect gene expression on a global scale. We therefore undertook global gene expression studies of the stringent response are required for the highly pathogenic microorganisms *F. tularensis, Y. pestis* or *B. pseudomallei*.

5.2. *Francisella tularensis* Regulatory Analysis

5.2.1. Serine Hydroxamate Induction of the Stringent Response

The stingent respnse can be induced with the amino acid analogue serine hydroxamate, which inhibits Ser tRNA synthetase leading to an accumulation of uncharged tRNA, in turn causing ribosome stalling and RelA-dependent (p)ppGpp production (191). In our experiments we wished to induce the stringent response using a low concentration of serine hydroxamate, sufficient to induce the stringent response, whilst being present at concentrations that do not inhibit the growth of *F. tularensis* SCHU S4 in Chamberlain's Defined Medium (CDM) without DL-serine. A titration was initially carried out to establish the highest concentration of serine hydroxamate that could be added to cultures without inhibiting growth, but which did trigger the stringent response (figure 89).

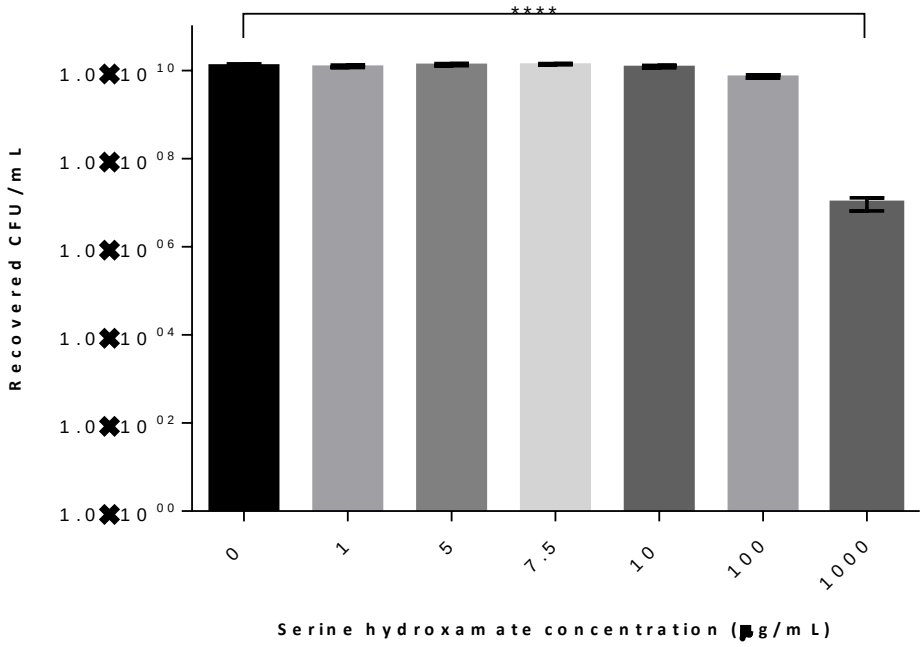

Figure 89. Serine hydroxamate titration to establish at which concentration growth of *F. tularensis* SCHU S4 is inhibited. Statistical significance determined by 1 Way ANOVA at the 95% confidence interval with Bonferroni's correction for multiple comparisons. (**** - P < 0.0001).

The addition of up to 100 μg/mL serine hydroxamate had no significant effect on the growth of *F. tularensis* SCHU S4 (figure 89). Addition of 1000 μg/mL serine hydroxamate had a toxic effect, significantly reducing the number of viable bacteria recovered from cultures, possibly inducing more general stress responses as well as the stringent response. Nearly 3000 fold fewer viable bacteria were recovered from cultures grown in the presence of 1000 μg /mL serine hydroxamate. Consequently, it was decided that cultures containing concentrations of between 0 and 100 μg /mL serine hydroxamate would be analysed by RT-PCR for virulence gene expression. A range of serine hydroxamate concentrations was envisaged to reveal any incremental differences in gene expression in response to different concentrations of serine hydroxamate.

5.2.2. Genetic Marker of Active Stringent Response - *iglC*

To establish the concentration of serine hydroxamate required to initiate the stringent response, reverse-transcriptase PCR (RT-PCR) targeting the *iglC* gene on the FPI was used to determine if the FPI genes were being expressed, as a marker of stringent response activation (86, 239). Primers iglCrtpcrF and iglCrtpcrR (table 29, appendix section 8.11) were used to assess *iglC* expression (557 bp) and mouse β-actin gene was used as a control gene with mouse total liver cDNA (540 bp). A dilution series of serine hydroxamate concentrations were tested to establish the lowest concentration at which *iglC* expression could be observed. RT-PCR showed that *iglC* was induced in the presence of very low concentrations of serine hydroxamate (1 μg /mL), and was not expressed in media without serine hydroxamate supplementation (figure 90).

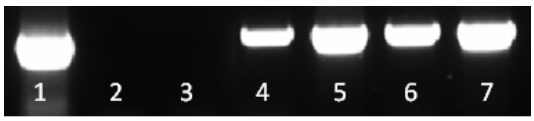

Figure 90. Expression of *iglC* in *F. tularensis* SCHU S4 can be induced or repressed by supplementing growth media with serine hydroxamate as determined by RT-PCR. Lane 1, mouse β-actin gene control amplified from mouse liver total RNA; Lane 2, no DNA control; Lane 3, cDNA from 0 μg /mL serine hydroxamate; Lane 4, cDNA from 1 μg /mL serine hydroxamate; Lane 5, cDNA from 10 μg /mL serine hydroxamate; Lane 6, cDNA from 50 μg /mL serine hydroxamate; Lane 7, cDNA from 100 μg /mL serine hydroxamate.

5.2.3. Whole Genome RNA-Sequencing

Following RT-PCR, total RNA was isolated from each *F. tularensis* culture for analysis of whole genome transcriptomic profiles by RNA-seq. In brief, the Qiagen RNA Bacteria Protect Reagent and subsequent RNeasy isolation kit was used for RNA isolation. Primer pairs specific to a region on the *iglC* gene on the FPI were then used in each RT-PCR (Appendix 8.11). RT-PCR was carried out using the Titanium one-step RT-PCR kit (ClonTech Palo Alto, USA) (394), which allows complementary DNA (cDNA) synthesis and subsequent PCR to occur in the same tube (full method outlined in section 7.3.6). The initial samples tested indicated that *iglC* is expressed in the presence of a very low concentration of serine hydroxamate (1 μg/mL), and is not expressed in media without serine hydroxamate supplementation (figure 91) indicating that *F. tularensis* is very sensitive to serine hydroxamate treatment.

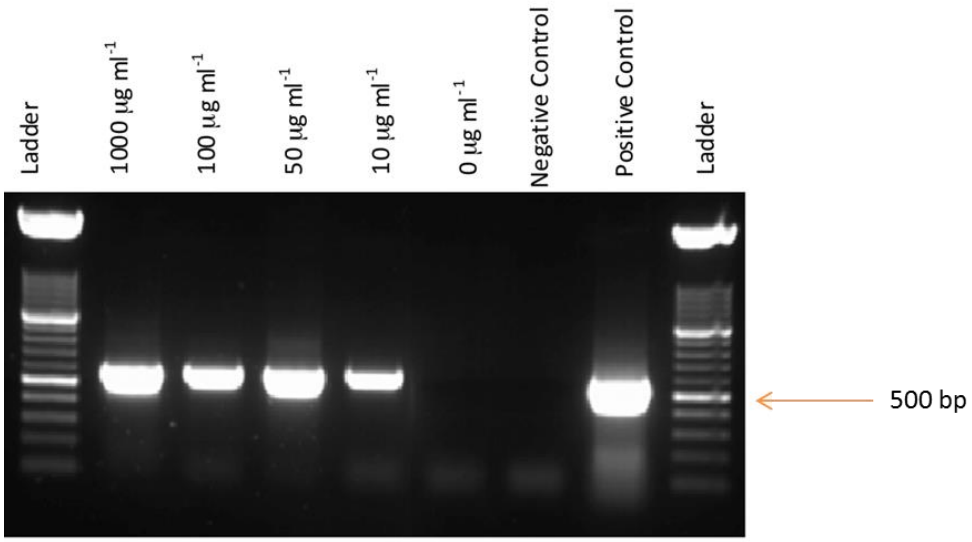

Figure 91. RT-PCR targeting the *iglC* gene on the FPI, from total RNA isolated from overnight cultures in the presence of various concentrations of serine hydroxamate. The target fragment size of 500 bp was observed in all lanes apart from RNA isolated from *F. tularensis* cultured without serine hydroxamate.

A further serine hydroxamate titration experiment was carried out in order to obtain three biological replicates for RNA isolation and subsequent RNA-Seq (figure 92).

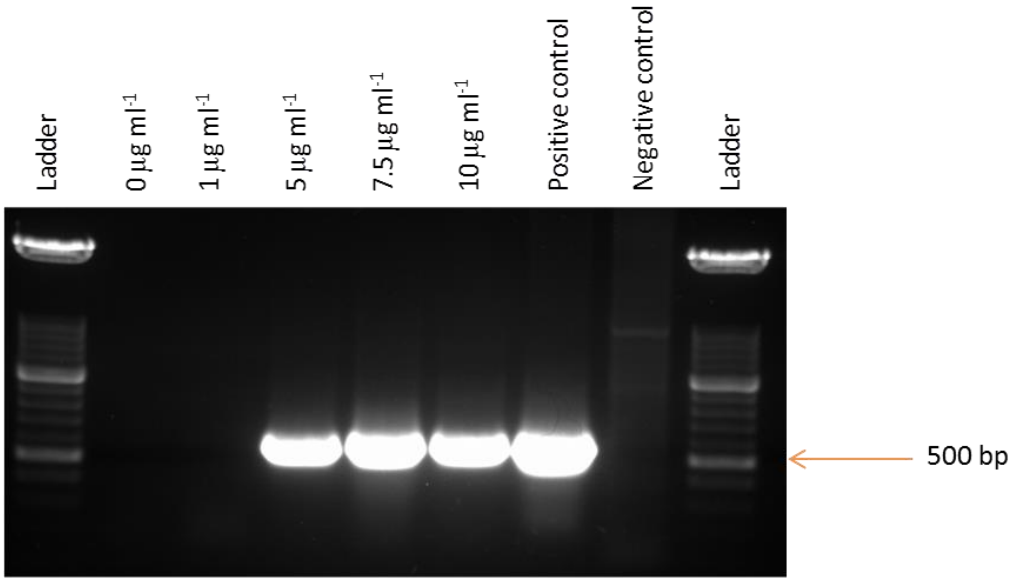

Figure 92. RT-PCR targeting the *iglC* gene on the FPI, from total RNA isolated from two further biological replicates of overnight cultures in the presence of various concentrations of serine hydroxamate. The desired fragment size of 500 bp was observed in all lanes apart from *F. tularensis* total RNA isolated from cultures in the presence of 1 μg /mL and 0 μg /mL serine hydroxamate.

Prior to sample preparation for transcriptional analysis, total RNA quality and quantity were assessed using the Agilent Bioanalyzer, shown in figures 93 and 94. Total RNA isolates from three conditions (0 μg /mL, 1 μg /mL and 10 μg /mL serine hydroxamate) in biological replicates of three were sent to the University of Exeter for RNA-seq on the Illumina MiSeq. All samples selected for RNA-Seq met the specified criteria for processing for high throughput sequencing (Bioanalyzer traces for all samples are shown in section 8.10, figures 138-146).

RNA sequencing was used to analyse the global gene expression profiles of *F. tularensis* cultures supplemented with 1 and 10 μg /mL serine hydroxamate, compared to a control culture containing no serine hydroxamate. 1 μg /mL serine hydroxamate was selected as the lowest concentration at which the stringent response was expected to be switched on, and 10 μg /mL serine hydroxamate was selected as a concentration 10 fold higher, to determine if more significant and widespread global gene expression effects could be observed.

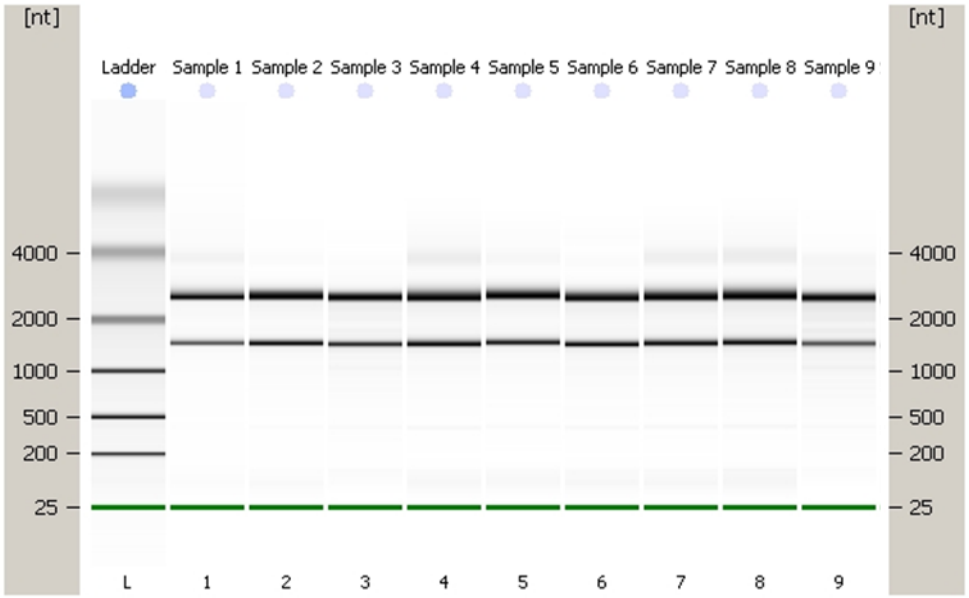

Figure 93. Electropherogram of 9 RNA samples prepared from *F. tularensis* SCHU S4 cultured in the presence of different concentrations of serine hydroxamate; samples 1, 2 and 3 – 0 μg /mL serine hydroxamate, samples 4, 5 and 6 - 1 μg /mL serine hydroxamate, samples 7, 8 and 9 - 10 μg /mL serine hydroxamate. All samples show distinct 16S and 23S ribosomal RNA bands with no high molecular weight genomic DNA contamination present. Band clarity varies indicating variable concentrations of total RNA.

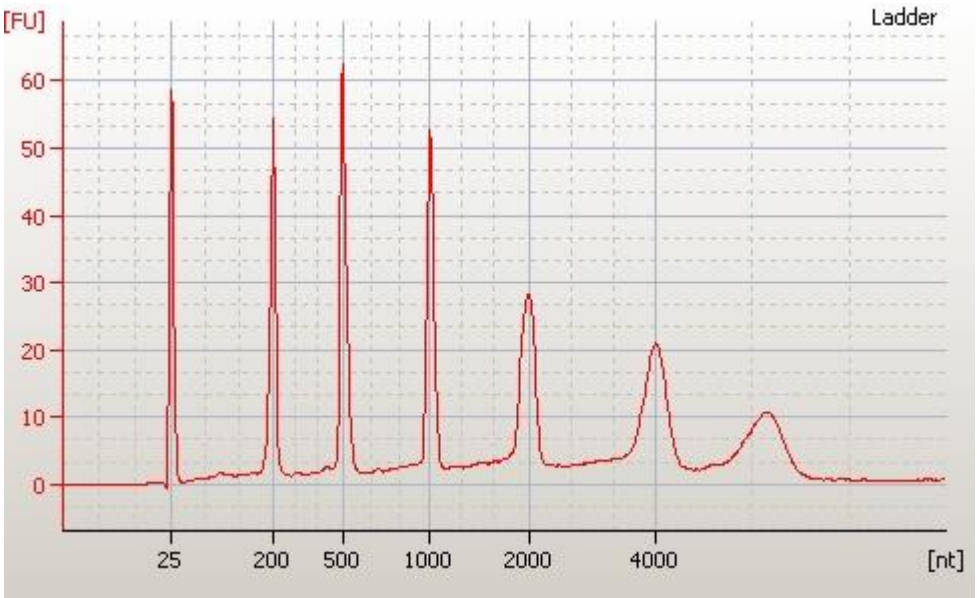

Figure 94. mRNA Nano series II RNA control ladder analysed on the Bioanalyzer (Agilent). The seven visible peaks indicate RNA fragments of a specific size as indicated on the trace.

5.2.4. *Francisella tularensis* Global Gene Expression Profile

The gene expression profiles obtained from *F. tularensis* cultures treated with either 1 μg/mL or 10 μg/mL serine hydroxamate were compared to the control culture with no serine hydroxamate, and revealed a total of 1005 (60.80 % of *F. tularensis* total genes) genes showed changes in gene expression in the comparison between 0 μg/mL and 1 μg/mL serine hydroxamate treatments, and a total of 1089 (65.88 % of total genes) genes showed changes in expression in the comparison between 0 μg/mL and 10 μg/mL serine hydroxamate treatments (figure 95). Of those, 219 genes showed more than two fold expression changes in the comparison between conditions 0 and 1 μg/mL, and 316 genes in the comparison between 0 and 10 μg/mL. Interestingly, there were no genes that passed the significance filters for differential expressed between 1 μg /mL and 10 μg/mL serine hydroxamate as shown by the volcano plots in Fig. 5. This indicated that increasing the concentration of serine hydroxamate did not significantly increase the global effects of the stringent response on gene expression, but was also consistent with the observations made from the RT-PCR experiments (figure 96). These results suggested that, in the range of serine hydroxamate concentrations studied, the stringent control of gene expression in response to stress was very much an on/off response as opposed to a gradual adaptive process.

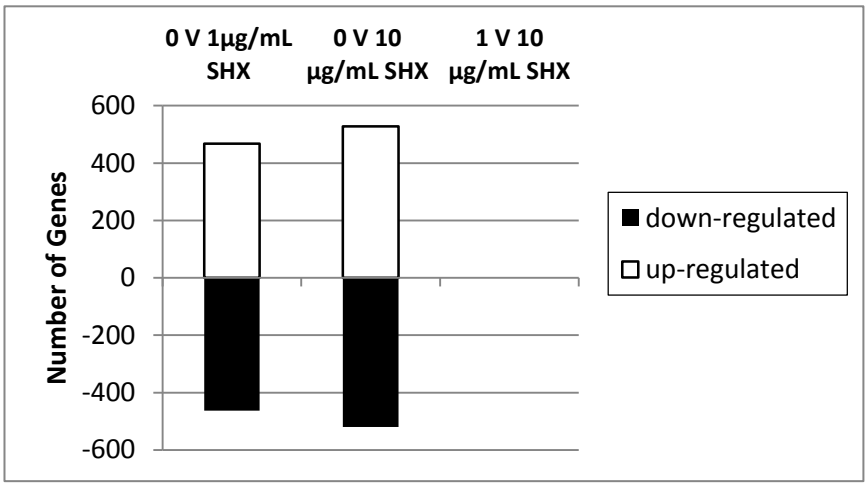

Figure 95. Total number of significantly differentially expressed genes in each serine hydroxamate condition tested.

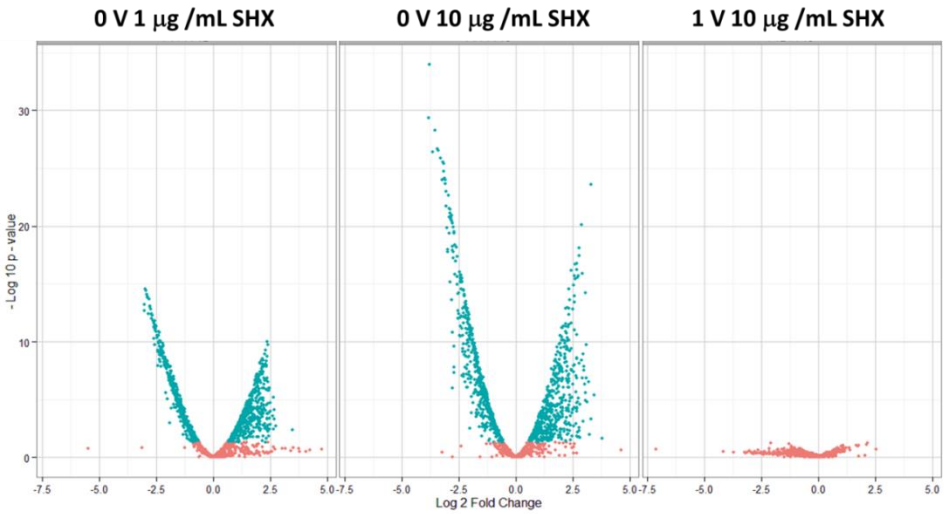

Figure 96. Volcano plots showing significantly differentially expressed genes derived from analysis at the 95% confidence interval. Negative log of P-values are plotted on the y axis versus log 2 fold change between the two conditions on the x axis. More significant data points are nearer the top of the plot and greater magnitude of fold change are to the far left or right of the plot. Data points in blue are significant, points in red are not significant. Far left image represents gene expression in the 0 versus 1 μg /mL serine hydroxamate (SHX) condition. Middle image represents gene expression in the 0 versus 10 μg /mL serine hydroxamate condition and far right image represents gene expression in the 1 μg /mL versus 10 μg /mL serine hydroxamate condition.

Hierarchical cluster analysis was used to generate a heat map of the global gene expression profile of *F. tularensis* cultured in the presence of either 0, 1 or 10 μg/mL serine hydroxamate which was used to induce the stringent response and associated gene expression changes (figure 97) (395, 396). Hierarchical clustering of differential gene expression data designated the "no serine hydroxamate" control group as the outlier and the two serine hydroxamate-treated conditions as a clustered group in the distance matrix tree (figure 97). Genes were clustered according to expression level, and it was apparent that the significance of differential gene expression generally increased in the higher concentration of serine hydroxamate used. By increasing the concentration of serine hydroxamate, global gene expression changes become slightly more widespread and significant; however the gene expression levels between the two serine hydroxamate-treated conditions remained relatively consistent as demonstrated by the lack of statistically significant differences between these conditions and the clustering in the heat map.

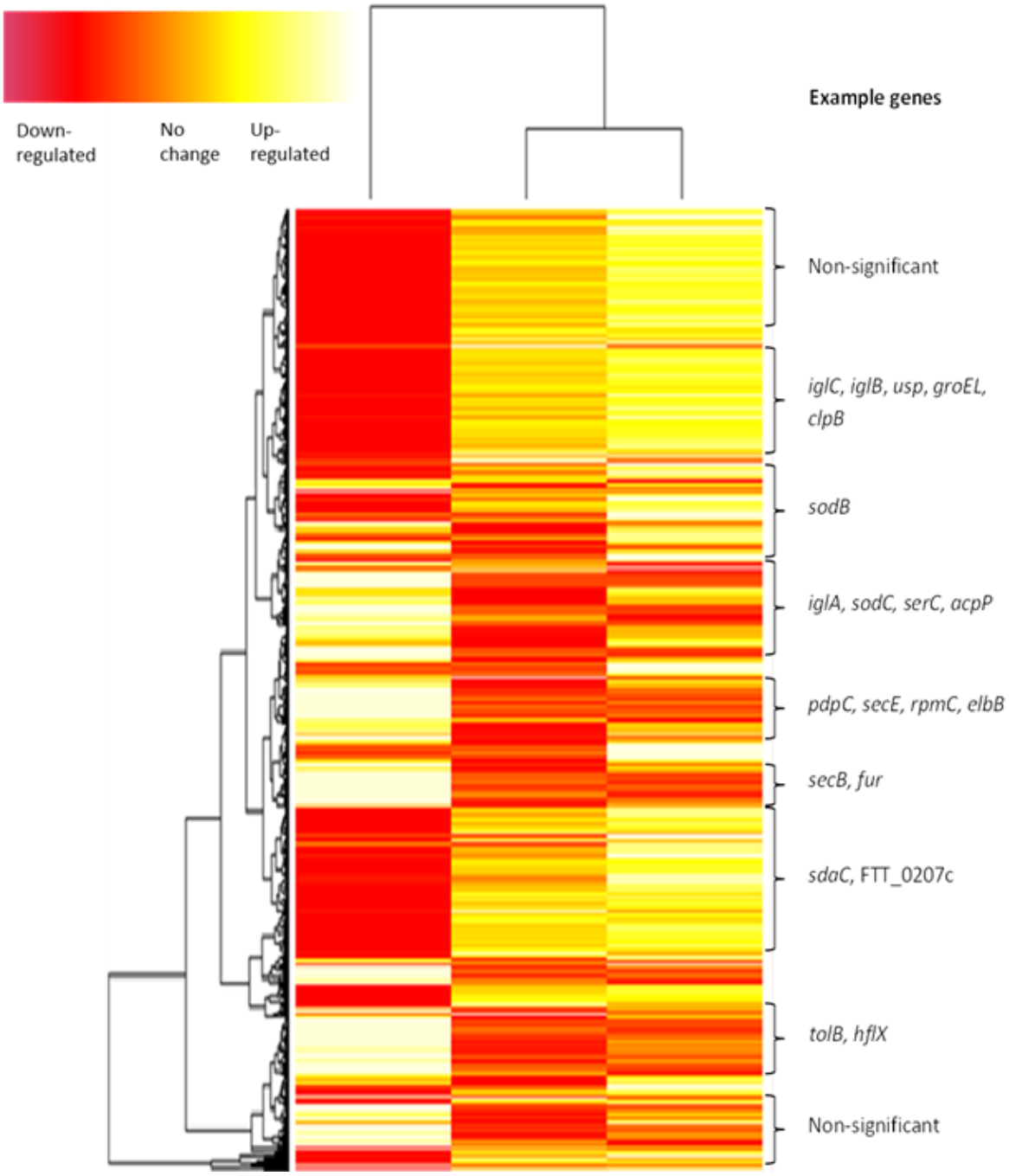

Figure 97. Heat map showing global gene expression profiles of *F. tularensis* SCHU S4 isolated from cultures treated with different concentrations of serine hydroxamate. Far left 0 μg /mL serine hydroxamate condition, middle 1 μg /mL serine hydroxamate condition and far right 10 μg /mL serine hydroxamate condition. Individual genes are indicated on the x axis and clustered according to expression level in the different serine hydroxamate conditions.

It was also apparent that expression levels of genes which belonged to particular functional groups were collectively up-regulated or down-regulated in the serine hydroxamate-treated

samples. Fig. 98 shows the distribution of genes allocated to various functional categories and their associated expression level. Although categories such as virulence genes and transport showed clear up- or down-regulation patterns (fold change shown in supplemental material), many genes were categorised as hypothetical or unknown function, which highlighted the need for more studies into characterising the *F. tularensis* genome.

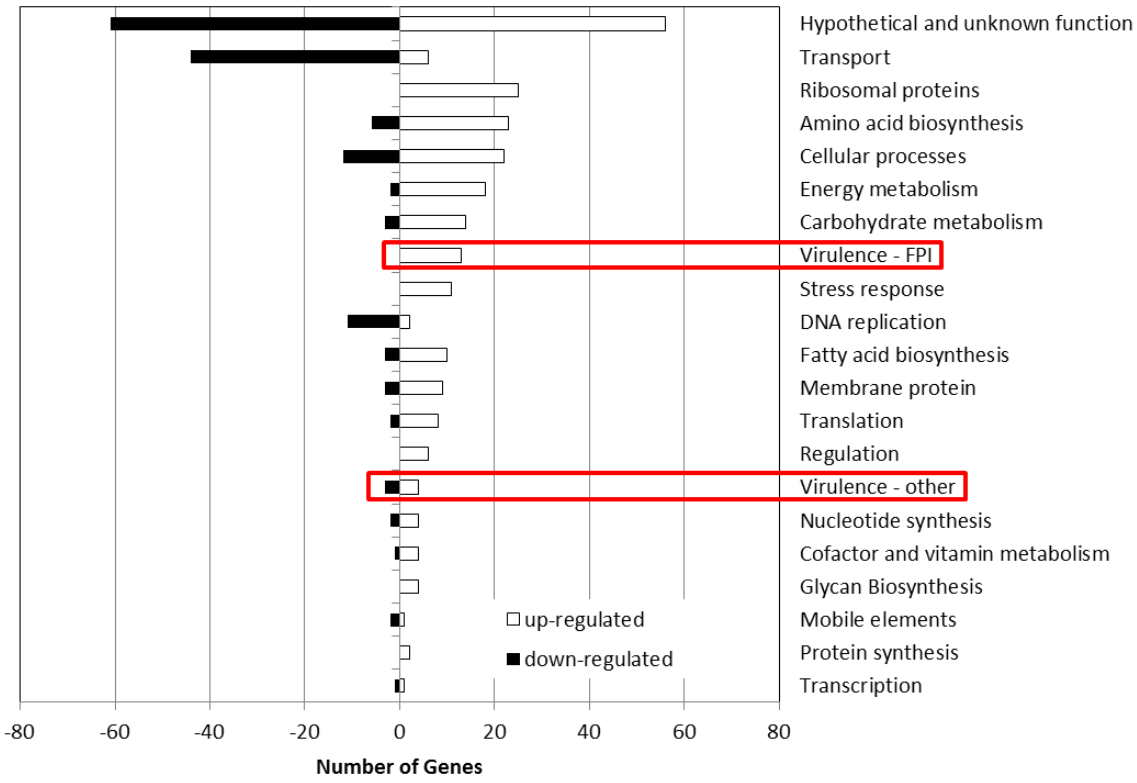

Figure 98. Number of genes up-regulated or down-regulated from the top 400 most significantly differentially expressed genes in the 1 μg /mL serine hydroxamate condition, classified by functional category. Virulence genes, particularly FPI-virulence genes are significantly up-regulated and are highlighted in red.

5.2.5. Virulence Gene Expression

Whole genome transcriptomics of starved *F. tularensis* samples revealed a significant upregulation of virulence associated genes, particularly those encoded on the FPI. Previous

research has suggested an association of virulence gene expression and the stringent response in *Francisella* (86). The genes *iglA1, iglA2, iglB1, iglB2, iglC1, iglC2, iglD1, iglD2, pdpA1, pdpA2, pdpD1* and *pdpD2* encoded on the FPI showed a significant increase of at least 2.5 fold change and a significance score of at least $P = 2.75x10^{-09}$ in expression level in the active stringent response cultures of *F. tularensis* compared to the untreated control culture (figure 99). This supports previous observations by Charity *et al* (239) who noted a significant decrease in expression levels of FPI virulence genes, including the intracellular growth locus genes and the pathogenicity determinant proteins in Δ*mglA* and Δ*sspA* mutants compared to wild type *Francisella* (239). This showed that, without the regulatory protein, MglA (in cooperation with SspA), expression levels of FPI genes cannot be sufficiently regulated (239). Wehrly *et al* (90) reported an upregulation of *Francisella* virulence determinants inside macrophages, which would be expected to be an environment that would activate the stringent response due to lack of nutrient availability and an abundance of ROS (90). Wehrly *et al* (90) also reported FPI gene expression rapidly increased within the first hour post-infection, and then reached maximum expression levels by the end of the cytosolic replication stage of infection, approximately 12-16 hours post infection (90). They also found that *iglC* mRNA levels were much higher than other FPI genes whereas *pdpC* was significantly down regulated (90). As previous research has shown gene expression during stationary phase to be most representative of gene expression during the stressful conditions associated with *in vivo* survival (90, 105, 397), it was anticipated that serine hydroxamate treatment would simulate starvation conditions and result in similar gene expression profiles. As anticipated, gene expression analysis presented herein also found *iglC* to show high expression levels compared to some other FPI encoded genes, however it was also found that *iglB* showed comparable expression levels, conversely to Wehrly *et al* (90). The *pdpC* gene did not show a significant difference in its expression level in our study either. Additionally, in support of the observation that Wehrly *et al* (90) made that mRNA levels of FPI genes increased rapidly in the initial stages of infection then decreased after 16 hours, analysis from this study showed that expression levels of the FPI genes were higher in the 1 μg/mL serine hydroxamate condition compared to the 10 μg/mL serine hydroxamate condition. This result could indicate that increasing the concentration of serine hydroxamate mimics a later stage of the infection lifecycle of *F. tularensis*.

In addition to the evident contribution of FPI genes to *Francisella* virulence, various metabolic pathways have also been shown to contribute to the pathogenesis of this microorganism. One such pathway, which remains relatively unstudied, is the glycine cleavage system (GCS) (398). This system facilitates the degradation of glycine to acquire 5, 10-methylene-tetrahydrofolate, a one carbon donor utilised in the production of serine, thymidine and purines. This pathway contributes to pathogen fitness *in vivo*, where metabolites such as serine are limited (398). As such, it has been reported that homologs of the GCS are transcriptionally up-regulated during *F. tularensis* infection of macrophages (90). A *gcvH* homolog was discovered to be strongly induced in *Francisella* isolated from mouse spleens (397). In support of this finding, *gcvH* was the most significantly up-regulated gene in the comparison between 1 and 10 μg/mL serine hydroxamate conditions, reported here. Further evidence for the importance of the GCS has been reported by Brown *et al* (398) where *gcvT* was required for full *in vivo* virulence of *F. tularensis* following investigation of this pathway using deletion mutants lacking *gcvT* (398). Studies of this deletion mutant also revealed a requirement of the GCS in *F. tularensis* SCHU S4 in serine limiting conditions in broth, however had no effect on the survival of *F. tularensis* in rich media in macrophages or lung epithelial cells (398). However intracellular growth assays performed in minimal media, depleted for serine, intracellular growth defects were apparent in *F. tularensis* strains lacking a functional *gcvT* homolog. These findings by Brown *et al* (398) indicate that the culture conditions reported in this work accurately represented serine starvation conditions that *F. tularensis* might encounter in the host environment.

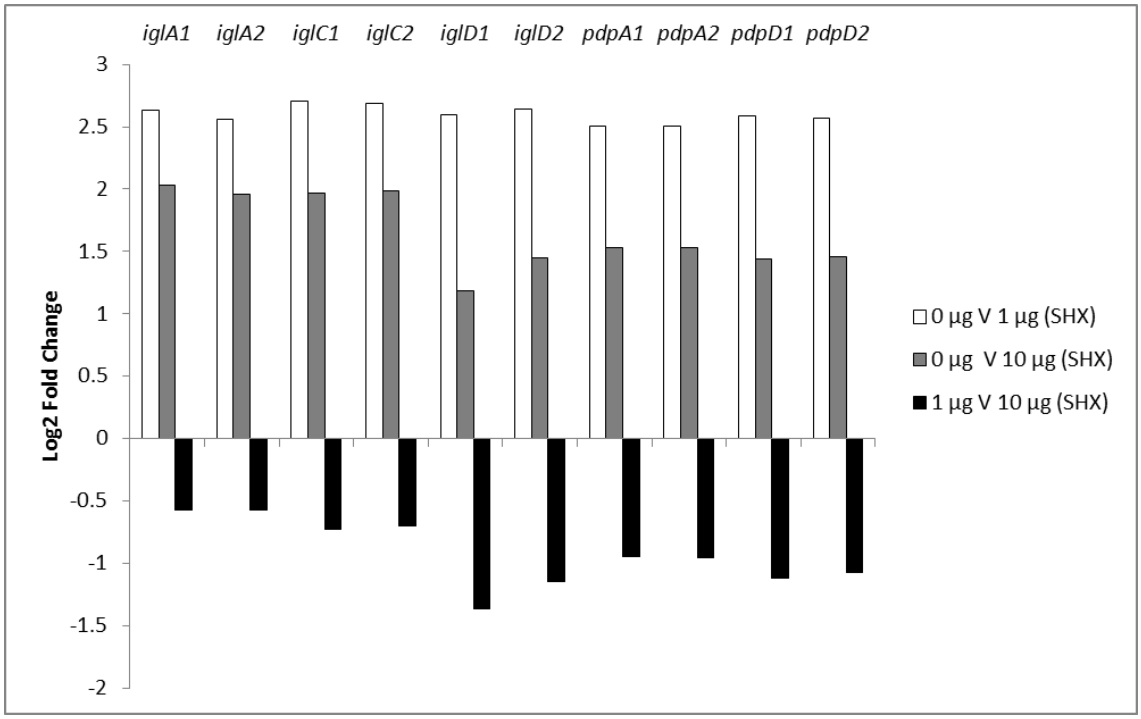

Figure 99. Log_2 fold change in gene expression levels of genes encoded on the FPI in the different serine hydroxamate conditions tested. *iglA1* encodes the intracellular growth locus A1 protein (IglA1), *iglA2* encodes the intracellular growth locus A2 protein (IglA2), *iglC1* encodes the intracellular growth locus C1 protein (IglC1), *iglC2* encodes the intracellular growth locus C2 protein (IglC2), *iglD1* encodes the intracellular growth locus D protein (IglD1), *iglD2* encodes the intracellular growth locus D protein (IglD2), *pdpA1* encodes the pathogenicity determinant protein A1 (PdpA1), *pdpA2* encodes the pathogenicity determinant protein A2 (PdpA2), *pdpD1* encodes the pathogenicity determinant protein D1 (PdpD1), *pdpD2* encodes the pathogenicity determinant protein D2 (PdpD2).

5.2.6. Stress Response Gene Expression

In addition to virulence gene expression, significant differences were observed in expression of stress response genes, particularly those involved in responding to oxidative stress. The genes encoding the superoxide dismutases *sodB* and *sodC* were among the most significantly up-regulated genes in this study. Additionally, the gene encoding the universal stress protein *usp* showed a 2.7 fold change increase in expression level in 1 µg/mL serine hydroxamate-treated cultures. Other stress response genes such as *groEL* and *clpP* which had previously been identified as being up-regulated in studies of *Francisella* gene expression in macrophages (90)

also showed increased expression in the 1 μg/mL serine hydroxamate treated culture conditions in our study.

5.2.7. Metabolic Gene Expression

As expected during stringent conditions, many processes such as cell division and DNA replication are significantly down-regulated in order to conserve cellular resources for survival during stationary phase. FTT0244, which encodes a DNA helicase, was found to be significantly down regulated in *Francisella* cultures treated with serine hydroxamate. The gene *ftsW* which encodes FtsW a key protein in cell division, specifically septum formation, also showed significantly lower expression levels in both stringent response simulated conditions. However, bacterial cells undergoing the stringent response will also up-regulate processes in preparation for when nutrient availability improves. Such processes include metabolic pathways for the synthesis of amino acids, fatty acids and energy production. FTT_1666c, a 3-hydroxyisobutyrate dehydrogenase, a protein involved in amino acid metabolism, showed the third most significant upregulation in the 1 μg/mL serine hydroxamate condition. This gene was previously shown by Charity *et al* (86) to be significantly down regulated in Δ*mglA* and Δ*sspA* mutant backgrounds compared to wild type *Francisella*, implying that FTT1666c could be an important virulence determinant in *F. tularensis* as MglA, in cooperation with SspA is a known regulator of virulence gene expression in *F. tularensis*. SdaA, another protein involved in amino acid production also showed a 2.5 fold increase in expression in the 1 μg/mL serine hydroxamate condition. The genes *pepA, serC* and FTT_1253 also showed at least a 2.5 fold increase in their expression levels in the 1 μg/mL serine hydroxamate condition. The gene *pepA* encodes a protein involved in turnover of intracellular proteins, serC encodes a protein involved in serine synthesis and FTT_1253 encodes an oligopeptide transport protein (82, 399).

5.2.8. Regulatory gene expression

Bacterial gene expression is mediated by proteins, and more recently established small regulatory RNAs, that either act on a global scale or at specific sites in the genome to either activate or repress transcription. Regulatory systems in *F. tularensis* remain poorly characterised, with the majority of two-component regulatory system components being identified as orphans (400). Well characterised regulatory proteins such as sigma factors are

generally not affected by environmental conditions and maintain a constant basal level of expression regardless of stressful environmental conditions. For example, *rpoD* (σ70) did not show a significant difference in its expression level in any of the conditions in this experiment. Conversely, a gene from a two component regulatory system, which are involved in sensing environmental conditions, such as FTT1557c, part of a two component response regulator, was among the most significantly up-regulated genes in the serine hydroxamate-treated samples. Previous research has demonstrated that targeted deletion of the gene *fevR,* which encodes a transcriptional regulator, causes attenuation of *F. tularensis* SCHU S4 in a murine model of infection and is unable to survive or proliferate in macrophages (90). In addition, this gene showed a significant decrease in expression in a Δ*mglA* and Δ*sspA* mutant background compared to wild type *Francisella*, which implied that *fevR* could be an important virulence determinant in *F. tularensis.*

The conserved RNA chaperone, Hfq, has recently been implicated in stringent response regulation, whereby RelA facilitates binding of low affinity RNAs to Hfq to enable gene expression changes in response to starvation conditions (278). *hfq* was found to be among the most significantly up-regulated genes in both serine hydroxamate treated cultures. However, the stringent response gene *relA* did not reveal a significant difference in its expression level, whereas *spoT* showed a significant increase in expression level in the starved *Francisella* cultures.

A possible reason for the upregulation of *spoT* but not *relA* is perhaps due to the fact that the serine hydroxamate-induced stringent response leads to the accumulation of (p)ppGpp and the eventual downstream metabolism of (p)ppGpp requires the pyrophosphate hydrolase activity of SpoT. Our working model for the expression levels of *relA* and *spoT* during the stringent response included a basal level of un-activated RelA present in bacteria which could be activated in response to amino acid deficiency-induced ribosome stalling. The synthesised (p)ppGpp results in global changes in expression levels, including upregulation of *spoT*. The (p)ppGpp synthatase activity of SpoT can supplement the activity of RelA in response to nutrient deficiency, but if nutrient levels are restored, the SpoT (p)ppGpp pyrophosphate hydrolase activity can participate in restoring (p)ppGpp levels to the resting state (lower) level, thus switching off the stringent response.

5.2.9. Reverse Transcriptase Polymerase Chain Reaction Verification

Two genes that showed significant up-regulation in serine hydroxamate-treated cultures of *F. tularensis* were selected for RT-PCR validation of the aforementioned differential expression. FTT0613 and FTT1334 were the top ranking differentially expressed hypothetical proteins selected from the dataset comparing *F. tularensis* treated with 0 μg/mL serine hydroxamate and *F. tularensis* treated with 1 μg/mL serine hydroxamate. Primers 0613rtpcrF/0613rtpcrR and 1334rtpcrF and 1334rtpcrR (listed in appendix section 8.11) were used to amplify 350 bp and 382 bp products, respectively to determine expression levels of FTT0613 and FTT1334 in the serine hydroxamate-treated *F. tularensis* cultures. 16S rRNA was selected as a stable reference gene to which expression levels of the targets genes could be compared. Primers 16SrtpcrF and 16SrtpcrR (listed in appendix section 8.11) were used to amplify a 287 bp product targeting the 16SrRNA gene. The 16S rRNA reference gene showed stable expression levels across all serine hydroxamate conditions tested (figure 100), whereas FTT0613 showed no expression in *F. tularensis* cultured without serine hydroxamate and stable expression in those cultures treated with 1 μg/mL, 10 μg/mL and 100 μg/mL serine hydroxamate (figure 101). FTT1334 also revealed no expression in the 0 μg/mL serine hydroxamate condition, low expression levels at 1 μg/mL serine hydroxamate and higher expression levels at 10 μg/mL and 100 μg/mL serine hydroxamate (figure 102).

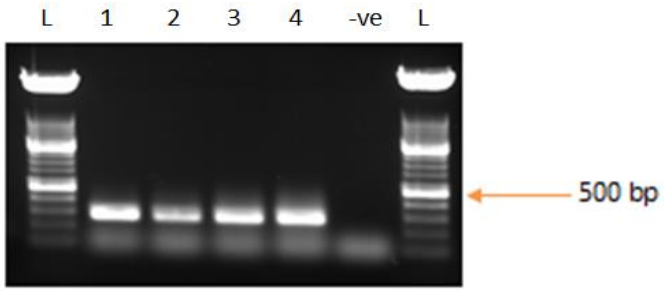

Figure 100. Expression of the 16S rRNA housekeeping gene in *F. tularensis* SCHU S4 grown in media supplemented with or without serine hydroxamate as determined by RT-PCR. Lane 1, cDNA from 0 μg /mL serine hydroxamate; Lane 2, cDNA from 1 μg /mL serine hydroxamate; Lane 3, cDNA from 10 μg /mL serine hydroxamate; Lane 4, cDNA from 100 μg /mL serine hydroxamate; Lane 5, No cDNA control.

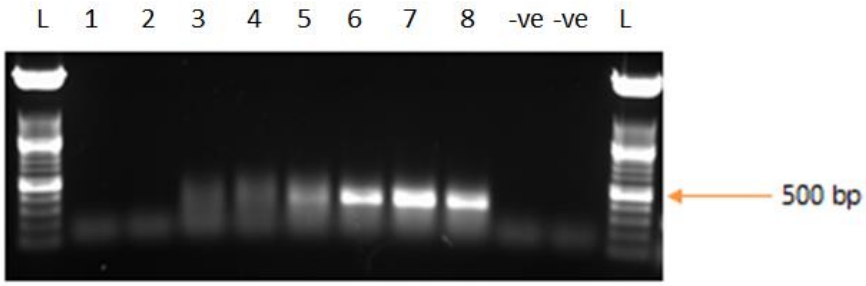

Figure 101. Expression of FTT0613 (350 bp product) in *F. tularensis* SCHU S4 can be induced or repressed by supplementing growth media with serine hydroxamate as determined by RT-PCR. Lanes 1 and 2, cDNA from 0 μg /mL serine hydroxamate; Lanes 3and 4, cDNA from 1 μg /mL serine hydroxamate; Lanes 5 and 6, cDNA from 10 μg /mL serine hydroxamate; Lanes 7 and 8, cDNA from 100 μg /mL serine hydroxamate; Lanes 9 and 10 no cDNA controls.

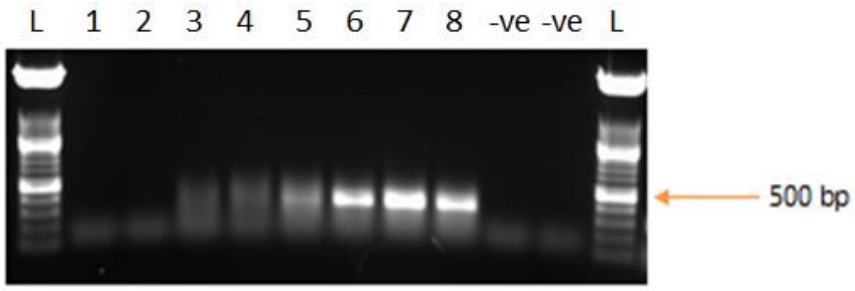

Figure 102. Expression of FTT0613 (350 bp product) in *F. tularensis* SCHU S4 can be induced or repressed by supplementing growth media with serine hydroxamate as determined by RT-PCR. Lanes 1 and 2, cDNA from 0 μg /mL serine hydroxamate; Lanes 3 and 4, cDNA from 1 μg /mL serine hydroxamate; Lanes 5 and 6, cDNA from 10 μg /mL serine hydroxamate; Lanes 7 and 8, cDNA from 100 μg /mL serine hydroxamate; Lanes 9 and 10 no cDNA controls.

5.2.10. Proteomics

High performance Liquid Chromatography Mass spectrometry (HPLC-MS) was performed on prepared protein lysates of *F. tularensis* cultures grown in active stringent response conditions using the same serine hydroxamate concentrations as the previously discussed transcriptional analysis (0 μg/mL, 1 μg/mL or 10 μg/mL serine hydroxamate). Lysates were either inactivated at 60 °C or 100 °C for subsequent proteomic analysis. Inactivation at 60 °C was expected to produce a higher quality lysate for protein analysis, but would potentially be less effective for inactivating the bacteria and result in either inactivated cells or contaminants in the samples for sterility check. Inactivation at 100 °C was expected to be more effective at inactivating the bacteria, but might result in a lower quality sample for proteomics, therefore both temperature were used. Of the predicted protein coding sequences, 1804 ORFs, 1104 proteins (61%) were detected in this screen. When the *F. tularensis* proteome of the 0 μg/mL serine hydroxamate condition was compared to the 10 μg/mL serine hydroxamate condition 14 proteins showed a greater than two fold down regulation and 25 proteins showed a greater than two fold upregulation in expression levels. This finding is somewhat different to the transcriptomics data which revealed 1005 (60.80 % of *F. tularensis* total genes) and a total of 1089 (65.88 % of total genes) genes showed significant changes in expression in the comparison between 0 μg/mL and 1 μg/mL serine hydroxamate and 0 μg/mL and 10 μg/mL serine hydroxamate treatments. Proteins that showed a significant increase in expression in the comparison between 0 μg/mL and 10 μg/mL serine hydroxamate treatments included IglC

(accession number Q5NEC5), which is an intracellular growth locus protein and resides on the FPI showed a 1.27 fold increase in expression (figure 103). UbiE (accession number Q5NFE1), a methyltransferase involved in ubiquinone biosynthesis showed a 6.35 fold increase in expression, one of the highest and statistically significant expression levels observed in the dataset (figure 104). Hfq (accession number Q5NH41) which binds RNAs facilitated by the stringent response protein RelA showed a 2 fold increase in expression (figure 105). Stress response proteins that also showed a correlating increase in expression in the proteomic and transcriptomic data sets were Usp (accession number Q5N144) the universal stress protein and SspA (accession number Q5NHJ6) the stringent starvation protein (figures 106 and 107 respectively). Whereas SodB (accession number Q5NIJ9) a super oxide dismutase showed no significant change in expression when comparing 0 μg/mL and 10 μg/mL serine hydroxamate treatments, however showed a 1.32 fold increase in expression when comparing 0 μg/mL and 1 μg/mL serine hydroxamate treatments. Contrary however to the transcriptomics and RT-PCR results, the hypothetical proteins FTT_1334c and FTT_0613 did not show a significant change in expression levels in the proteomic results when comparing serine hydroxamate treated samples to the control. It was unclear was to why this was however, it is becoming more apparent that proteomic data often does not correlate well with transcriptomic data.

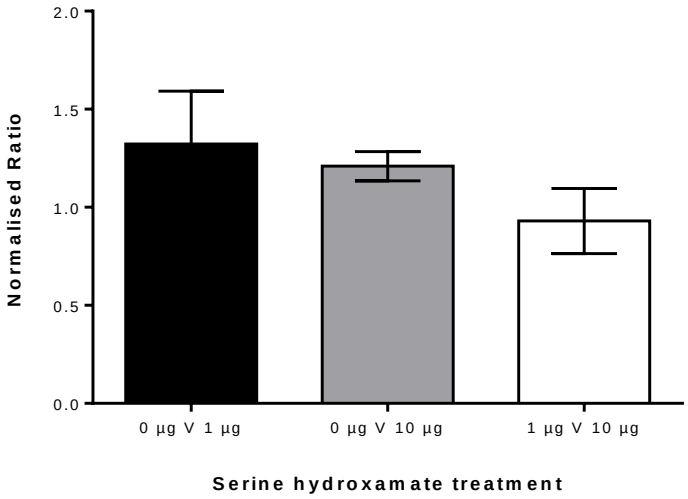

Figure 103. Protein level of IglC determined from whole proteome mass spectrometry, comparing ratios derived from *F. tularensis* SCHU S4 total protein isolated from cultures treated with different concentrations of serine hydroxamate. IglC showed a 1.27 fold increase in expression in cultures treated with serine hydroxamate, however this was not statistically significant as determined by two-way ANOVA (P = 0.0989).

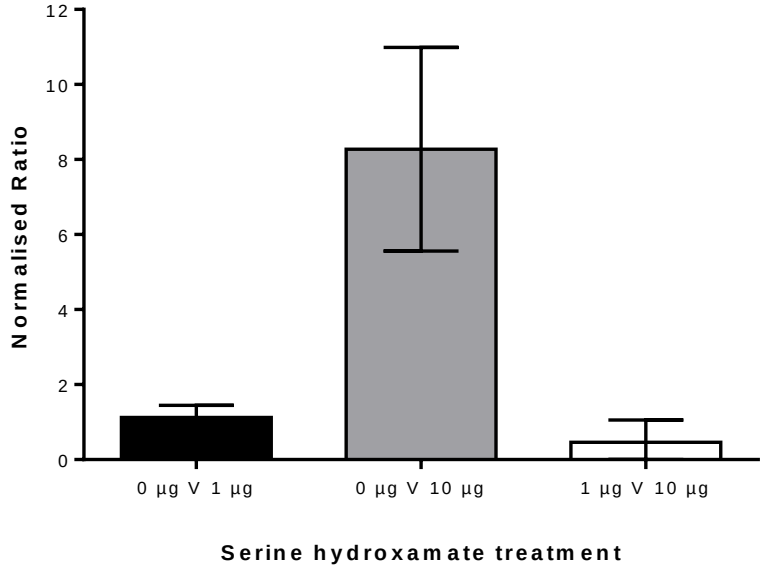

Figure 104. Protein level of UbiE determined from whole proteome mass spectrometry, comparing ratios derived from *F. tularensis* SCHU S4 total protein isolated from cultures treated with different concentrations of serine hydroxamate. UbiE showed a 6.35 fold increase in expression in cultures treated with serine hydroxamate, which was statistically significant as determined by two-way ANOVA (P = 0.0018).

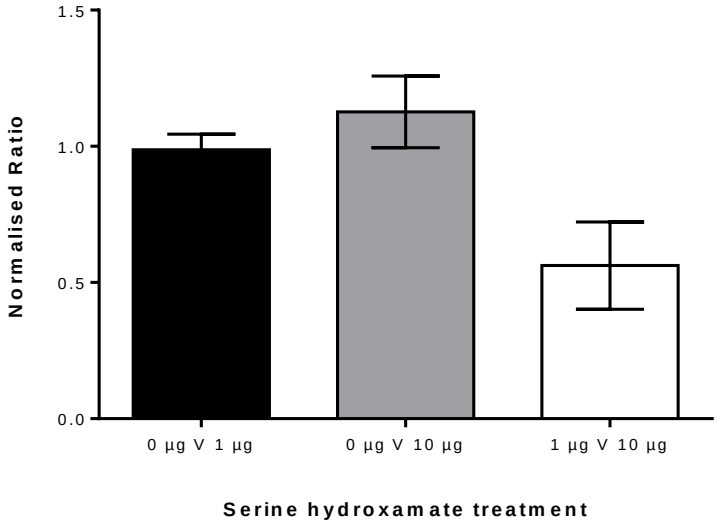

Figure 105. Protein level of Hfq determined from whole proteome mass spectrometry, comparing ratios derived from *F. tularensis* SCHU S4 total protein isolated from cultures treated with different concentrations of serine hydroxamate. Hfq showed a 2 fold increase in expression in cultures treated with serine hydroxamate, which was statistically significant as determined by two-way ANOVA (P = 0.0178).

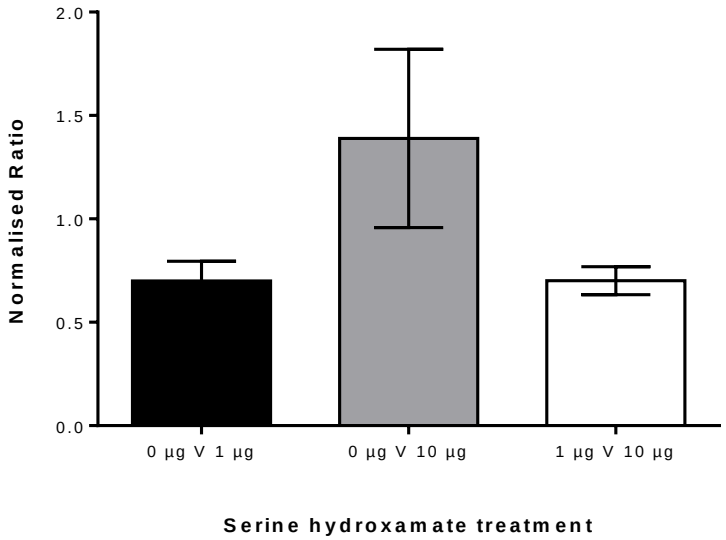

Figure 106. Protein level of Usp determined from whole proteome mass spectrometry, comparing ratios derived from *F. tularensis* SCHU S4 total protein isolated from cultures treated with different concentrations of serine hydroxamate. Usp showed a 1.4 fold increase in expression in cultures treated with serine hydroxamate, which was statistically significant as determined by two-way ANOVA (P = 0.0259).

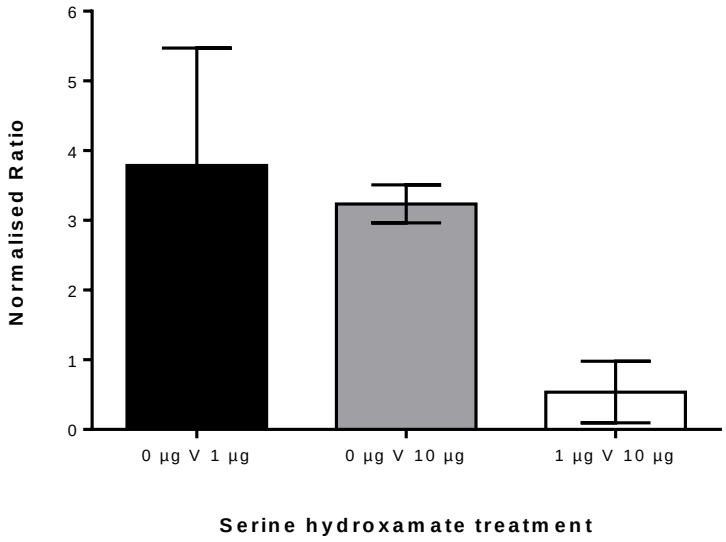

Figure 107. Protein level of SspA determined from whole proteome mass spectrometry, comparing ratios derived from *F. tularensis* SCHU S4 total protein isolated from cultures treated with different concentrations of serine hydroxamate. SspA showed a 3.8 fold increase in expression in cultures treated with serine hydroxamate, which was statistically significant as determined by two-way ANOVA (P = 0.0166).

5.2.11. Genetic Targets Selected for Mutagenesis from Transcriptomics

In light of the RNAseq analysis from serine hydroxamate-treated *F. tularensis* cultures it was decided that the two most up-regulated hypothetical genes, that showed that same level of up-regulation in both the 1 µg/mL, and 10 µg/mL serine hydroxamate-treated samples would be selected for new mutant targets. There are many proteins in the *F. tularensis* genome whose functions are still to be elucidated, and two of those proteins, FTT_1334c and FTT_0613 showed upregulation during the stringent response indicating that they may have a key role in stress response or virulence. Hypothetical proteins FTT_1334c and FTT_0613 were selected based on the significance value of their differential expression and the fact they were significantly differentially expressed genes in both conditions mentioned above. FTT_1334c appears to be part of a small operon with one other, as yet, hypothetical protein FTT_1333c. This small operon is adjacent to an ABC transporter operon comprising the genes *cydC* and *cydD*, but appears to be relatively uncharacterised. FTT_0613 does not appear to be part of an operon with any other genes. FTT_0613 falls adjacent to a cluster of genes which encode proteins of various functions including FTT_0614c, an apolipoprotein N-acyltransferase and FTT_0617, a PhoH-like protein involved in phosphate starvation. Bioinformatic analyses were

carried out to search for homologues to previously characterised genes, and none were identified for either gene.

Synthetic gene constructs were commercially sourced for creating unmarked isogenic allelic replacement mutants as previously described herein. Mutants were successfully made as described in the method section 7.5, and characterisation assays including *in vitro* growth kinetics assessment and antibiotic disc diffusion assays were carried out to establish if any phenotypes different to that of the wild type strain were apparent.

Firstly, *in vitro* growth was assessed using the MultiSkan™ FC microplate photometer, as described in the method section 7.7.1 Optical density readings were taken every 15 minutes for 24 hours and the data plotted to generate growth curves (figure 108).

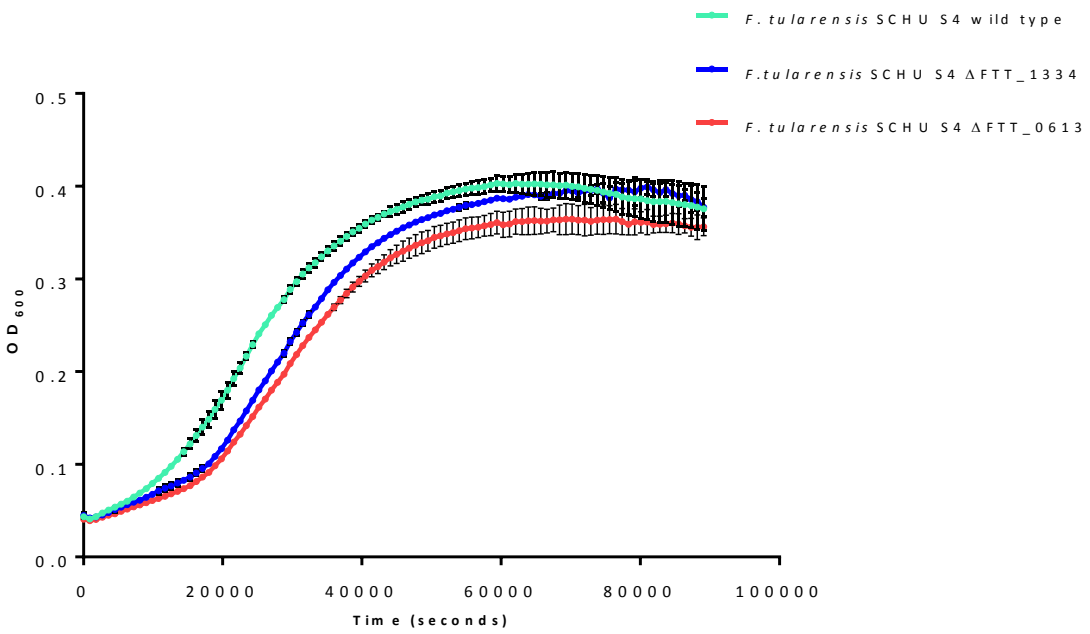

Figure 108. Growth curve showing the *F. tularensis* ΔFTT_1334c and ΔFTT_0613 mutant's growth kinetics *in vitro* compared to wild type *F. tularensis* SCHU S4. Each data point represents combined results from 3 biological replicates in which 6 technical replicates were analysed. Error bars are shown for each data point.

These data were statistically analysed by one way ANOVA and a statistically significant difference was observed between the ΔFTT_0613 mutant and the wild type strain (P = 0.0176) but not between the ΔFTT_1334c mutant and wild type. These results indicated that deletion of these genes resulted in *F. tularensis* strains that were slightly defective for growth in comparison to the wild type. Further characterisation of these mutants is required to understand the importance of this observed growth defect, and ultimately if these strains display diminished virulence during infection. If further characterisation of these strains indicates decreased virulence these gene could make appropriate broad spectrum targets for future antibiotics.

5.3. *Yersinia pestis* Regulatory Analysis

5.3.1. Serine Hydroxamate Induction of the Stringent Response

Similarly to results observed for *F. tularensis* it was expected that the addition of serine hydroxamate to induce the stringent response in cultures of *Y. pestis* GB would similarly result in modified expression levels of various genes involved in either virulence related mechanisms or stress response mechanisms. However, unlike in *F. tularensis* there are no known genetic markers of active stringent response. Initially, the concentration of serine hydroxamate required to inhibit the growth of *Y. pestis* was titrated. Optical density readings (OD_{600}) and viable counts were measured from samples taken from overnight cultures of *Y. pestis* GB in the presence of 1 mg/mL , 100 µg /mL, 50 µg /mL, 10 µg /mL, and 0 µg /mL of the amino acid analogue serine hydroxamate. It was found that a concentration of serine hydroxamate of 1 mg/mL inhibited the growth of *Y. pestis*, whereas concentrations of 100 µg /mL and below had no effect of the growth of *Y. pestis* as shown below in figures 109 and 110 by OD_{600} readings and viable counts.

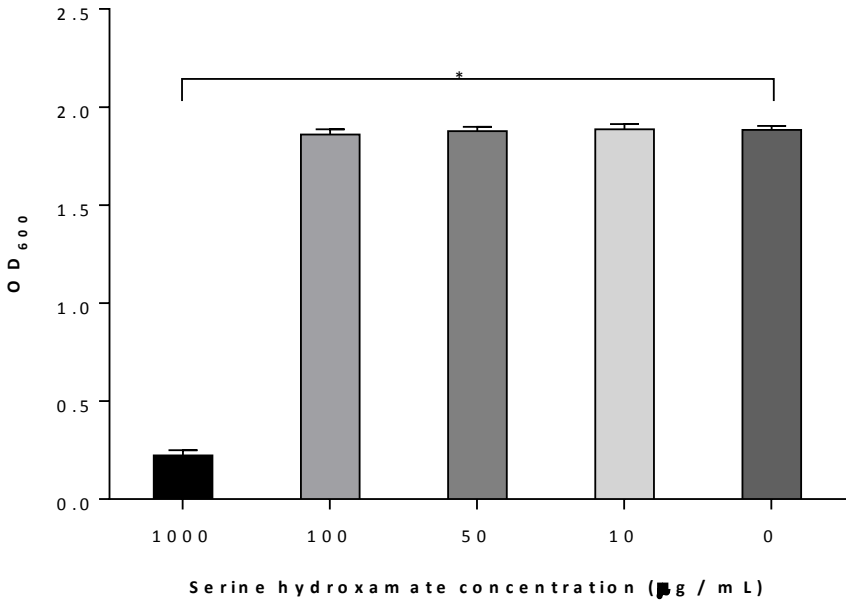

Figure 109. Optical density reading recorded from *Y. pestis* GB cultures incubated in the presence of various concentrations of serine hydroxamate (1 mg / mL , 100 µg / mL, 50 µg / mL, 10 µg / mL, and 0 µg / mL).

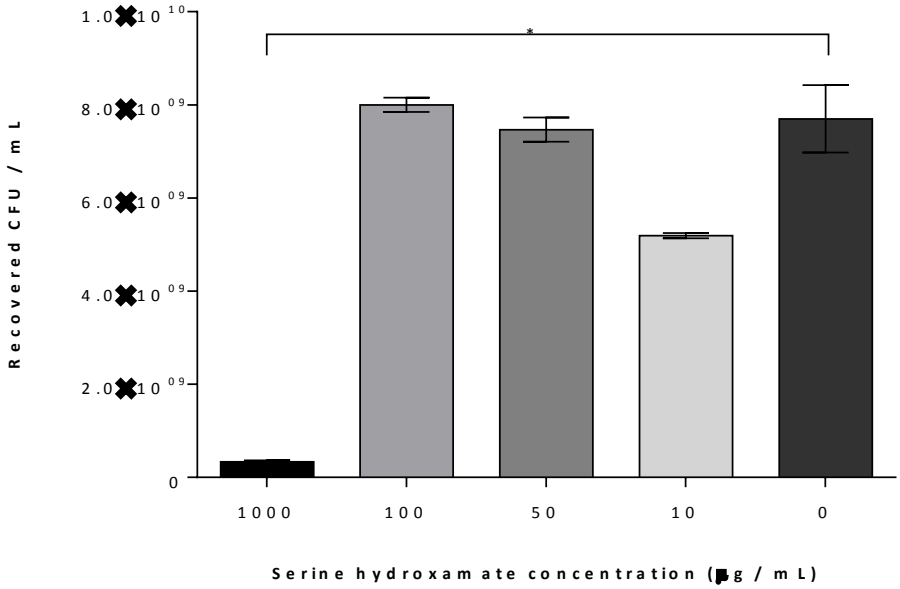

Figure 110. Viable counts taken from *Y. pestis* GB cultures incubated in the presence of various concentrations of serine hydroxamate (1 mg / mL , 100 µg / mL, 50 µg / mL, 10 µg / mL, and 0 µg / mL).

5.3.2. Whole Genome RNA-Sequencing

RNA was isolated from cultures treated with a range of serine hydroxamate concentrations (0 µg/mL, 10 µg/mL and 100 µg/mL) for RNA sequencing and assessed for quality and RNA concentration on the Bioanalyzer (Agilent) (methodologies described in section 7.3.4). Figure 111 shows the electropherogram results from this quality assessment.

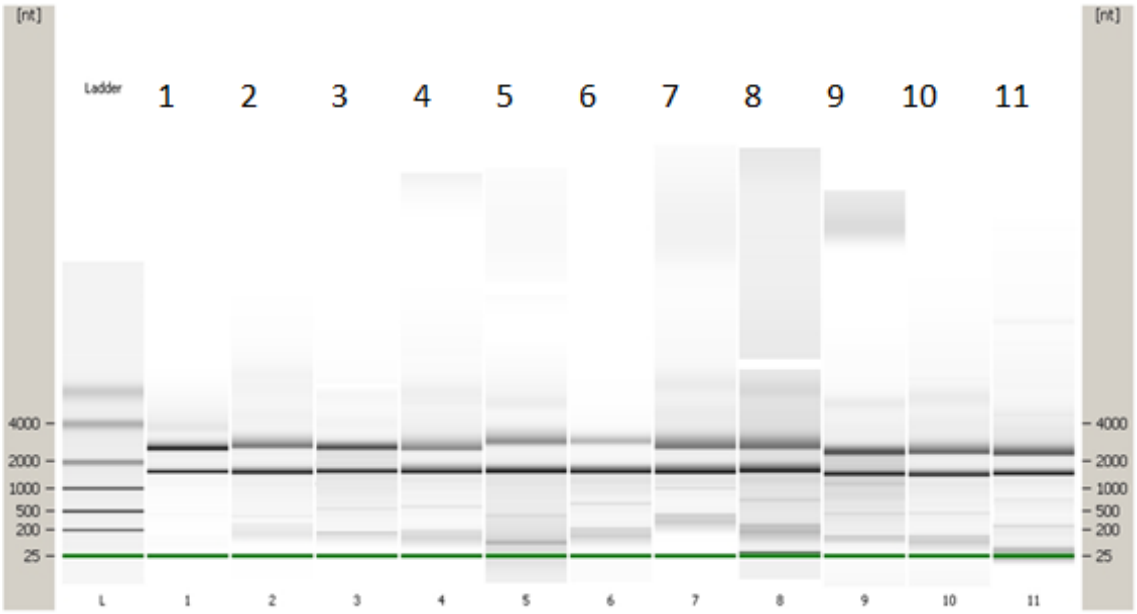

Figure 111. Electropherogram of 11 RNA samples prepared from *Y. pestis* GB cultured in the presence of different concentrations of serine hydroxamate. Lanes 1-3, 0 μg/mL serine hydroxamate, lanes 4-7, 10 μg/mL serine hydroxamate and lanes 8-11, 100 μg/mL serine hydroxamate. All samples show distinct 16S and 23S ribosomal RNA peaks with minimal high molecular weight genomic DNA contamination present. Band clarity varies indicating variable concentrations of total RNA.

The gene expression profiles obtained from *Y. pestis* cultures treated with either 10 μg/mL or 100 μg/mL serine hydroxamate compared to the control culture with no serine hydroxamate revealed a total of 163 genes (4.08 % of *Y. pestis* total genes) showed changes in expression in the comparison between 0 μg/mL and 10 μg/mL serine hydroxamate treatments, and a total of 215 genes (5.38 % of total genes) showed changes in expression in the comparison between 0 μg/mL and 100 μg/mL serine hydroxamate treatments (figures 97 and 98). Of those, 48 genes showed more than two fold expression changes in the comparison between conditions 0 and 10 μg/mL, and 50 genes in the comparison between 0 and 100 μg/ mL. Interestingly, there were no genes that passed the significance filters for differential expressed between 10 μg /mL and 100 μg/mL serine hydroxamate (figures 97 and 98). This indicated that increasing the concentration of serine hydroxamate did not significantly increase the global effects of the stringent response on gene expression. These results suggested that, in the range of serine hydroxamate concentrations studied, the stringent control of gene expression in response to stress was an on/off response as opposed to a gradual adaptive process.

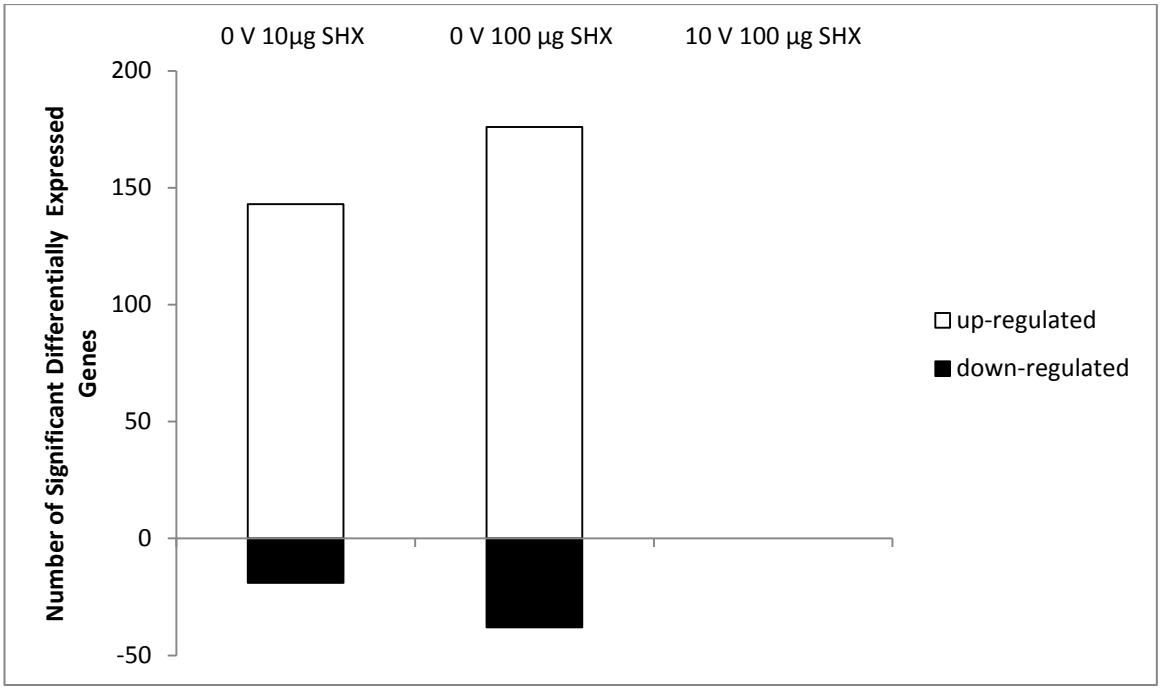

Figure 112. Total number of significantly differentially expressed genes in each serine hydroxamate condition tested.

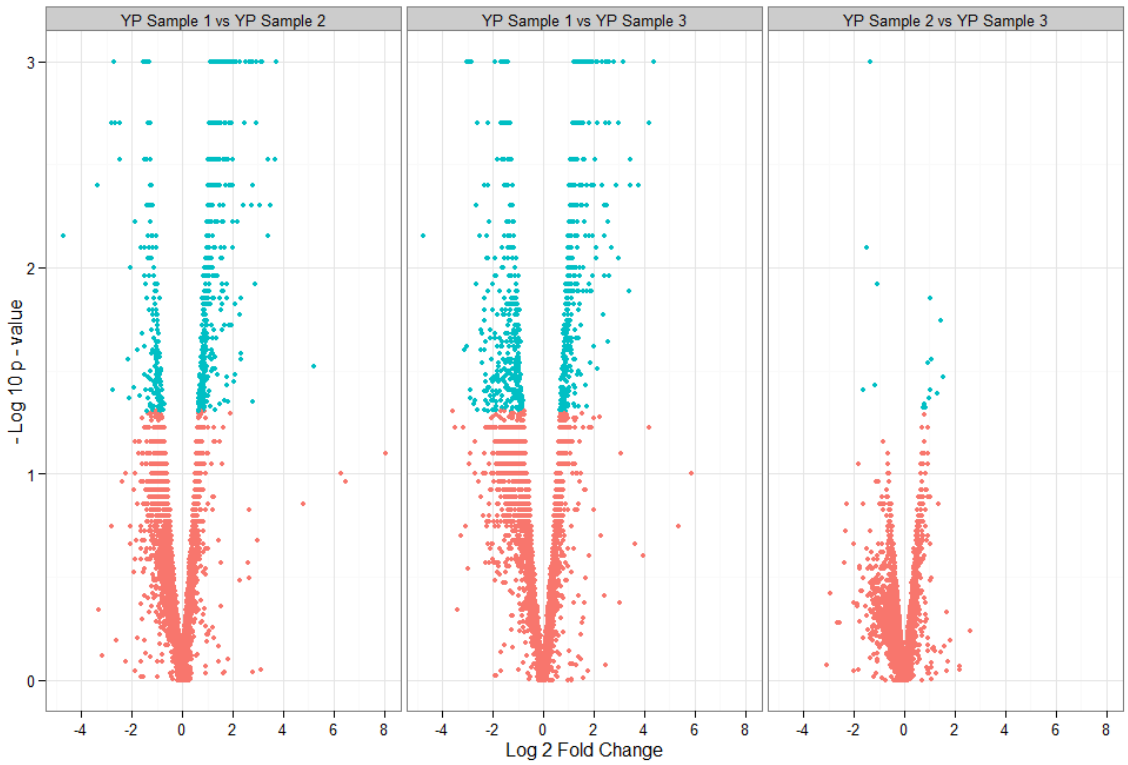

Figure 113. Volcano plots showing significantly differentially expressed genes derived from analysis at the 95% confidence interval. Negative log of P-values are plotted on the y axis versus log 2 fold change between the two conditions on the x axis. More significant data points are nearer the top of the plot and greater magnitude of fold change are to the far left or right of the scatter plot. Data points in blue are significant, points in red are not significant. Far left image represents gene expression in the 0 versus 10 μg /mL serine hydroxamate condition. Middle image represents gene expression in the 0 versus 100 μg /mL serine hydroxamate condition and far right image represents gene expression in the 10 versus 100 μg /mL serine hydroxamate condition.

The global gene expression profile of *Y. pestis* was different from that which was observed for *F. tularensis,* as discussed above. *F. tularensis* up-regulated a similar number of genes to those down regulated under starvation conditions, whereas here we observed that *Y. pestis* up-regulated significantly more genes than the number of genes down regulated under starvation conditions (figures 99 and 100). *Y. pestis* also differentially expresses far fewer genes in total than *F. tularensis* under serine hydroxamate treatment, indicating that *Y. pestis* is perhaps more tolerant of amino acid starvation conditions than *F. tularensis* and required fewer genes

to be differentially expressed to adapt to the nutrient limitation. Although both organisms are auxotrophic for certain amino acids, and require acquisition of these from their host environment, *Y. pestis* may have more compensatory mechanisms for amino acid acquisition during the stringent response.

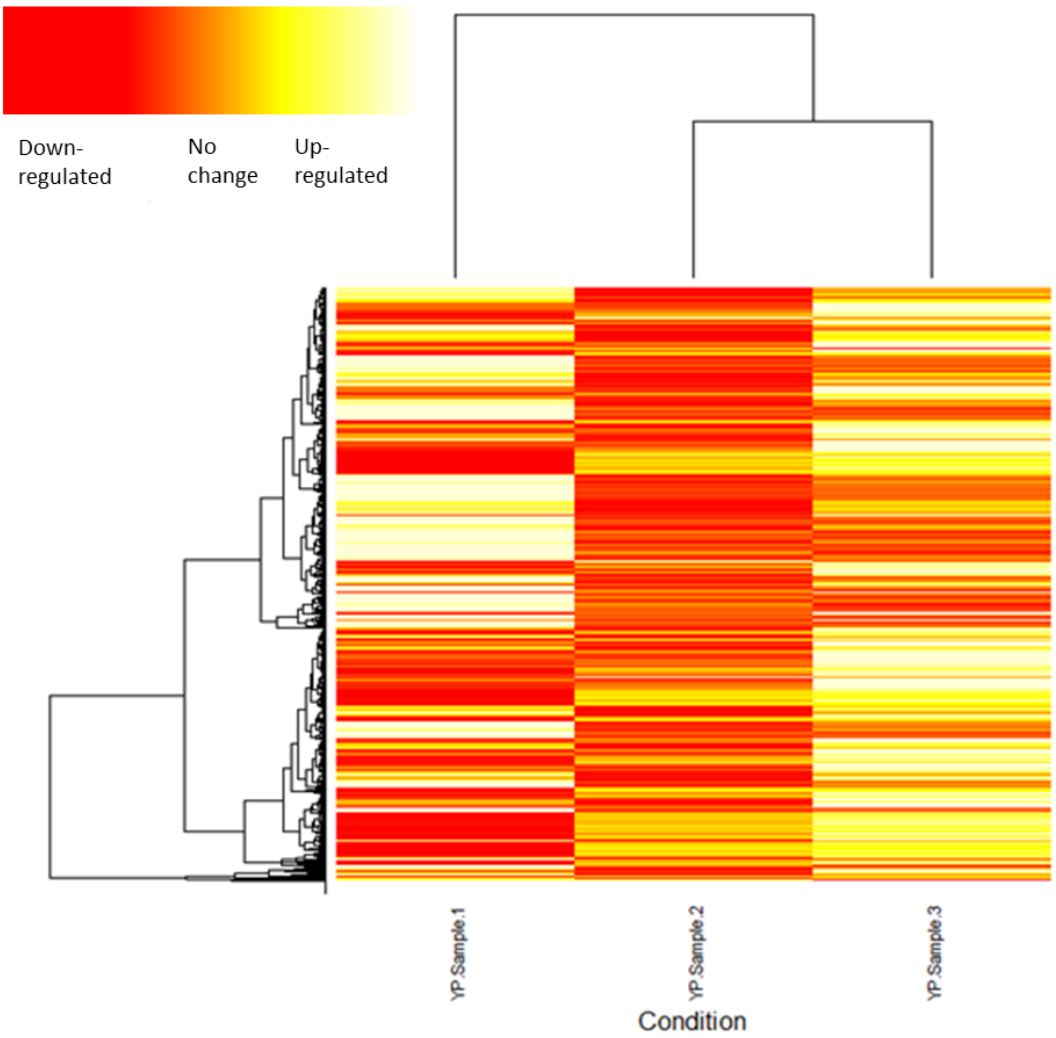

Figure 114. Heat map showing global gene expression profiles of *Y. pestis* GB isolated from cultures treated with different concentrations of serine hydroxamate. Far left profile corresponds to the control 0 μg /mL serine hydroxamate condition, the middle profile corresponds to the 10 μg /mL serine hydroxamate condition and the far right profile corresponds to the 100 μg /mL serine hydroxamate condition. Individual genes are indicated on the x axis and clustered according to expression level in the different serine hydroxamate conditions.

Expression levels of genes which belonged to particular functional groups were collectively up-regulated or down-regulated in the serine hydroxamate-treated samples (figure 100). Although categories such as genes encoding proteins involved in regulatory and transport functions showed clear up- or down-regulation patterns respectively, many genes were categorised as hypothetical or unknown function, which highlights the need for further studies into characterisation of the *Y. pestis* genome.

Extensive research has been conducted into the stringent response of *E. coli,* including artificially inducing the stringent response using serine hydroxamate (190, 191, 286, 401-404). As both *Y. pestis* and *E. coli* are members of the *Enterobacteriaceae*, comparisons can be made between the two organisms. Durfee *et al* (405) reported a significant increase in the number of genes that were up-regulated in the early stages of a serine hydroxamate treatment time course, similar to our observation that more genes were up-regulated than down regulated in the presence of 10 μg/mL serine hydroxamate (405). Durfee *et al* (405) also reported that the majority of transport genes in *E. coli* were down regulated under starvation conditions (405). This observation supports the idea that bacteria need to conserve energy during the stringent response as active transport of amino acids, nucleosides and peptides and other molecules requires energy that is not available during conditions of nutrient limitation.

An unexpected pattern that was apparent in the global gene expression profiles of both *F. tularensis* and *Y. pestis* under active stringent response was the increase in the expression of ribosomal proteins. For *Y. pestis* 13 ribosomal proteins were up-regulated in the significantly differentially expressed genes, whereas none were down regulated. This was also discussed above for *F. tularensis*, where 25 ribosomal proteins showed increased expression and none were down regulated. It has been found in *E. coli* that ribosomal proteins which lack a particular amino acid are expressed at a higher level when bacteria are starved for the same amino acid compared to other amino acids (406). This indicates that bacteria are able to sense specific amino acid starvation and only synthesise ribosomal proteins that do not require depleted amino acid. However, it has generally been found that starvation and subsequent accumulation of (p)ppGpp leads to a reduction in ribosomal protein synthesis and has been reported as such for *E. coli* (407). Therefore, it was unexpected to see all ribosomal proteins showing increased gene expression in this transcriptomics experiment.

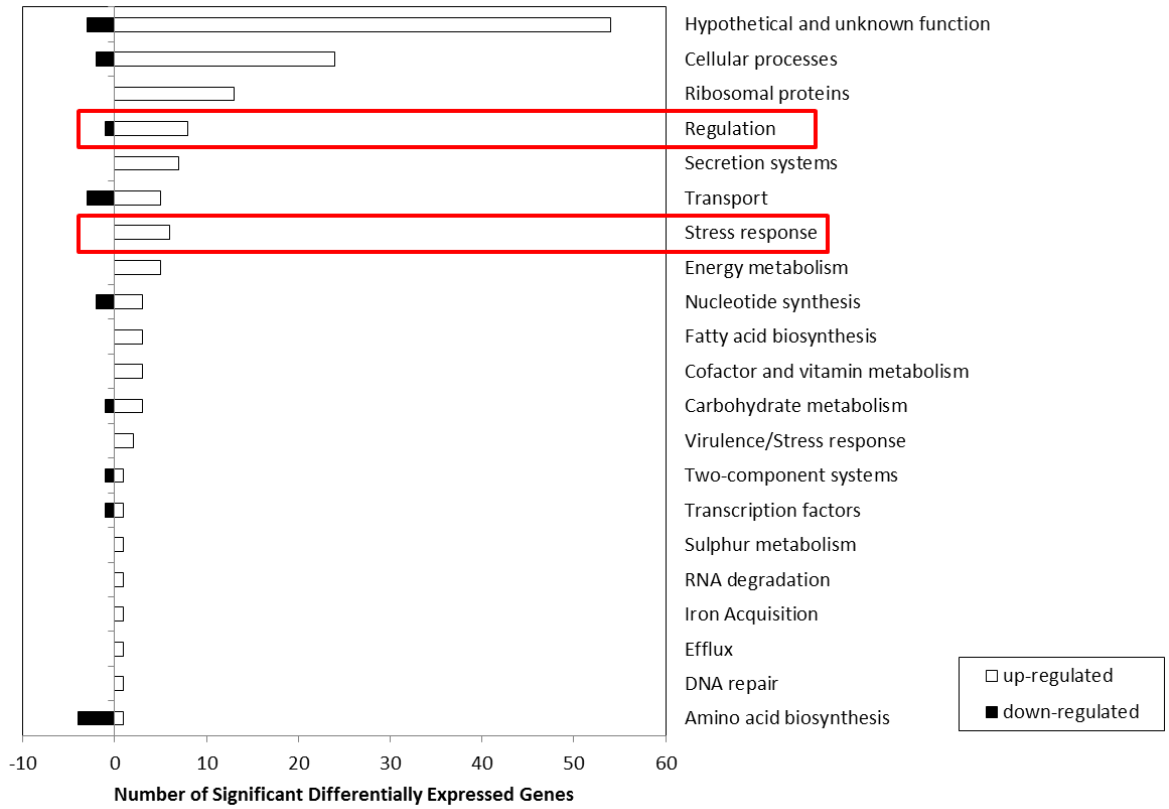

Figure 115. Number of genes up-regulated or down-regulated from the most significantly differentially expressed genes in the 10 μg /mL serine hydroxamate condition, classified by functional category.

5.3.3. Virulence gene expression

Previous research into gene expression in *Y. pestis* during infection has shown that the most highly expressed genes are those involved in virulence (408). Known virulence factors such as the antiphagocytic F1 protein capsule, the plasminogen activator required for invasion of the lymph node, the iron acquisition system encoded on the *Y. pestis* pathogenicity island and the TTSS have all been shown to be significantly up-regulated *in vivo* (408). Studies have also shown that *Y. pseudotuberculosis* induces virulence gene expression upon contact with host cells, specifically the YpoE cytotoxin, which is an essential virulence factor in antiphagocytic activity (409). Many gene expression studies in *Yersinia* have reported specific gene expression patterns associated with temperature shifts from flea/ambient temperature, 28˚C to mammalian temperature, 37˚C. Motin *et al* (105) carried out whole genome microarrays during temperature transition in *Y. pestis* from which transcriptional profiles revealed many

genes being differentially expressed in a temperature dependent manner (105). Genes involved in pathogenicity and stress responses such as *sodC*, *katA* and *gsrA* (encoding a superoxide dismutase, and catalase and a serine protease, respectively) showed strong induction upon temperature shift to 37 ˚C (105).

In contrast to observations that were made for virulence gene expression *F. tularensis*, in which *Francisella* Pathogenicity Island (FPI) gene expression was significantly up-regulated in serine hydroxamate-treated cultures, altered patterns of virulence gene expression were not apparent in *Y. pestis*. One may have anticipated TTSS virulence genes to be up-regulated in the starved *Y. pestis* cultures as this effect was observed in our *F. tularensis* data and the stringent response has been shown to induce virulence related phenotypes in other organisms such as *C. jejuni* and *S. flaxneri* as discussed in the introduction section 1.5.7 (194, 240); however this was not observed. This could be due to the culture conditions used to grow *Y. pestis* using 28 °C, rather than 37 °C, to ensure pCD1 was stably maintained in the bacteria, as 37 °C is an environmental cue that *Y. pestis* uses for expression of TTSS factors. The only TTSS genes that showed upregulation in serine hydroxamate-treated samples were *yopE* and *yopH*, similar to observations by Fukuto *et al* (410) who reported a global transcriptional profile of intracellular *Y. pestis* (410). Fukuto *et al* (410) also noted a down regulation of all TTSS genes residing on the plasmid pCD1 in intra-macrophage *Y. pestis*, except for *yopE* and *yopH* (410). This could mean that a serine hydroxamate-treated *Y. pestis* culture is more representative of intracellular *Y. pestis* during the early stages of infection, prior to escape from macrophages, than *Y. pestis* cultured in non-starvation media (410). Most of the virulence genes encoded on pCD1 were not captured by the RNA-seq most likely due to isolated RNA becoming degraded in processing or *Y. pestis* losing the virulence plasmid during laboratory culture. In total, across the entire genome, no sequence data was generated for 91 genes following RNAseq. As such, it is difficult to comment with certainty whether the *Y. pestis* virulence genes are affected in expression during the stringent response.

5.3.4. Stress response gene expression

Similarly to *F. tularensis*, it was observed that genes involved in stress responses were significantly up-regulated in the serine hydroxamate-treated *Y. pestis* cultures, as highlighted in figure 115. As with *F. tularensis*, the superoxide dismutase, *sodB,* was among the most

significant genes that showed an increased expression level. Genes involved in cold shock response *cspD* and *cspE* which encode a DNA replication inhibitor and a regulator of stress response proteins respectively (411), showed increased expression levels in both serine hydroxamate-treated growth conditions tested in the work presented here. This finding has also been observed during transcriptional profiling of intracellular *Y. pestis* (410).

5.3.5. Metabolic gene expression

Although the stringent response results in a global down shift of cellular processes in order to conserve resources and energy, cells undergoing the stringent response will also upregulate various metabolic pathways to prepare the bacterial cell for when growth condition return to favourable. Examples of metabolic processes that showed an increase in expression level were *acpP* and *fabG* which are genes involved in fatty acid metabolism. This pattern was observed in the *F. tularensis* RNA-seq data as well, indicating fatty acid biosynthesis is a process that intracellular bacteria prioritise for upregulation during adaptation to nutrient limitation.

5.3.6. Regulatory gene expression

Durfee *et al* (405) noted that *E. coli* cultures treated with serine hydroxamate up-regulated many more regulatory genes than were seen to be down regulated (405). Similarly, *Y. pestis* showed more regulatory genes being up-regulated than down-regulated in active stringent response conditions in our experiments presented herein (highlighted in figure 115). Moreover, *Y. pestis* appeared to upregulate many similar types of regulatory genes, particularly transcriptional regulators such as *metR* which encodes a transcriptional activator required for methionine synthesis, *fis* which encodes a global regulatory protein that activates rRNA transcription and *hns* which encodes a DNA binding protein involved in transcription repression (103).

5.4. *Burkholderia pseudomallei* Regulatory Analysis

To establish if the amino acid analogue serine hydroxamate could be used to induce the stringent response in *B. pseudomallei* in the same way that had previously been used for *F. tularensis* and *Y. pestis*, serine hydroxamate titrations were carried out on wild type cultures of *B. pseudomallei* K96243. It was hypothesised that a higher concentration of serine hydroxamate might be required to induce the stringent response and impact the growth of *B. pseudomallei* compared to the other previously studied microorganisms, due to the many stress and antibiotic resistance mechanisms present in *B. pseudomallei*.

5.4.1. Serine Hydroxamate Induction of the Stringent Response

Initial serine hydroxamate titration experiments showed that addition of up 100 µg/mL serine hydroxamate to cultures resulted in no negative impact on the overnight OD_{600} reading of the *B. pseudomallei* cultures (figure 101). However viable counts revealed a dose dependent growth inhibition effect from the same cultures (figure 102). This had not previously been observed when *F. tularensis* or *Y. pestis* were treated with serine hydroxamate using the same approach. Previously, addition of up to 100 µg/mL serine hydroxamate had no effect on the OD_{600} or viable counts of *F. tularensis* and *Y. pestis,* whereas addition of 1000 µg/mL significantly reduced the overnight OD_{600} readings and associated viable counts. To confirm this observation the same serine hydroxamate titration experiments were repeated, and the same effect was again observed for both the overnight OD_{600} readings and the associated viable counts (figures 103 and 104). These results indicate that, surprisingly, *B. pseudomallei* is perhaps more sensitive to the effects of serine hydroxamate than the other intracellular bacteria described in this thesis. The gradual decrease in viable counts also indicates that *B. pseudomallei* is unable to survive as well during stationary phase compared to *Y. pestis* and *F. tularensis*. To this end it was decided that the transcriptional study would focus on samples from *B. pseudomallei* cultures treated with 1 or 10 µg/mL serine hydroxamate and 0 µg/mL serine hydroxamate as a baseline control sample.

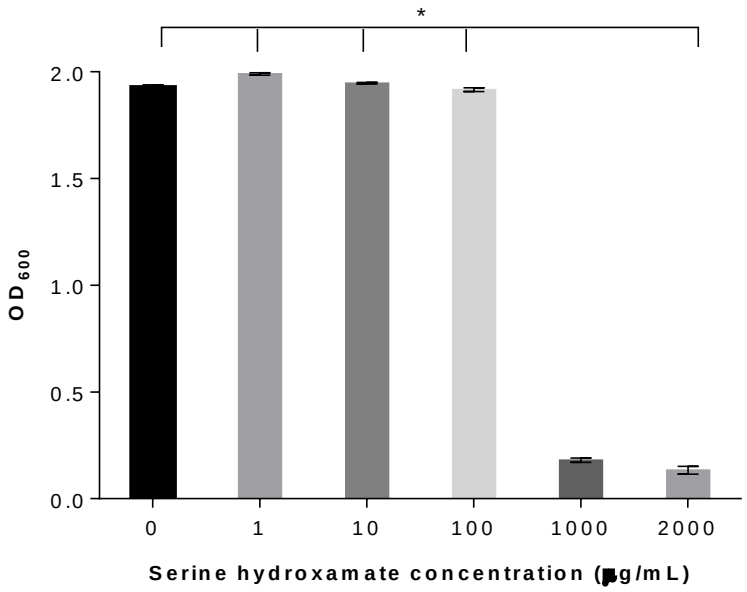

Figure 116. Optical density readings recorded from *B. pseudomallei* K96243 cultures incubated in the presence of various concentrations of serine hydroxamate (2000 µg/mL, 1000 µg/mL, 100 µg/mL, 10 µg/mL, 1 µg/mL and 0 µg/mL). Statistical significance determined by unpaired t-test with Welch's correction for unequal variance (* - $P \leq 0.05$).

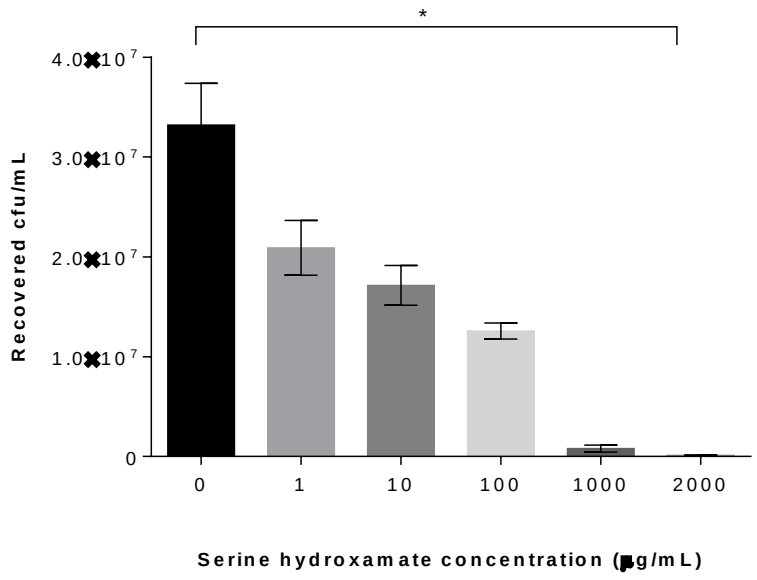

Figure 117. Viable counts recorded from *B. pseudomallei* K96243 cultures incubated in the presence of various concentrations of serine hydroxamate (2000 µg/mL, 1000 µg/mL, 100 µg/mL, 10 µg/mL, 1 µg/mL and 0 µg/mL). Statistical significance determined by unpaired t-test with Welch's correction for unequal variance (* - $P \leq 0.05$).

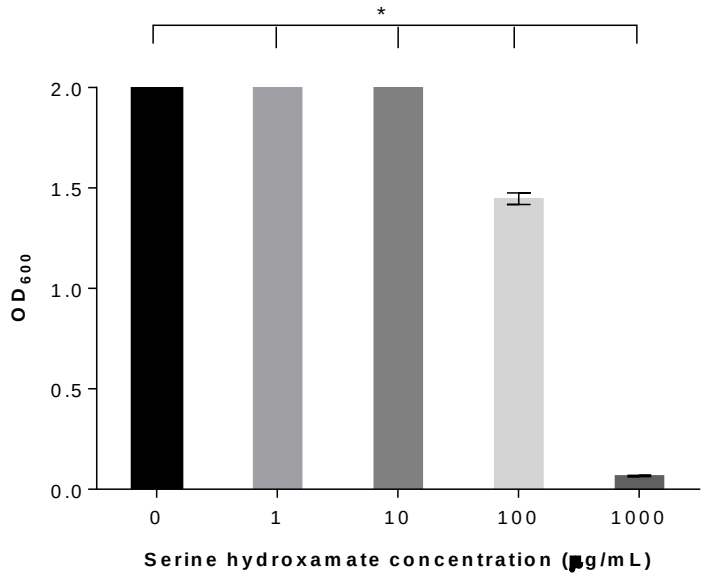

Figure 118. Repeat serine hydroxamate titration experiment showing optical density readings recorded from *B. pseudomallei* K96243 cultures incubated in the presence of various concentrations of serine hydroxamate (1000 µg/mL, 100 µg/mL, 10 µg/mL, 1 µg/mL and 0 µg/mL). Statistical significance determined by unpaired t-test with Welch's correction for unequal variance (* - P ≤ 0.05).

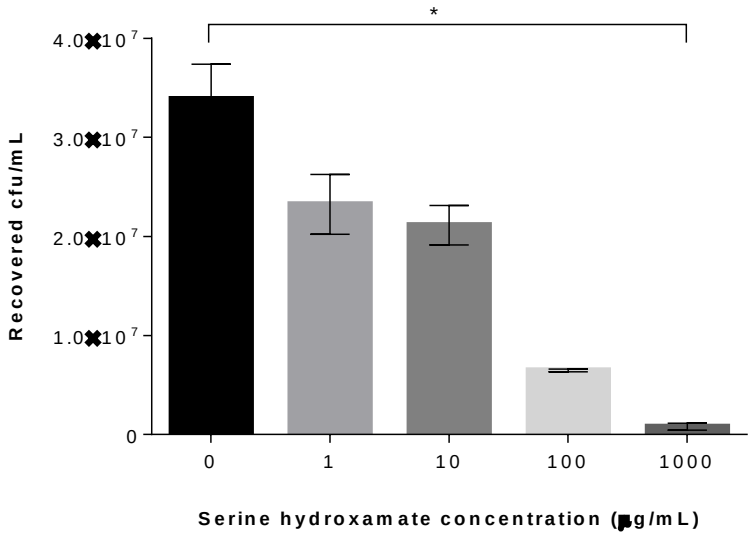

Figure 119. Repeat serine hydroxamate titration experiment showing viable counts recorded from *B. pseudomallei* K96243 cultures incubated in the presence of various concentrations of serine hydroxamate (1000 µg/mL, 100 µg/mL, 10 µg/mL, 1 µg/mL and 0 µg/mL). Statistical significance determined by unpaired t-test with Welch's correction for unequal variance (* - P ≤ 0.05).

RNA was isolated from *B. pseudomallei* cultures treated with either, 0, 1 or 10 µg/mL serine hydroxamate for subsequent whole transcriptome RNAseq analysis. RNA isolation, purification and on-column DNase digestion was carried out using the Qiagen RNeasy bacteria protect kit, according to the manufacturer's instructions. RNA isolates were then subjected to a two week sterility check. Following release from high containment, the samples were assessed for quality and quantity using the Bioanalyzer to ensure the samples met the minimum criteria required for high throughput RNAseq. The Bioanalyzer procedure is outlined in the method section 7.3.4 and the electropherogram is shown in figure 120 and the individual sample traces and concentrations are shown in Appendix 8.15. All samples met the quality and quantity criteria for high throughput RNAseq. A final concentration of 500 ng total RNA is required; therefore even the sample at the lowest concentration (SC06/0919) which was recorded at 42 ng/µL will provide enough material for sequencing due to the 60 µL volume that was prepared.

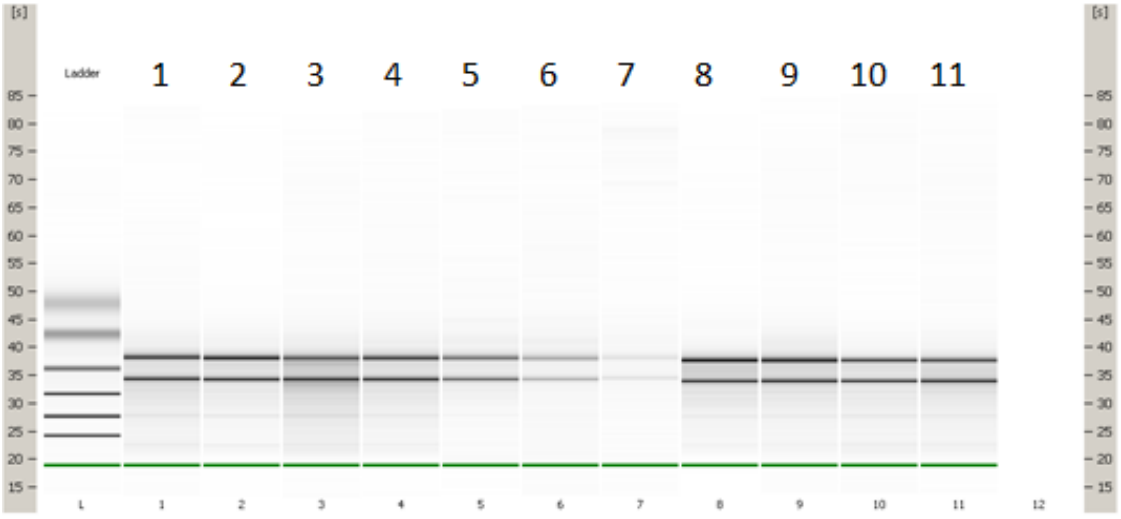

Figure 120. Electropherogram of 11 RNA samples prepared from *B. pseudomallei* K96243 cultured in the presence of different concentrations of serine hydroxamate. Lanes 1-3, 0 µg/mL serine hydroxamate, lanes 4-7, 1 µg/mL serine hydroxamate and lanes 8-11, 10 µg/mL serine hydroxamate. All samples show distinct 16S and 23S ribosomal RNA peaks with no high molecular weight genomic DNA contamination present. Band clarity varies indicating variable concentrations of total RNA.

5.4.2. Whole Genome RNA-Sequencing

Whole genome transcriptional profiling of *B. pseudomallei* strain K96243 revealed gene expression changes on a global scale in response to culturing in the presence of the amino acid analogue serine hydroxamate (figure 121). Significant differences were observed in the comparison between the baseline culture condition and the high concentration serine hydroxamate condition, which revealed 114 genes being differentially expressed (1.99% of the total genome). Significant differences were also observed when the low concentration serine hydroxamate condition was compared to the high concentration condition, which revealed 115 genes being differentially expressed (2.00% of the total genome), suggesting a titration effect from artificial induction of the stringent response (figure 122). This titration effect supports that of the *in vitro* starvation experiments that were carried out with to determine the concentration of serine hydroxamate that would inhibit the growth of *B. pseudomallei*. These experiments revealed an increasing degree of growth inhibition as the serine hydroxamate concentration was increased. Although the scale of differential expression observed in the *B. pseudomallei* dataset was less extensive that that observed for *F. tularensis* or *Y. pestis*, the changes were spread across many different biological processes, some of which having key roles in the virulence of *B. pseudomallei* (figure 123).

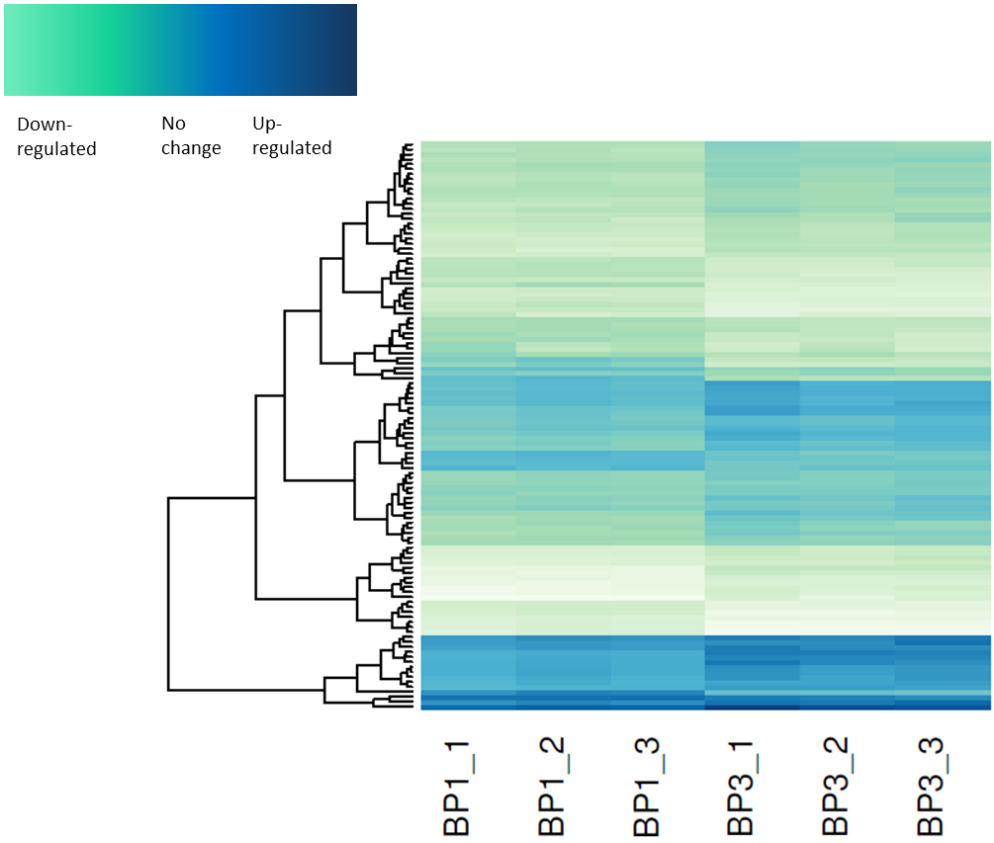

Figure 121. Heat map showing global gene expression profiles of B. pseudomallei K96243 isolated from cultures treated with different concentrations of serine hydroxamate. Left profile corresponds to the three samples from the control 0 μg /mL serine hydroxamate condition, right profile corresponds to the three samples from the 10 μg /mL serine hydroxamate condition. Individual genes are indicated on the x axis and clustered according to expression level in the different serine hydroxamate conditions. BP1_1, BP1_2 and BP1_3 are samples treated with 0 μg /mL serine hydroxamate, and BP3_1, BP3_2 and BP3_3 are samples treated with 10 μg /mL serine hydroxamate.

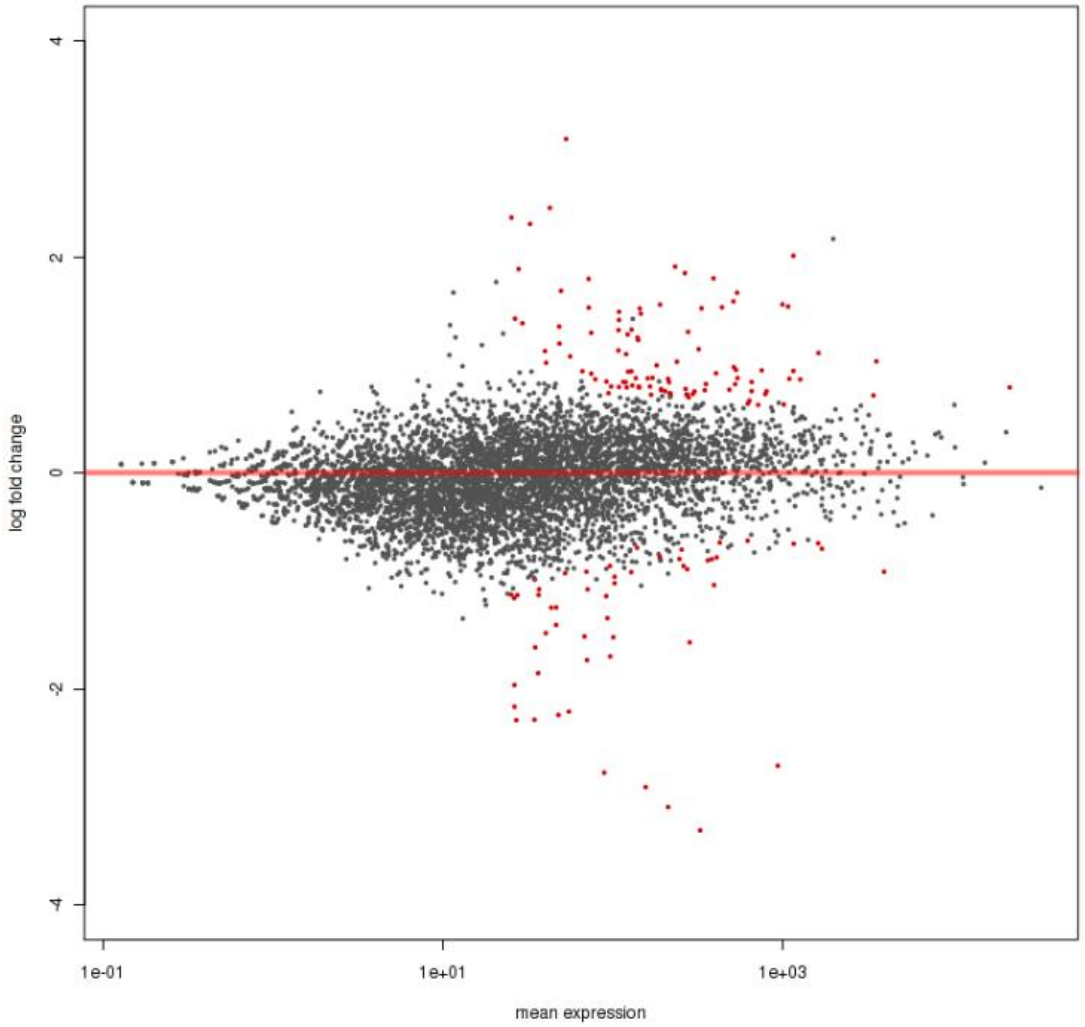

Figure 122. Volcano plot showing significantly differentially expressed genes derived from analysis at the 95% confidence interval of the data produced from the 0 versus 100 μg /mL serine hydroxamate conditions. Log fold change between the two conditions is plotted on the y axis and the mean P-values are plotted on the x axis versus. More significant data points are nearer the right of the plot and greater magnitude of fold change are to the top or bottom of the scatter plot. Data points in red are significant, points in grey are not significant.

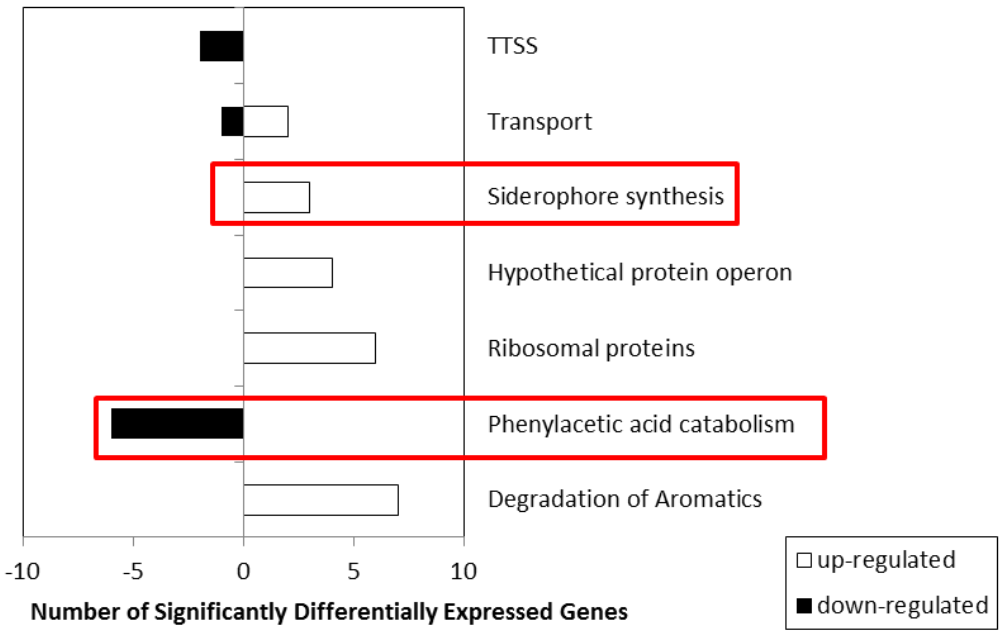

Figure 123. Number of genes up-regulated or down-regulated from the 115 most significantly differentially expressed genes in the 10 μg /mL serine hydroxamate condition, classified by functional category.

5.4.3. Phenylacetic Acid Degradation

The most significantly differentially expressed genes formed part of an operon involved in phenylacetic acid (PA) degradation (as highlighted in the red box in figure 123) (412). The PA catabolic pathway is the central route by which many aromatic compounds are degraded and directed to the Krebs cycle and has been shown to be required for full virulence of other *Burkholderia* species (412). The following genes all showed a significant down regulation in the presence of serine hydroxamate; *paaA*, *paaB*, *paaC*, *paaD*, *paaE*, *paaI* and *paaZ*. Previous studies have found that PA catabolic genes were up-regulated in *Burkholderia cenocepacia* cultured in synthetic cystic fibrosis sputum medium, which is particularly rich in amino acids, and that specific aromatic amino acids such as phenylalanine induce PA catabolism (413). It is therefore expected that under a growth condition in which amino acid starvation is simulated by the addition of serine hydroxamate, that PA catabolic gene would be down regulated as the bacterium assumes a lack of amino acids in its surrounding environment, and consequently induces the stringent response pathway.

5.4.4. Iron Acquisition

It has been widely published that iron acquisition plays a key role in the survival and virulence of *Burkholderia* species (59, 414-418). As such, *B. pseudomallei* has a dedicated siderophore, known as malleobactin (structure shown in figure 124), encoded by BPSL1776 and BPSL1774, which are designated *mbaA* and *mbaF* respectively and are involved in malleobactin synthesis (416). BPSL1775 designated *fmtA*, has also been shown to be involved in the transport of malleobactin (416). These genes are part of an operon including BPSL1778, designated *mbaJ,* which is also involved in malleobactin non-ribosomal peptide synthetase (416). Previous studies have demonstrated that siderophore synthesis is up-regulated under iron limiting conditions (415). Our results showed an increased expression level of siderophore-related genes under serine hydroxamate conditions (as highlighted in figure 123), which simulated amino acid limitation and induced the stringent response, thus siderophore synthesis is potentially up-regulated in response to a more diverse range of nutrient limitation cues, including amino acids, or the ability of *B. pseudomallei* to sequester the siderophore back into the cell is impeded.

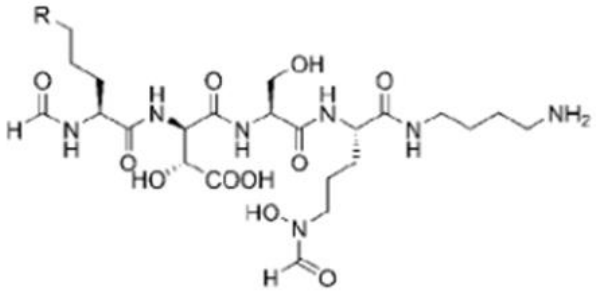

Figure 124. Structure of *B. pseudomallei* malleobactin A (figure adapted from Franke *et al* (419)).

To validate the significance of this results Chrome Azurol S (CAS) agar was prepared and the stringent response mutant strains and wild type *B. pseudomallei* K96243 grown on the indicator agar (figure 125) (420). The CAS agar comprises CAS dye and hexadecyltrimethylammonium bromide (HDTMA) which form a tight complex with ferric iron to produce a blue colour. When a strong iron chelator such as a siderophore, in the case of *B. pseudomallei* melleobactin, removes iron from the dye complex, the colour of the agar

changes from blue to orange (420). Therefore a deeper orange colour or larger area of orange agar indicates increased siderophore secretion or decreased siderophore transport back into the cell.

When compared to *B. pseudomallei* K96243 wild type both the Δ*relA* and Δ*relA/spoT* mutants showed darker orange and larger haloes surrounding bacterial growth on CAS agar plates. The Δ*relA/spoT* double mutant showed the most deep orange and largest haloes (figure 125). This result validates the gene expression results discussed previously as it demonstrates that the stringent response affects the *B. pseudomallei* siderophore both at the transcriptional level and phenotypic level.

A hypothesis that could explain these results is that disruption of the stringent response genes gives rise to increased siderophore secretion or decreased siderophore gene expression inhibition. As without the stringent response genes *relA* and *spoT* the bacterium cannot sense nutrient limitation in the environment, therefore as a protective mechanism *B. pseudomallei* may increase siderophore production to compensate for a potential lack of iron or other nutrients in the surrounding environment. An alternative hypothesis is that upon disruption of the stringent response genes *B. pseudomallei* can no longer retrieve secreted siderophores back into the cell meaning larger haloes in the CAS agar being observed. This effect has previously been observed in other organisms including *F. tularensis,* the *Bacillus* siderophore, bacillibactin and the *E. coli* siderophore enterobactin (372, 393, 421, 422).

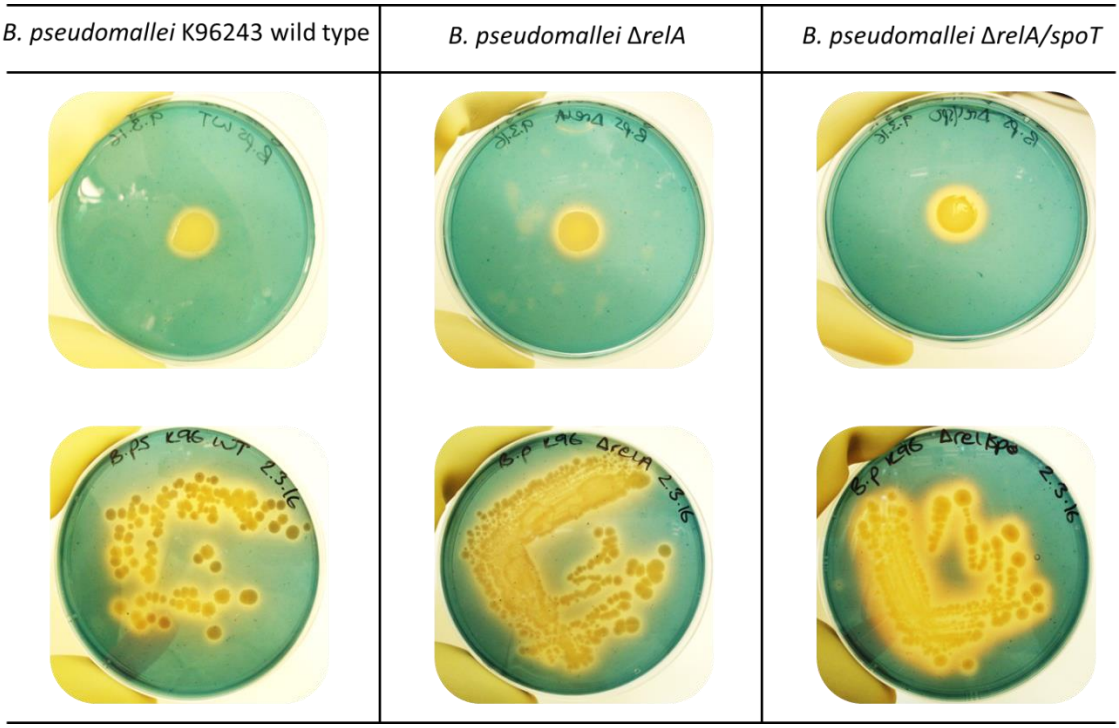

Figure 125. CAS agar plates showing *B. pseudomallei* K96243 wild type and mutants (Δ*relA* and Δ*relA*/*spoT*) growth. More intense yellow colouring and larger halo surrounding bacterial growth indicates increased siderophore production and thus removal of iron from the CAS agar. The top panels show siderophore production surrounding *B. pseudomallei* spotted onto CAS agar. The bottom panels show siderophore production surrounding *B. pseudomallei* streaked onto CAS agar.

5.5. Conserved Targets between Organisms

There were no common targets identified between all three pathogens; *B. pseudomallei, Y. pestis* and *F. tularensis*. Each pathogen studied in this work has a different mechanism of virulence and survival. Therefore, the fact that no conserved targets were identified between all three pathogens may not be surprising due to the complexities of the stringent response. This was highlighted whereby the similarities observed in the characterisation experiments between the organisms did not correlate with the same gene expression changes in the transcriptomics experiments. However, conserved genes were identified between the *Y. pestis* and *F. tularensis* gene expression data sets with genes being selected for inactivation to elucidate their contribution to the stringent regulon (table 10 and figure 126). In total there were only nine conserved genes identified between the stringent response regulons, four of these encoded ribosomal proteins, genes *fabI and fabG* which encode proteins involved in fatty acid biosynthesis, *dsbA* and *dsbB* which encode proteins involved in disulfide bond formation, *clpB* which encodes a heat shock protein, *feoA* which encodes a protein involved in ferrous iron (Fe^{2+}) transport and *acpP* which encodes an ACP response regulator involved in fatty acid starvation response. The gene *clpB* which encodes a heat shock protein involved in stress tolerance and an essential gene for intracellular replication and virulence *in vivo* in *F. tularensis* LVS (371), was established to be the most significantly differentially expressed gene that was present in both organism data sets. *dsbA* and *dsbB,* which are genes encoding proteins involved in disulfide bond formation were also significantly upregulated in our *F. tularensis* transcriptomic data. Specifically, *dsbA* encodes a periplasmic dithiol oxido-reductase that functions as a direct disulfide bond donor to folding proteins (423). *dsbB* encodes DsbB, a cytoplasmic embedded protein which oxidises and concurrently activates DsbA (424). Activation of DsbA by DsbB also requires association of either ubiquinone or menaquinone to oxidise and activate DsbB (425). The DsbB-quinolone complex forms a disulphide bond *de novo* which is then donated to DsbA, and subsequently to a plethora of other cellular proteins (426). The requirement of quinolone for DsbA/B activity perhaps explains why higher protein levels of UbiE, a ubiquinone biosynthesis protein, were observed in the *F. tularensis* proteomics results. Both *dsbA* and *dsbB* have also been shown to be essential for virulence for *F. tularensis in vivo* (427) and were significantly up-regulated in our *Y. pestis* and *F. tularensis* transcriptomics datasets presented herein so therefore may also be appropriate for further investigation as novel antimicrobial targets.

The genes *fabI and fabG* which encode ACP reductases were significantly up-regulated (428). FabG is a β-ketoacyl ACP-reductase and FabI is an enoyl-ACP-reductase and together form part of the FAS-II fatty acid biosynthetic pathway (429). *fabI* and *fabG* have already been shown to be essential in the FAS-II pathway in bacteria and have been evaluated as potential drug targets in *Plasmodium falciparum* for example (430, 431). *feoA* which encodes a protein involved in ferrous iron (Fe^{2+}) transport, was significantly up-regulated in *Y. pestis* and *F. tularensis* under stringent conditions. The Feo system is the only transport pathway that is widely distributed and that is dedicated to the transport of ferrous iron in bacteria (432, 433). The Feo system has been shown to be essential for iron acquisition in *Y. pestis*, with the *feoA* and *feoB* genes being essential for iron uptake (434). Previous studies have reported iron limitation inducing a SpoT-dependent accumulation of (p)ppGpp in *E. coli* (180) therefore the stringent response may also bring about gene expression changes to ensure other key survival mechanisms such as iron acquisition pathways are also upregulated.

Finally, *acpP* which encodes the ACP response regulator involved in fatty acid starvation response was also significantly up-regulated in *Y. pestis* and *F. tularensis* under stringent conditions. The ACP response regulator has been found to be an essential component of fatty acid biosynthesis in bacteria (367, 435-439). Our results indicate that fatty acid biosynthesis is a key process that intracellular pathogens prioritise during times of nutritional stress, as several components of this pathway including FabI, FabG and AcpP, were significantly up-regulated in *F. tularensis* and *Y. pestis* when cultures of which were treated with serine hydroxamate and analysed by whole genome transcriptomics.

Gene	Function	Bacteria in which conserved (↑ or ↓ expression)
clpB	Encodes a heat shock protein involved in stress tolerance, essential for intracellular replication and virulence *in vivo* (*F. tularensis* LVS). Solubilises protein aggregates and redirects misfolded proteins for re-folding via *dnaK* (440).	*Y. pestis* ↑ / *F. tularensis* ↑
dsbA/B	Encodes proteins involved in disulfide bond formation, essential for virulence *in vivo* (*F. tularensis*). Disulfide bond donor for various cellular proteins (423).	*Y. pestis* ↑/ *F. tularensis* ↑
FabI/G	Encodes ACP reductases. *fabG* encodes a β-ketoacyl ACP-reductase and *fabI* encodes is an enoyl-ACP-reductase and are involved in the elongation step in the bacterial fatty acid biosynthetic pathway (430).	*Y. pestis* ↑/ *F. tularensis* ↑
acpP	Encodes an essential fatty acid starvation response regulator. Mediates *de novo* fatty acid biosynthesis. AcpP acts as an anchor for the growing fatty acid chain (435).	*Y. pestis* ↑/ *F. tularensis* ↑
feoA	Encodes a ferrous iron transport protein essential for iron acquisition activity in bacteria including *Y. pestis* (441).	*Y. pestis* ↑/ *F. tularensis* ↑
rpsO	Encodes ribosomal protein S15 which binds 16S rRNA during ribosomal assembly (442, 443).	*Y. pestis* ↑/ *F. tularensis* ↑
rpsA	Encodes ribosomal protein S1 which is the largest ribosomal protein and plays a role in initiating protein synthesis (444-446).	*Y. pestis* ↑/ *F. tularensis* ↑
rpsJ	Encodes ribosomal protein S10 (447).	*Y. pestis* ↑/ *F. tularensis* ↑
rplD	Encodes ribosomal protein L4 (448, 449).	*Y. pestis* ↑/ *F. tularensis* ↑

Table 10. Summary of conserved targets that were differentially expressed in *Y. pestis* and *F. tularensis* in serine hydroxamate-treated cultures. *clpB* was selected as a new conserved target for mutagenesis in *F. tularensis* and *Y. pestis*.

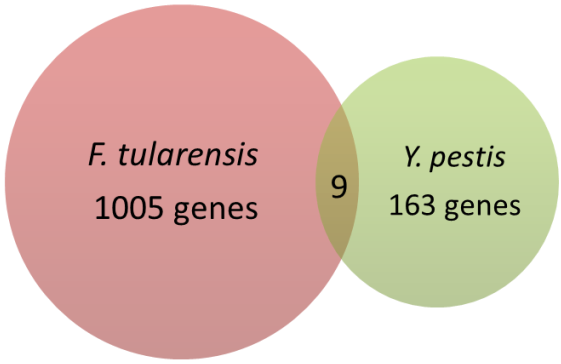

Figure 126. Venn diagram of the number of significantly differentially regulated genes in starved cultures of *F. tularensis* and *Y. pestis*, indicating those genes whose expression level were conserved in both organisms. The nine conserved genes are listed in table 10.

A gene that showed a significant increase in expression in both organisms was *clpB*, which encodes a heat shock protein chaperone with a known role in stress tolerance (371, 450), including resistance to oxidative stress, which has also been shown to be essential for intracellular replication and virulence *in vivo* in *F. tularensis* sub spp. *holarctica* LVS (371). In contrast, Motin *et al* (451) found that *clpB* was neither significantly up- nor down-regulated during temperature shift experiments from 26 °C to 37 °C to simulate *in vivo* infection (105). Some overlap of conserved pathways has been observed for bacteria undergoing the stringent response with other stresses, such as FPI gene expression being up-regulated inside macrophages which are likely to be a source of oxidative stress (373).

The *dsbA* gene, encoding a membrane lipoprotein involved in disulfide bond formation, showed significant increased expression levels in the starved cultures of both *F. tularensis* and *Y. pestis*. Straskova *et al* (452) demonstrated *dsbA* to be required for survival and replication in macrophages and that *dsbA* was required for *in vivo* virulence in a mouse infection model of tularemia (452). DsbA has also been shown to play a key role in the expression of essential virulence factors in *Y. pestis* (453). It was demonstrated that secretion of Yop effector proteins was significantly diminished in a *dsbA* deletion mutant (453). Another key virulence factor in *Y. pestis*, Ysc, showed specific instability in a *dsbA* mutant (453).

The enoyl-ACP reductase enzyme FabI, a protein that catalyses a key regulatory step in fatty acid biosynthesis, specifically the elongation process, was also observed to be up-regulated in both *F. tularensis* and *Y. pestis* under starvation conditions according to our transcriptional analysis. FabI has been shown to have essential activity for the growth of *F. tularensis* during the infection process (367). This protein has also been a target for novel antibacterial inhibitor development in various bacteria, including *F. tularensis* (454).

The acyl carrier protein, AcpP, was found to be significantly up-regulated in both our *F. tularensis* and *Y. pestis* data sets. The AcpP is known to be involved in the stringent response, being required for SpoT activity in response to fatty acid starvation conditions, and subsequent initiation of the stringent response. Although SpoT was not found to be up-regulated in either transcriptional analysis, this could indicate that, similarly to RelA, SpoT is already present in cells in sufficient quantities ready to respond to nutrient starvation conditions, and its activity is switched on during this process. However, AcpP appeared to require an increase in its expression to meet the demands of the bacterium under these stressful conditions. The *acpP* gene has also been shown to be essential in *E. coli* (436).

The gene *feoA*, is found as part of an iron uptake operon with *feoB* and *feoC*. However *feoA* was the only gene from this operon to be up-regulated under stringent conditions in our transcriptional analysis of *F. tularensis* and *Y. pestis*. Links have also been made between this iron uptake system and the ability of *Francisella* spp. to resist killing by ROS so has been implicated in stress responses (455). It has been proposed that *feoA* encodes a transport protein (441), and thus was surprising to see up-regulated during the stringent response in *F. tularensis* as generally, transport-associated genes showed a pattern of down-regulation in this experiment. However, in *Y. pestis* transport-associated genes showed almost equal levels of up- and down-regulation.

A group of genes that showed increased expression levels in *F. tularensis* and *Y. pestis* were the ribosomal proteins, *rpsO*, *rpsA*, *rpsJ* and *rplD*. This was an unexpected pattern as the stringent response initiates following a stalled ribosome and subsequent production of (p)ppGpp which then acts on various cellular targets to down-regulate various biochemical pathways to conserve resources until conditions become favourable again. One would expect

ribosomal protein synthesis to be a process that would scale back during the stringent response. As discussed earlier, this observation of up-regulated ribosomal proteins could be part of the adaptive process bacteria undergo before normal growth can resume following the stringent response. As (p)ppGpp levels increase, in turn giving rise to an increase in polyphosphate, ribosomal proteins are directed to the Lon protease for degradation. The supply of ribosomal subunits will run out unless more are generated to replenish those ribosomal proteins that have been degraded to provide the pool of free amino acids for starvation response protein synthesis.

5.6. Discussion and Conclusions

This study has demonstrated the direct association of *Francisella* virulence gene expression with an active stringent response, triggered by amino acid starvation conditions. In this study we demonstrated the ability to induce the stringent response artificially by culturing *F. tularensis* in the presence of low concentrations of the amino acid analogue serine hydroxamate. This allowed the stringent response to be studied *in vitro* at the global gene expression level by high throughput technologies such as RNA-seq. Using the *iglC* virulence gene as a genetic marker of active stringent response, it was anticipated that upon artificial amino acid starvation by the addition of serine hydroxamate, *iglC* expression would be switched on or up-regulated. This was first demonstrated by RT-PCR, and then confirmed by whole genome transcriptomics. Whole genome transcriptomics also revealed differential expression of the other genes comprising the type VI secretion system on the FPI and other genes involved in *Francisella* virulence such as *groEL* and *dsbA*. It has previously been established in *Y. pestis* that bacterial cells in stationary phase of growth, *in vitro*, show a greater similarity at the gene expression level to bacterial cells isolated from infection. Such stresses are likely to be representative of those encountered *in vivo* (408). It is hypothesised, as a result of this study, that artificial induction of the stringent response with serine hydroxamate can mimic the *in vivo* environment bacteria encounter during the infection process and result in a similar pattern of gene expression.

Interestingly, during active stringent response, *F. tularensis* up-regulated an equal number of genes to the number of genes down-regulated. From the 400 most significantly differentially expressed genes in the 1 μg/mL serine hydroxamate condition, 243 were up-regulated and 156 were down-regulated, which demonstrated that *F. tularensis* undergoes genome-wide gene expression changes as a result of nutrient starvation.

The *Y. pestis* transcriptomic data revealed predominantly different gene expression patterns compared to that of *F. tularensis* and *B. pseudomallei*. It was hypothesised that one would detect a significant upregulation of the TTSS genes residing on the virulence plasmid due to the stringent response simulating an in vivo stressful environment, and the fact the bacterium was grown at 37 °C, mammalian host body temperature, which should switch on virulence gene

expression. However, only two TTSS genes were significantly up-regulated, *yopE* and *yopH*. This anomaly could be explained by the fact the majority of pCD1-residing genes were not covered in the RNASeq and showed a complete absence of sequence reads. It is unclear as to why two pCD1 genes were sequenced in full and the remainder were not. It would therefore be recommended that this sequencing be repeated to ensure complete genome coverage is achieved so a realistic picture of the total gene expression changes *Y. pestis* undergoes when under active stringent response conditions. In contrast, a result that supported the proposed hypothesis was the increase in gene expression of stress response genes including *sodB*, which also showed upregulation in *F. tularensis*, and cold shock proteins, which have previously been shown to be up-regulated in intracellular *Y. pestis*. One would expect to see various stress response gene up-regulated during the stringent response as many different environmental cues can trigger the stringent response. As the RelA-dependent stringent response pathway was induced artificially, using serine hydroxamate rather than starving cultures of amino acids, it is plausible that the bacteria might upregulate more diverse stress response mechanisms to cover a range of environmental stresses including heat and cold stress, oxidative stress and nutrient limitation.

The *B. pseudomallei* transcriptomic data revealed far fewer genes being differentially regulated compared to the other two organisms, with only 2% of its genes showing changes in expression level. As the pathogen with the largest genome it is possible that *B. pseudomallei* has much more redundancy in its genome, and is able to maintain normal levels of gene expression during conditions of stress. However, some key pathways did show gene expression changes. One such pathway was the phenylacetic acid degradation pathway, which is the central route by which many aromatic compounds are degraded and directed to the Krebs cycle and has been shown to be required for full virulence of other *Burkholderia* species . Nearly the entire PA operon (*paaA*, *paaB*, *paaC*, *paaD*, *paaE*, *paaG*, *paaZ* and *paaI*) showed a significant down regulation in the presence of serine hydroxamate. This result supports previous studies which found that PA catabolic genes were up-regulated in *Burkholderia cenocepacia* cultured in synthetic cystic fibrosis sputum medium, which is particularly rich in amino acids (413, 456). It is therefore expected that under a growth condition in which amino acid starvation is simulated by the addition of serine hydroxamate, that PA catabolic genes would be down regulated as the bacterium assumes a lack of amino acids in its surrounding environment, and consequently induces the stringent response pathway.

Another pathway that showed significant alteration in its expression level in *B. pseudomallei* was the siderophore synthesis pathway. It is well established that iron acquisition plays a key role in the survival and virulence of *Burkholderia* species (414, 418, 457). As such, *B. pseudomallei* has a dedicated siderophore, known as malleobactin, encoded by *mbaA* and *mbaF* which are involved in malleobactin synthesis. The gene *fmtA*, has also been shown to be involved in the transport of malleobactin. These genes are part of an operon including *mbaJ,* which is also involved in malleobactin synthesis. Previous studies have demonstrated that siderophore synthesis is up-regulated under iron limiting conditions. Our results showed an increased expression level of siderophore-related genes under serine hydroxamate conditions, which simulated amino acid limitation, thus siderophore synthesis is potentially up-regulated in response to a more diverse range of nutrient limitation cues, including amino acids. It is also likely that the ability of *B. pseudomallei* to sequester the siderophore back into the cell is impeded if stress response genes, including those of the stringent response pathway, are inactivated. This hypothesis was tested by the growth of *B. pseudomallei* K96243 wild type and mutants on CAS agar plates. These plates revealed that the stringent response mutants showed either increased malleobactin synthesis, as visualised by the larger and deeper yellow halos surrounding bacterial growth, or that that secreted siderophore cannot be sequestered back into the cell in the deletion mutant strains.

Overall, this work has revealed that *F. tularensis* alters gene expression on a truly global scale under active stringent response conditions *in vitro* with over 60% of its genomic content significantly changing expression level. This global gene expression change consistent with the stringent response was observed for neither *Y. pestis* nor *B. pseudomallei* whose gene expression alterations were much less widespread.

The global gene expression profiles generated in this work will inform the selection of future targets for antimicrobial development. Many hypothetical proteins have also been highlighted as being significantly differentially expressed under active stringent response conditions, whose functions are yet to be elucidated, which could have important roles in bacterial virulence and stress responses.

6. Conclusions and Further Work

6.1. Conclusions

The overall objective of this project was to investigate the stringent response and polyphosphate biosynthesis pathways from a microbiological perspective by characterising bacterial mutants of the respective gene components of the pathways in three intracellular pathogens. The aim of this work was to inform the identification and development of potent inhibitors of *ppk, ppX* and *relA* as potential alternatives or adjuvants to current antibiotic prophylaxis. Treatment of tularaemia, plague and melioidosis is primarily by administration of antibiotics such as ciprofloxacin, but unfortunately all these infections are often associated with fatal outcomes, latent infection and resistant strains. In addition, there are no licenced vaccines for any these infections despite continued research into novel candidates.

Inherent antibiotic resistance and bacterial persistence are key issues for melioidosis and plague infections, but less so for tularaemia. This being said, all three agents discussed in this thesis are considered potential BWA and present a critical threat to both public health and biodefence. The stringent response has been the subject of preliminary research projects looking to exploit this pathway for the development of novel medical countermeasures (458). However, to date, there has been no single compound developed that can target Gram negative bacteria successfully. Therefore, we have taken a cross-genus approach to identify whether a small molecule inhibitor strategy is viable for Gram negative intracellular pathogens.

6.1.1. *Yersinia pestis* Mutants

In vitro and *in vivo* characterisation of *Y. pestis* mutants defective in stringent response and polyphosphate metabolism genes revealed phenotypes that suggest targeting the these pathways for novel bacterial small molecule inhibitors could be successful. Interesting phenotypes observed included particularly pronounced fitness defects for the double Δ*ppK/ppX* mutant. The Δ*ppK/ppX* mutant showed a significant growth defect compared to the wild type and other mutants when grown in laboratory media; the Δ*ppK/ppX* mutant was completely attenuated in a murine model of infection, whether challenged at a low or high dose via that sub cutaneous route of infection; the Δ*ppK/ppX* mutant also recorded

significantly lower levels of intracellular polyphosphate when tested for free phosphate with a malachite green spectrophotometric assay; finally, the Δ*ppK/ppX* mutant showed increased sensitivity to various antibiotics in disc diffusion assays. These results indicate that targeting the polyphosphate biosynthetic pathway, with small molecule inhibitors that can inhibit the activity of both the polyphosphate kinase, *ppK* and the exopolyphosphatease, *ppX,* could significantly inhibit the ability of *Y. pestis* to cause disease, or could indeed enhance the activity of antibiotics currently used to treat plague infection and thus improve patient outcome.

The *Y. pestis* Δ*relA* mutant also revealed results that indicated that the stringent response could also be a worthwhile target for antimicrobial development. Although the Δ*relA* mutant did not demonstrate an in vitro growth defect or attenuation in a murine model of infection, this mutant did show an increased sensitivity to various antibiotics in disc diffusion assays, again suggesting that targeting RelA for the development of a small molecule inhibitor could result in enhanced antibiotic activity, when used in the capacity as an adjuvant. Inactivation of RelA also increased persister cell formation compared to the wild type, in accordance with a recent model proposed by Maisonneuve *et al* (252) which proposes hierarchical control over bacterial persistence involving cascade effects due to (p)ppGpp, polyphosphate and toxin-antitoxin systems (169, 253, 342, 364, 459).

6.1.2. *Francisella tularensis* Mutants

Previous research undertaken at DSTL (14, 15) suggested that targeting the stringent response and polyphosphate biosynthetic pathways could be beneficial for the development of novel small molecule *Francisella* inhibitors. Work presented herein supports this notion and extends these preliminary studies by broadening the range of relevant phenotypes associated with *F. tularensis* and the stringent response. Specifically, assays which were carried out to test antibiotic sensitivity of *F. tularensis* mutants revealed that strains with mutations in *ppK*, *relA* and *relA*/*spoT* had increased sensitivity to various antibiotics irrespective of their mechanism of action. This indicated that small molecules inhibitors targeting these genes could be used as antibiotic adjuvants to enhance current antibiotic efficacy.

6.1.3. *Burkholderia pseudomallei* Mutants

Inactivation of genes involved in the stringent response in *B. pseudomallei* resulted in an increase in sensitivity to various classes of antibiotics; *B. pseudomallei* mutants displayed increased sensitivity to the tetracyclines, whereas the same mutants in *F. tularensis* and *Y. pestis* displayed increased sensitivity to various classes of antibiotics. However, *B. pseudomallei* may have further compensatory or alternative stress response mechanisms at play that are yet to be investigated and beyond the scope of this work. For example, *B. pseudomallei* has a very effective efflux mechanism which may have provided sufficient activity to resist the action of the antibiotics tested in this study.

Although the inactivation of stringent response genes did not result in a generic increases in sensitivity to various antibiotics, targeting the stringent response did result in attenuation in mice, which indicates that this pathway could provide appropriate targets for small molecule bacterial inhibitors, vaccines or antibiotic adjuvants.

6.1.4. Whole Genome Transcriptional Analysis of the Stringent Response

Overall, this work has revealed that *F. tularensis* alters gene expression on a truly global scale under active stringent response conditions *in vitro* with over 60% of its genomic content significantly changing expression level. This global gene expression change consistent with the stringent response was observed for neither *Y. pestis* nor *B. pseudomallei* whose gene expression alterations were much less widespread. The identification of few conserved targets between *F. tularensis*, *Y. pestis* and *B. pseudomallei* indicated that the stringent regulon is not conserved between organisms, whereas stringent-associated phenotypes are conserved.

The global gene expression profiles generated in this work will inform the selection of future targets for antimicrobial development. Many hypothetical proteins have also been highlighted as being significantly differentially expressed under active stringent response conditions, whose functions are yet to be elucidated, which could have important roles in bacterial virulence and stress responses.

6.2. Further Work

6.2.1. Additional Mutants Characterisation

A key experiment to complete for the currently generated mutants in all organisms presented herein is complementation of wild type copies of the targeted genes to ensure wild type phenotypes are restored. This will validate that the phenotypes presented herein are due to the mutations introduced to the organisms and not due to any off target effects.

Whole genome transcriptomics revealed two hypothetical proteins to be significantly and highly up-regulated during the *F. tularensis* stringent response (discussed in section 5.2.9). The genes FTT_1334c and FTT_0613, which currently have no annotation in the *F. tularensis* genome other than being assigned as putative ORFs encoding hypothetical proteins, were among the most significantly up-regulated genes following DESeq analysis. These mutants have been generated and initially tested for *in vitro* growth kinetics (section 5.2.11). There were no statistically significant growth difference between these mutant strains and the wild type *F. tularensis* SCHU S4. Further characterisation including *in vivo* virulence assessment, MIC experiments, persister assays, and protein characterisation and expression studies should be carried out to determine the suitability of these targets for novel bacterial inhibitors or antimicrobials.

Another target that was selected for mutation from the conserved target list between *F. tularensis* and *Y. pestis* was *clpB*. ClpB has been characterised as a caseinolytic peptidase B and acts as a protein chaperone generally induced during stress. ClpB binds damaged protein aggregates via ATP hydrolysis and unfolds the denatured protein aggregate. Work has been done to generate a Δ*clpB* mutant in *Y. pestis* GB and a Δ*clpB* mutant has been obtained for *F. tularensis* SCHU S4. These mutants are yet to be characterised *in vitro* and *in vivo*, however it is planned to conduct phenotypic assays as mentioned previously in this work, including growth kinetics *in vitro*, antibiotic sensitivity assays, virulence assessments in an insect model and murine model of infection, intracellular polyphosphate quantification and *in vitro* persister assays. These experiments will help determine which stringent response-affected phenotypes ClpB activity contributes to and enable a better understanding of the stringent response regulon.

In addition to novel targets for mutagenesis identified from transcriptomics data, a mutant targeting the Lon protease (Lon) due to its direct association with the (pp)ppGpp and polyphosphate cascade leading to bacterial persistence would provide additional evidence for a direct link of the stringent response and bacterial persistence. This would be the first time that this would be demonstrated in *F. tularensis*, *Y. pestis* and *B. pseudomallei*.

6.2.2. Inhibitor Screening *in vitro* and *in vivo*

Enzymatic activity screening conducted at the University of Southampton have identified a potential inhibitory compound for *F. tularensis* PPK. As such, the compound should be tested in a biological assay, such as an *in vitro* MIC experiment, to look for a biological effect that could then be optimised to create an effective small molecule *Francisella* inhibotor. The inhibitor is likely to have most efficacious biological function when used as an antibiotic adjuvant. It is therefore recommended that the PPK inhibitor is tested in combination with an antibiotic that showed increased action in the previosuly described antibiotic disc diffusion experiemnts.

Should any testing of the potential *F. tularensis* PPK inhibitor suggest that the compound has biological activity further assessment of the compound should then be carried out including *in vivo* experiments using the murine Balb/C model of tularaemia. Additionally, as our results have indicated that a PPK inhibitor is perhaps a more suitable target for an antibiotic adjuvant, the inhibitor compound should be tested in a murine model in combination with an antibiotic of relevance for the treatment of tularaemia to establish if the antibiotic activity against *F. tularensis* infection is enhanced.

6.2.3. Whole Genome Transcriptional Analysis of Current Mutants Strains

Whole genome transcriptomics was carried out on wild type strains of the bacteria of interest in this work. As mutants have been created targeting stringent response and polyphosphate biosynthesis genes it would be recommended that further transcriptomics be carried out on cultures of *F. tularensis*, *Y. pestis* and *B. pseudomallei* mutant strains including Δ*relA*, Δ*relA/spoT,* Δ*ppK, and* Δ*ppX* to look for novel patterns of gene expression in response to

stringent response induction by serine hydroxamate. It would be expected that without the activity of these key genes the bacteria would initiate alternative stress response mechanisms or perhaps display a dysregulation of stress response genes due to the lack of the appropriate biosynthetic pathways. It would also be interesting to carry out proteomic studies on these mutants to elucidate if protein expression effects are still observed when components of the stringent response pathway and polyphosphate biosynthesis pathway are disrupted and how these effects compare to the transcriptional profiles of stringent response and polyphosphate defective mutants.

7. Materials and Methods

7.1. Materials

7.1.1. Preparation of Media and Supplements

All media and supplements were prepared as described below unless otherwise stated.

7.1.2. Luria-Bertani Medium

Luria-Burtani (LB) broth consisted of 10 g/L bacto-tryptone (Difco), 5 g/L bacto-yeast extract (Difco) and 5 g/L NaCl dissolved in the require volume of distilled water (dH_2O) and autoclaved at 121°C for 15 min. LB broth was subsequently stored at 4°C. LB agar was prepared as described for LB broth, except 20 g/L bacto-agar (Difco) was added before making up to the required volume in dH_2O and autoclaving at 121 °C for 15 min. Agar was cooled to 50°C before any supplements were added.

7.1.3. Blood Agar Base Medium

Blood agar base (BAB) broth consisted of 15 g/L Proteose Peptone (Oxoid), 2.5 g/L Neutralised Liver Digest (Oxoid), 5 g/L Yeast Extract (Oxoid) 5 g/L NaCl dissolved in the required volume of dH_2O and autoclaved at 121 °C for 15 min. BAB hemin agar consisted of 40 mL blood agar base (Oxoid) made up to the required volume with dH_2O and autoclaved at 121 °C for 15 min. After cooling to 50 °C 8 mL hemin (sigma), made up as described below, was added, then the agar was filter sterilised.

7.1.4. Blood Cysteine Glucose Agar Medium

Blood cysteine glucose agar (BCGA) consisted of 3 g/L Lab Lemco (Oxoid), 20 g/L Bacteriological peptone (Oxoid), 12. 5 g/L technical agar (Oxoid), 5 g/L NaCl dissolved in the desired volume of dH_2O. After cooling 50 °C, 10% L-cysteine 10 mL/l, 10 % L-histidine 10 mL/l, 50 % glucose solution and 50 mL/L and defibrinated horse blood (Oxoid) 50 mL/L, was added, then autoclaved at 121 °C for 15 min.

7.1.5. Chamberlain's Defined Medium

Chamberlain's defined medium (CDM) consisted of 0.4 g/L L-arginine, 0.4 g/L L-aspartic acid, 0.2 g/L L-cysteine, 0.2 g/L L-histidine, 0.4 g/L DL-isoleucine, 0.4 g/L L-leucine, 0.4 g/L L-lysine, 0.4 g/L DL- methionine, 2 g/L L-proline, 0.4 g/L DL-serine, 2 g/L DL-threonine (allofree), 0.4 g/L L-tyrosine, 0.4 g/L DL-valine, 0.04 g/L spermine diphospahte, 4 mg/L thiamine HCl, 2 mg/L DL-calcium pantothenate, 4 g/L D(+)-glucose, 10 g/L K2HPO4 dissolved in the required volume of dH_2O and autoclaved at 121 °C for 15 min.

7.1.6. Thayer Martin Agar

Thayer Martin agar plates consisted of 100mL 2% Haemoglobin, 100mL 2xGC Agar base, 2ml IsoVitalex (BD), 10-100µg/mL kanamycin or 10% w/v sucrose, depending on the selection required. GC agar base and haemoglobin were autoclaved at 121 °C for 15 min and antibiotic or sucrose was added to haemoglobin. GC agar base was then melted and cooled to 50 50 °C and combined with haemoglobin, antibiotic or sucrose.

7.1.7. Antibiotics and Supplements

Antibiotics were routinely prepared as stock solutions and were used at the final concentrations listed in table 3 in both liquid and solid media. Hemin was routinely made to a stock concentration of 0.25% (v/v) and consisted of 0.75 g hemin powder (sigma) and 10mM NaOH made up to 300 mL in dH2O and filter sterilised using 0.2 µm filters. For every 200 mL growth media, 16 mL 0.25% (v/v) hemin was added.

Serine hydroxamate was sourced from Sigma Aldrich reconstituted in in dH_2O to make a 25 mM stock solution then diluted as required in dH_2O and stored at -20 °C.

Supplement	Stock solution	Final concentration
Ampicillin (Sigma Aldrich)	25 mg/mL	55 μg/mL or 100 μg/mL
Chloramphenicol (Sigma Aldrich)	50 mg/mL	50 μg/mL
Doxycycline(Sigma Aldrich)	25 mg/mL	Various – as stated in specific methods
Gentamicin (Sigma Aldrich)	25 mg/mL	Various – as stated in specific methods
Kanamycin (Sigma Aldrich)	25 mg/mL	50 μg/mL
Polymyxin B (Sigma Aldrich)	50 mg/mL	100 μg/mL
Streptomycin (Sigma Aldrich)	25 mg/mL	Various – as stated in specific methods
Tetracycline (Sigma Aldrich)	25 mg/mL	Various – as stated in specific methods
Trimethoprim (Sigma Aldrich)	50 mg/m	100 μg/mL
Sucrose(Sigma Aldrich)	20 % (w/v)	10% (w/v)
Serine Hydroxamate (Sigma Aldrich)	25 mg/mL	Various – as stated in specific methods

Table 11. Supplements used in this study

7.2. General Microbiology Methods

7.2.1. *Escherichia coli*

All *E. coli* strains (table 12) were grown and stored as follows unless otherwise stated. For long-term storage, -80 °C freezer stocks were made. For short-term storage, bacteria from a -80 °C stock were streaked onto LB agar containing the appropriate supplements. The streak plate was then incubated for 18 – 22 hours at 37 °C or at 37 °C with agitation for 18 – 22 hours in LB broth containing the appropriate supplements.

7.2.2. *Francisella tularensis*

All *F. tularensis* strains (table 12) were grown and stored as follows unless otherwise stated. For long-term storage, -80 °C freezer stocks were made as described below. For short-term storage, bacteria from -80 °C freezer stock were streaked onto BCGA agar supplemented with 10% L-cysteine 10 mL/L, 10 % L-histidine (10 mL/L), 50 % glucose solution (50 mL/L) and defibrinated horse blood (Oxoid) (50 mL/L), incubated at 37 °C for 2 - 4 days, before storage at 4 °C for up to three weeks. For routine culture of bacteria, chamberlain's defined medium was inoculated with bacteria scraped from a streak plate to an OD_{600} of 0.1, and incubated at either 37 °C with agitation for 18 – 22 hours.

7.2.3. *Yersinia pestis*

All *Y. pestis* strains (table 12) were grown and stored as follows unless otherwise stated. For long term storage, -80 °C freezer stocks were made as described below. For short term storage, bacteria from -80 °C freezer stock were streaked onto BAB agar supplemented with 0.25% hemin and incubated at 28 °C for two days, before storage at 4 °C for up to three weeks. For routine culture of bacteria, BAB broth was inoculated with an isolated colony from a streak plate and incubated at either 28 °C or 37 °C with agitation for 18 – 22 hours.

7.2.4. *Burkholderia pseudomallei*

All strains of *Burkholderia pseudomallei* (table 12) were grown and stored as follows unless otherwise stated. For long-term storage, -80 °C freezer stocks were made as described below. For short-term storage, bacteria from -80 °C freezer stock were streaked onto LB agar and incubated at 37 °C for 48 hours, before storage at 4 °C for up to three weeks. For routine culture of bacteria, LB broth was inoculated with an isolated colony from a streak plate and incubated at 37 °C with agitation for 18 – 22 hours.

7.2.5. Bacterial Staining

Bacteria that had grown on solid media were tested by Gram's staining. A portion of a single colony was homogenised in dH_2O and spotted onto a glass microscope slide. The slide was air dried and then placed at 65 °C for 20 min. The fixed bacteria were stained in crystal violet (0.8 % ammonium oxalate-crystal violet) (sigma) for 30 seconds then washed in d dH_2O. The slide was then submerged in Lugol's iodine (5 % iodine, 10 % potassium iodide) (sigma) for 30 seconds then briefly in acetone before being washed in dH_2O. Finally, bacteria were counter-stained in saffranin red (0.5 % saffrinin) (sigma) for 30 seconds and washed in dH_2O. The slide was air dried before being analysed under oil immersion using a light microscope (x 1000).

7.2.6. Glycerol stocks

Bacterial broth cultures were prepared as described above for each species and were incubated under the required conditions for 18-22 hours. An aliquot of 0.7 mL of bacterial culture was transferred into a cryotube and 0.3 mL sterile glycerol was added. The stock was stored in a -80 °C freezer.

7.2.7. Sterility Check Procedure

A sterility check was performed on nucleic acid products prepared in ACDP containment level 3 laboratories if they were to be used in an ACDP containment level 2 laboratory. A volume of 10 % of the product was transferred to a flask containing the original volume of the require broth. The flask was incubated statically at the required growth temperature for the organism

for 7 days. After 7 days the broth was spread onto appropriate agar plates, and incubated at the required temperature for a further 7 days. Following incubation plates were checked for bacterial growth and visible colonies were picked and stained as described above. If no colonies were present on the plates or if low numbers of Gram positive bacteria were identified by staining, the culture was considered to have passed the sterility check, and was used in a containment level 2 laboratory.

Strain	**Relevant properties**	**Source/Reference**
Escherichia coli		
S17 λ *pir*	*recA thi pro hsdR-M*$^{+}$ <RP4 : 2-Tc : Mu : Kn : Tn7>Tp^{R} Sm^{R} . Mobilising strain to act as donor for conjugation	(307)
DH5 α λ *pir*	F_ _80*lacZ*_M15 _(*lacZYA-argF*) *U169 deoR recA1 endA1 hsdR17*(r_K _ m_K _) *phoA supE44*	(460)
JM109 (strain K12)	F´ *traD36 proA*$^{+}$*B*$^{+}$ *lacI*^{q} *Δ(lacZ)M15/ Δ(lac-proAB) glnV44 e14*$^{-}$ *gyrA96 recA1 relA1 endA1 thi hsdR17*	Promega, UK
SCS110 (derivative of JM110)	*rpsL* (Strr) *thr leu endA thi-1 lacY galK galT ara tonA tsx dam dcm supE44* Δ(*lac-proAB*) [F´ *traD36 proAB lacI*qZΔ*M15*] Dam and Dcm deficient. streptomycin resistant.	Stratagene
Yersinia pestis		
GB	Orientalis (Virulent)	Human – UK
Francisella tularensis		
SCHU S4	Isolated 1941, *tularensis*	Human – USA
Burkholderia pseudomallei		
K96243	Isolated 1996, female, Khon Kaen	Human – Thailand

Table 12. Bacterial strains used in this study.

7.3. General Molecular Biology Methods

7.3.1. Isolation of Genomic DNA

Bacteria were grown in a liquid volume of 10 mL for 18-22 hours in the appropriate media containing the required supplements. The Qiagen Puregene DNA isolation kit was used to isolate genomic DNA (gDNA), according to the manufacturer's instructions.

All nucleic acids were subjected to a sterility check prior to removal from the ACDP containment level 3 laboratory. Meanwhile the gDNA was stored at 4 °C.

7.3.2. Isolation of Plasmid DNA

For small-scale isolation of plasmid DNA, 3 mL of an overnight culture grown in the appropriate broth containing the required supplements was used in the Qiagen plasmid mini-prep kit. The manufacturer's instructions were followed and plasmid DNA was routinely eluted in a final volume of 50 µL deionised water or elution buffer.

7.3.3. Isolation of Total RNA

F. tularensis SCHU S4 was grown in a volume of 50 mL for 18-22 hours in Chamberlain's defined medium (17) with or without serine. Cells were pelleted and stored in Qiagen's RNA bacteria protect reagent and the Qiagen RNeasy RNA isolation kit was used, according to the manufacturer's instructions to extract total RNA.

Y. pestis GB was grown in a volume of 50 mL for 16 hours in BAB broth with or without serine. Cells from overnight growth were pelleted and stores in 2X volume in Qiagen's RNA bacteria protect reagent and the Qiagen RNeasy RNA isolation kit was used, according to the manufacturer's instructions to extract total RNA.

B. pseudomallei K96243 was grown in a volume of 50 mL L-broth for 16 hours with or without serine. Cells from overnight growth were pelleted and stores in 2X volume in Qiagen's RNA bacteria protect reagent and the Qiagen RNeasy RNA isolation kit was used, according to the manufacturer's instructions to extract total RNA.

RNA was subjected to a sterility check prior to removal from the ACDP containment level 3 laboratory. Meanwhile the RNA was stored at -80 °C.

7.3.4. Bioanalyser Quality Assessment of Total Isolated RNA

The chip priming station was set up with a new syringe and the old syringe was discarded. Using the RNA 6000 pico reagent set (Agilent Technologies), the supplied RNA ladder was heat denatured at 70°C for 2 minutes. The ladder was immediately cooled on ice and 90 µL RNase free dH_2O added, mixed and aliquoted into single use amounts then stored at -80°C. Reagents were allowed to equilibrate to room temperature for 30 minutes. 550 µL gel matrix was filtered through a spin filter by centrifugation at 1500 g for 10 minutes. The gel matrix was aliquoted into 65 µL amounts. 1 µL RNA 6000 pico dye concentrate was added to an aliquot of gel matrix, mixed and spun down at 13000 g for 10 minutes. The chip was then loaded according to the kit instructions and each sample to be analysed was added to the appropriate well along with an RNA marker. The chip was then vortexed for 1 minute and loaded onto the BioAnalyzer and run on the appropriate protocol.

7.3.5. Polymerase Chain Reaction

PCR was routinely used to amplify specific regions of DNA from lysed bacteria, genomic DNA or plasmid DNA. A typical 50 µL PCR consisted of 10 µL 5x High Fidelity reaction buffer, 31.3 µL dH_2O, 2.5 µL of each 10 pm/µL primer, 1 µL 10 mM dNTPs, 0.5 µL Phusion polymerase, and 2 µL DNA template. A negative control of sterile water was included. Where possible a positive template control, containing the expected DNA region was also included. The amplified DNA fragments were analysed by agarose gel electrophoresis (explained below). PCR cycling conditions used were as follows; Initial denaturation cycle of 98 °C for 30 s, followed by 30 cycles of 98 °C for 10 s, 55 °C (or other appropriate annealing temperature) for 30 s, 72 °C for 1

min, followed by a final extension of 72 °C for 10 min, then 4 °C on hold. For colony PCR, lysates were prepared by picking a single colony into 50 µL sterile dH_2O, then boiling the sample for 5 min to lyse the bacterial cells. Each lysate was then centrifuged at 12 000 g for 5 min. 1 µL of the supernatant was used as template for PCR. PCR primers were synthesised by Eurofins MWG.

7.3.6. Reverse-Transcriptase Polymerase Chain Reaction

The Titanium® One-Step RT-PCR Kit (ClonTech) was used to generate a cDNA template and amplify a target region of a gene. A typical reaction comprised a mastermix of 5 µL 10x One-step buffer, 1 µL 50X dNTP mix, 0.5 µL recombinant RNase inhibitor (40 units/µL), 25 µL thermostabilising reagent, 10 µL GC melt, 1 µL oligo (dT) primer and 1 µL 50X Titanium *Taq* RT enzyme mix. A typical experimental reaction comprised 43.5 µL the above mastermix, 2 µL experimental primer mix (45 µM each), 1 µL experimental RNA and 3.5 µL dH_2O to give a total volume of 50 µL. A positive control reaction comprised 43.5 µL mastermix, 1 µL control mouse β-actin primer mix, 1 µL control mouse liver total RNA and 4.5 µL dH_2O to give a final volume of 50 µL. A negative control of sterile water was also included. PCRs were run on the following thermal cycling protocol; Initial cDNA synthesis 50 °C I hour, then denaturation at 94 °C 5 minutes, then 30 cycles of 94 °C 30 seconds, 65 °C 30 seconds, 68 °C 1 minute, then a final extension of 68 °C 2 minutes then 4 °C on hold. PCR products were analysed by agarose gel electrophoresis. PCR primers were synthesised by Eurofins MWG.

7.3.7. GC-Advantage Polymerase Chain Reaction

The Advantage ® GC 2 PCR kit (ClonTech) was used to amplify flanking regions of the target genes for inactivation from the highly GC rich genome of *B. pseudomallei* K96243. A typical reaction comprised 10 µL 5X GC 2 PCR Buffer, 30 µL dH_2O, 2 µL Primer mix (10 µM each primer), 1 µL 50X dNTP mix (10mM each nucleotide), 5 µL GC-Melt (0.5M), 1 µL Advantage GC 2 Polymerase Mix (50X) and 1 µL template DNA to give a total volume of 50 µL. A negative control of sterile water was included. Where possible a positive template control, containing the expected DNA region was also included. The amplified DNA fragments were analysed by agarose gel electrophoresis. A two-step PCR cycling protocol was used as follows; Initial denaturation cycle of 94 °C for 3 minutes, followed by 25 cycles of 94 °C for 30 seconds, 68 °C

for 1.5 minutes, followed by a final extension of 68 °C for 3 min, then 4 °C on hold. PCR primers were synthesised by Eurofins MWG.

7.3.8. Agarose Gel Electrophoresis

The method of agarose gel electrophoresis described by Sambrook *et al*. (1989) was followed (118). A 1% (w/v) agarose gel was routinely used for the visualisation of DNA fragments of 0.8 kb – 10 kb, and a2 % gel was used for the visualisation of fragments less than 0.8 kb. The appropriate amount of agarose was added to a suitable volume of tris-acetate-EDTA (0.04 M Tris-acetate, 0.001 M EDTA) buffer and melted until the solution was transparent. The molten agarose was cooled to ~ 50 °C then ethidium bromide was added to give a final concentration of 0.5 µg/mL. DNA samples were routinely prepared for loading onto an agarose gel by adding 6 sample buffer (0.25 % bromophenol blue (w/v) and 40 % sucrose (w/v) in dH_2O). Molecular weight markers used (Roche Diagnostics) were XIV, which is digested into fragments of 2642 bp, 1500 bp, 1400 bp, 1300 bp, 1200 bp, 1100 bp, 900 bp, 800 bp, 700 bp, 600 bp, 500 bp, 400 bp, 300 bp, 200 bp and 100 bp. Molecular weight marker III is digested into fragments of 21, 226 bp, 5148 bp, 4973 bp, 4268 bp, 3530 bp, 2027 bp, 1904 bp, 1584 bp, 1375 bp, 947 bp, 831 bp, 564 bp and 125 bp. An aliquot of 10 µL was routinely loaded onto agarose gels. A voltage of 90 – 110 V was applied to the agarose gel until the dye front had migrated an appropriate distance through the gel. Gels were examined using an ultraviolet transilluminator.

7.3.9. Determination of DNA Concentration

DNA concentration was measured using the Qubit 2.0 fluorometer (Life Technologies™) and associated high sensitivity dsDNA quantification PicoGreen dye kit (for double stranded DNA), according to the manufacturer's instructions. Samples quantified were in concentration from 100 pg⁄µl–1,000 ng⁄µl. The PicoGreen dye was diluted 1:200 in the supplied buffer, and between 1 – 20 µL of sample was added to be read in the fluorimeter.

7.3.10. Restriction Endonuclease Digest

DNA digestion reactions (tables 13 and 14) were prepared in reaction mixes of the following composition. Digests were incubated at 37 °C for 90 minutes or overnight and the products were separated by gel electrophoresis and gel extracted and purified using the Qiagen Gel Extraction and Purification kit according to the manufacturer's instructions.

Component	**1x / µL**
NEB Buffer 3	5
***Mlu*I Restriction Enzyme**	1
pSMP75 (1 µg)	1
dH_2O	43
Final Volume	**50**

Table 13. Restriction enzyme digests reaction composition for pSMP75.

Component	**1x / µL**
NEB Buffer 3 or 4	8
***Xba*I or *Bgl*II Restriction Enzyme**	8
pDM4 (1 µg)	60
dH_2O	4
Final Volume	**80**

Table 14. Restriction enzyme digests reaction composition for pDM4.

7.4. Creation of Mutants – *Yersinia pestis*

7.4.1. Ligation of DNA Fragments into Plasmid Vectors

For selected targets synthetic deletion constructs were synthesised at LifeTechnologies™ GeneArt® synthesis service, for sub-cloning into vectors required for transformation procedures.

A ratio of 1:1 or 1:2 insert:vector DNA concentration was used per ligation reaction. A final concentration of 1X ligation buffer and 1 U T4 DNA ligase (Roche Diagnostics) were added to each reaction before being made up to the required volume in dH_2O. Each reaction was incubated at 16 °C for 18-22 hours. In order to ligate a concentrated PCR product into a T-cloning vector, the manufacturer's instructions were followed.

7.4.2. Electro-competent *Yersinia pestis* Cells

A 20 mL volume of BAB broth was inoculated with the required *Y. pestis* strain and incubated aerobically at 28 °C for 18 – 22 hours. An aliquot of 1 mL of this culture was inoculated into a volume of 40 mL BAB broth and incubated aerobically at 28 °C for a further 6 hours. Following incubation, the culture was chilled and centrifuged at 10 000 g at 4 °C for 12 min to pellet cells. Cells were then washed three times in sterile 10 % glycerol (w/v) before being resuspended in a final volume of 300 µL sterile, chilled 10 % glycerol (w/v). Aliquots of 60 µL of cells were transferred to cryotubes and stored at -80 °C.

7.4.3. Transformation of *Yersinia pestis* by Electroporation

Electro-competent *Y. pestis* cells were thawed on ice for 2 – 3 min prior to use. 1 µL of cleaned up PCR products were added to the cells and mixed by pipetting. The cells were then transferred to a pre-chilled and dried electroporation cuvette (Bio-Rad) and were transformed by electroporation at 200 Ω, 25 µF and 1.6 kV. Cells were resuspended in 1 mL BAB broth containing the appropriate antibiotic, and were incubated aerobically for 2 – 3 hours at 28 °C. Following incubation, the required volumes of the recovered cultures, typically 10 µL, 50 µL and 100 µL, were spread onto BAB-hemin plates supplemented with the appropriate

antibiotics to select for the plasmid vector and the marked mutation. Spread plates were incubated at 28 °C for 2 days.

7.4.4. Selection of *Yersinia pestis* Mutants

Bacterial colonies that grew on BAB-hemin plates supplemented with the appropriate antibiotics were picked and streaked onto BAB-hemin plates supplemented with only the appropriate antibiotic to select for incorporation of the resistance marker. Bacterial growth from each grid plate was then tested by PCR using gene-specific primers to check for a difference in size that corresponded with the insertion of the kanamycin gene. PCR was also used to confirm that the kanamycin resistance marker had been inserted in the correct gene using gene-specific and Kanamycin-specific primer pairs.

7.4.5. Cure Mutant Strains of pAJD434

Mutant strains were cured of the temperature sensitive pAJD434 plasmid by growth of mutant strains in 20mL BAB broth supplemented with 50 µg/mL Kanamycin and 2.5mM $CaCl_2$ for approximately 30 hours with continuous shaking at 37°C. This culture was then serially diluted to 10^{-6} and spread out on to BAB- hemin agar plates supplemented with 50 µg/mL Kanamycin. These plates were incubated at 28°C for 48 hours. Duplicate plates were then prepared from a selection of colonies and plated onto a BAB-hemin agar plate supplemented with 50 µg/mL kanamycin and onto a BAB-hemin agar plates supplemented with 100 µg/mL trimethoprim. Plates were incubated at 28°C for 24 hours. From these plates colonies that were kanamycin resistant but trimethoprim sensitive were selected as cured strains. PCR was used to verify pAJD434 plasmid curing using primers targeting the recombinase exonuclease and gam gene products. Cured mutant strains were tested for the presence of the virulence plasmid pYV by PCR using primer pairs targeting the *lcrV* gene. Glycerol stocks were then made of mutant strains.

7.5. Creation of Mutants – *Francisella tularensis*

7.5.1. Ligation of DNA Fragments into Plasmid Vectors

For selected targets synthetic deletion constructs were synthesised at LifeTechnologies™ GeneArt® synthesis service, for sub-cloning into vectors required for transformation procedures. A ratio of 1:1 or 1:2 insert:vector DNA concentration was used per ligation reaction. Suicide vector pSMP75 was digested with *Mlu*I restriction endonuclease to create compatible ends for ligation of the deletion construct into the suicide vector. Dephosphorylation of the cut pSMP75 was also conducted to prevent self-ligation of the plasmid. A final concentration of 1X ligation buffer and 1 U T4 DNA ligase (Roche Diagnostics) were added to each reaction before being made up to the required volume in dH_2O. Each reaction was incubated at 16 °C for 18-22 hours.

7.5.2. Conjugation of *Francisella tularensis*

Conjugations were performed to introduce the suicide vector pSMP75 construct into *F. tularensis* SCHU S4. A BCGA plate containing cultured *F. tularensis* and a 10 mL culture of *E. coli* S17λpir donor strain were inoculated from -70 ^{o}C freezer stocks and grown overnight at 37 ^{o}C. For each mating, 3 mL *E. coli* S17 λ *pir* donor strain was aliquoted into separate microcentrifuge tubes and spun at 13 000 rpm / 1 min. The supernatant was removed from the pellet. The pellet was then resuspended in 100 μL of PBS. *F. tularensis* was harvested with a loop from the overnight lawn culture and resuspended in the *E. coli* S17 λ *pir* suspension. The bacterial suspension was then spotted onto the centre of a dried BCGA plate and incubated at 25 °C overnight. Following incubation the resulting bacterial growth was harvested with a loop and resuspended in 500 μL PBS. 100 μL aliquots of the suspension were spread onto five Thayer Martin agar plates supplemented with 15 μg/mL kanamycin and 100 μg/mL polymyxin B. The plates were incubated at 37 $^{\circ}$C for a period of up to 4 weeks or until colonies were visible.

7.5.3. Selection for Putative Integrants in *Francisella tularensis*

Bacterial growth from the conjugation plates was inoculated on to Thayer Martin kanamycin agar supplemented with 25 μg/mL to confirm incorporation of the plasmid and thus antibiotic

resistance. Isolated colonies from this inoculation plate were then sub-cultured onto Thayer Martin agar supplemented with sterile sucrose at a final concentration of 10 % (w/v) without any antibiotics. Plates were incubated at 37 °C for a period of up to two weeks or until well isolated colonies were present.

7.5.4. Selection of Deletion Mutants in *Francisella tularensis*

Sucrose-resistant colonies were sub-cultured onto duplicate Thayer Martin agar plates supplemented with kanamycin at 25 mg/mL and Thayer Martin agar plates without antibiotics. All kanamycin sensitive clones were screened by PCR.

Plasmids used in this study are listed in table 15.

Plasmid	**Relevant properties**	**Source/Reference**
pGEM-T Easy	T-cloning vector, Amp^R	Promega
pK2	pGEMT-Easy containing kanamycin resistance cassette	(289)
pAJD434	Encodes *λ* Red Recombinase genes under the control of an arabinose-inducible promoter	(271)
pSMP75	Modified pSMP22 suicide vector; Kan^R introduced under the control of FTT1441 promoter using *Mul*I and *Pst*I restriction sites	(427)
pCVD442	Suicide vector, *sacB*, Amp^R	(461)
pDM4	derivative of pNQ705; encodes *sacBR* gene from *Bacillus subtilis*	(291)
pBAD33	Complementation plasmid for *Y. pestis*	(357)
pUC57	Standard cloning vector used for synthetic inserts in this study. Amp^R	(462)

Table 15. Plasmids used in this study.

7.6. Creation of Mutants – *Burkholderia pseudomallei*

7.6.1. Ligation of DNA Fragments into Plasmid Vectors

For selected targets synthetic deletion constructs were synthesised at LifeTechnologies™ GeneArt® synthesis service, for sub-cloning into vectors required for transformation procedures. A ratio of 1:1 or 1:2 insert:vector DNA concentration was used per ligation reaction. Suicide vector pDM4 was digested with *Xba*I or *Bgl*II restriction endonucleases to create compatible ends for ligation of the deletion construct into the suicide vector. Dephosphorylation of the cut pDM4 was conducted to prevent self-ligation of the plasmid. A final concentration of 1X ligation buffer and 1 U T4 DNA ligase (Roche Diagnostics) were added to each reaction before being made up to the required volume in dH_2O. Each reaction was incubated at 16 °C for 18-22 hours.

7.6.2. Conjugation of *Burkholderia pseudomallei*

The *E. coli* S17 λ *pir* donor strain and *B. pseudomallei* K96243 recipient strain were grown overnight to stationary phase in 10 mL LB broth supplemented with appropriate antibiotics. Cultures were then pelleted and the supernatant replaced with half of the original volume of antibiotics-free LB broth to concentrate cells so as not to flood the conjugation filter. Sterile nitrocellulose filters were then placed onto LB-agar plates without supplements and 10 µL of the donor and recipient strains were pipetted onto the sterile filters, including separate donor and recipient filters to demonstrate filters can support the growth of both strains. Filter plates were incubated for 8 hours at 37°C. Filters were then removed and placed into separate Eppendorf tubes containing 1 mL sterile phosphate buffered saline (PBS) and vortexed thoroughly to remove bacteria from filters. 100 µL aliquots were then spread onto solid selective media supplemented with the appropriate antibiotics to counter-select against the donor *E. coli* strain and *B. pseudomallei* that did not conjugate, and select for *B. pseudomallei* strains which had incorporated the plasmid. The plates were incubated for at least two days at 37 °C.

7.6.3. Selection for Putative Integrants in *Burkholderia pseudomallei*

Bacterial growth from the conjugation plates was inoculated on to LB-agar plates supplemented with appropriate antibiotics to confirm the incorporation of the plasmid and thus antibiotic resistance. Isolated colonies from this inoculation plate were then sub-cultured onto LB agar supplemented with sterile sucrose at a final concentration of 10 % (w/v) without any antibiotics. Plates were incubated at 37 °C for a period of up to two weeks or until well isolated colonies were present.

7.6.4. Selection of Deletion Mutants in *Burkholderia pseudomallei*

Sucrose-resistant colonies were sub-cultured onto duplicate LB- agar plates supplemented with appropriate antibiotic and LB-agar plates without antibiotics. All antibiotic sensitive clones were screened by PCR to confirm deletion of the target gene and subsequent loss of the plasmid.

7.7. Bacterial Mutant Characterisation *in Vitro*

7.7.1. *In vitro* Growth Kinetics

For inoculation into BAB broth, bacteria from a glycerol freezer stock were grown on BAB hemin agar with the appropriate antibiotic for mutant strains, and incubated at 28 °C overnight. The following day, bacteria from the plate were inoculated into 50 mL BAB broth containing the appropriate antibiotics for mutant strains to an OD_{600} of 1.5. Liquid cultures were incubated at 28 °C with shaking overnight. The following day OD_{600} readings were taken from 50 mL cultures to check for growth, and an expected OD_{600} reading of 2.0. 1 mL of overnight culture was then pelleted by centrifugation at 10000 rpm for four minutes. The supernatant was removed and discarded and cells were resuspended in 500 µL fresh media supplemented with the appropriate antibiotics. 20-40 µL of this cell suspension was added to 5 mL fresh media supplanted with the appropriate antibiotics to an OD_{600} of exactly 0.6. A 96-well plate was then prepared by aliquoting 200 µL dH_2O to the outer most wells, and then 200 µL of replicates of six were added to each remaining row of the plate for each condition being tested and each strain being tested. A negative control row containing no bacteria was incorporated to blank the system. The plate was then sealed with a breathable membrane plate sealer and transferred to the MultiSkan FC microplate photometer. The MultiSkan FC was programmed to run for 24 hours incubating at 28°C with shaking, taking OD_{600} readings every 15 minutes.

7.7.2. Intracellular Polyphosphate Quantification Assay

Wild-type and mutant strains of *Y. pestis* were streaked from a glycerol stock onto BAB plates supplemented with the appropriate antibiotics, and incubated for 24 hours at 28 °C. Polyphosphate extraction was performed using a modification of the acidic extraction method (45). 0.5 g bacterial growth from streak plates was removed with a 10 µL loop and resuspended in 10 mL 0.5 N $HClO_4$ and vortexed to a homogenous suspension. Cell suspensions were incubated on ice for 30 minutes, with occasional inversion. Bacterial cells were then pelleted by centrifugation at 7000 rpm for 20 minutes. The supernatant was retained for analysis. Nucleoside phosphates were removed by adsorption by the addition of 0.75 g acid-washed activated charcoal (Sigma) to the supernatants. Activated charcoal suspensions were then centrifuged at 9000 rpm for 20 minutes at 4 °C. The free phosphates in

the acid-soluble extract were determined before and after hydrolysis at 100 °C for 10 min. An increase in detectable free phosphate following hydrolysis is a measure of the amount of intracellular polyphosphate present in the bacteria. The concentration of free phosphate was determined using a spectrophotometric phosphorus assay kit based on phosphate complex formation with malachite green and molybdate (BioAssay Systems). The mean results from six replicates were analysed by a two-way analysis of variance with Bonferroni's post-tests using GraphPad Prism v5.0.

7.7.3. Antibiotic Sensitivity Assay

To test susceptibility to various antibiotics, *Y. pestis* GB, and the mutant strains Δ*ppK*, Δ*ppX* Δ*ppK/ppX* and *ΔrelA* were grown overnight in BAB broth supplemented with 50 mg/mL kanamycin for mutant strains, and adjusted to an OD_{600} of 0.5. Cultures were vortexed thoroughly to ensure a completely homogenous lawn of bacteria would grow on the plates. In three biological replicates aliquots of 1000 µL *Y. pestis* GB and mutant strains were aliquoted onto BAB-hemin agar, with surplus media being poured off. Filter paper discs 5 mm in diameter were placed in each quadrant of a divided plate, to which 10 µL of the appropriate antibiotic at the appropriate concentration (Sigma) was added. The plates were incubated upright, overnight at 28 °C and zones of inhibition surrounding the discs were measured.

7.7.4. Superoxide Anion Assay

To test susceptibility to exogenous superoxide anions, *Y. pestis* GB, and the mutant strains Δ*ppK*, Δ*ppX* Δ*ppK/ppX* and *ΔrelA* were grown overnight in BAB broth supplemented with 50 mg/mL kanamycin for mutant strains, and diluted to an OD_{590} of 0.5. Cultures were vortexed thoroughly to ensure a completely homogenous lawn of bacteria would grow on the plates. In three biological replicates aliquots of 1000 µL *Y. pestis* GB and mutant strains were aliquoted onto BAB-hemin agar, with surplus media being poured off. Filter paper discs 5 mm in diameter were placed in each quadrant of a divided plate, to which 10 µL 1 M, 8 M, 6 M and 4 M pyrogallol (Sigma) was added. The plates were incubated upright, overnight at 28 °C and zones of inhibition surrounding the discs were measured.

7.7.5. Sodium Azide Sensitivity Assay

To test susceptibility to endogenous ROS (H_2O_2), *Y. pestis* GB, and the mutant strains Δ*ppK*, Δ*ppX* Δ*ppK/ppX* and *ΔrelA* were grown overnight in BAB broth supplemented with 50 mg/mL kanamycin for mutant strains, and diluted to an OD_{590} of 0.5. Cultures were vortexed thoroughly to ensure a completely homogenous lawn of bacteria would grow on the plates. In three biological replicates aliquots of 1000 µL *Y. pestis* GB and mutant strains were aliquoted onto BAB-hemin agar, with surplus media being poured off. Filter paper discs 5 mm in diameter were placed in each quadrant of a divided plate, to which 10 µL NaN_3 (Sigma) was added. The plates were incubated upright, overnight at 28 °C and zones of inhibition surrounding the discs were measured.

7.7.6. Persister Assay – *Yersinia pestis*

From a freezer stock, a fresh BAB-hemin agar plate was inoculated with the appropriate strain of *Y. pestis* and then incubated for 48 hours at 28 °C. Using fresh growth from streak plate, 50 mL BAB broth was inoculated with each mutant strain and wild type *Y. pestis* GB in a 250 mL conical flask to OD_{600} 0.1. Flasks were incubated with shaking at 200 rpm overnight at 28 °C. This starter culture was used to inoculate a fresh 50 mL BAB broth to OD_{600} 0.06. This culture was incubated with shaking for 3.5 hours at 28 °C to ensure cells reached mid-exponential phase. 5 mL cells were removed, in triplicate, and pelleted by centrifugation at 10,000 rpm at room temperature for 10 minutes. Cells were then resuspended in 5 mL fresh BAB broth in universals and antibiotic was added to the desired final concentration (start with 10X MIC90). 100 µl was removed immediately and serially diluted and 100 µl plated out onto BAB-hemin agar plates for viable counts. 5 mL cultures were incubated with shaking for 3 hours in total and samples were removed (100 µl, serially diluting and plating 100 µl onto BAB-hemin plates) at the following time points: 0.0, 0.5, 1.0, 1.5, 2.0, 2.5 and 3.0 hours. Plates were Incubated for 48 hours at 28 °C or until visible colonies appeared large enough to count. Colonies on plates were then counted and results were input into GraphPad Prism v5.0 for statistical analysis.

7.7.7. RNA-sequencing Library preparation

RNA isolates were prepared in triplicate to provide sufficient biological replicates for RNA-seq. Total RNA was depleted for ribosomal RNA using the Ribo-Zero™ kit (Epibio) according to the manufacturer's instructions. mRNA libraries were then prepared using Script-Seq™ RNA-seq library preparation kit (Epicentre®), according to the manufacturer's instructions. The University of Exeter performed 300-bp, paired end read RNA sequencing using a single lane on the Illumina HiSeq2500.

7.7.8. Lysate Preparation for Proteomics

50 mL CDM without serine, supplemented with 0, 1 or 10 µg/mL serine hydroxamate, was inoculated to OD_{600} 0.1 from a fresh BCGA plate of *F. tularensis* SCHU S4 and incubated at 37˚C with shaking, overnight. OD_{600} readings were taken to check for growth the following day. 1 mL of culture was then centrifuged at 13,000 rpm for 1 minute to pellet cells. Cells were then resuspended in 1 mL SDS buffer comprising 125mM Tris pH 6.8, 20% SDS, 20% glycerol made up to 1 mL with dH_2O. SDS cell suspensions were then heated to either 60 °C for 60 minutes or 100 °C for 10 minutes then stored at -80 °C. Prior to freezing, 10% of each cell sample was inoculated into 1 mL CDM and immediately plated onto BGGA plates. After incubation for one week at 37 °C BCGA plates were inspected for bacterial growth and samples deemed non-viable were subsequently subjected to proteomic analysis.

7.7.9. Sample preparation for Mass Spectrometry

5 µl *F. tularensis* lysates were resuspended in 5 µl Tris-SDS-Glycerol buffer and protein concentrations measured using a Direct Detector spectrometer. Volumes equating to 120 mg protein were added to 0.5 µl DTT solution and incubated at 56 °C for 30 mins. Protein digest was carried out using FASP protein digestion kit according to the manufacturer's instructions. Samples were lyophilised using a vacuum concentrator then cleaned up using the C18 Protea Tip SpinTips Sample Prep Kit (Protea) according to the manufacturer's instructions. Samples were then reconstituted in 60 µl dH_20 + 0.1% formic acid buffer (buffer A). An internal standard for subsequent mass spectrometry was prepared comprising 8 µl of Enolase stock and 32 µl of buffer A.

7.7.10. Mass Spectrometry

Samples were separated using a nanoAcquity UPLC system (Waters). For the first dimension separation, 1.0 µl of the prepared protein digest (500 ng on column) containing 100 fmol of the internal standard digest Enolase digest was injected onto a Symmetry C18, 180µm x 20mm trapping cartridge (Waters). After 5 min washing of the trap column, peptides were separated using a 75µm ID x 200mm, 1.7 µm BEH130 C18, column (Waters) using a linear gradient of 5 to 40% B (buffer A = 0.1% formic acid in water, buffer B = 0.1% formic acid in acetonitrile) over 90 min with a wash to 85% B at a flow rate of 300 nL/min. All separations were automated and performed on-line to a Waters G2-S HDMS mass spectrometer operating in MS^e mode with ion mobility enabled. Data was acquired from 50 to 2000 *m/z* using alternate low and high collision energy (CE) scans. Low CE was 5V and elevated, ramped from 20-40V. The lock mass Glu-fibrinopeptide, $(M+2H)^{+2}$, *m/z* = 785.8426) at a concentration of 500 fmol/µL was infused at 250 nL/min and acquired every 13 seconds.

7.7.11. Chrome Azurol S Agar Siderophore Detection Assay

The following solutions were prepared:

Blue dye solution:

Solution 1: 0.06 g of CAS dye (Sigma Aldrich) was dissolved in 50 ml of ddH_2O

Solution 2: 0.0027 g of $FeCl_3 \cdot 6H_2O$ was dissolved in H_2O the added to 10 ml of 10 mM HCl

Solution 3: 0.073 g of HDTMA was dissolved in 40 ml of ddH_2O.

Solution 1 was mixed with 9 mL of Solution 2, and then mixed with Solution 3. This solution was a dark blue colour. This solution was autoclaved and stored in a glass bottle.

Minimal Media 9 (MM9) Salt Solution Stock

MM9 salt solutions stock was made by dissolving 15 g KH_2PO_4, 25 g NaCl, and 50 g NH_4Cl in 500 mL of ddH_2O. A 20% Glucose Stock was made by dissolving 20 g glucose in 100 ml of ddH_2O. A NaOH Stock was made by dissolving 25 g of NaOH in 150 ml ddH_2O, the pH of this solution should be 12.

Casamino acid solution

The casamino acid solution was made by dissolving 3 g of casamino acid in 27 ml of ddH_2O. This casamino acid solution was extracted with 3% 8-hydroxyquinoline in chloroform to remove any trace iron, by mixing equal volumes of casamino acid solution with 3% 8-hydroxyquinoline in chloroform. The extraction was left overnight, and then the extracted casamino acids left for a further day to ensure the chloroform had evaporated. This solution was then filter sterilized.

The CAS agar was prepared by addition of 100 ml of MM9 salt solution to 750 ml of ddH_2O. 32.24 g piperazine-N,N'-bis(2-ethanesulfonic acid) (PIPES) was then dissolved into the MM9 solution. As PIPES will not dissolve below pH of 5 the pH was adjusted up to pH 6 or pH 6.8 and PIPES slowly added while stirring. The pH dropped as PIPES dissolved. It was ensured that the solution did not exceed 6.8 as this turns the solute on green. 15 g Bacto agar was then added and then autoclaved and cooled to 50^{o}C. 30 ml of sterile casamino acid solution and 10 ml of sterile 20% glucose solution was then added to MM9/PIPES mixture. 100 ml of the Blue Dye solution was slowly added along the glass wall with enough agitation to mix thoroughly. Plates were then aseptically poured and cooled overnight.

7.8. Bacterial mutant Characterisation *In vivo*

7.8.1. *Francisella tularensis* Murine Challenge

For inoculation into mice, bacteria were grown on BCGA plates and incubated at 37 °C for 2 – 4 days then scraped into 20 % sterile sucrose solution until a homogenous solution was achieved. Stocks of sucrose captured bacteria were transferred to cryotubes and stored at -80 °C. Bacteria were then thawed and diluted in phosphate-buffered saline (PBS) as required. Duplicate 100 µL volumes of dilutions of 10^{-4}, 10^{-5}, 10^{-6}, 10^{-7} and 10^{-8} of either mutant *F. tularensis* strains or the wild type *F. tularensis* SCHU S4 were spread onto BCGA agar plates and incubated at 37 °C for 2 – 4 days. After incubation bacterial colonies on plates were enumerated to give viable counts. Groups of the required number of female BALB/c mice were inoculated subcutaneously with 100 CFU / 100 µL of the appropriate strain of *F. tularensis*. Humane end-points were strictly observed and animals deemed incapable of survival were humanly sacrificed by cervical dislocation. Spleens of each mouse in each group were removed and processed through a sieve. 100 µL of dilutions of processed spleen from 10^{-1} – 10^{-4} were plated onto BCGA agar plates and incubated at 37 °C for 2 – 4 days. Following incubation plates were enumerated to give viable counts.

7.8.2. Virulence Assessment of *Yersinia pestis* in *Galleria mellonella*

G. mellonella larvae were purchased from Porton Pet and Aquatic Centre, UK. Larvae were infected with wild type *Y. pestis* GB, or the mutant strains Δ*ppK*, Δ*ppX*, Δ*relA* or Δ*ppk*/*ppX*. For dosing, the larvae were inverted over a 5 mm diameter plastic tube and 10 µl given by micro-injection (Hamilton) into the right foremost leg. The larvae were incubated at 37 °C and survival and appearance recorded at 24 hour intervals. Larvae were scored as dead when they ceased moving, changed from their normal pale cream coloration to brown and failed to respond when gently manipulated with a pipette tip. PBS-injection and no- injection controls were used for visual comparison to infected larvae. Survival 24 hours post-infection was recorded. To determine the numbers of bacteria and site of localization in the haemocoel, larvae were chilled on ice for 20 min. The bottom 2 mm of each larva was aseptically removed and haemocoel was drained into a sterile 1.5 mL microcentrifuge tube. For enumeration haemocoel was serially diluted in PBS (10^{-1}, 10^{-2}, 10^{-3} and 10^{-4}) and the bacterial load per larva was quantified by enumeration of CFU on BAB agar.

7.8.3. Virulence Assessment of *Yersinia pestis* in a Murine Model of Infection

For inoculation into mice, bacteria from a glycerol freezer stock were grown on BAB hemin agar with the appropriate antibiotic for mutant strains, and incubated at 28 °C overnight. The following day, bacteria from the plate were inoculated into 10 mL BAB broth containing the appropriate antibiotics for mutant strains. Liquid cultures were incubated at 28 °C with shaking overnight. On the day of the challenge, 10 mL BAB broths supplemented with the antibiotics as required were inoculated with the overnight culture to a starting OD_{600} of 0.2. Liquid cultures were incubated at 28 °C with shaking until an OD_{600} of 0.6 was achieved (up to 5 hours for some mutant strains). Once an OD_{600} of 0.6 was reached, cultures were serially diluted in 10 mL PBS. Dilutions 10^{-3} and 10^{-5} were supplied for the challenge to provide doses of approximately 100 CFU / 100 µL and 10^5 CFU / 100 µL respectively. Duplicate 100 µL aliquots of dilutions were plated out onto BAB hemin agar containing antibiotics as required and incubated for 48 hours at 28 °C. Following incubation plates were enumerated to give viable counts.

7.9. Data Analysis and Statistical Analysis

7.9.1. GraphPad Prism Statistical Analysis

GraphPad Prism V6 was used for statistical analysis of *in vitro* and *in vivo* characterisation data generated for all the mutants discussed in this thesis. One way ANOVA was used to determine the statistical significance of growth kinetic data by comparing the means of multiple groups of data. Welch's correction was used to compare two groups at a time to account for unequal variances between the groups tested. Multiple comparisons were used to determine significance values (P values) for each mutant group compared to the wild type group. An unpaired t-test was used to compare means of unmatched groups and with Welch's correction was used to account for potential unequal variance and standard deviation from the mean.

7.9.2. RNA-Seq Data Analysis

Raw images were captured using RTA 1.13.48 (Real Time Analysis), then raw sequence files were de-multiplexed and filtered using CASAVA 1.8.2 (Consensus Assessment of Sequence and Variance), a quality filter designed to remove low quality reads or sections of reads, as well as any sequences derived from the sequencing adaptors or primers. The quality filtered FASTQ files were mapped to the *F. tularensis* subsp. *tularensis* SCHU S4 genome (NC_006570.2) with TopHat in local alignment mode. The short read alignments were used as input for HTSeq, a python framework for working with high-throughput sequencing data (463). Read counts were generated for each CDS in the reference sequence in HTSeq. Differentially expressed genes were then identified in each condition using the R package DESeq, by comparing the read counts of each CDS in each serine hydroxamate condition. The DESeq package tests for differential expression through the application of negative binomial distribution and shrinkage estimator for the distribution of variance. Normalised expression levels among the samples were obtained by estimating the total sequencing depths for each sample as the median of the ratios of the samples' counts to geometric mean across all samples. Genes were identified as being differentially expressed when the DESeq-calculated adjusted p-value was less than 0.05 and the change in expression was at least 1.5-fold up or down. Further information about statistical analyses can be found in the DESeq vignette (http://www.bioconductor.org/packages/devel/bioc/vignettes/DESeq/inst/doc/DESeq.pdf). Heat maps were generated in the software environment R, for statistical computing and

graphics generation, using the gplots package. Volcano plots were also generated in R using the VolcanoPlot function (395, 396).

7.9.3. Mass Spectrometry Database Searching

The raw mass spectra were processed using ProteinLynx Global Server Version 3.0 (Waters, Manchester, UK) and the data processed to generate reduced charge state and de-isotoped precursor and associated product ion mass lists. These mass lists were searched against the *Francisella tularensis* protein sequence. A maximum of one-missed cleavage was allowed for tryptic digestion and the variable modification was set to contain oxidation of methionine, carboxyamidomethylation of cysteine and hydroxylation of aspartic acid, lysine, asparagine and proline.

8. Appendix

8.1. Protein Alignments for *Yersinia pestis*: PPK, PPX, RelA and SpoT

Figure 127. Amino acid sequence alignment of PPK (YPO_2836) of *Y. pestis* with the Catalytic C-terminal domain, second repeat, of *E. coli* polyphosphate kinase 1. Amino acid residues denoted in red indicate a high degree of conservation and amino acid residues in blue indicate a low degree of conservation.

Figure 128. Amino acid sequence alignment of PPX (YPO_2837) of *Y. pestis* with exopolyphosphatase/guanosine pentaphosphate phosphohydrolase/nucleoside triphosphate diphosphohydrolase family, propionate kinase/acetate kinase family, glycerol dehydratase reactivase, 2-hydroxyglutaryl-CoA dehydratase component A, N-acetylglucosamine kinase, butyrate kinase 2 of *E. coli*. Amino acid residues denoted in red indicate a high degree of conservation and amino acid residues in blue indicate a low degree of conservation.

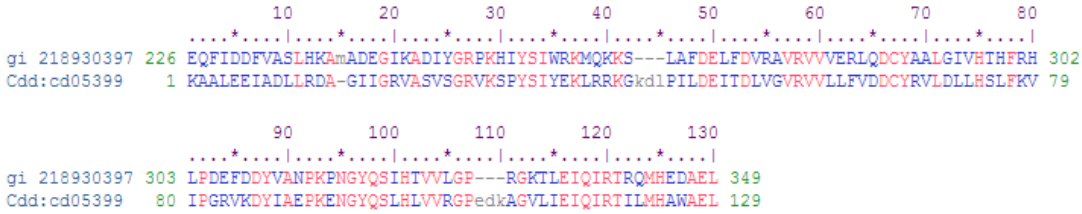

Figure 129. Amino acid sequence alignment of RelA (YPO_3380) of *Y. pestis* CO92 with the catalytic domain of *E. coli* ppGpp synthetase (RelA). Amino acid residues denoted in red indicate a high degree of conservation and amino acid residues in blue indicate a low degree of conservation.

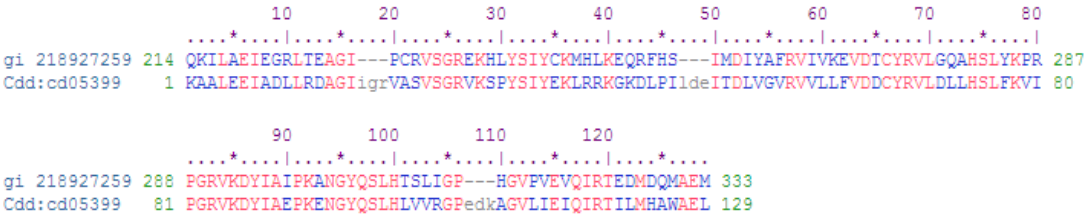

Figure 130. Amino acid sequence alignment of SpoT (YPO_0038) of *Y. pestis* CO92 with the Nucleotidyltransferase (NT) domain of RelA- and SpoT-like ppGpp synthetases and hydrolases; This family includes the catalytic domains of *E. coli* ppGpp synthetase (RelA), ppGpp synthetase/hydrolase (SpoT), and related proteins. Amino acid residues denoted in red indicate a high degree of conservation and amino acid residues in blue indicate a low degree of conservation.

8.2. Primer sequences for *Yersinia pestis* Mutants

Primer Designation	Oligonucleotide sequence
ppk_ppX_F	5'TGTTTACGGACACTAAATACTCCCACAATAATCTTAATGGAGTTGCAATGGATCT GCCACGTTGTGTCTC 3'
ppX_R	5'CGGTGCACGATTTTATTAGCGTCAGATCACTCTTCAGGGGCCACTTTTGCGCTCT GCCAGTGTTACAACC 3'
ppX_single_F	5'TGATTATTTAAAAGCACTGGAACAACCGGAGCAGTAGACCTAACACTATGGATC TGCCACGTTGTGTCTC 3'

Table 16. Oligonucleotide primers for the amplification of the kanamycin resistance gene incorporating sequences homologous flanking regions of the target genes. Bases underlined are specific for the kanamycin resistance gene of plasmid pK2.

Primer Designation	Oligonucleotide sequence
Kan Forward	TTCAACAGGCCAGCCATTAC
Kan Reverse	CAACCTTAAATTAGCGCCGG

Table 17. Kanamycin resistance gene specific screening PCR primers.

Name	Sequence	Gene Target
ppk_out_F1	CCCACCAAGGCGAATAAACAC	*pstC*
ppk _out_R1	ATTGTTGATGCGCTGGCAGTG	Kan^R
ppk _out_R2	TCAGCAAACAGGGCCAGACAG	*ppX*

Table 18. Oligonucleotide primers for the determination of the orientation of the kanamycin resistance gene in the genome of the Δ*ppK* mutant.

Name	Sequence	Gene Target
ppkx_out_F1	CCCACCAAGGCGAATAAACAC	*pstC*
ppkx_out_R1	ATTGTTGATGCGCTGGCAGTG	Kan^R
ppkx _out_R2	TCAGCAAACAGGGCCAGACAG	*mtgE*

Table 19. Oligonucleotide primers for the determination of the orientation of the kanamycin resistance gene in the genome of the Δ*ppK/ppX* mutant.

Primer Designation	Oligonucleotide sequence
RelA_F	5' GCAAAGTAGGGAGAAGTTATGGATCTGCCACGTTGTGTCTC 3'
RelA_R	5' TCGCCGTCCAGATTAAAAAGCGCTCTGCCAGTGTTACAACC 3'

Table 20. Table showing primer sequences for the amplification of the kanamycin resistance cassette incorporating sequences homologous flanking regions of the target gene. Bases underlined are specific for the kanamycin resistance gene of plasmid pK2. Bases in bold indicate the start codon of *relA*.

Name	Sequence	Gene Target
relA_out_F1	CCCAGTATCTGGTCACTTTCC	*barA*
relA_out_R1	ATTGTTGATGCGCTGGCAGTG	Kan^R
relA_out_R2	TCAAGGCGGGCAATGCATCAG	*mazG*

Table 21. Oligonucleotide primers for the determination of the orientation of the kanamycin resistance gene in the genome of the Δ*relA* mutant.

Primer	Sequence
lcrV_Forward	TCTACCCGAGGATGCCATTC
lcrV_Reverse	TCTAGCAGACGTTGCATCAC

Table 22. *Y. pestis lcrV* specific primers for verification of pCD1

Primer	Sequence
PPK_comp_For_linked	AAGCTT GGAGTTGCAATGGGTCAGGA (HindIII)
PPK_comp_Rev_linked	TCTAGATAGGTCTACTGCTCCGGTTG (XbaI)

Table 23. *Y. pestis ppK* complementation primers.

8.3. Synthetic Construct Sequence for *Yersinia pestis* Δ*relA*

***Y. pestis* Δ*relA* Synthetic Construct:**

AGATCTCGGTGACATCGCGCATCAGGCGGTAAGCAAACAAAATGGCGACACACATACAGAACAGCAG
TAGCAAAGTTGAAATGAATATTTCTTTATATTGTTTCAGGCGCACTGATTGTAAATCTAAATCAATGGCG
ATATAGCCCAGTATCTGGTCACTTTCCCCCTGCCCGGAGGCTTGTTCACTGGATAAATTAGATTCTGAGA
CAATGGGCATTCGTAGGATCAGCGAATCCCCACGGTACGAAAGCATCAAAGAGTCGGGGACGGGTTC
GCCTGGAGGGAGTCTTAATTGTGAGGAATTGTAATTGTAGTTGGATGTGACAAAAAGCTTATTATCTAC
GTCAAAAACAGAAATTGACCGAACAATATTCGAGTGCCTTCGGTGTAGTAGATTAATCAACTGCCGAAC
GGTGTCGCGGTTGCGGAAGCTCATCCCGTATTCACTGGCAACGGCCAACGGTTCAATAATATTGGTGCC
GGCACTAACTATTTGGTTTTGCAGCTCATTATAGCGATTGACCATAAAGGATGTACTGAGTAACAGCCC
TAGAAGCAGCGTGGGTGCCAAGATTAAAATCATCATGCGCGCGCGAAGACTGTATTTGGTCATGGTAT
TCCAATGTGGGAGAATGGGTGACTAATGAAACTGATGCTTGATCAATCAATGTGGTGCAATTCTACTCT
CCAAACAGGCGTGTGACGACCCGGTAAACAATAACTGTGACAGTATATTTTCTTGGCCCCTTTACGTTA
GGGGCTGTACTCCATCAGGGAGTGATCGTTTTTATCCCTGATATCTTACCGGGAGGGCGAGTTTATCTT
GCTGCGGGTAGCCTGTTTGGTAAGCCGTTGAGGGTGAAGGAGTTGCGGCGTTTGTCGCTAATGGGCTG
TATAATGCGTTAAGCAATAATTTACCCAATGCGCCATGTTTTATCAGGAGTGGGTTATCGTCTTGCTCAG
GTGCGTACGTTGGATATGTTCCCGCACACCGGGCATCTTGAATCTATGGCGCTGTTTATTCAGGCGTCA
GAGGTCGCAAAGTAGGGAGAAGTTATGGTTACGCGTACGCGTTCTGGACGGCGATTACGTTTTGCTCT
ATTGATCTTGCGCTTTGCTCTATTGATCTTGCGCGGTGCTCGCCCTCCTCATGTACCGGTTTTTATAAGAT
CGGGTATACATTTCGGGGGCGTGGCGGGTCGCAATCAATCTGCCTGTGCTTTCGACGCTTTGAATTTAA
AAAACAAAAAAAGTGAATAAATTGAAATGACTCAACCTGTTACTTCCCCTGATTCTACAGCAGTCGCCCT
GCAACGTTTATTGGATATTATGCGCGCTCTGCGTGACCCAGAGCAGGGGTGCCCATGGGATCGCAAAC
AGACCTTTGACACCATCGCCCCTTATACGTTGGAAGAGACTTACGAGGTGCTTGATGCGATTGCGCGCA
AGGACTTTGATGACCTTCGAGACGAACTGGGTGATTTGCTGTTCCAGGTGGTGTTTTATGCCCAAATGG
GGCAGGAGCAAGGGCTGTTTACCTTTGATGACGTTTGCCATGCGATTAGCGATAAGCTTGAGCGCCGC
CATCCCCATGTCTTCTCTGATACGTCTCAAAACGTCACTCAGGCGGCGGTTAACAGAGAGGCCGCTCTG
GCGGGCTGGGAATCACGAAAAGCCGAGGAACGAGCAGAAAAAGCATTGTATTCGGCATTGGACGATA
TTCCTGATGCATTGCCCGCCTTGATGAAGGCCCATAAAATTCAGAAGCGTTGTGCGTCAGTCGGTTTTG
ATTGGAACACGCTAGGGCCGGTACTCGATAAGGTCTACGAAGAGATTGACGAGGTCATGTTTGAAGCG
CGTCAGGCAGTCGTCGATGAGGACAAATTGGGAGAGGAAATTGGCGATTTACTCTTTGCCACGGTTAA
TCTATCGCGCCATCTGGGCCATAAAGCTGAGAATGCGCTGCAAGCGGCTAATCGTAAGTTTGAACGGC
GTTTTCGTCAGGTAGAACAAATAGTTACGGCATCAGGTCAAACCATGGAGAGTGCGACGCTTGATGAA
ATGGAAGCAGCCTGGCAGCAAGTTAAAAAGCAAGAAACTGAAATGTAAGGTGTTTTAATTCATTTCACT
GATAGTTGTGGAATT**AGATCT**

Figure 131. Commercially sourced synthetic gene sequence for *Y. pestis* Δ*relA* mutant generation. Left flank highlighted in yellow and right flank highlighted in blue.

8.4. Protein Alignments for *Francisella tularensis* PPK, PPX, RelA and SpoT

Figure 132. Amino acid sequence alignment of PPK (FTT_1564) of *F. tularensis* with PPK2 from *Pseudomonas aeruginosa*. Amino acid residues denoted in red indicate a high degree of conservation and amino acid residues in blue indicate a low degree of conservation.

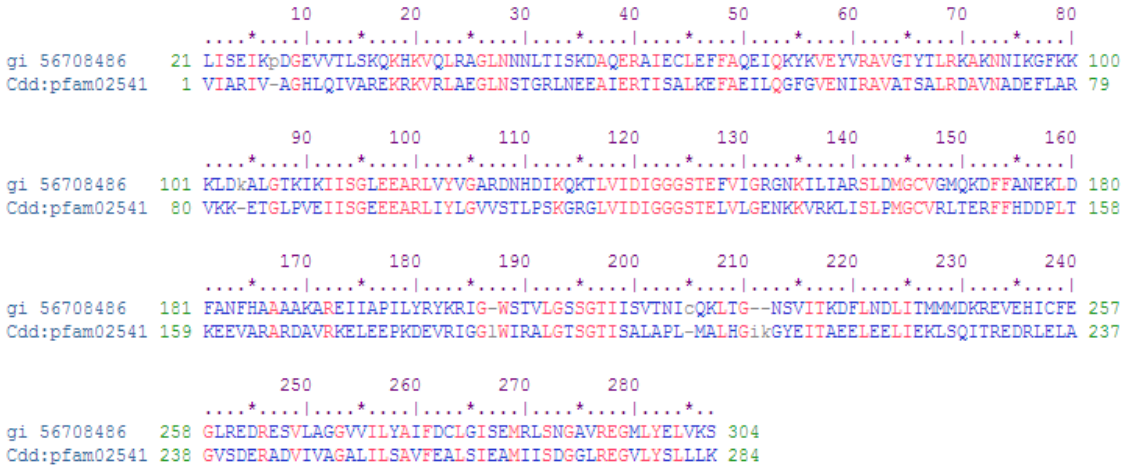

Figure 133. Amino acid sequence alignment of PPX (FTT_1444c) of *F. tularensis* with PPX_GPPA family protein. Amino acid residues denoted in red indicate a high degree of conservation and amino acid residues in blue indicate a low degree of conservation

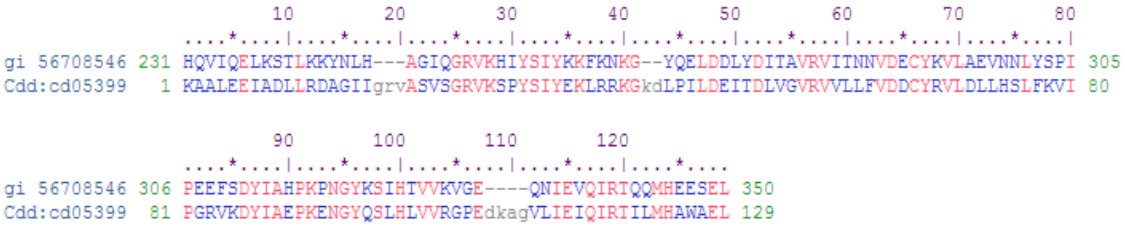

Figure 134. Amino acid sequence alignment of relA (FTT_1508) of *F. tularensis* with the catalytic domain of RelA from *E. coli*. Amino acid residues denoted in red indicate a high degree of conservation and amino acid residues in blue indicate a low degree of conservation.

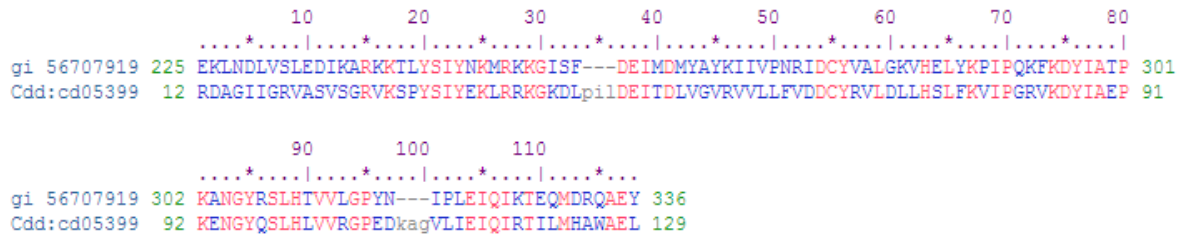

Figure 135. Amino acid sequence alignment of SpoT (FTT_0808) of *F. tularensis* with SpoT from *E. coli.* Amino acid residues denoted in red indicate a high degree of conservation and amino acid residues in blue indicate a low degree of conservation.

8.5. Primer Sequences for *Francisella tularensis* Mutants

Primer designation	Oligonucleotide sequence
ppXLF-F	AATTACGCGTTATATCCATTAGCTCATTAAC
ppXLF-R	**AGATCT**CAAAAGCTTATTCCTTAAC
ppXRF-F	**AGATCT**TAGAAAATCATGGACTAGGTATAAGG
ppXRF-R	AATTACGCGTCAATCGCGAAACTAAAGCATC

Table 24. Oligonucleotide primers for creation of *ppX* mutagenesis construct. Engineered *Mlu*I restriction sites are underlined, and engineered *Bgl*II restriction sites are in **bold.** Left Flank Amplicon: 624 bp. Right Flank Amplicon: 679 bp

Primer designation	Oligonucleotide sequence
Kan_PSMP_F	GCGATAATGTCGGGCAATCAG
Kan_PSMP_R	CTCACCGAGGCAGTTCCATAG

Table 25. Oligonucleotide primers for the amplification of the kanamycin cassette from suicide plasmid pSMP75. Kanamycin cassette amplicon: 626 bp.

8.6. Synthetic Construct Sequence for FTT_0613 and FTT_1334

Sequence for synthetic insert FTT_0613c :

ACGCGTTTAGCAGAATAAGATATTTAGAAGAAACATTATCGCAACATAACAATAATCAAGATGCTGCGA
TTAATGAAATTGTAGAAAAAATAAATGTAGCATATGAAAAAAGGAAGAATAAACAAAATCTAGATTGT
GATGAAAAAAATTATTAGATATATTAAATTGGTTTGATGGAGTTCAAATATACCAAAATCACAATAAAC
TATTATCTGGAGGTCAAAGTTATGAGAATGCAACAAACTTTTTCTCAGCTAATACAAATCAAAATGAAA
AAGAAAATAGAAAAATCTTTGTTATAGCTAAAGAATTAAATATATTAACAAAAGAGTTGATAGATGATA
TTTTTAATAAGATTGATAACAGTAAAGAACCTATTGCTTTTTCATTAAGCGCCCCAGGTCATATTATTTCG
ATAGGTAAAAGCTCTAATTATAAACCGATATATTTAGTTAATCATAATATTCATAAACATATATTAAATA
AGAAATCGTTATATAGTGAAGTATTTTGTGCATTTAAGTATTCGATGAGGATAGCTTTGAGCATTTTTAG
ATATTCATACCAAGAAGAAAATATTTCAATTAAATATGTTACTAATAATTTAGATAAAGATGATTTATGT
GAATTATTATGTATAGCTTTGCAAGATGGCCACGCAGAAGCTATCAAAGTTTATAGAGGGGATATTTAA
TCTTTCTGGAATTAATAGACGAGAACTGTTAGCTGCTAAAATGCCAGATGGAACACCTGGTTTACATAT
AGCTTTGCAACAGTATCATTCAGAAGCTGTTAAAACTTATAGAGAAATGATATCTAAATTGAAGATCTT
AAGTAATGGATTACCAGGATTTTTGCTTTAGGTATGATTGTCAATGCTATTCGAAAAATAACTTTTTTAA
CAAAAGATTTTAATCTGAGCTTAAAATATTTAGAACTCAATTTATGAAAAATCTTGGTTAATTTATTAATT
AGAATTCTATATTTCATATATTAGAGAAAAGTTAACTTTATTTAGTTAGAGAAGAAGCTAGCTTGATCTT
TAGTAATTTGGCAGCAGATCTTACTAAAAGCAATACTAGTTAGAGATATTAATAGTAATGTTGATAGTG
TAATTATCTTTTTCATTTTTTTCTCCTTAATTTACTATTATTTGTTTTATGTTTGTTAAAATCTAAATAGTAA
ATAAAAACATCTGCATGAAACTTTTTTATCCAGTAAAAATTTTAGCTTTTACTATGATAAAATGATTCTAC
TAGAACAATAAATTATAAAAGTATTTAATAAAATATAATTTATAGCAAATTAATTTATTTTTATTAATTTT
TTATTTATAAGACAGTTTGATTAATTATGCAGAAAATTATTATAAATTATTTGGAGTATTTCTCTTTAATA
ATTAGCCCAATCGCTATACTAAATATCAACAATAGCCAAACTAATGACATACCAATATTCATCCAAATAG
TATGATAATCATTTAAATATATCGTTTGCTCAAGTGTCGCACGAGTATCCTTAGGTAGTTCTTTAATAATT
TCGCCATTAGGCTCAATAACAGCAGTGATACCATTACTAGTAGTCGTAAGAACATATTTAGCATTCTCAA
TTGCTCTAACTTGAGATATTTGCAATTGTTGCTCACGCGCGATCGAGTCACCAAACCAAGAGTCATCACT
AATGATAGAAATAAGCTTAGCGCCTTGTAGCTGATCACGAACTTGTTCAGGATATGCAACTTCATAGCA
GATAAAATTAGCTAGAGGTTGACCAAAGGCTGTCATAATTAGTTGAATCTTATCACCAGCATTAAAACT
ACTTAAACCAACACTATCAACATAGCCAAAAAATTTGATTGGGAAATATTCACCGAATGGAACTAGGTG
ATGCTTATTATATACTCCTTGACCATTTCCAATAATGATTGAACTATTGTAAATCTTAGCTCTAGATGCTG
TTTGTTCAATACTTAGTGATCCAATAAGCATAGCATTATTATTTTCATCAGCTAGCTCTTTAAGCTTACTA
AAATATGAATTCATATATTGTCTATAATTAGGGATAGCATTTTCAGAGAGAATTATTAATGAGTTTTTGT
ATTCAGTGGCAGCTTGTTGATAGTATTTTTGCATCTTAGCAAAATTATCAGGATCCCACTTAAATCCTTG
GACGAAATCTCC**ACGCGT**

Figure 136. Commercially sourced synthetic insert sequence for *F. tularensis* FTT_0613 mutant generation. Left flank highlighted in yellow and right flank highlighted in blue.

Sequence for synthetic insert FTT_1334c :

ACGCGTAGAGTCGTTATCCTTGCTAACTTCCTTCAACTTAGTCTGCGAATTATAATGCTCTTGTTGACTAT
AGTTTTATGTCTTTGTACATAAAAGATACTGCTTTGCTTATTGGTACAATGATGATTATAATGACAATAT
ATACAACATCTATTTGGCTTAGCCAAACATCAAAATATACTTTCACCAGCTCAAAGCCAATCGGTAGTAA
TATCTCATTTGCTCTAATGCAATGGGGATTATTATTACTATCACAAATCGATATCATAATCTTAAAAGTAC
TAGCAACTCCCGCAGATATCGCTCTCTACGGTGTAGCACTACAACTTGGCGCATTAGTTATTTTTGTATT
AAATGCGGTTAATTCAAATGTCCTATCACAAATTGCTGATGATTATAAAAACTGCTCTAGAAAAGAATTT
CAAAATAAAATAACCTCTTATACTAGAATTATCTTTATACTCTCAATATTTGCTATTTTAGGAATTATTATT
TGTGGATATCCAATTACTTTAATGTATGGTAAACAATATACCGCATCATATTTTATCTTTTGTATATTAAT
GGTTGGGCAAATAGTAAATGTTCTATCTGGTTGCGTTGCTACGATTCTAAATATGGCAGGATATGAGAA
AAGTACATGTTTTGCTTTCTATATTGCACTTGCTATTAATATATTGCTAGGAGTAGTTTTTACGCTTTATT
GGGGTGTATATGGTCTTGCAATTGCCTCAAGCTTATCAATGATATATTGGAATATTCATCTACTTTACAA
AGTAATTACACAGATAAAAATTAACCCAACAATATTTATAATTAGATAAAACCTAATCTACAGAGTTATT
ACTAGTAGCAGCATTATTGAGTGTTTTTGAAACATTATTAACGGCTTTGTTAACTGTCTCTTTAGCAACTT
TTATAGGCTCGCTCCTAATATTTGCTACTAACAGTAAAGCTCCAACAAGTAACAAAAAAATCACAAGAG
GGATATTTATATTTTTGACAATTCTTCTAAGGAAGTTCTTCATATAGCTATCACCATAATATTTATTTAGA
GATCTTAAAGCTACTTTCTTCATAATAACTCTCCTTTTACTTTTTTATCTACAACTTCATATCAGATTACAA
ATCTCAATAATTTTGTTTGTAATTATATATGTTAGTTGATTTATTTTTCCGTTTTCTCACTAGTTTTAAATG
ACTATCAAAATCATTTTTTATATATAAATATCTATATCGTACTGTAATACTATAATCAGTATGTTAGTAAG
CTTATTATTAATAAATAAAAATATTTATTTTGCATATTCTCCCCTTAACCTTTATTTGGTTAATATAGAAAT
TATCATAAAACTTGTAAATTTACTATATTTTGGAGCCGAGTTTAGCTAGGTTTAAGAAGTTTAAGCTGAT
TATGCTATAATCTAAACAATACTAAATTTAATAAATATCTAAATGCTTTCAGATGCTTCACAAGAAGATA
AAAAAGTAGCTAGGAAATGGCTCAAACAAATATCATATCCCGCTAAGAGATGGATTAAATTAACTATAT
TGATAGCTTTTTTAAGCGGCTTACTACTAGTTGGACAATTATATTTATTAGCTCATATTTCTTATGCTGCA
TACATCGATAAATCTAACTTTGGTCAACTAAGTAACTACTTTATAGTTATTGTTTTAATAGTCATAATTAG
AGCAGCTCTTGCTTGGTTACGAGAAATTGTCAGTTATAAAGCCGCGACAATTGTCAAAAAGCAAATTAG
AGAAGATATCTTGGCTCATGTAAACCAACTCGGTCCAATTCAGTTAAACAAAACTTCTAATGCAAATATA
ATTACAAGTGCGATGGAACAAGTCGAAGGACTAACTGGGTTCCTAACAAAATTTCTACCACAAATAACT
TTATCAGGACTATTACCTTTAGCTGTTTTAGTATTTATATTCCCTCAAAGTATTGTCTGTGGAATCCTTCT
ACTAATAAGCGCACCACTTATTCCACTTTTTATGGTATTAGTTGGTTTAGGCGCTGAATCTGAAAGCCAA
AAGCATTTCAAAGCACTTGCTAGAATGAGTCTAACTTTTCTAGATACGCT**ACGCGT**

Figure 137. Commercially sourced synthetic insert sequence for *F. tularensis* FTT_1334c mutant generation. Left flank highlighted in yellow and right flank highlighted in blue.

8.7. Protein Alignments for *Burkholderia pseudomallei* PPK and PPX

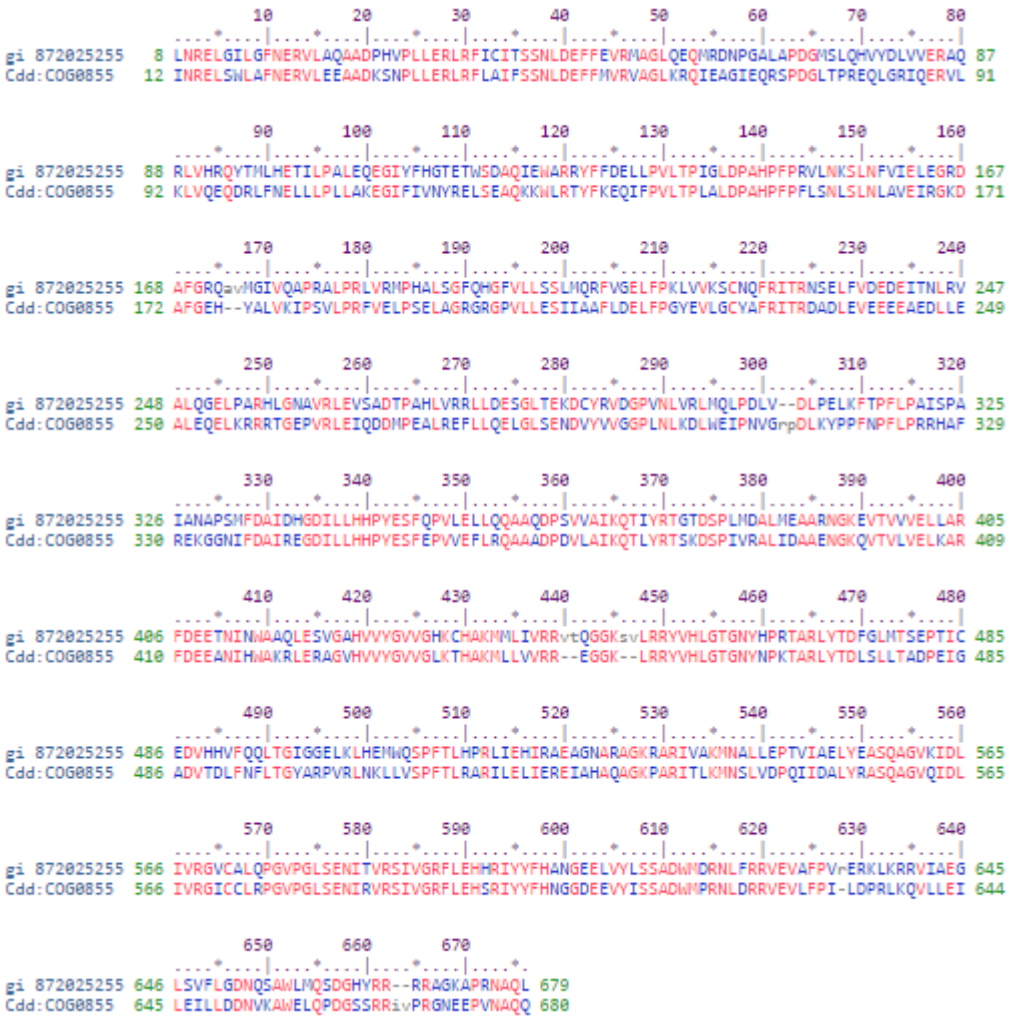

Figure 138. Amino acid sequence alignment of PPK (BPSL_1366) of *B. pseudomallei* with PPK from *E. coli.* Amino acid residues denoted in red indicate a high degree of conservation and amino acid residues in blue indicate a low degree of conservation.

Figure 139. Amino acid sequence alignment of PPX (BPSL_1367) of *B. pseudomallei* K96243 with PPX from *E. coli.* Amino acid residues denoted in red indicate a high degree of conservation and amino acid residues in blue indicate a low degree of conservation

Figure 140. Amino acid sequence alignment of RelA (BPSL_1946) of *B. pseudomallei* K96243 with RelA from *E. coli.* Amino acid residues denoted in red indicate a high degree of conservation and amino acid residues in blue indicate a low degree of conservation.

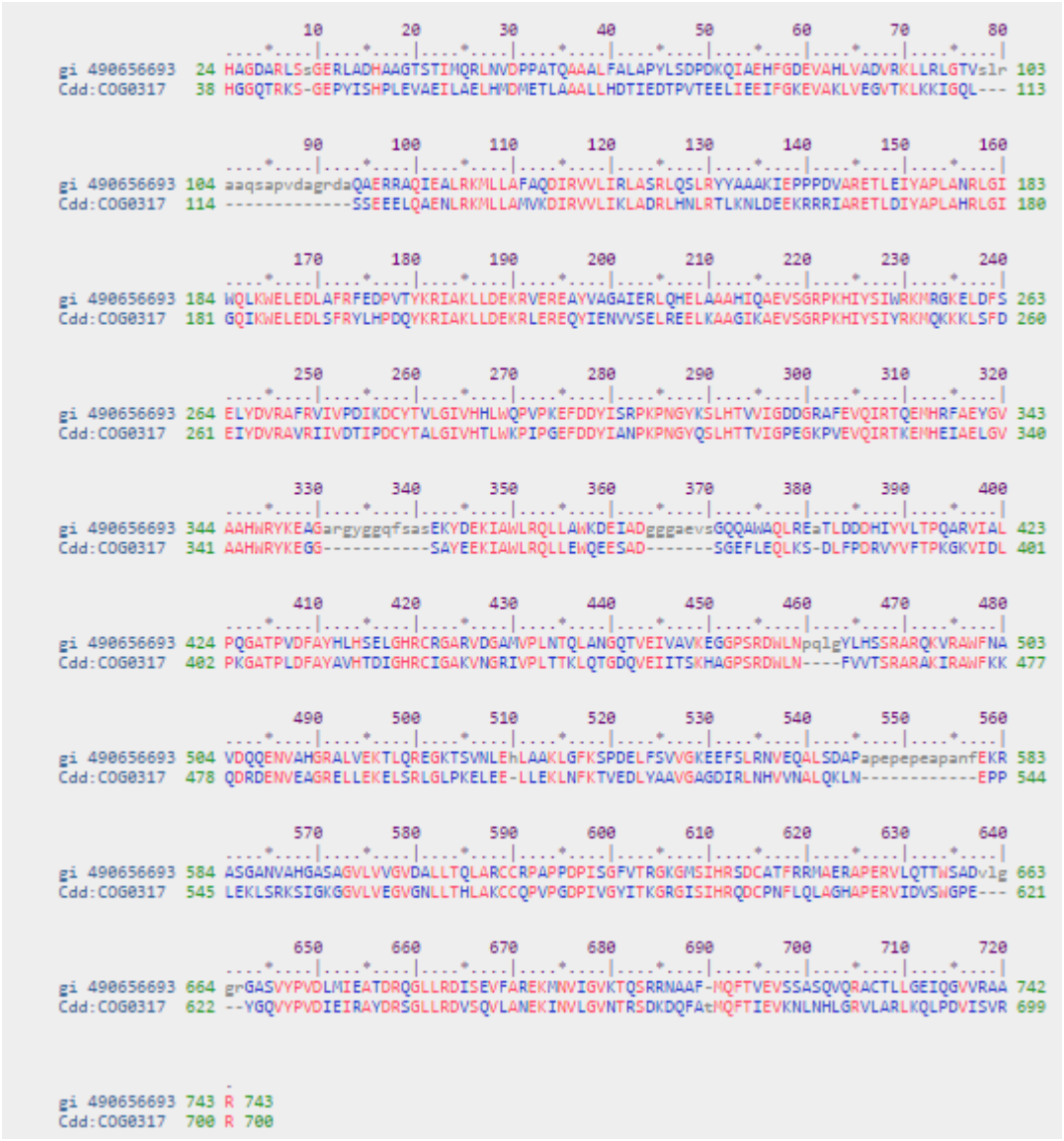

Figure 141. Amino acid sequence alignment of SpoT (BPSL_ 2561) of *B. pseudomallei* K96243 with SpoT from *E. coli.* Amino acid residues denoted in red indicate a high degree of conservation and amino acid residues in blue indicate a low degree of conservation

8.8. Primer Sequences for *Burkholderia pseudomallei* Mutants

Primer	Sequence
BP_PPK_LFF_ xbaI_linked	TCTAGAGATTTCGTCCGCTATCTGAAC
BP_PPK_LFR_xmaI _linked	**CCCGGG**CAGGCGCCGGCGCGTGCG
BP_PPK_RFF_ xmaI_linked	**CCCGGG**GAGGCGCGCAGCGCTTAAAATGGC
BP_PPK_RFR_xbaI _linked	TCTAGAGCGGCCGAGCAGGTCGTACAG

Table 26. *B. pseudomallei Δppk* mutant. Bases underlined denote the *Xba*I restriction site. Bases in **bold** denote the *Xma*I restriction site.

Primer	Sequence
BP_PPX_LFF_ BglII_linked	AGATCTCACGAGATGCGCAGGCGTGTC
BP_PPX_LFR_scaI _linked	**AGTACT**ACGCGCCGAAAAGATCAAAGG
BP_PPX_RFF_ scaI_linked	**AGTACT**CCGGCGGCGCAACGGCGCTTC
BP_PPX_RFR_BglII _linked	AGATCTGCTCGCCCTCGCCCGACTCCC

Table 27. *B. pseudomallei ΔppX* mutant. Bases underlined denote the *Bgl*II restriction site. Bases in **bold** denote the *Sca*I restriction site.

Primer	Sequence
BP_PPK_X_LFF_Xba	TCTAGAGATTTCGTCCGCTATCTGAAC
BP_PPK_X_LFR_Xma	**CCCGGG**CAGGCGCCGGCGCGTGCG
BP_PPK_X_RFF_Xma	**CCCGGG**CCGGCGGCGCAACGGCGCTTC
BP_PPK_X_RFR_Xba	TCTAGAGCTCGCCCTCGCCCGACTCCC

Table 28. *B. pseudomallei Δppk/ppX* mutant. Bases underlined denote the *Xba*I restriction site. Bases in **bold** denote the *Xma*I restriction site.

8.9. Synthetic Construct Sequences for *Burkholderia pseudomallei* Mutants

***B. pseudomallei* ∆*ppK* Synthetic Construct:**

TCTAGAGATTTCGTCCGCTATCTGAACGGCCAGCATTACGACGAAACGCTCGTGATGCGCGGCATGGG
CGGCAATCGGCAGAACGTGCTTGCCGTGCAGGTGTTTCCGTACGGCGAGAACCGCAAGCTGCTGCTCA
CGCAGGATATCACCGAGCTCGAGCGCACCGATGCGATGCGGCGCGACTTCGTCGCGAACGTGTCGCAC
GAACTGAAGACGCCGCTTACCGTGCTGTCGGGCTTTCTCGAGACGATGCGCGAGCTGCCGCTGTCGGA
CGACGAGCGCGCGCGCTATCTCGAACTGATGGAGCAGCAGGCGTCGCGGATGCGGCACATCGTCACC
GATCTGCTCGTGCTCGCGAAGCTCGAGGGCGAAAGCAAGCCGCCCGCCGATCGCGCGGTCGACATGC
GCACGGTGCTCGACCATCTGCGGGACGATGCGCAGACGCTATCGGGCGGCCATCACGAGATCACGTTC
AAGGTTGACGAGACGCTCGCGGTGACGGGCGCGCAGACCGAGATCTTCAGCGCGCTCGGCAACCTCG
TGACGAATGCGATCCGCTATACGCCGGAGGGCGGGACGATCCGCGTCGAATGGCGGCGCGACGGCGC
GCAGGCGGTGTTCTCGGTCACCGATAGCGGGCTCGGCATTCCGGCCGCCGAACTGCCGCGGCTCACCG
AGCGGTTCTATCGCGTCGACCGCAGCCGCTCGCGCGACACGGGCGGCACGGGGCTCGGGCTCGCGAT
CGTCAAGCATGTGTTGCAACGGCACGATGCGCAACTGTCGATCCAGAGCGAGGAGGGGCGTGGCAGC
ACGTTTACCGCGCGTTTTCCCGCGCATCGGACGATCAGCCGGAGGCATGCGGCGTGACGTGAGCGGCG
CGCGGGGGGCATGGCGTTGCTTCGGGAGAGCCGTTCGATTCGGCGGAGCCGCGCGCCGCATCGCCGT
GCGGAGCCGGCGTCTTCGCGGCGTCGGGCCGCGCGGCGGGCGCGCCCGCCGCGCCCTCGTTCGAGGT
TTGAGCGGCGCGGCGCTTGCCGCGGCGCGGCACCGCGCACGCGCCGGCGCCTGCCCGGGCCCGGGGA
GGCGCGCAGCGCTTAAAATGGCGCCTTTGATCTTTTCGGCGCGTGCAGCGTCGCCTGCGCGCGCCAGG
CGAGAACGGAGCCCCCTCGATGGTTACATCCCCGCATCTACTGGCTGCCGTCGATCTCGGCTCGAACAG
CTTCCGGCTCATCGTCGGGCGCGTCGAGGAGACGCCCGCCGGCAGCCAGATCTATCCCGTCGACGCGC
TGCGCGAACCCGTGCGGCTCGCCGCCGGCCTGTCCCGCGACAAGATGCTCGATCGCGCGTCGCAGGAG
CGCGGCTGGGAAGCGCTCAAGCGTTTCGGCGAGCGGCTGCGCGATTTCCACCCGGATCACGTGCGCGC
GGTCGCGACGAACACGCTGCGCGTCGCGAAGAACGCCGGGGAGTTTCTCGCCGAGGCGCAGGCGGCG
CTCGGCTTTCCGATCGAAGTGATCGCGGGCCGCGAGGAAGCGCGCCTCATTTACGCGGGCGCCGCGCA
CTCGGTGCCGGCGAACGCCGGCAAGCGGCTCGTCGTCGACATCGGCGGCGGCTCGACCGAATTCATCA
TCGGCCAGCATTACACGCCGCTTGTGATGGAGAGCCTCTACATCGGCTGCGTGAGCCACAGCCGCGCG
TTCTTTCCGGCCGGCAACGTCGACGAATACATGATGCGCCAGGCCGAACTCGCCGCGAAGCGCGAGAT
CCAGATCATCTCCGGCGAATACAAGAAGGCGGGGGTGGGATCAGGCGATCGGCTCGTCCGGCACCGCG
CGCGCGCTCGCGGAACTCGTCGAGGCGAACGGCTTCAACGACGCGGGCGTGTCGCACGGCATCTCGC
GCGGCGGCCTCGAGCGCCTGAAGCGCGCGCTCATCAAGGCCGAGAACGTGAACCGCCTGAAGCTCGT
CGCGCTGAAGCCCGATCGCGTGCCGGTGCTCGCGGGCGGGCTGTCGATCATGCTCGCGGTGTTCGAG
GAACTCGGCGTCGACTACGTCGACACGACGGACGGCGCGCTGCGTCTGGGTGTGCTGTACGACCTGCT
CGGCCGC**TCTAGA**

Figure 142. Commercially sourced synthetic insert sequence for *B. pseudomallei* ∆*ppK* synthetic insert mutant generation. Left flank highlighted in yellow and right flank highlighted in blue.

***B. pseudomallei* ΔppX Synthetic Construct:**

AGATCTCACGAGATGCGCAGGCGTGTCGGCCGACACCTCGAGCCGCACCGCGTTGCCGAGATGGCGC
GCGGGCAGCTCGCCCTGCAGCGCGACGCGCAGGTTCGTGATTTCGTCTTCGTCGACGAAGAGCTCGCT
GTTGCGCGTGATCCGAAACTGGTTGCAGCTCTTCACGACGAGTTTGGGAAACAGCTCGCCGACGAAGC
GCTGCATCAGCGAGCTCAGCAGCACGAAGCCGTGCTGGAAACCCGACAGCGCGTGCGGCATGCGCAC
GAGGCGCGGCAGCGCGCGCGGCGCCTGCACGATGCCCATCACCGCCTGGCGGCCGAACGCGTCGCGG
CCCTCGAGCTCGATCACGAAGTTCAGGCTCTTGTTCAGCACGCGCGGGAACGGGTGCGCGGGGTCGAG
CCCGATCGGCGTGAGAACGGGCAGCAGCTCGTCGAAGAAGTAGCGGCGCGCCCATTCGATCTGCGCG
TCACTCCATGTCTCGGTGCCGTGGAAATAGATGCCTTCCTGCTCGAGCGCGGGCAGGATCGTTTCGTGC
AGCATCGTATATTGCCGGTGCACGAGCCGCTGCGCGCGCTCGACGACGAGATCGTACACGTGCTGCAG
CGACATGCCGTCCGGCGCGAGCGCCCCCGGATTGTCGCGCATCTGCTCTTGCAGCCCGGCCATCCGGA
CTTCGAAGAATTCGTCGAGGTTGCTGCTCGTGATGCAGATGAAGCGCAGACGCTCGAGGAGGGGGAC
GTGCGGATCGGCGGCTTGGGCGAGCACGCGCTCGTTGAAGCCCAGGATGCCGAGTTCGCGATTCAGG
AGCGGATAACGGAGGGACATCGGCAGAGAATACGGAAGGTCAGGCGCAGACTCGAAAGGTCGCTCG
GAAATTCTCACGGTGCGATGACGTGCTGATGACAGTTTGATGTTTGTCGGCAAATCATACGCTCGAAAA
CCGGGGATTTCATAAAAGCATCCTCTAGATACAATGAAAGCATGTGTGGGCCGGCTCGCGGCCGACAC
CGGGAGGCGCGCAGCGCTTAAAATGGCGCCTTTGATCTTTTCGGCGCGTAGTACTAGTACTCCGGCGG
CGCAACGGCGCTTCCGCTCCCGCTTTCGCCAGCACGCGAGGGGGCGTGTTCGTTGGCCGCGTTAACGG
ACCTTCGCGGGCGTTTGCGTACCTTTGTGGGTGTTTGGGGCCGTGTTTCCGGACGATTTCGGCCGCAAC
TGCGCGCGTAGCGTCGCGCGCGCGTCGAATGCCGGCGGGCTGCCGATGCTGCGCGTCCCGCACGGGC
GCGGCGCGCCGGGCATCAGCGGGGCGTGGGCCGCGCCGGTGCCAGCGGGCCACGCTGCGCGGCGAG
GTGCCCGCGTGCCGGCCGCCGTGCCGCCACGCTTACGGAGACGTGCAGACGATCGCCGTCAGAAACG
GAAACGCATCCTTGACCACCGCCTGGCTGCCCGCCGCGCGCACCTTCGCCTCCACCGCCTGCTTCGAGC
CCCGGACGACGACCCCATATGCCCAGTCGCCGATCGGCTCGCCGTCGCCATGCGCGAAGAGCGGGTCG
TTCGCCTGGTAGCCGAGCACGACGTAGACGGAGAAACCGTAGGCGCTCAGCGAGCGGTTCGTGCGGA
ACGCATTCATCGAGTTCGCCTCGACGTGCATCGGCTGCGAGCGGACCGCGCCGCTCGCGACGAGCGGC
GCGACGAACGCGTGGCCCGTCGACGAACAGTCGAGCGCGGCGTCGAGCGCTTGCGAATCGGCGGACG
CGGCGGGCGCGGCCGCAAGCGTCGCGAACGGGATCAGCAGTCGGGCAATCAGGCGGAGTGGGTTGT
TCATGCGATGGCGCTCGCCGCACGGGCGGCGGGTTGTCGACGGCCCGAGGCGGGCCGCTCGGTCGAG
GTCGGGCGGGAAAGGCGCGGCCTCGCGGCCGCGGGCCTTTCGACTGGCTTTGCTTTCGAACCTTACGG
ATCGGGCGCGGGTTGCCGGCGCCGTTTGCCCGATGATAGCGAAAACACCGGCCATACGCAGGCGGAT
CCACGCGGAGGCGTCCGGCGCGTGAGGCCTGGGGCGGGCAGCGCCGTCGTGCGGGCGGGGAGTCGG
GCGAGGGCGAGC**AGATCT**

Figure 143. Commercially sourced synthetic insert sequence for *B. pseudomallei* Δ*ppX* synthetic insert mutant generation. Left flank highlighted in yellow and right flank highlighted in blue.

***B. pseudomallei* ΔppK/ppX Synthetic Construct:**

TCTAGAGATTTCGTCCGCTATCTGAACGGCCAGCATTACGACGAAACGCTCGTGATGCGCGGCATGGG
CGGCAATCGGCAGAACGTGCTTGCCGTGCAGGTGTTTCCGTACGGCGAGAACCGCAAGCTGCTGCTCA
CGCAGGATATCACCGAGCTCGAGCGCACCGATGCGATGCGGCGCGACTTCGTCGCGAACGTGTCGCAC
GAACTGAAGACGCCGCTTACCGTGCTGTCGGGCTTTCTCGAGACGATGCGCGAGCTGCCGCTGTCGGA
CGACGAGCGCGCGCGCTATCTCGAACTGATGGAGCAGCAGGCGTCGCGGATGCGGCACATCGTCACC
GATCTGCTCGTGCTCGCGAAGCTCGAGGGCGAAAGCAAGCCGCCCGCCGATCGCGCGGTCGACATGC
GCACGGTGCTCGACCATCTGCGGGACGATGCGCAGACGCTATCGGGCGGCCATCACGAGATCACGTTC
AAGGTTGACGAGACGCTCGCGGTGACGGGCGCGCAGACCGAGATCTTCAGCGCGCTCGGCAACCTCG
TGACGAATGCGATCCGCTATACGCCGGAGGGCGGGACGATCCGCGTCGAATGGCGGCGCGACGGCGC
GCAGGCGGTGTTCTCGGTCACCGATAGCGGGCTCGGCATTCCGGCCGCCGAACTGCCGCGGCTCACCG
AGCGGTTCTATCGCGTCGACCGCAGCCGCTCGCGCGACACGGGCGGCACGGGGCTCGGGCTCGCGAT
CGTCAAGCATGTGTTGCAACGGCACGATGCGCAACTGTCGATCCAGAGCGAGGAGGGGCGTGGCAGC
ACGTTTACCGCGCGTTTTCCCGCGCATCGGACGATCAGCCGGAGGCATGCGGCGTGACGTGAGCGGCG
CGCGGGGGGCATGGCGTTGCTTCGGGAGAGCCGTTCGATTCGGCGGAGCCGCGCGCCGCATCGCCGT
GCGGAGCCGGCGTCTTCGCGGCGTCGGGCCGCGCGGCGGGCGCGCCCGCCGCGCCCTCGTTCGAGGT
TTGAGCGGCGCGGCGCTTGCCGCGGCGCGGCACCGCGCACGCGCCGGCGCCTGCCCGGGCCCGGGCC
GGCGGCGCAACGGCGCTTCCGCTCCCGCTTTCGCCAGCACGCGAGGGGGCGTGTTCGTTGGCCGCGTT
AACGGACCTTCGCGGGCGTTTGCGTACCTTTGTGGGTGTTTGGGGCCGTGTTTCCGGACGATTTCGGCC
GCAACTGCGCGCGTAGCGTCGCGCGCGCGTCGAATGCCGGCGGGCTGCCGATGCTGCGCGTCCCGCA
CGGGCGCGGCGCGCCGGGCATCAGCGGGGCGTGGGCCGCGCCGGTGCCAGCGGGCCACGCTGCGCG
GCGAGGTGCCCGCGTGCCGGCCGCCGTGCCGCCACGCTTACGGAGACGTGCAGACGATCGCCGTCAG
AAACGGAAACGCATCCTTGACCACCGCCTGGCTGCCCGCCGCGCGCACCTTCGCCTCCACCGCCTGCTT
CGAGCCCCGGACGACGACCCCATATGCCCAGTCGCCGATCGGCTCGCCGTCGCCATGCGCGAAGAGCG
GGTCGTTCGCCTGGTAGCCGAGCACGACGTAGACGGAGAAACCGTAGGCGCTCAGCGAGCGGTTCGT
GCGGAACGCATTCATCGAGTTCGCCTCGACGTGCATCGGCTGCGAGCGGACCGCGCCGCTCGCGACGA
GCGGCGCGACGAACGCGTGGCCCGTCGACGAACAGTCGAGCGCGGCGTCGAGCGCTTGCGAATCGGC
GGACGCGGCGGGCGCGGCCGCAAGCGTCGCGAACGGGATCAGCAGTCGGGCAATCAGGCGGAGTGG
GTTGTTCATGCGATGGCGCTCGCCGCACGGGCGGCGGGTTGTCGACGGCCCGAGGCGGGCCGCTCGG
TCGAGGTCGGGCGGGAAAGGCGCGGCCTCGCGGCCGCGGGCCTTTCGACTGGCTTTGCTTTCGAACCT
TACGGATCGGGCGCGGGTTGCCGGCGCCGTTTGCCCGATGATAGCGAAAACACCGGCCATACGCAGG
CGGATCCACGCGGAGGCGTCCGGCGCGTGAGGCCTGGGGCGGGCAGCGCCGTCGTGCGGGCGGGGA
GTCGGGCGAGGGCGAGC**TCTAGA**

Figure 144. Commercially sourced synthetic insert sequence for *B. pseudomallei* Δ*ppK/ppX* synthetic insert mutant generation. Left flank highlighted in yellow and right flank highlighted in blue.

8.10. Bioanalyzer Traces of *Francisella tularensis* RNA samples

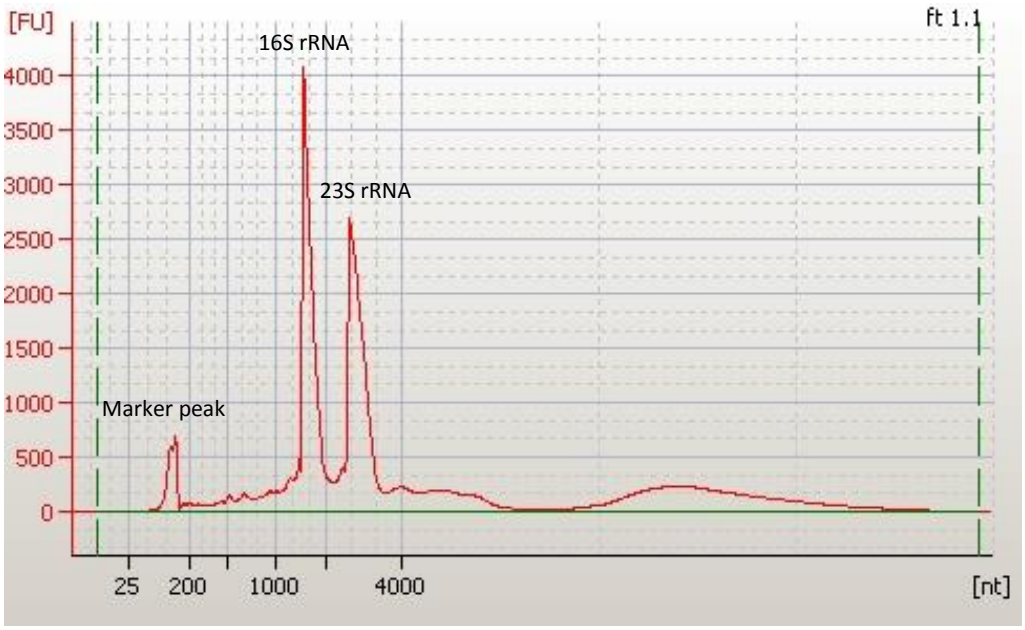

Figure 145. Electropherogram trace of *F. tularensis* RNA sample FT1.1 from the 0 µg/mL serine hydroxamate condition. Distinct and high peaks observed for 16S and 23S rRNA. These peaks are labelled on this trace for reference. Sample SB03/0228. 185194.9 pg/µL.

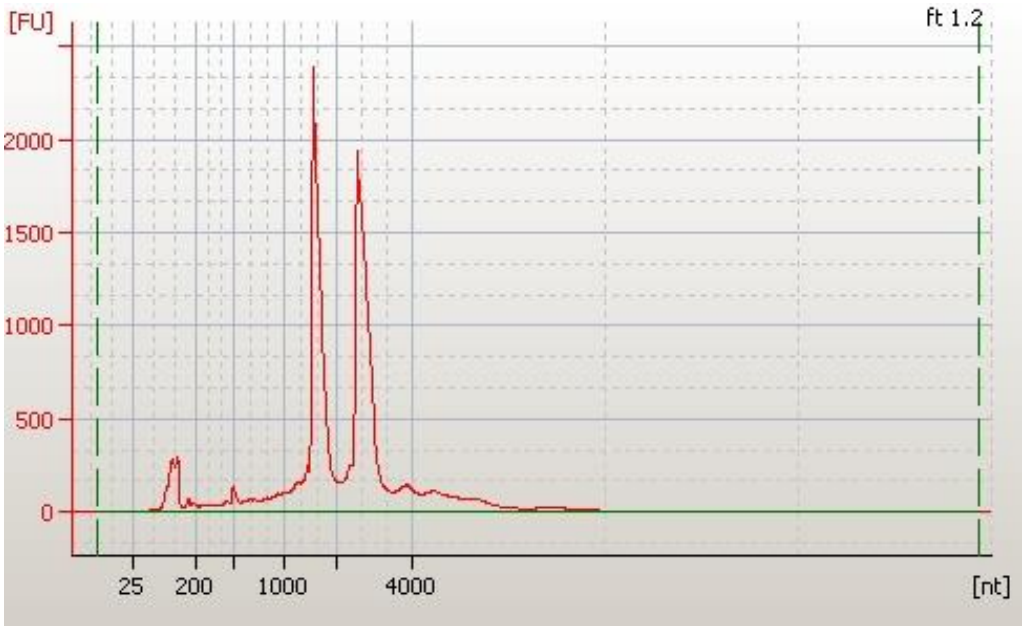

Figure 146. Electropherogram trace of *F. tularensis* RNA sample FT1.2 from the 0 µg/mL serine hydroxamate condition. Distinct and high peaks observed for 16S and 23S rRNA. Sample SB03/0229. 89240.43 pg/µL.

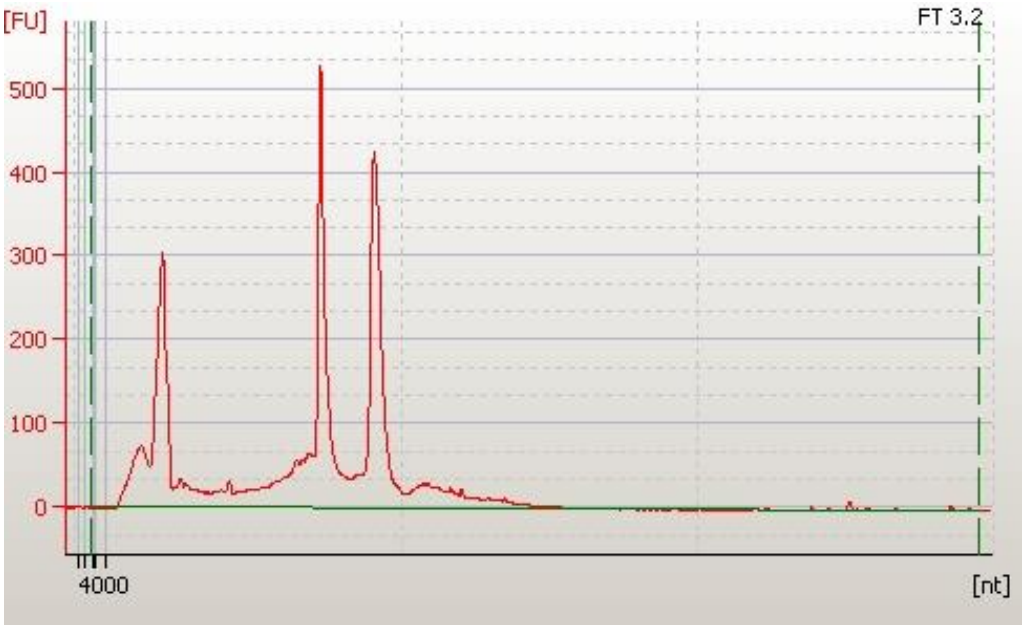

Figure 147. Electropherogram trace of *F. tularensis* RNA sample FT1.3 from the 0 µg/mL serine hydroxamate condition. Distinct and high peaks observed for 16S and 23S rRNA. Sample SB03/0213. 13052.46 pg/µL.

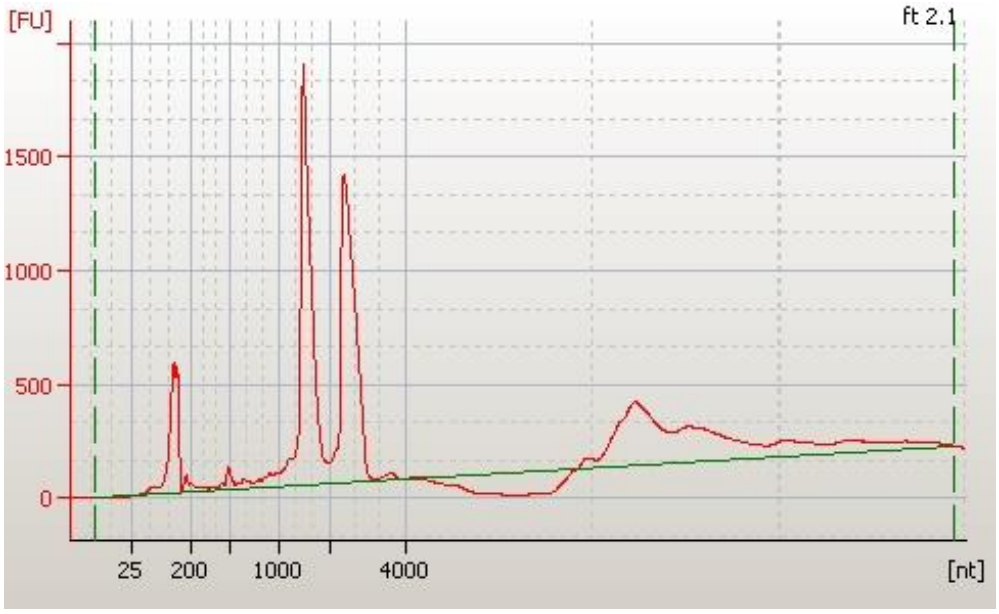

Figure 148. Electropherogram trace of *F. tularensis* RNA sample FT2.1 from the 1 µg/mL serine hydroxamate condition. Distinct and high peaks observed for 16S and 23S rRNA. Sample SB03/0230. 85913.35 pg/µL.

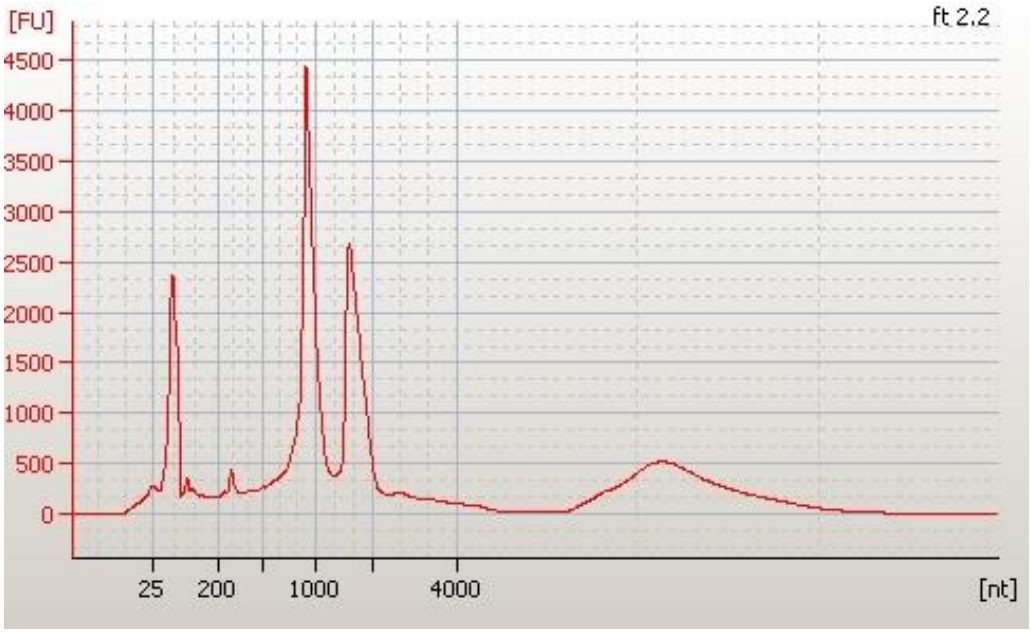

Figure 149. Electropherogram trace of *F. tularensis* RNA sample FT2.2 from the 1 µg/mL serine hydroxamate condition. Distinct and high peaks observed for 16S and 23S rRNA. Sample SB03/0231. 229727.8 pg/µL.

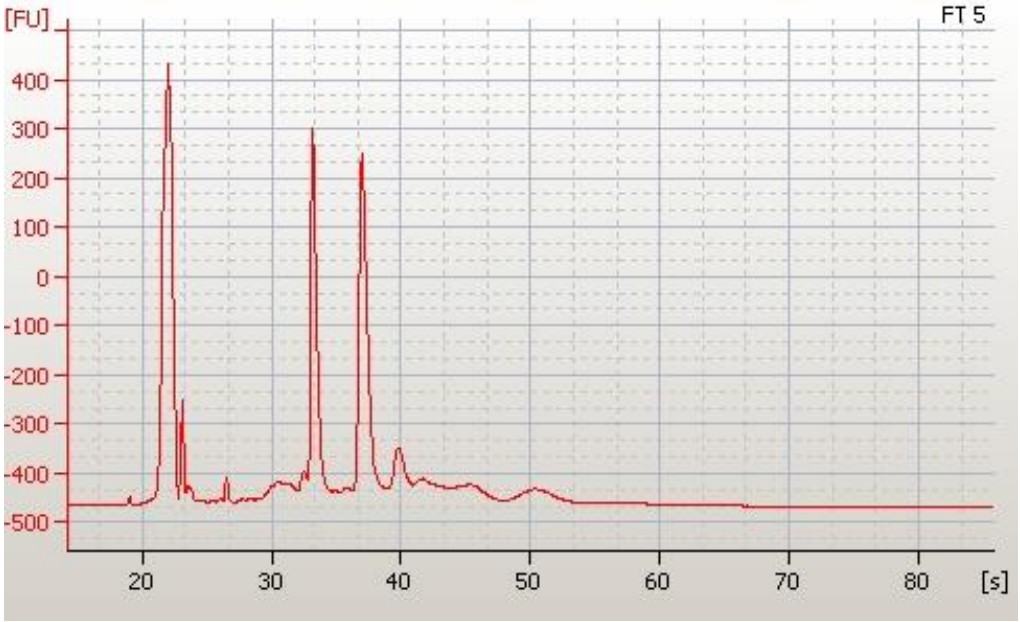

Figure 150. Electropherogram trace of *F. tularensis* RNA sample FT2.3 from the 1 µg/mL serine hydroxamate condition. Distinct and high peaks observed for 16S and 23S rRNA. Sample SB03/0212. 15064.5 pg/µL.

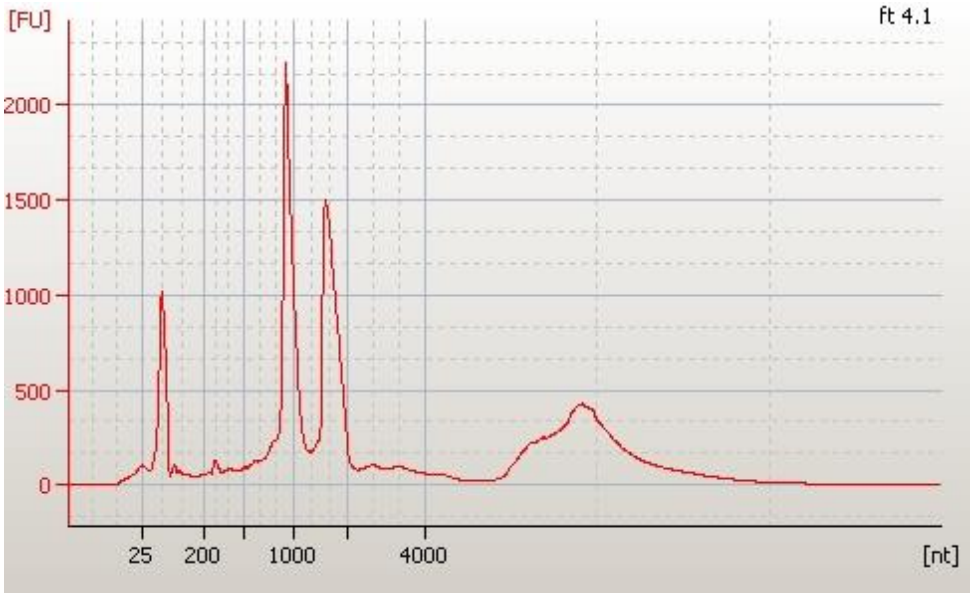

Figure 151. Electropherogram trace of *F. tularensis* RNA sample FT3.1 from the 10 µg/mL serine hydroxamate condition. Distinct and high peaks observed for 16S and 23S rRNA. Sample SB03/0235. 56185.21 pg/µL.

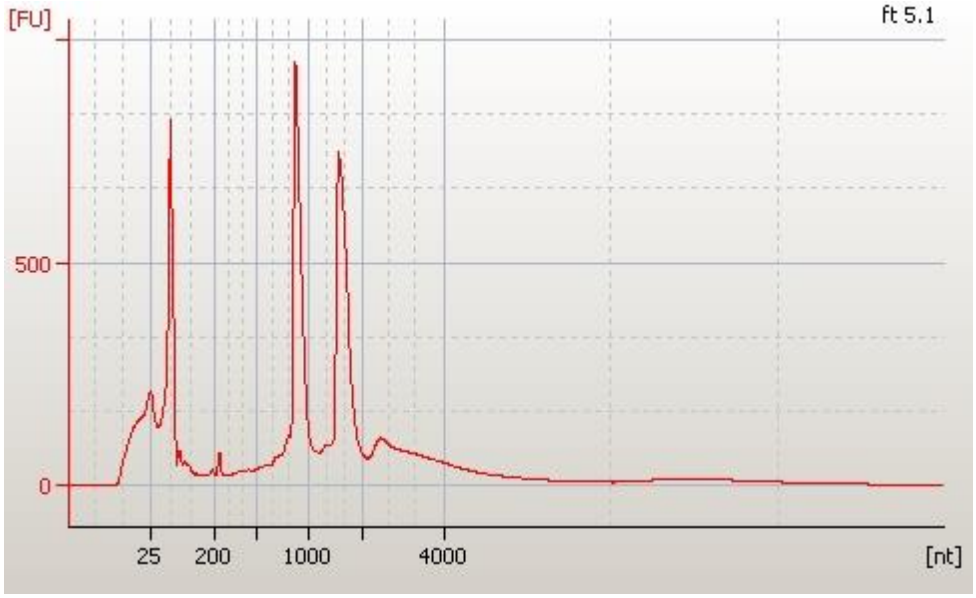

Figure 152. Electropherogram trace of *F. tularensis* RNA sample FT3.2 from the 10 µg/mL serine hydroxamate condition. Distinct and high peaks observed for 16S and 23S rRNA. Sample SB03/0236. 42767.46 pg/µL.

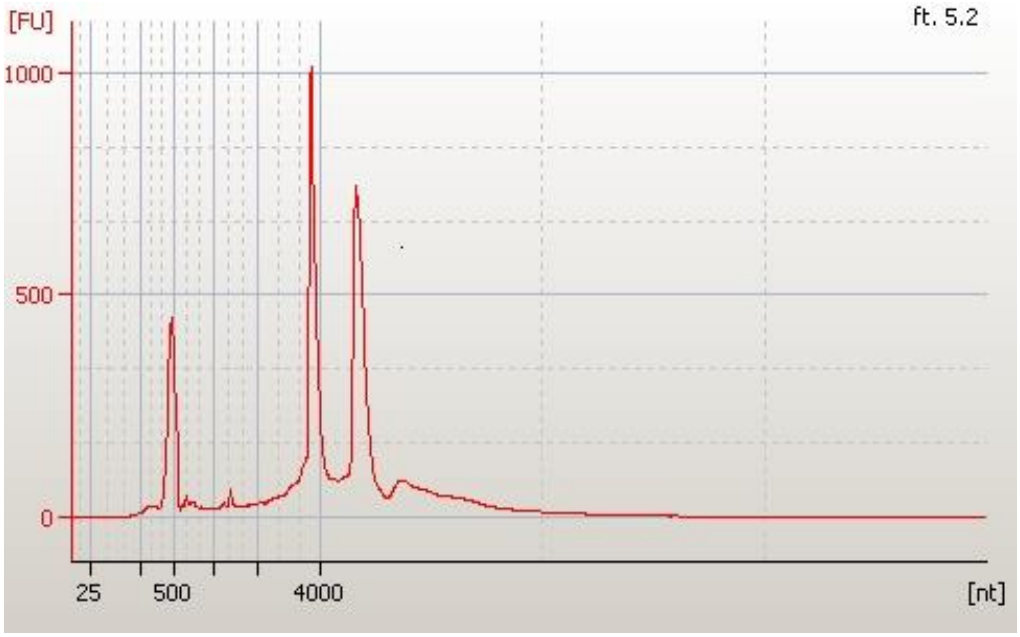

Figure 153. Electropherogram trace of *F. tularensis* RNA sample FT3.3 from the 10 µg/mL serine hydroxamate condition. Distinct and high peaks observed for 16S and 23S rRNA. Sample SB03/0237. 36902.04 pg/µL.

8.11. Primer Sequences for *Francisella tularensis* Transcriptional Analysis Validation

Primer	Sequence
IglC_For	ACAGGTAACAAGTGGCGAGACCATTC
IglC_Rev	CTGCGCAACATACTGGCAAACTTCC
FT_16S_F	AATTGCTATTGCTGGCAGTGAAC
FT_16S_R	GAGCAGTTTCTGCTTTAAGTATTC
FTT_0613c_For	TAATATCTCTAACTAGTATTG
FTT_0613c_Rev	TTGGCAGCCAATTGTAATACG
FTT_1334_For	TTACCACGATAGGTTTGTCTG
FTT_1334_Rev	GTTTGCTGGACTAGCTTAGAC

Table 29. *F. tularensis* specific primers for RT-PCR validation of RNA-seq results

8.12. Raw Data Output from *Francisella tularensis* RNA-Sequencing

Sample ID	Yield (Mbases)	# Reads	% of >= Q30 Bases	Mean Quality Score
FT1_1	4,286	42,855,794	95.12	37.03
FT1_2	3,628	36,283,622	95.13	37.01
FT1_3	3,618	36,182,144	95.09	37.01
FT2_1	3,375	33,754,344	95.21	37.07
FT2_2	4,320	43,197,050	95.39	37.15
FT2_3	3,082	30,818,746	93.34	36.33
FT3_1	5,009	50,091,740	95.30	37.11
FT3_2	5,289	52,889,968	94.53	36.81
FT3_3	2,937	29,371,816	95.25	37.12

Table 30. Summary of raw data output statistics for a paired-end RNA-seq run on the Illumina HiSeq2500. Three biological replicates are shown for each condition tested. Total number of reads and sequence yield for each sample are shown. Quality scores for each sample are shown as the percentage of bases with high quality scores and the average quality score for each sample.

8.13. Bioanalyzer Traces of *Yersinia pestis* RNA samples

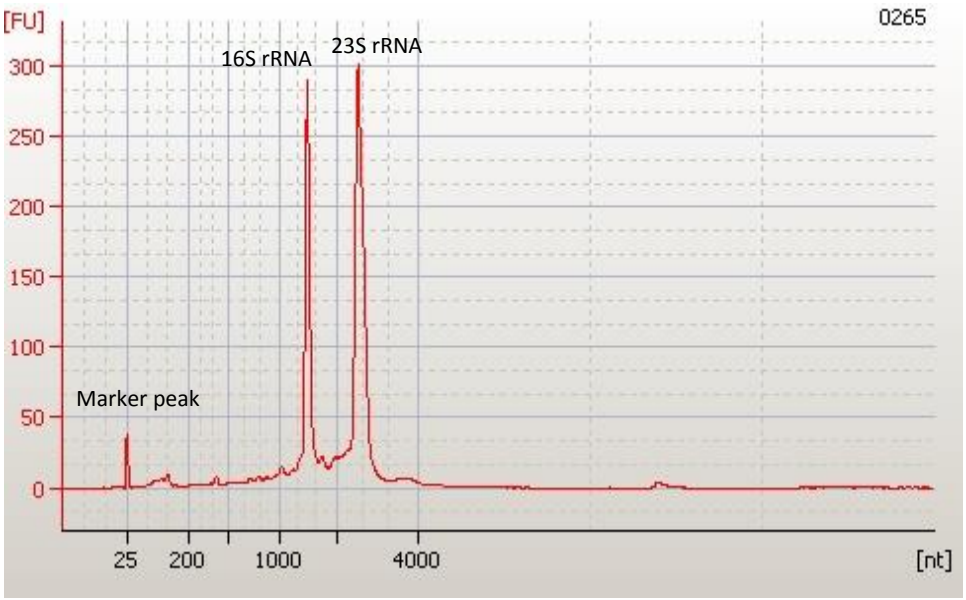

Figure 154. Electropherogram trace of *Y. pestis* RNA sample YP1.1 from the 0 µg/mL serine hydroxamate condition. Distinct and high peaks observed for 16S and 23S rRNA. These peaks are labelled on this trace for reference. Sample SC06/0265. 5625.304 ng/µL. RIN: 9.8.

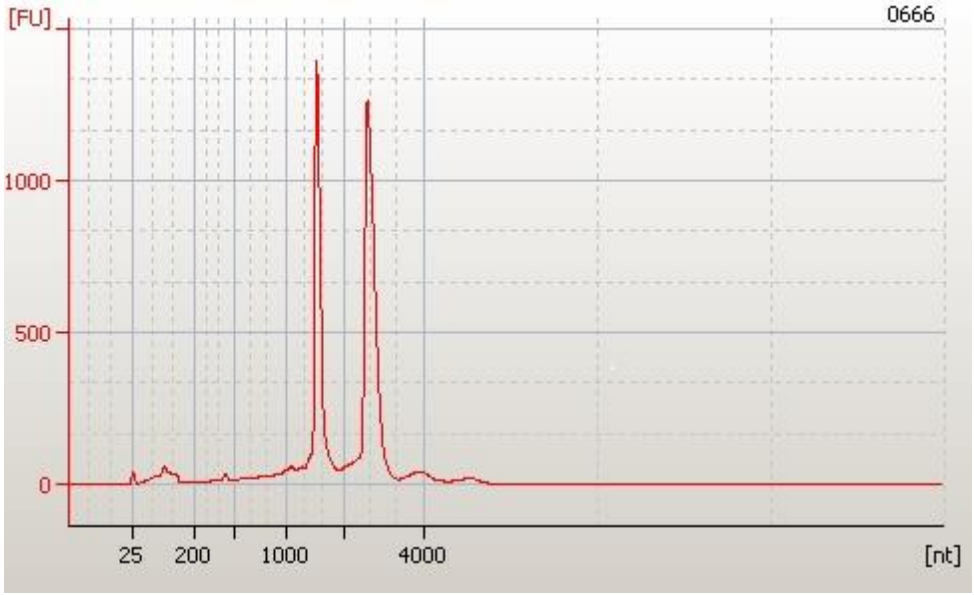

Figure 155. Electropherogram trace of *Y. pestis* RNA sample YP1.2 from the 0 µg/mL serine hydroxamate condition. Distinct and high peaks observed for 16S and 23S rRNA. Sample SC06/0666. 27936.41 ng/µL. RIN: 9.8.

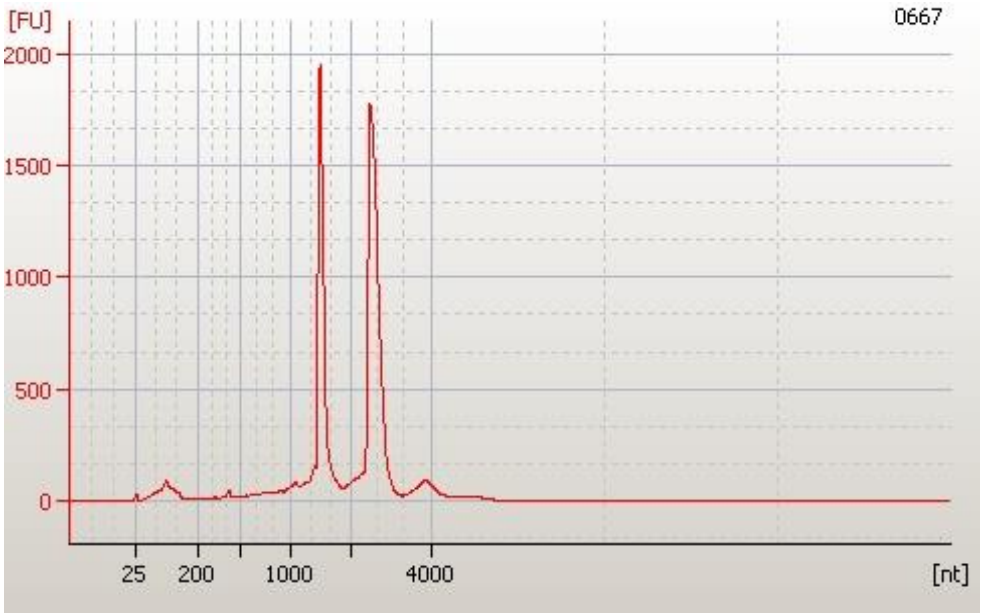

Figure 156. Electropherogram trace of *Y. pestis* RNA sample YP1.3 from the 0 µg/mL serine hydroxamate condition. Distinct and high peaks observed for 16S and 23S rRNA. Sample SC06/0667. 39491.84 ng/µL. RIN: 9.8.

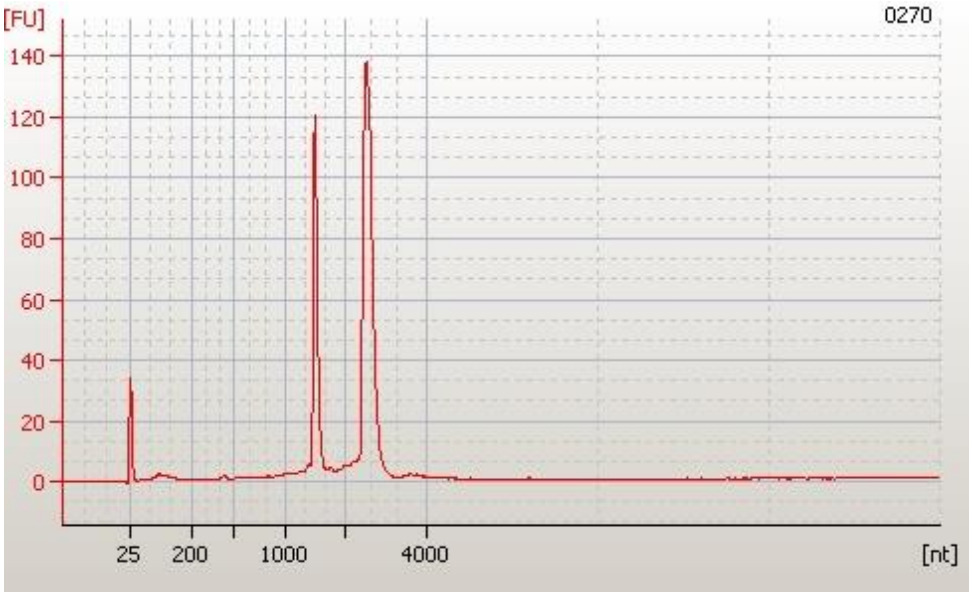

Figure 157. Electropherogram trace of *Y. pestis* RNA sample YP2.1 from the 10 µg/mL serine hydroxamate condition. Distinct and high peaks observed for 16S and 23S rRNA. Sample SC06/0270. 2147.219 ng/µL. RIN: 10

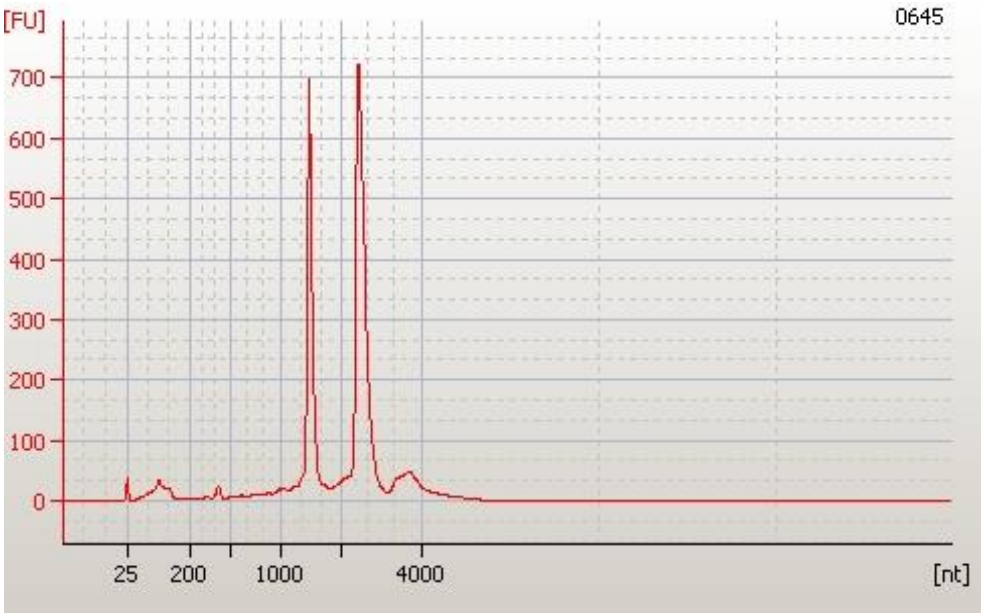

Figure 158. Electropherogram trace of *Y. pestis* RNA sample YP2.2 from the 10 µg/mL serine hydroxamate condition. Distinct and high peaks observed for 16S and 23S rRNA. Sample SC06/0645. 14130.71 ng/µL. RIN: 9.9.

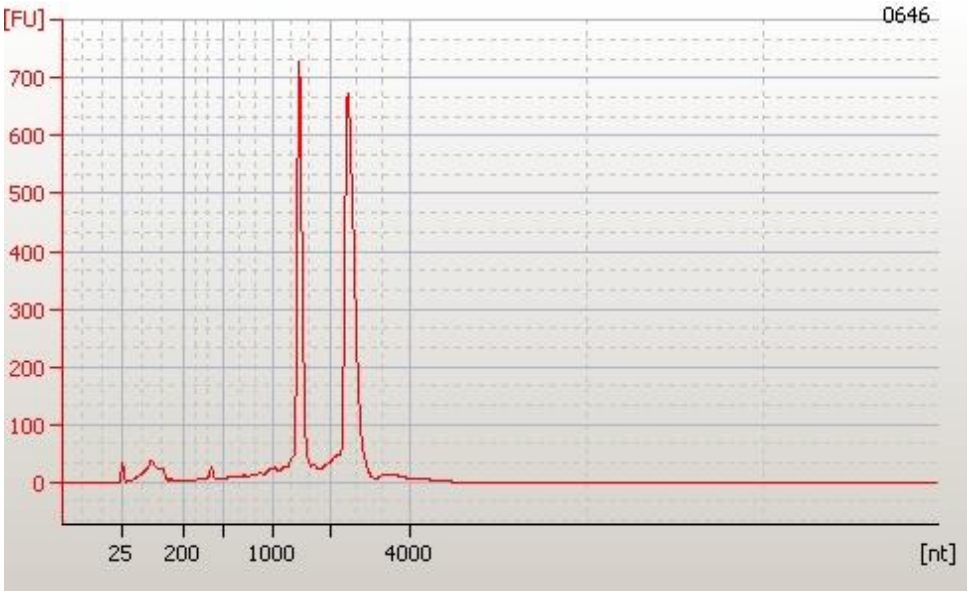

Figure 159. Electropherogram trace of *Y. pestis* RNA sample YP2.3. from the 10 µg/mL serine hydroxamate condition. Distinct and high peaks observed for 16S and 23S rRNA. Sample SC06/0645. 13889.29 ng/µL. RIN: 9.9.

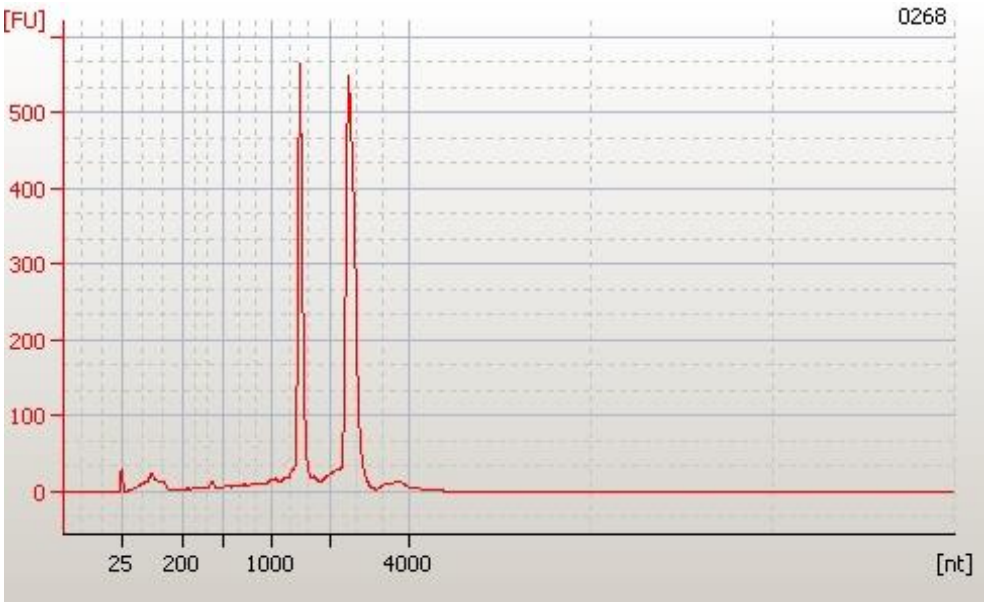

Figure 160. Electropherogram trace of *Y. pestis* RNA sample YP3.1 from the 100 µg/mL serine hydroxamate condition. Distinct and high peaks observed for 16S and 23S rRNA. Sample SC06/0268. 10273.82 ng/µL. RIN: 9.9.

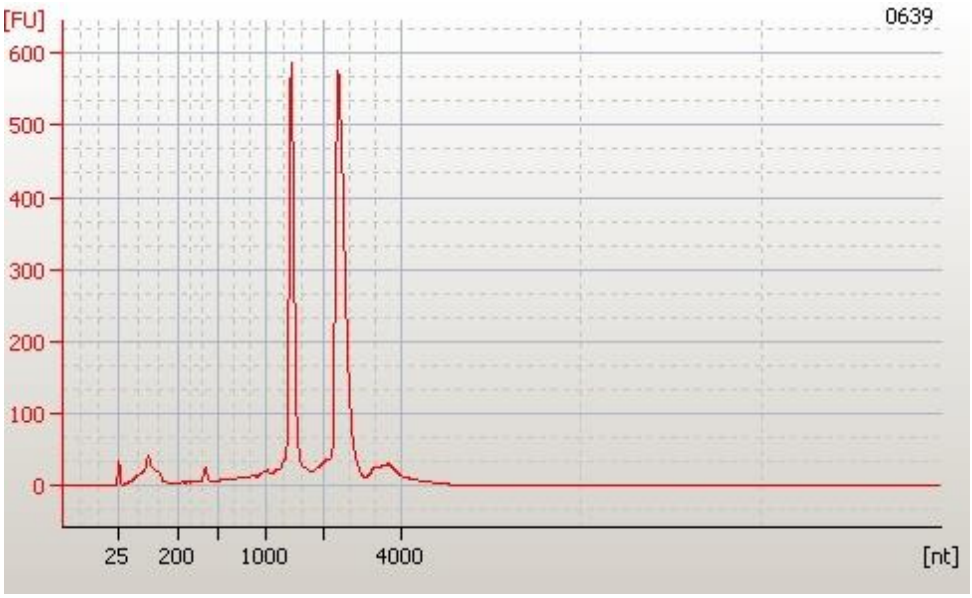

Figure 161. Electropherogram trace of *Y. pestis* RNA sample YP3.2 from the 100 µg/mL serine hydroxamate condition. Distinct and high peaks observed for 16S and 23S rRNA. Sample SC06/0239. 12154.31 ng/µL. RIN: 9.9.

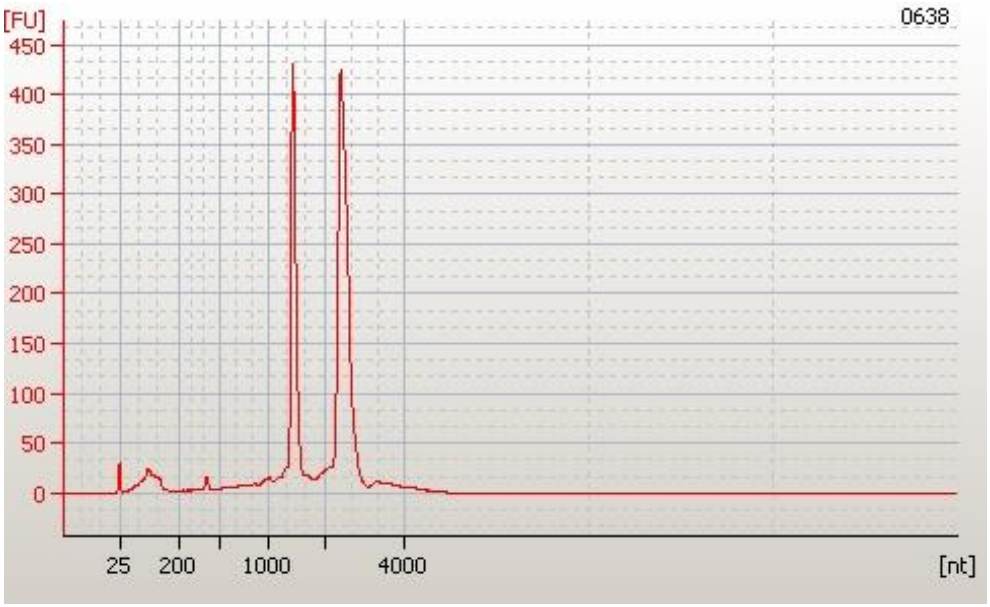

Figure 162. Electropherogram trace of *Y. pestis* RNA sample YP3.3 from the 100 µg/mL serine hydroxamate condition. Distinct and high peaks observed for 16S and 23S rRNA. Sample SC06/0238. 8779.569 ng/µL. RIN: 10.

8.14. Raw Data Output from *Yersinia pestis* RNA-Sequencing

Sample ID	Yield (Mbases)	# Reads	% of >= Q30 Bases	Mean Quality Score
YP1_1	4,286	42,855,794	95.12	37.03
YP1_2	3,628	36,283,622	95.13	37.01
YP1_3	3,618	36,182,144	95.09	37.01
YP2_1	3,375	33,754,344	95.21	37.07
YP2_2	4,320	43,197,050	95.39	37.15
YP2_3	3,082	30,818,746	93.34	36.33
YP3_1	5,009	50,091,740	95.30	37.11
YP3_2	5,289	52,889,968	94.53	36.81
YP3_3	2,937	29,371,816	95.25	37.12

Table 31. Summary of raw data output statistics for a paired-end RNA-seq run on the Illumina HiSeq2500. Three biological replicates are shown for each condition tested. Total number of reads and sequence yield for each sample are shown. Quality scores for each sample are shown as the percentage of bases with high quality scores and the average quality score for each sample.

8.15. Bioanalyzer Traces of *Burkholderia pseudomallei* RNA samples

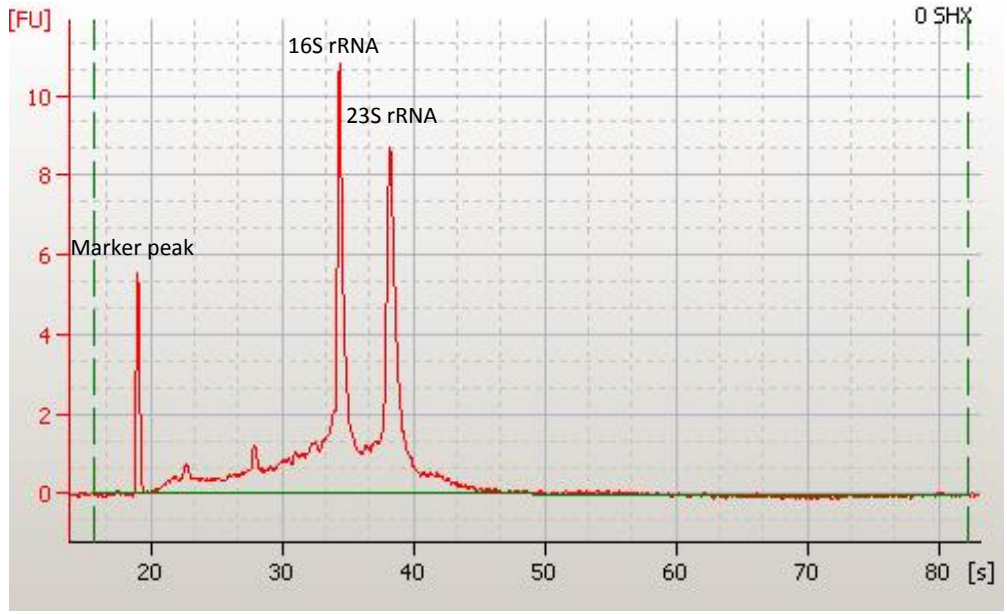

Figure 163. Electropherogram trace of *B. pseudomallei* RNA sample from the 0 µg/mL serine hydroxamate condition. Distinct and high peaks observed for 16S and 23S rRNA. These peaks are labelled on this trace for reference. Sample SC06/0913. 111 ng/µL.

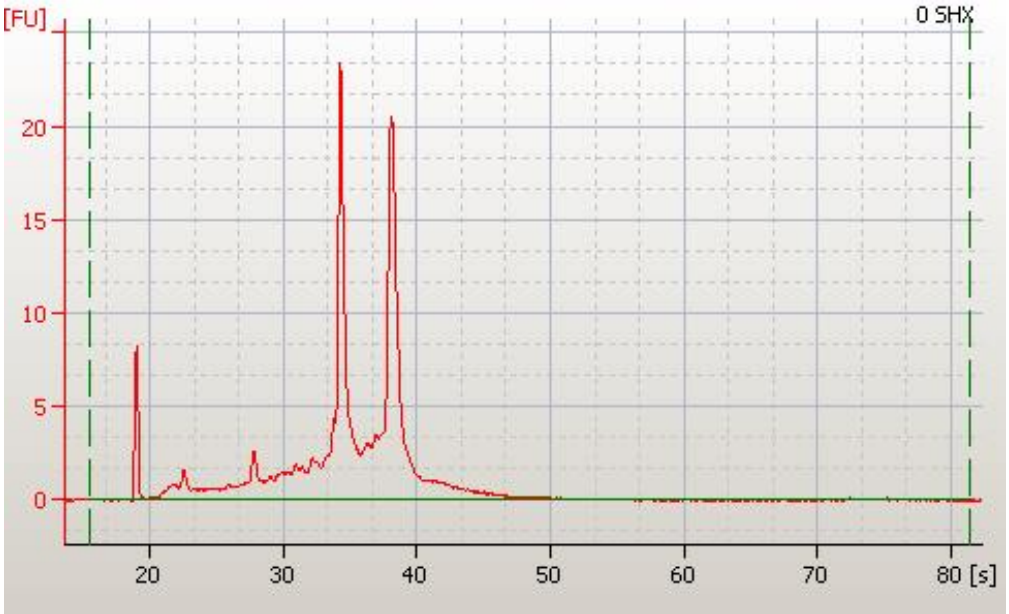

Figure 164. Electropherogram trace of *B. pseudomallei* RNA sample from the 0 µg/mL serine hydroxamate condition. Distinct and high peaks observed for 16S and 23S rRNA. Sample SC06/0914. 237 ng/µL.

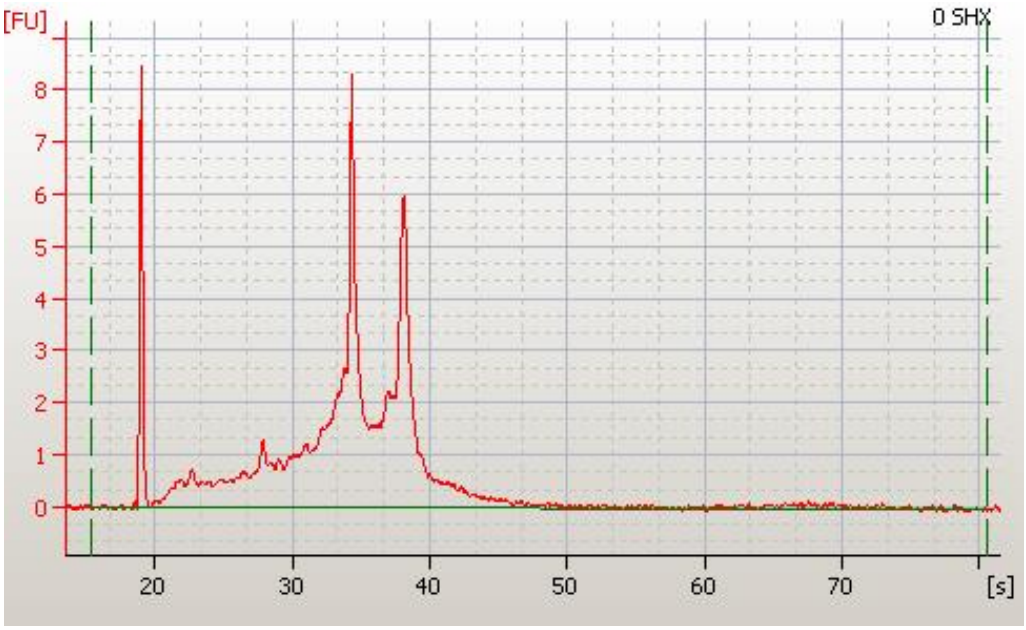

Figure 165. Electropherogram trace of *B. pseudomallei* RNA sample from the 0 µg/mL serine hydroxamate condition. Distinct and high peaks observed for 16S and 23S rRNA. Sample SC06/0916. 125 ng/µL.

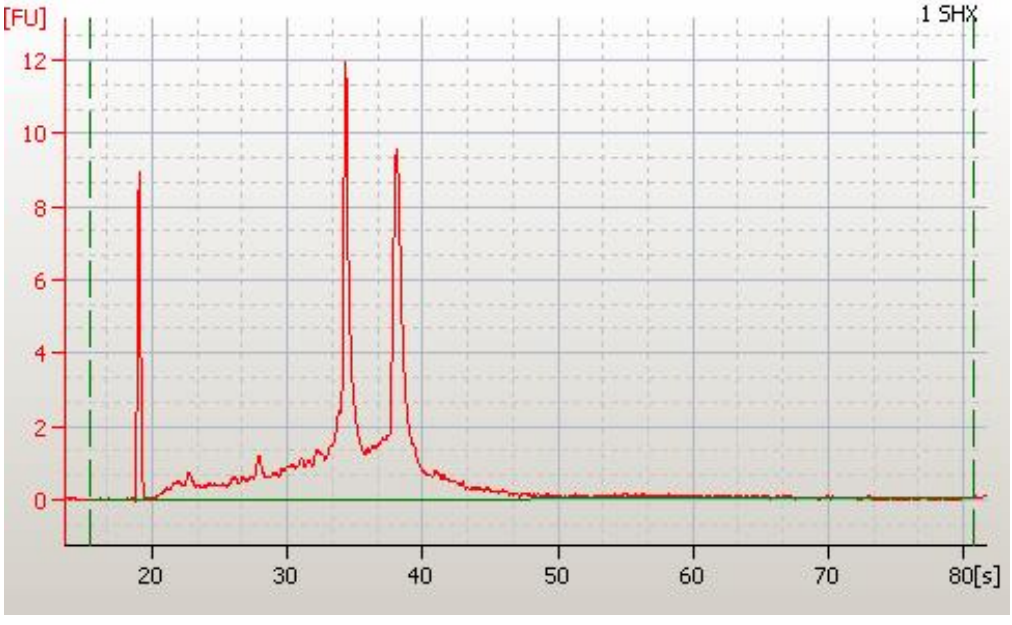

Figure 166. Electropherogram trace of *B. pseudomallei* RNA sample from the 1 µg/mL serine hydroxamate condition. Distinct and high peaks observed for 16S and 23S rRNA. Sample SC06/0917. 129 ng/µL.

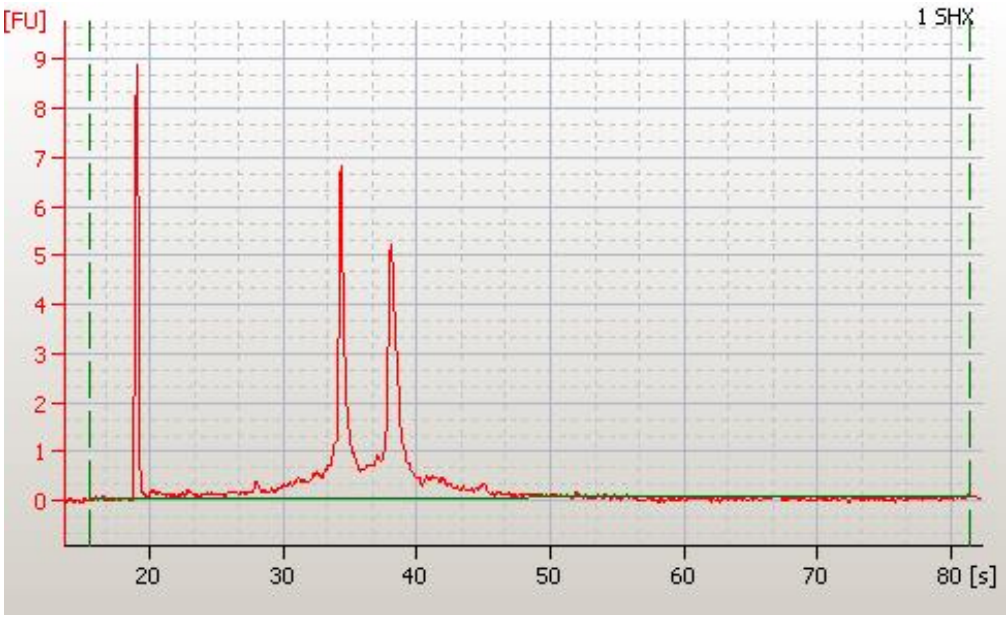

Figure 167. Electropherogram trace of *B. pseudomallei* RNA sample from the 1 µg/mL serine hydroxamate condition. Distinct and high peaks observed for 16S and 23S rRNA. Sample SC06/0918. 59 ng/µL.

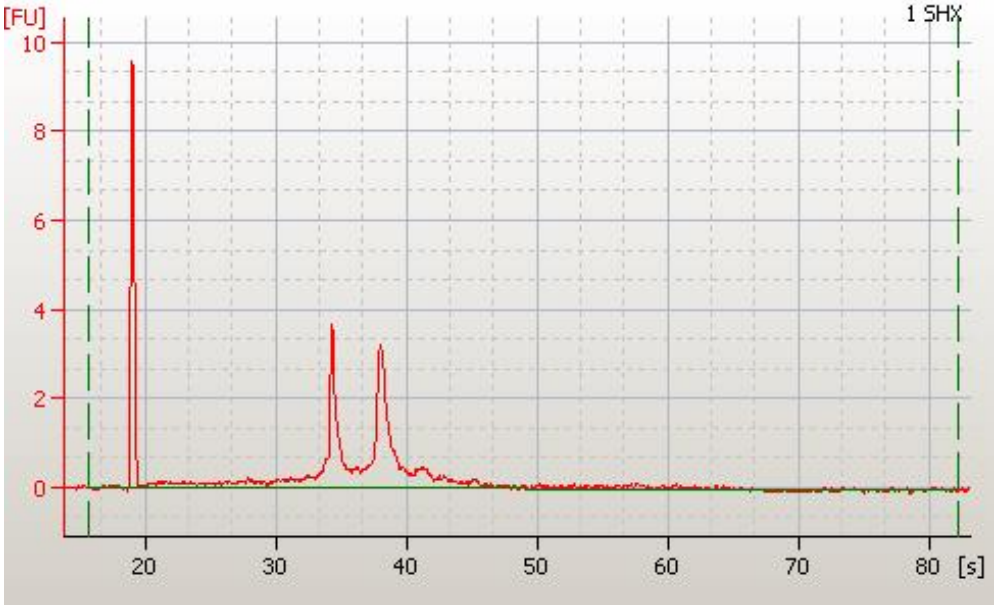

Figure 168. Electropherogram trace of *B. pseudomallei* RNA sample from the 0 µg/mL serine hydroxamate condition. Distinct and high peaks observed for 16S and 23S rRNA. Sample SC06/0919. 42 ng/µL.

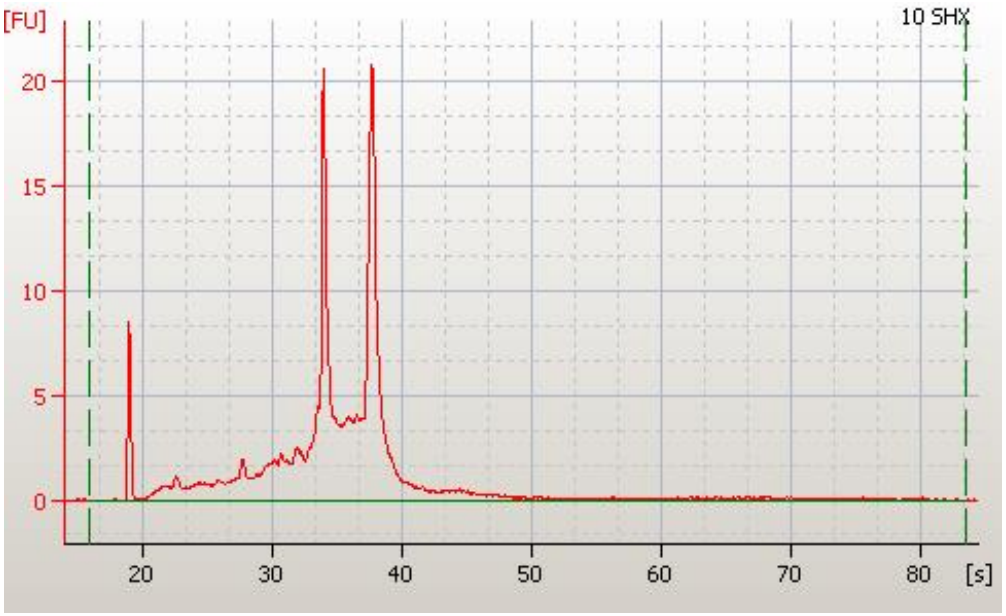

Figure 169. Electropherogram trace of *B. pseudomallei* RNA sample from the 0 µg/mL serine hydroxamate condition. Distinct and high peaks observed for 16S and 23S rRNA. Sample SC06/0921. 240 ng/µL.

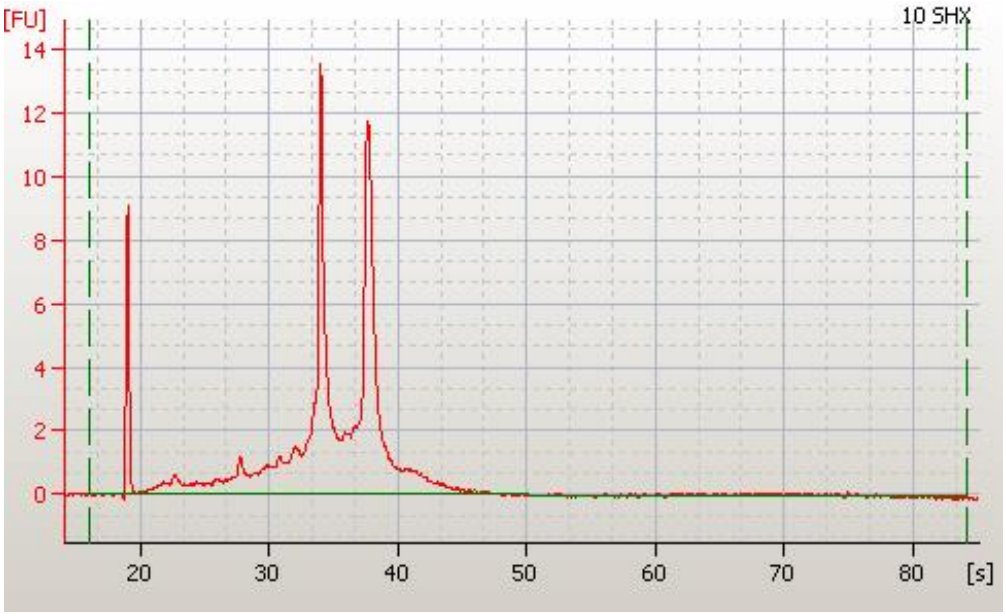

Figure 170. Electropherogram trace of *B. pseudomallei* RNA sample from the 0 µg/mL serine hydroxamate condition. Distinct and high peaks observed for 16S and 23S rRNA. Sample SC06/0922. 139 ng/µL.

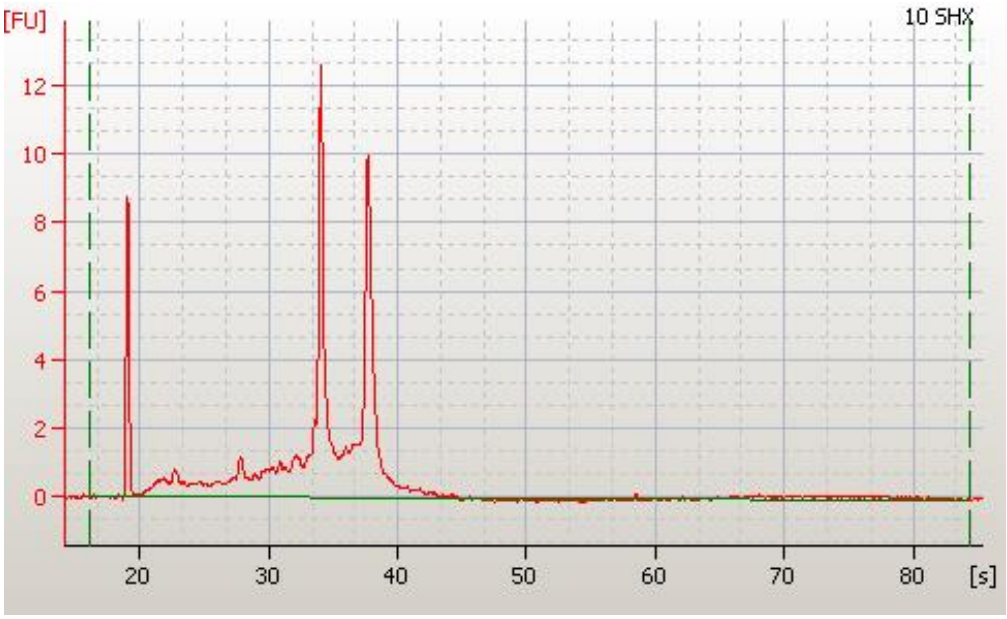

Figure 171. Electropherogram trace of *B. pseudomallei* RNA sample from the 0 µg/mL serine hydroxamate condition. Distinct and high peaks observed for 16S and 23S rRNA. Sample SC06/0923. 111 ng/µL.

8.16. Raw Data Output from *Burkholderia pseudomallei* RNA-Sequencing

Sample ID	Yield (Mbases)	# Reads	% of >= Q30 Bases	Mean Quality Score
BP1_1	4,286	42,855,794	95.12	37.03
BP1_2	3,628	36,283,622	95.13	37.01
BP1_3	3,618	36,182,144	95.09	37.01
BP2_1	3,375	33,754,344	95.21	37.07
BP2_2	4,320	43,197,050	95.39	37.15
BP2_3	3,082	30,818,746	93.34	36.33
BP3_1	5,009	50,091,740	95.30	37.11
BP3_2	5,289	52,889,968	94.53	36.81
BP3_3	2,937	29,371,816	95.25	37.12

Table 32. Summary of raw data output statistics for a paired-end RNA-seq run on the Illumina HiSeq2500. Three biological replicates are shown for each condition tested. Total number of reads and sequence yield for each sample are shown. Quality scores for each sample are shown as the percentage of bases with high quality scores and the average quality score for each sample.

8.17. Testing Southampton-Manufactured Serine Hydroxamate

Serine hydroxamate that was produced at the University of Southampton was compared to that manufactured by a commercial company, Sigma Aldrich. Both serine hydroxamate batches were used to supplement media in which *Y. pestis* GB was to be cultured and optical density reading were taken after 16 hours incubation at 28 °C (table 33).

SHX concentration (μg /mL)	OD_{600} from Sigma Aldrich serine hydroxamate supplementation	$OD_{600}$from Southampton serine hydroxamate supplementation
1000	0.25	0.24
100	1.98	1.95
50	2.0	1.97
10	2.0	2.0
0	2.0	2.0

Table 33. Southampton-produced serine hydroxamate efficacy results in comparison to serine hydroxamate purchased from a commercial supplier.

9. References

1. **Riedel S.** 2004. Biological warfare and bioterrorism: a historical review. Proceedings (Baylor University. Medical Center) **17:**400-406.
2. **Nicholas JB, David ABD, Alastair ROM, Robert CS.** 2002. Biological warfare and bioterrorism. BMJ **324**.
3. **Wheelis M.** 1945. 2. Biological warfare before 1914.
4. **Poupard JA, Miller LA.** 1992. History of Biological Warfare: Catapults to Capsomeres. Annals of the New York Academy of Sciences **666:**9-20.
5. **Christopher LW, Cieslak LJ, Pavlin JA, Eitzen EM, Jr.** 1997. Biological warfare: A historical perspective. JAMA **278:**412-417.
6. **McLendon MK, Apicella MA, Allen L-AH.** 2006. *Francisella tularensis*: taxonomy, genetics, and immunopathogenesis of a potential agent of biowarfare. Annual review of microbiology **60:**167.
7. **Meselson M, Hugh-Jones G.** Public Health Assessment of Potential Biological Terrorism Agents.
8. **Garcia-del Portillo F, Finlay BB.** 1995. The varied lifestyles of intracellular pathogens within eukaryotic vacuolar compartments. Trends in Microbiology **3:**373-380.
9. **Pujol C, Bliska JB.** 2003. The Ability To Replicate in Macrophages Is Conserved between *Yersinia pestis* and *Yersinia pseudotuberculosis*. Infection and Immunity **71:**5892-5899.
10. **Lai X-H, Golovliov I, Sjöstedt A.** 2001. *Francisella tularensis* Induces Cytopathogenicity and Apoptosis in Murine Macrophages via a Mechanism That Requires Intracellular Bacterial Multiplication. Infection and Immunity **69:**4691-4694.
11. **Du Y, Rosqvist R, Forsberg Å.** 2002. Role of Fraction 1 Antigen of *Yersinia pestis* in Inhibition of Phagocytosis. Infection and Immunity **70:**1453-1460.
12. **Clemens DL, Lee B-Y, Horwitz MA.** 2004. Virulent and Avirulent Strains of *Francisella tularensis* Prevent Acidification and Maturation of Their Phagosomes and Escape into the Cytoplasm in Human Macrophages. Infection and Immunity **72:**3204-3217.
13. **Golovliov I, Baranov V, Krocova Z, Kovarova H, Sjöstedt A.** 2003. An Attenuated Strain of the Facultative Intracellular Bacterium *Francisella tularensis* Can Escape the Phagosome of Monocytic Cells. Infection and Immunity **71:**5940-5950.
14. **Richards MI, Michell SL, Oyston PCF.** 2008. An intracellularly inducible gene involved in virulence and polyphosphate production in *Francisella*. Journal of Medical Microbiology **57:**1183-1192.
15. **Dean RE, Ireland PM, Jordan JE, Titball RW, Oyston PCF.** 2009. RelA regulates virulence and intracellular survival of *Francisella novicida*. Microbiology **155:**4104-4113.
16. **Sun W, Roland KL, Branger CG, Kuang X, Curtiss R.** 2009. The Role of *relA* and *spoT* in *Yersinia pestis* KIM5 Pathogenicity. PLoS ONE **4:**e6720.
17. **Holden MTG, Titball RW, Peacock SJ, Atkins T, Crossman LC, Pitt T, Oyston PCF, Parkhill J*ea*.** 2004. Genomic plasticity of the causative agent of melioidosis, *Burkholderia pseudomallei*. Proceedings of the National Academy of Sciences of the United States of America **101:**14240-14245.
18. **Dance DA.** 1991. Melioidosis: the tip of the iceberg? Clinical Microbiology Reviews **4:**52-60.
19. **Inglis TJJ, Garrow SC, Adams C, Henderson M, Mayo M, Currie BJ.** 1999. Acute melioidosis outbreak in Western Australia. Epidemiology and infection **123:**437-443.
20. **Pilatz S, Breitbach K, Hein N, Fehlhaber B, Schulze J, Brenneke B, Eberl L, Steinmetz I.** 2006. Identification of *Burkholderia pseudomallei* Genes Required for the Intracellular Life Cycle and *In Vivo* Virulence. Infection and Immunity **74:**3576-3586.

21. **Subsin B, Thomas MS, Katzenmeier G, Shaw JG, Tungpradabkul S, Kunakorn M.** 2003. Role of the Stationary Growth Phase Sigma Factor RpoS of *Burkholderia pseudomallei* in Response to Physiological Stress Conditions. Journal of Bacteriology **185:**7008-7014.
22. **Cheng AC, Currie BJ.** 2005. Melioidosis: Epidemiology, Pathophysiology, and Management. Clinical Microbiology Reviews **18:**383-416.
23. **Limmathurotsakul D, Golding N, Dance DA, Messina JP, Pigott DM, Moyes CL, Rolim DB, Bertherat E, Day NP, Peacock SJ.** 2016. Predicted global distribution of *Burkholderia pseudomallei* and burden of melioidosis. Nature microbiology **1:**15008.
24. **Dance DAB.** 2002. Melioidosis. Current Opinion in Infectious Diseases **15:**127-132.
25. **Jones AL, Beveridge TJ, Woods DE.** 1996. Intracellular survival of *Burkholderia pseudomallei*. Infection and Immunity **64:**782-790.
26. **Tunpiboonsak S, Mongkolrob R, Kitudomsub K, Thanwatanaying P, Kiettipirodom W, Tungboontina Y, Tungpradabkul S.** 2010. Role of a *Burkholderia pseudomallei* polyphosphate kinase in an oxidative stress response, motilities, and biofilm formation. The Journal of Microbiology **48:**63-70.
27. **Chua KL, Chan YY, Gan YH.** 2003. Flagella Are Virulence Determinants of *Burkholderia pseudomallei*. Infection and Immunity **71:**1622-1629.
28. **Poxton I, Arbuthnott J.** 1990. Determinants of bacterial virulence. Principles of bacteriology, virology and immunity **1:**332-351.
29. **Steinmetz I, Rohde M, Brenneke B.** 1995. Purification and characterization of an exopolysaccharide of *Burkholderia (Pseudomonas) pseudomallei*. Infection and Immunity **63:**3959-3965.
30. **Reckseidler-Zenteno SL, Viteri D-F, Moore R, Wong E, Tuanyok A, Woods DE.** 2010. Characterization of the type III capsular polysaccharide produced by Burkholderia pseudomallei. Journal of Medical Microbiology **59:**1403-1414.
31. **Reckseidler-Zenteno SL, DeVinney R, Woods DE.** 2005. The Capsular Polysaccharide of Burkholderia pseudomallei Contributes to Survival in Serum by Reducing Complement Factor C3b Deposition. Infection and Immunity **73:**1106-1115.
32. **DeShazer D.** 2004. Genomic Diversity of *Burkholderia pseudomallei* Clinical Isolates: Subtractive Hybridization Reveals a *Burkholderia mallei*-Specific Prophage in *B. pseudomallei* 1026b. Journal of Bacteriology **186:**3938-3950.
33. **Yu Y, Kim HS, Chua HH, Lin CH, Sim SH, Lin D, Derr A, Engels R, DeShazer D, Birren B, Nierman WC, Tan P.** 2006. Genomic patterns of pathogen evolution revealed by comparison of *Burkholderia pseudomallei*, the causative agent of melioidosis, to avirulent *Burkholderia thailandensis*. BMC Microbiology **6:**1-17.
34. **Pitt TL, Trakulsomboon S, Dance DAB.** 2000. Molecular phylogeny of *Burkholderia pseudomallei*. Acta Tropica **74:**181-185.
35. **Godoy D, Randle G, Simpson AJ, Aanensen DM, Pitt TL, Kinoshita R, Spratt BG.** 2003. Multilocus Sequence Typing and Evolutionary Relationships among the Causative Agents of Melioidosis and Glanders, *Burkholderia pseudomallei* and *Burkholderia mallei*. Journal of Clinical Microbiology **41:**2068-2079.
36. **Valvano MA, Keith KE, Cardona ST.** 2005. Survival and persistence of opportunistic *Burkholderia* species in host cells. Current Opinion in Microbiology **8:**99-105.
37. **Lowe W, March JK, Bunnell AJ, O'Neill KL, Robison RA.** 2013. PCR-based methodologies used to detect and differentiate the *Burkholderia* pseudomallei complex: *B. pseudomallei, B. mallei, and B. thailandensis*. Curr Issues Mol Biol **16:**23-54.
38. **Schmoock G, Elschner M, Sprague LD.** 2015. Clear distinction between *Burkholderia mallei* and *Burkholderia pseudomallei* using fluorescent *motB* primers. Acta Veterinaria Scandinavica **57:**1-5.

39. **Janse I, Hamidjaja RA, Hendriks AC, van Rotterdam BJ.** 2013. Multiplex qPCR for reliable detection and differentiation of *Burkholderia mallei* and *Burkholderia pseudomallei*. BMC Infectious Diseases **13:**1-8.
40. **Koh SF, Tay ST, Sermswan R, Wongratanacheewin S, Chua KH, Puthucheary SD.** 2012. Development of a multiplex PCR assay for rapid identification of *Burkholderia pseudomallei, Burkholderia thailandensis, Burkholderia mallei* and *Burkholderia cepacia* complex. Journal of Microbiological Methods **90:**305-308.
41. **Thibault FM, Valade E, Vidal DR.** 2004. Identification and discrimination of Burkholderia pseudomallei, B. mallei, and B. thailandensis by real-time PCR targeting type III secretion system genes. J. Clin. Microbiol. **42:**5871-5874.
42. **Wiersinga WJ, van der Poll T, White NJ, Day NP, Peacock SJ.** 2006. Melioidosis: insights into the pathogenicity of *Burkholderia pseudomallei*. Nat Rev Micro **4:**272-282.
43. **Fernández L, Hancock REW.** 2012. Adaptive and Mutational Resistance: Role of Porins and Efflux Pumps in Drug Resistance. Clinical Microbiology Reviews **25:**661-681.
44. **Dance D, Davong V, Soeng S, Phetsouvanh R, Newton P, Turner P.** 2014. Trimethoprim/sulfamethoxazole resistance in *Burkholderia pseudomallei*. International journal of antimicrobial agents **44:**368.
45. **Aunkham A, Schulte A, Winterhalter M, Suginta W.** 2014. Porin Involvement in Cephalosporin and Carbapenem Resistance of *Burkholderia pseudomallei*. PLoS ONE **9:**e95918.
46. **Chan YY, Tan TMC, Ong YM, Chua KL.** 2004. BpeAB-OprB, a Multidrug Efflux Pump in *Burkholderia pseudomallei*. Antimicrobial Agents and Chemotherapy **48:**1128-1135.
47. **Mima T, Schweizer HP.** 2010. The BpeAB-OprB Efflux Pump of *Burkholderia pseudomallei* 1026b Does Not Play a Role in Quorum Sensing, Virulence Factor Production, or Extrusion of Aminoglycosides but Is a Broad-Spectrum Drug Efflux System. Antimicrobial Agents and Chemotherapy **54:**3113-3120.
48. **Chan YY, Chua KL.** 2005. The *Burkholderia pseudomallei* BpeAB-OprB efflux pump: expression and impact on quorum sensing and virulence. J. Bacteriol. **187:**4707-4719.
49. **Moore RA, DeShazer D, Reckseidler S, Weissman A, Woods DE.** 1999. Efflux-Mediated Aminoglycoside and Macrolide Resistance in *Burkholderia pseudomallei*. Antimicrobial Agents and Chemotherapy **43:**465-470.
50. **Yamaguchi A, Nakashima R, Sakurai K.** 2015. Structural basis of RND-type multidrug exporters. Frontiers in Microbiology **6**.
51. **Siritapetawee J, Prinz H, Samosornsuk W, Ashley RH, Suginta W.** 2004. Functional reconstitution, gene isolation and topology modelling of porins from *Burkholderia pseudomallei* and *Burkholderia thailandensis*. Biochemical Journal **377:**579-587.
52. **Jaffe A, Chabbert YA, Semonin O.** 1982. Role of porin proteins OmpF and OmpC in the permeation of beta-lactams. Antimicrobial Agents and Chemotherapy **22:**942-948.
53. **Medeiros AA, O'Brien TF, Rosenberg EY, Nikaido H.** 1987. Loss of OmpC Porin in a Strain of *Salmonella typhimurium* Causes Increased Resistance to Cephalosporins During Therapy. Journal of Infectious Diseases **156:**751-757.
54. **Armand-Lefèvre L, Leflon-Guibout V, Bredin J, Barguellil F, Amor A, Pagès JM, Nicolas-Chanoine M-H.** 2003. Imipenem Resistance in *Salmonella enterica* Serovar Wien Related to Porin Loss and CMY-4 β-Lactamase Production. Antimicrobial Agents and Chemotherapy **47:**1165-1168.
55. **Toro CS, Lobos SR, Calderón I, Rodríguez M, Mora GC.** 1990. Clinical isolate of a porinless *Salmonella typhi* resistant to high levels of chloramphenicol. Antimicrobial Agents and Chemotherapy **34:**1715-1719.
56. **Suginta W, Mahendran KR, Chumjan W, Hajjar E, Schulte A, Winterhalter M, Weingart H.** 2011. Molecular analysis of antimicrobial agent translocation through the

membrane porin BpsOmp38 from an ultraresistant *Burkholderia pseudomallei* strain. Biochimica et Biophysica Acta (BBA) - Biomembranes **1808:**1552-1559.

57. **Choh L-C, Ong G-H, Vellasamy KM, Kalaiselvam K, Kang W-T, Al-Maleki AR, Mariappan V, Vadivelu J.** 2013. *Burkholderia* Vaccines: Are We Moving Forward? Frontiers in Cellular and Infection Microbiology **3**.
58. **Elkins KL, Burns DL, Schmitt MP, Weir JP.** 2004. Vaccines against Bioterror Agents, p. 529-545, Novel Vaccination Strategies. Wiley-VCH Verlag GmbH & Co. KGaA.
59. **Lazar Adler NR, Govan B, Cullinane M, Harper M, Adler B, Boyce JD.** 2009. The molecular and cellular basis of pathogenesis in melioidosis: how does *Burkholderia pseudomallei* cause disease? FEMS Microbiology Reviews **33:**1079-1099.
60. **Vasu C, Vadivelu J, Puthucheary DS.** 2003. The Humoral Immune Response in Melioidosis Patients during Therapy. Infection **31:**24-30.
61. **Puthucheary SD.** 2009. Melioidosis in Malaysia. Med J Malaysia **64:**266-274.
62. **Peacock SJ, Limmathurotsakul D, Lubell Y, Koh GCKW, White LJ, Day NPJ, Titball RW.** 2012. Melioidosis Vaccines: A Systematic Review and Appraisal of the Potential to Exploit Biodefense Vaccines for Public Health Purposes. PLoS Negl Trop Dis **6:**e1488.
63. **Sarkar-Tyson M, Titball RW.** 2010. Vaccines Progress toward development of vaccines against melioidosis: A review. Clinical Therapeutics **32:**1437-1445.
64. **Sjöstedt A.** 2007. Tularemia: history, epidemiology, pathogen physiology, and clinical manifestations. Annals of the New York Academy of Sciences **1105:**1-29.
65. **Oyston PCF, Sjostedt A, Titball RW.** 2004. Tularaemia: bioterrorism defence renews interest in *Francisella tularensis*. Nat Rev Micro **2:**967-978.
66. **Morner T.** 1992. The ecology of tularaemia. Revue scientifique et technique (International Office of Epizootics) **11:**1123-1130.
67. **Olsufiev NG, Emelyanova OS, Dunayeva TN.** 1959. Comparative study of strains of *B. tularense* in the old and new world and their taxonomy. Journal of hygiene, epidemiology, microbiology, and immunology **3:**138.
68. **Isabel Lopes de C, Raquel E, Cristina G-A, Helena F, Pedro A, Maria Sofia N.** 2007. *Francisella tularensis,* Portugal. Emerging Infectious Disease journal **13:**666.
69. **Organization WH.** 2007. WHO Guidelines on Tularaemia.
70. **Bosio CM, Bielefeldt-Ohmann H, Belisle JT.** 2007. Active Suppression of the Pulmonary Immune Response by *Francisella tularensis* Schu4. The Journal of Immunology **178:**4538-4547.
71. **Bosio C.** 2011. The subversion of the immune system by *Francisella tularensis*. Frontiers in Microbiology **2**.
72. **Rossow H, Ollgren J, Klemets P, Pietarinen I, Saikku J, Pekkanen E, Nikkari S, Syrjälä H, Kuusi M, Nuorti J.** 2014. Risk factors for pneumonic and ulceroglandular tularaemia in Finland: a population-based case-control study. Epidemiology and infection **142:**2207-2216.
73. **Dennis DT, Inglesby TV, Henderson DA, Perl TM, Russell PK, Tonat K, null.** 2001. Tularemia as a biological weapon: medical and public health management. JAMA : the journal of the American Medical Association **285:**2763-2773.
74. **Enderlin G, Morales L, Jacobs RF, Cross JT.** 1994. Streptomycin and Alternative Agents for the Treatment of Tularemia: Review of the Literature. Clinical Infectious Diseases **19:**42-47.
75. **McDermott W.** 1947. Symposium on StreptomycinToxicity of streptomycin. The American Journal of Medicine **2:**491-500.
76. **Hamblin KA, Wong JP, Blanchard JD, Atkins HS.** 2014. The potential of liposome–encapsulated ciprofloxacin as a tularemia therapy. Frontiers in Cellular and Infection Microbiology **4:**79.

77. **Pérez-Castrillón JL, Bachiller-Luque P, Martín-Luquero M, Mena-Martín FJ, Herreros V.** 2001. Tularemia Epidemic in Northwestern Spain: Clinical Description and Therapeutic Response. Clinical Infectious Diseases **33:**573-576.
78. **Meric M, Willke A, Finke EJ, Grunow R, Sayan M, Erdogan S, Gedikoglu S.** 2008. Evaluation of clinical, laboratory, and therapeutic features of 145 tularemia cases: the role of quinolones in oropharyngeal tularemia. Apmis **116:**66-73.
79. **Meric M, Willke A, Finke E-J, Grunow R, Sayan M, Erdogan S, Gedikoglu S.** 2008. Evaluation of clinical, laboratory, and therapeutic features of 145 tularemia cases: the role of quinolones in oropharyngeal tularemia. APMIS **116:**66-73.
80. **Piercy T, Steward J, Lever MS, Brooks TJ.** 2005. *In vivo* efficacy of fluoroquinolones against systemic tularaemia infection in mice. The Journal of antimicrobial chemotherapy **56:**1069-1073.
81. **Oyston PCF.** 2008. *Francisella tularensis*: unravelling the secrets of an intracellular pathogen. Journal of Medical Microbiology **57:**921-930.
82. **Larsson P, Oyston PC, Chain P, Chu MC, Duffield M, Fuxelius HH, Garcia E, Forsman M, Titball RW.** 2005. The complete genome sequence of *Francisella tularensis*, the causative agent of tularemia. Nature genetics **37:**153-159.
83. **Ireland PM, LeButt H, Thomas RM, Oyston PCF.** 2011. A *Francisella tularensis* SCHU S4 mutant deficient in glutamyltransferase activity induces protective immunity: characterization of an attenuated vaccine candidate. Microbiology **157:**3172-3179.
84. **Postic G, Dubail I, Frapy E, Dupuis M, Dieppedale J, Charbit A, Meibom KL.** 2012. Identification of a Novel Small RNA Modulating *Francisella tularensis* Pathogenicity. PLoS ONE **7:**e41999.
85. **de Bruin OM, Duplantis BN, Ludu JS, Hare RF, Nix EB, Schmerk CL, Robb CS, Boraston AB, Hueffer K, Nano FE.** 2011. The biochemical properties of the *Francisella* pathogenicity island (FPI)-encoded proteins IglA, IglB, IglC, PdpB and DotU suggest roles in type VI secretion. Microbiology **157:**3483-3491.
86. **Charity JC, Blalock LT, Costante-Hamm MM, Kasper DL, Dove SL.** 2009. Small molecule control of virulence gene expression in *Francisella tularensis*. PLoS pathogens **5:**e1000641.
87. **Abd H, Johansson T, Golovliov I, Sandström G, Forsman M.** 2003. Survival and Growth of *Francisella tularensis* in *Acanthamoeba castellanii*. Applied and Environmental Microbiology **69:**600-606.
88. **Cuthbert BJ, Brennan RG, Schumacher MA.** 2015. Structural and Biochemical Characterization of the *Francisella tularensis* Pathogenicity Regulator, Macrophage Locus Protein A (MglA). PLoS ONE **10:**e0128225.
89. **Hazlett KRO, Caldon SD, McArthur DG, Cirillo KA, Kirimanjeswara GS, Magguilli ML, Malik M, Shah A, Broderick S, Golovliov I, Metzger DW, Rajan K, Sellati TJ, Loegering DJ.** 2008. Adaptation of *Francisella tularensis* to the Mammalian Environment Is Governed by Cues Which Can Be Mimicked *In Vitro*. Infection and Immunity **76:**4479-4488.
90. **Wehrly TD, Chong A, Virtaneva K, Sturdevant DE, Child R, Edwards JA, Brouwer D, Nair V, Fischer ER, Wicke L, Curda AJ, Kupko JJ, Martens C, Crane DD, Bosio CM, Porcella SF, Celli J.** 2009. Intracellular biology and virulence determinants of *Francisella tularensis* revealed by transcriptional profiling inside macrophages. Cellular Microbiology **11:**1128-1150.
91. **Horzempa J, Carlson P, O'Dee D, Shanks R, Nau G.** 2008. Global transcriptional response to mammalian temperature provides new insight into *Francisella tularensis* pathogenesis. BMC Microbiology **8:**172.
92. **Lenco J, Link M, Tambor V, Zaková J, Cerveny L, Stulik, Jiri.** 2009. iTRAQ quantitative analysis of *Francisella tularensis* ssp. *holarctica* live vaccine strain and *Francisella*

tularensis ssp. *tularensis* SCHU S4 response to different temperatures and stationary phases of growth. PROTEOMICS **9:**2875-2882.

93. **Scheel O, Reiersen R, Hoel T.** 1992. Treatment of tularemia with ciprofloxacin. European Journal of Clinical Microbiology and Infectious Diseases **11:**447-448.
94. **Matyas BT, Nieder HS, TELFORD SR.** 2007. Pneumonic tularemia on Martha's Vineyard. Annals of the New York Academy of Sciences **1105:**351-377.
95. **Feldman KA, Enscore RE, Lathrop SL, Matyas BT, McGuill M, Schriefer ME, Stiles-Enos D, Dennis DT, Petersen LR, Hayes EB.** 2001. An outbreak of primary pneumonic tularemia on Martha's Vineyard. New England Journal of Medicine **345:**1601-1606.
96. **Perry RD, Fetherston JD.** 1997. *Yersinia pestis*--etiologic agent of plague. Clinical Microbiology Reviews **10:**35-66.
97. **Raoult D, Mouffok N, Bitam I, Piarroux R, Drancourt M.** Plague: History and contemporary analysis. Journal of Infection.
98. **Parkhill J, Wren BW, Thomson NR, Titball RW, Holden MTG, Prentice MB, Sebaihia M, James KD, Churcher C, Mungall KL, Baker S, Basham D, Bentley SD, Brooks K, Cerdeno-Tarraga AM, Chillingworth T, Cronin A, Davies RM, Davis P, Dougan G, Feltwell T, Hamlin N, Holroyd S, Jagels K, Karlyshev AV, Leather S, Moule S, Oyston PCF, Quail M, Rutherford K, Simmonds M, Skelton J, Stevens K, Whitehead S, Barrell BG.** 2001. Genome sequence of *Yersinia pestis*, the causative agent of plague. Nature **413:**523-527.
99. **Pieper R, Huang S-T, Robinson JM, Clark DJ, Alami H, Parmar PP, Perry RD, Fleischmann RD, Peterson SN.** 2009. Temperature and growth phase influence the outer-membrane proteome and the expression of a type VI secretion system in Yersinia pestis. Microbiology **155:**498-512.
100. **Deng W, Burland V, Plunkett III G, Boutin A, Mayhew GF, Liss P, Perna NT, Rose DJ, Mau B, Zhou S, Schwartz DC, Fetherston JD, Lindler LE, Brubaker RR, Plano GV, Straley SC, McDonough KA, Nilles ML, Matson JS, Blattner FR, Perry RD.** 2002. Genome Sequence of *Yersinia pestis* KIM. Journal of Bacteriology **184:**4601-4611.
101. **Song Y, Tong Z, Wang J, Wang L, Guo Z, Han Y, Zhang J, Pei D, Zhou D, Qin H, Pang X, Han Y, Zhai J, Li M, Cui B, Qi Z, Jin L, Dai R, Chen F, Li S, Ye C, Du Z, Lin W, Wang J, Yu J, Yang H, Wang J, Huang P, Yang R.** 2004. Complete Genome Sequence of *Yersinia pestis* Strain 91001, an Isolate Avirulent to Humans. DNA Research **11:**179-197.
102. **Morelli G, Song Y, Mazzoni CJ, Eppinger M, Roumagnac P, Wagner DM, Feldkamp M, Kusecek B, Vogler AJ, Li Y, Cui Y, Thomson NR, Jombart T, Leblois R, Lichtner P, Rahalison L, Petersen JM, Balloux F, Keim P, Wirth T, Ravel J, Yang R, Carniel E, Achtman M.** 2010. *Yersinia pestis* genome sequencing identifies patterns of global phylogenetic diversity. Nat Genet **42:**1140-1143.
103. **Chain PSG, Hu P, Malfatti SA, Radnedge L, Larimer F, Vergez LM, Worsham P, Chu MC, Andersen GL.** 2006. Complete Genome Sequence of *Yersinia pestis* Strains Antiqua and Nepal516: Evidence of Gene Reduction in an Emerging Pathogen. Journal of Bacteriology **188:**4453-4463.
104. **Chain PSG, Carniel E, Larimer FW, Lamerdin J, Stoutland PO, Regala WM, Georgescu AM, Vergez LM, Land ML, Motin VL.** 2004. Insights into the evolution of *Yersinia pestis* through whole-genome comparison with *Yersinia pseudotuberculosis*. Proceedings of the National Academy of Sciences of the United States of America **101:**13826-13831.
105. **Motin VL, Georgescu AM, Fitch JP, Wyrobek AJ, Slezak TR, Brubaker RR, Garcia E.** 2004. Temporal Global Changes in Gene Expression during Temperature Transition in *Yersinia pestis*. Journal of Bacteriology **186:**6298-6305.
106. **Eisen RJ, Wilder AP, Bearden SW, Montenieri JA, Gage KL.** 2007. Early-Phase Transmission of *Yersinia pestis* by Unblocked *Xenopsylla cheopis* Is as Efficient as Transmission by Blocked Fleas. Journal of Medical Entomology **44:**678-682.

107. **Zhou D, Han Y, Qiu J, Song Y, Tan Y, Du Z, Yang R.** 2006. Genome-wide transcriptional response of *Yersinia pestis* to stressful conditions simulating phagolysosomal environments. Microbes and Infection **8:**2669-2678.
108. **Welch TJ, Fricke WF, McDermott PF, White DG, Cebula TA, Carniel E, Ravel J.** 2007. Multiple Antimicrobial Resistance in Plague: An Emerging Public Health Risk. PLoS ONE **2:**e309.
109. **Aminov RI.** 2010. A brief history of the antibiotic era: lessons learned and challenges for the future. Frontiers in microbiology **1:**134.
110. **Potter NB.** 1916. Salvarsan in the Treatment of Double Infections, Tuberculosis, and Syphilis. The American Journal of the Medical Sciences **152:**823-844.
111. **Ehrlich P.** 1957. collected works: Chemotherapy. Springer.
112. **Stein PD, Floyd DM, Bisaha S, Dickey J, Girotra RN, Gougoutas JZ, Kozlowski M, Lee VG, Liu ECK.** 1995. Discovery and Structure-Activity Relationships of Sulfonamide ETA-Selective Antagonists. Journal of Medicinal Chemistry **38:**1344-1354.
113. **Domagk G.** 1935. A contribution to the chemotherapy of bacterial infections. DMW-Deutsche Medizinische Wochenschrift **61:**250-253.
114. **Fleming A.** 1929. On the Antibacterial Action of Cultures of a Penicillium, with Special Reference to their Use in the Isolation of *B. influenzae*. British journal of experimental pathology **10:**226-236.
115. **O'Neill J.** 2016. Tackling drug-resistant infections globally: final report and recommendations. Review on Antimicrobial Resistance.
116. **Alanis AJ.** 2005. Resistance to Antibiotics: Are We in the Post-Antibiotic Era?, p. 697-705, Archives of Medical Research Infectious Diseases: Revisiting Past Problems and Addressing Future Challenges Infectious Diseases: Revisiting Past Problems and Addressing Future Challenges, vol. 36.
117. **Walsh C.** 2003. Where will new antibiotics come from? Nat Rev Micro **1:**65-70.
118. **Yoneyama H, Katsumata R.** 2006. Antibiotic Resistance in Bacteria and Its Future for Novel Antibiotic Development. Bioscience, Biotechnology, and Biochemistry **70:**1060-1075.
119. **Brodersen DE, Clemons J, Carter AP, Morgan-Warren RJ, Wimberly BT, Ramakrishnan V.** 2000. The Structural Basis for the Action of the Antibiotics Tetracycline, Pactamycin, and Hygromycin B on the 30S Ribosomal Subunit. Cell **103:**1143-1154.
120. **Carter AP, Clemons WM, Brodersen DE, Morgan-Warren RJ, Wimberly BT, Ramakrishnan V.** 2000. Functional insights from the structure of the 30S ribosomal subunit and its interactions with antibiotics. Nature **407:**340-348.
121. **Schlunzen F, Zarivach R, Harms J, Bashan A, Tocilj A, Albrecht R, Yonath A, Franceschi F.** 2001. Structural basis for the interaction of antibiotics with the peptidyl transferase centre in eubacteria. Nature **413:**814-821.
122. **Chen CR, Malik M, Snyder M, Drlica K.** 1996. DNA Gyrase and Topoisomerase IV on the Bacterial Chromosome: Quinolone-induced DNA Cleavage. Journal of Molecular Biology **258:**627-637.
123. **Campbell EA, Korzheva N, Mustaev A, Murakami K, Nair S, Goldfarb A, Darst SA.** 2001. Structural Mechanism for Rifampicin Inhibition of Bacterial RNA Polymerase. Cell **104:**901-912.
124. **Hancock REW, Chapple DS.** 1999. Peptide Antibiotics. Antimicrobial Agents and Chemotherapy **43:**1317-1323.
125. **Spratt BG.** 1988. Hybrid penicillin-binding proteins in penicillin-resistant strains of *Neisseria gonorrhoeae*. Nature **332:**173-176.
126. **Luzzatto L, Apirion D, Schlessinger D.** 1968. Mechanism of action of streptomycin in *E. coli*: interruption of the ribosome cycle at the initiation of protein synthesis. Proceedings of the National Academy of Sciences **60:**873-880.

127. **Hahn FE, Sarre SG.** 1969. Mechanism of Action of Gentamicin. The Journal of Infectious Diseases **119:**364-369.
128. **Schnappinger D, Hillen W.** 1996. Tetracyclines: antibiotic action, uptake, and resistance mechanisms. Archives of Microbiology **165:**359-369.
129. **Akamatsu H, Asada M, Komura J, Asada Y, Niwa Y.** 1992. Effect of doxycycline on the generation of reactive oxygen species: a possible mechanism of action of acne therapy with doxycycline. Acta Derm Venereol **72:**178-179.
130. **Sanders CC.** 1988. Ciprofloxacin: *In Vitro* Activity, Mechanism of Action, and Resistance. Review of Infectious Diseases **10:**516-527.
131. **Brogden RN, Carmine AA, Heel RC, Speight TM, Avery GS.** 1982. Trimethoprim: A Review of its Antibacterial Activity, Pharmacokinetics and Therapeutic Use in Urinary Tract Infections. Drugs **23:**405-430.
132. **Hitchings GH.** 1973. Mechanism of Action of Trimethoprim-Sulfamethoxazole—I. Journal of Infectious Diseases **128:**S433-S436.
133. **Newton BA.** 1956. The Properties and Mode of Action of the Polymyxins. Bacteriological Reviews **20:**14-27.
134. **Hsu Chen CC, Feingold DS.** 1973. Mechanism of polymyxin B action and selectivity toward biologic membranes. Biochemistry **12:**2105-2111.
135. **Walsh C, Wright G.** 2005. Introduction: antibiotic resistance. Chemical reviews **105:**391-394.
136. **Association CBR.** 2015. Fact Sheet: New Drug Development Process.
137. **Bowdish DME, Davidson DJ, Scott MG, Hancock REW.** 2005. Immunomodulatory Activities of Small Host Defense Peptides. Antimicrobial Agents and Chemotherapy **49:**1727-1732.
138. **Bowdish DME, Davidson DJ, Hancock R.** 2005. A Re-evaluation of the Role of Host Defence Peptides in Mammalian Immunity. Current Protein and Peptide Science **6:**35-51.
139. **Hancock REW, Sahl HG.** 2006. Antimicrobial and host-defense peptides as new anti-infective therapeutic strategies. Nat Biotech **24:**1551-1557.
140. **Hancock REW, Lehrer R.** 1998. Cationic peptides: a new source of antibiotics. Trends in Biotechnology **16:**82-88.
141. **Wilson DN.** 2014. Ribosome-targeting antibiotics and mechanisms of bacterial resistance. Nat Rev Micro **12:**35-48.
142. **Aminov RI, Mackie RI.** 2007. Evolution and ecology of antibiotic resistance genes. FEMS Microbiology Letters **271:**147-161.
143. **Kobayashi T, Suehiro F, Cach Tuyen B, Suzuki S.** 2007. Distribution and diversity of tetracycline resistance genes encoding ribosomal protection proteins in Mekong river sediments in Vietnam. FEMS Microbiology Ecology **59:**729-737.
144. **Nikaido H.** 1994. Prevention of drug access to bacterial targets: permeability barriers and active efflux. Science **264:**382-388.
145. **Davies J.** 1994. Inactivation of antibiotics and the dissemination of resistance genes. Science **264:**375-382.
146. **McMurry L, Petrucci RE, Levy SB.** 1980. Active efflux of tetracycline encoded by four genetically different tetracycline resistance determinants in *Escherichia coli*. Proceedings of the National Academy of Sciences **77:**3974-3977.
147. **Rushton L, Sass A, Baldwin A, Dowson CG, Donoghue D, Mahenthiralingam E.** 2013. Key Role for Efflux in the Preservative Susceptibility and Adaptive Resistance of *Burkholderia cepacia* Complex Bacteria. Antimicrobial Agents and Chemotherapy **57:**2972-2980.

148. **Galimand M, Guiyoule A, Gerbaud G, Rasoamanana B, Chanteau S, Carniel E, Courvalin P.** 1997. Multidrug Resistance in *Yersinia pestis* Mediated by a Transferable Plasmid. New England Journal of Medicine **337:**677-681.
149. **Galimand M, Carniel E, Courvalin P.** 2006. Resistance of *Yersinia pestis* to Antimicrobial Agents. Antimicrobial Agents and Chemotherapy **50:**3233-3236.
150. **Walsh C.** 2000. Molecular mechanisms that confer antibacterial drug resistance. Nature **406:**775-781.
151. **Zapun A, Contreras-Martel C, Vernet T.** 2008. Penicillin-binding proteins and lactam resistance. FEMS Microbiology Reviews **32:**361-385.
152. **Chesnel L, Pernot L, Lemaire D, Champelovier D, Croizé J, Dideberg O, Vernet T, Zapun A.** 2003. The Structural Modifications Induced by the M339F Substitution in PBP2x from *Streptococcus pneumoniae* Further Decreases the Susceptibility to β-Lactams of Resistant Strains. Journal of Biological Chemistry **278:**44448-44456.
153. **Weisblum B.** 1995. Erythromycin resistance by ribosome modification. Antimicrobial Agents and Chemotherapy **39:**577-585.
154. **Su Z, Honek J.** 2007. Emerging bacterial enzyme targets.
155. **Payne DJ, Gwynn MN, Holmes DJ, Pompliano DL.** 2007. Drugs for bad bugs: confronting the challenges of antibacterial discovery. Nat Rev Drug Discov **6:**29-40.
156. **Omura S.** 1976. The antibiotic cerulenin, a novel tool for biochemistry as an inhibitor of fatty acid synthesis. Bacteriological Reviews **40:**681-697.
157. **Magnuson K, Jackowski S, Rock CO, Cronan JE.** 1993. Regulation of fatty acid biosynthesis in *Escherichia coli*. Microbiological Reviews **57:**522-542.
158. **Flatman RH, Howells AJ, Heide L, Fiedler HP, Maxwell A.** 2005. Simocyclinone D8, an Inhibitor of DNA Gyrase with a Novel Mode of Action. Antimicrobial Agents and Chemotherapy **49:**1093-1100.
159. **Barrett JF, Hoch JA.** 1998. Two-Component Signal Transduction as a Target for Microbial Anti-Infective Therapy. Antimicrobial Agents and Chemotherapy **42:**1529-1536.
160. **Bush K.** 2012. Improving known classes of antibiotics: an optimistic approach for the future, p. 527-534, Current Opinion in Pharmacology Anti-infectives and New technologies, vol. 12.
161. **Belongia EA, Schwartz B.** 1998. Strategies for promoting judicious use of antibiotics by doctors and patients. British Medical Journal **317:**668.
162. **Keren I, Shah D, Spoering A, Kaldalu N, Lewis K.** 2004. Specialized Persister Cells and the Mechanism of Multidrug Tolerance in *Escherichia coli*. Journal of Bacteriology **186:**8172-8180.
163. **Keren I, Kaldalu N, Spoering A, Wang Y, Lewis K.** 2004. Persister cells and tolerance to antimicrobials. FEMS Microbiology Letters **230:**13-18.
164. **Klempner MS, Hu LT, Evans J, Schmid CH, Johnson GM, Trevino RP, Norton D, Levy L, Wall D, McCall J, Kosinski M, Weinstein A.** 2001. Two Controlled Trials of Antibiotic Treatment in Patients with Persistent Symptoms and a History of Lyme Disease. New England Journal of Medicine **345:**85-92.
165. **Bigger JW.** 1944. Treatment of Staphylococcal Infections with Penicillin by Intermittent Sterilisation. The Lancet **244:**497-500.
166. **Moyed HS, Bertrand KP.** 1983. hipA, a newly recognized gene of Escherichia coli K-12 that affects frequency of persistence after inhibition of murein synthesis. Journal of Bacteriology **155:**768-775.
167. **Balaban NQ, Merrin J, Chait R, Kowalik L, Leibler S.** 2004. Bacterial Persistence as a Phenotypic Switch. Science **305:**1622-1625.
168. **Kussell E, Kishony R, Balaban NQ, Leibler S.** 2005. Bacterial Persistence: A Model of Survival in Changing Environments. Genetics **169:**1807-1814.

169. **Germain E, Roghanian M, Gerdes K, Maisonneuve E.** 2015. Stochastic induction of persister cells by HipA through (p)ppGpp-mediated activation of mRNA endonucleases. Proceedings of the National Academy of Sciences **112:**5171-5176.
170. **Lewis K.** 2008. Multidrug Tolerance of Biofilms and Persister Cells, p. 107-131. *In* Romeo T (ed.), Bacterial Biofilms, vol. 322. Springer Berlin Heidelberg.
171. **Nguyen D, Joshi-Datar A, Lepine F, Bauerle E, Olakanmi O, Beer K, McKay G, Siehnel R, Schafhauser J, Wang Y, Britigan BE, Singh PK.** 2011. Active Starvation Responses Mediate Antibiotic Tolerance in Biofilms and Nutrient-Limited Bacteria. Science **334:**982-986.
172. **Ferullo DJ, Lovett ST.** 2008. The Stringent Response and Cell Cycle Arrest in *Escherichia coli*. PLoS Genet **4:**e1000300.
173. **Dalebroux ZD, Swanson MS.** 2012. ppGpp: magic beyond RNA polymerase. Nat Rev Micro **10:**203-212.
174. **Dalebroux ZD, Svensson SL, Gaynor EC, Swanson MS.** 2010. ppGpp Conjures Bacterial Virulence. Microbiology and Molecular Biology Reviews **74:**171-199.
175. **Chatterji D, Kumar Ojha A.** 2001. Revisiting the stringent response, ppGpp and starvation signaling. Current Opinion in Microbiology **4:**160-165.
176. **Cashel M, Gallant J.** 1969. Two compounds implicated in the function of the RC gene of Escherichia coli. Nature **221:**838-841.
177. **Kanjee U, Ogata K, Houry WA.** 2012. Direct Binding Targets of the Stringent Response Alarmone (p)ppGpp. Molecular Microbiology.
178. **Traxler MF, Summers SM, Nguyen HT, Zacharia VM, Hightower GA, Smith JT, Conway T.** 2008. The global, ppGpp-mediated stringent response to amino acid starvation in *Escherichia coli*. Molecular Microbiology **68:**1128-1148.
179. **Xiao H, Kalman M, Ikehara K, Zemel S, Glaser G, Cashel M.** 1991. Residual guanosine 3',5'-bispyrophosphate synthetic activity of *relA* null mutants can be eliminated by *spoT* null mutations. Journal of Biological Chemistry **266:**5980-5990.
180. **Vinella D, Albrecht C, Cashel M, D'Ari R.** 2005. Iron limitation induces SpoT-dependent accumulation of ppGpp in *Escherichia coli*. Molecular Microbiology **56:**958-970.
181. **Muller CM, Conejero L, Spink N, Wand ME, Bancroft GJ, Titball RW.** 2012. The role of RelA and SpoT in *Burkholderia pseudomallei* virulence and immunity. Infection and Immunity.
182. **Wendrich TM, Blaha G, Wilson DN, Marahiel MA, Nierhaus KH.** 2002. Dissection of the Mechanism for the Stringent Factor RelA. Molecular Cell **10:**779-788.
183. **Shyp V, Tankov S, Ermakov A, Kudrin P, English BP, Ehrenberg M, Tenson T, Elf J, Hauryliuk V.** 2012. Positive allosteric feedback regulation of the stringent response enzyme RelA by its product. EMBO reports **13:**835-839.
184. **Agirrezabala X, Fernandez IS, Kelley AC, Carton DG, Ramakrishnan V, Valle M.** 2013. The ribosome triggers the stringent response by RelA via a highly distorted tRNA. EMBO Rep.
185. **Loveland AB, Bah E, Madireddy R, Zhang Y, Brilot AF, Grigorieff N, Korostelev AA.** 2016. Ribosome/RelA structures reveal the mechanism of stringent response activation. eLife **5:**e17029.
186. **Hogg T, Mechold U, Malke H, Cashel M, Hilgenfeld R.** 2004. Conformational Antagonism between Opposing Active Sites in a Bifunctional RelA/SpoT Homolog Modulates (p)ppGpp Metabolism during the Stringent Response. Cell **117:**57-68.
187. **Battesti Al, Bouveret E.** 2006. Acyl carrier protein/SpoT interaction, the switch linking SpoT-dependent stress response to fatty acid metabolism. Molecular Microbiology **62:**1048-1063.

188. **Battesti Al, Bouveret E.** 2009. Bacteria Possessing Two RelA/SpoT-Like Proteins Have Evolved a Specific Stringent Response Involving the Acyl Carrier Protein-SpoT Interaction. Journal of Bacteriology **191:**616-624.
189. **Starosta AL, Lassak J, Jung K, Wilson DN.** 2014. The bacterial translation stress response. FEMS Microbiology Reviews **38:**1172-1201.
190. **Tosa T, Pizer LI.** 1971. Effect of Serine Hydroxamate on the Growth of *Escherichia coli*. Journal of Bacteriology **106:**966-971.
191. **Tosa T, Pizer LI.** 1971. Biochemical Bases for the Antimetabolite Action of l-Serine Hydroxamate. Journal of Bacteriology **106:**972-982.
192. **Brockmann-Gretza O, Kalinowski J.** 2006. Global gene expression during stringent response in Corynebacterium glutamicum in presence and absence of the rel gene encoding (p)ppGpp synthase. BMC Genomics **7:**1-15.
193. **Imlay JA.** 2013. The molecular mechanisms and physiological consequences of oxidative stress: lessons from a model bacterium. Nat Rev Micro **advance online publication**.
194. **Gaynor EC, Wells DH, MacKichan JK, Falkow S.** 2005. The *Campylobacter jejuni* stringent response controls specific stress survival and virulence-associated phenotypes. Molecular Microbiology **56:**8-27.
195. **Ligeza A, Tikhonov AN, Hyde JS, Subczynski WK.** 1998. Oxygen permeability of thylakoid membranes: electron paramagnetic resonance spin labeling study. Biochimica et Biophysica Acta (BBA) - Bioenergetics **1365:**453-463.
196. **Imlay JA.** 2008. Cellular defenses against superoxide and hydrogen peroxide. Annual review of biochemistry **77:**755-776.
197. **Park S, You X, Imlay JA.** 2005. Substantial DNA damage from submicromolar intracellular hydrogen peroxide detected in Hpx- mutants of *Escherichia coli*. Proceedings of the National Academy of Sciences of the United States of America **102:**9317-9322.
198. **Simpson JA, Smith SE, Dean RT.** 1989. Scavenging by alginate of free radicals released by macrophages. Free Radical Biology and Medicine **6:**347-353.
199. **Carlioz A, Touati D.** 1986. Isolation of superoxide dismutase mutants in *Escherichia coli*: is superoxide dismutase necessary for aerobic life? The EMBO journal **5:**623.
200. **Clements MO, Watson SP, Foster SJ.** 1999. Characterization of the Major Superoxide Dismutase of Staphylococcus aureus and Its Role in Starvation Survival, Stress Resistance, and Pathogenicity. Journal of Bacteriology **181:**3898-3903.
201. **Fridovich I.** 1995. Superoxide Radical and Superoxide Dismutases, p. 97-112, Annual Review of Biochemistry, vol. 64. Annual Reviews.
202. **Hopkin KA, Papazian MA, Steinman HM.** 1992. Functional differences between manganese and iron superoxide dismutases in *Escherichia coli* K-12. Journal of Biological Chemistry **267:**24253-24258.
203. **Khakimova M, Ahlgren HG, Harrison JJ, English AM, Nguyen D.** 2013. The Stringent Response Controls Catalases in *Pseudomonas aeruginosa* and Is Required for Hydrogen Peroxide and Antibiotic Tolerance. Journal of Bacteriology **195:**2011-2020.
204. **Keren I, Wu Y, Inocencio J, Mulcahy LR, Lewis K.** 2013. Killing by Bactericidal Antibiotics Does Not Depend on Reactive Oxygen Species. Science **339:**1213-1216.
205. **Bernhardt J, Weibezahn J, Scharf C, Hecker M.** 2003. *Bacillus subtilis* During Feast and Famine: Visualization of the Overall Regulation of Protein Synthesis During Glucose Starvation by Proteome Analysis. Genome Research **13:**224-237.
206. **Jenkins DE, Schultz JE, Matin A.** 1988. Starvation-induced cross protection against heat or H2O2 challenge in *Escherichia coli*. Journal of Bacteriology **170:**3910-3914.
207. **Cashel M.** 1975. Regulation of bacterial ppGpp and pppGpp. Annual Reviews in Microbiology **29:**301-318.

208. **Seyfzadeh M, Keener J, Nomura M.** 1993. spoT-dependent accumulation of guanosine tetraphosphate in response to fatty acid starvation in Escherichia coli. Proceedings of the National Academy of Sciences **90:**11004-11008.
209. **Yan X, Zhao C, Budin-Verneuil Al, Hartke A, Rinc+® A, Gilmore MS, Auffray Y, Pichereau V.** 2009. The (p)ppGpp synthetase RelA contributes to stress adaptation and virulence in *Enterococcus faecalis* V583. Microbiology **155:**3226-3237.
210. **Yamada A, Tsutsumi K, Tanimoto S, Ozeki Y.** 2003. Plant RelA/SpoT Homolog Confers Salt Tolerance in *Escherichia coli* and *Saccharomyces cerevisiae*. Plant and Cell Physiology **44:**3-9.
211. **Kristensen O, Laurberg M, Liljas A, Kastrup JS, Gajhede M.** 2004. Structural Characterization of the Stringent Response Related Exopolyphosphatase/Guanosine Pentaphosphate Phosphohydrolase Protein Family, p. 8894-8900, Biochemistry, vol. 43. American Chemical Society.
212. **Rao NN, Liu S, Kornberg A.** 1998. Inorganic Polyphosphate in *Escherichia coli*: the Phosphate Regulon and the Stringent Response. Journal of Bacteriology **180:**2186-2193.
213. **Kuroda A, Murphy H, Cashel M, Kornberg A.** 1997. Guanosine Tetra- and Pentaphosphate Promote Accumulation of Inorganic Polyphosphate in *Escherichia coli*. Journal of Biological Chemistry **272:**21240-21243.
214. **Rao NN, Gomez-Garcia MR, Kornberg A.** 2009. Inorganic polyphosphate: essential for growth and survival. Annual review of biochemistry **78:**605-647.
215. **Kornberg A.** 1999. Inorganic Polyphosphate: A Molecule of Many Functions, p. 1-18. *In* Schroder HC, Muller WEG (ed.), Inorganic Polyphosphates: Biochemistry, Biology, Biotechnology. Springer Berlin Heidelberg, Berlin, Heidelberg.
216. **Meyer A.** 1904. Investigations on proliferation , morphology and chemistry of volutins. A. Felix.
217. **Gunn JS, Lim KB, Krueger J, Kim K, Guo L, Hackett M, Miller SI.** 1998. PmrA PmrB-regulated genes necessary for 4-aminoarabinose lipid A modification and polymyxin resistance. Molecular Microbiology **27:**1171-1182.
218. **Kornberg A.** 1995. Inorganic polyphosphate: toward making a forgotten polymer unforgettable. Journal of Bacteriology **177:**491-496.
219. **Kornberg A.** 1999. Inorganic Polyphosphate: A Molecule of Many Functions, p. 1-18. *In* Schrader H, Muller W (ed.), Inorganic Polyphosphates, 23 ed. Springer Berlin Heidelberg.
220. **Fraley CD, Rashid MH, Lee SSK, Gottschalk R, Harrison J, Wood PJ, Brown MRW, Kornberg A.** 2007. A polyphosphate kinase 1 (*ppk1*) mutant of *Pseudomonas aeruginosa* exhibits multiple ultrastructural and functional defects. Proceedings of the National Academy of Sciences **104:**3526-3531.
221. **Kulaev IS, Vagabov V, Kulakovskaya T.** 2005. The biochemistry of inorganic polyphosphates. John Wiley & Sons.
222. **Ahn K, Kornberg A.** 1990. Polyphosphate kinase from *Escherichia coli*. Purification and demonstration of a phosphoenzyme intermediate. Journal of Biological Chemistry **265:**11734-11739.
223. **Akiyama M, Crooke E, Kornberg A.** 1992. The polyphosphate kinase gene of *Escherichia coli.* Isolation and sequence of the ppk gene and membrane location of the protein. Journal of Biological Chemistry **267:**22556-22561.
224. **Kumble KD, Ahn K, Kornberg A.** 1996. Phosphohistidyl active sites in polyphosphate kinase of *Escherichia coli*. Proceedings of the National Academy of Sciences **93:**14391-14395.
225. **Leipe DD, Koonin EV, Aravind L.** 2003. Evolution and Classification of P-loop Kinases and Related Proteins. Journal of Molecular Biology **333:**781-815.

226. **Brown MRW, Kornberg A.** 2008. The long and short of it – polyphosphate, PPK and bacterial survival. Trends in Biochemical Sciences **33:**284-290.
227. **Nocek B, Kochinyan S, Proudfoot M, Brown G, Evdokimova E, Osipiuk J, Edwards AM, Savchenko A, Joachimiak A, Yakunin AF.** 2008. Polyphosphate-dependent synthesis of ATP and ADP by the family-2 polyphosphate kinases in bacteria. Proceedings of the National Academy of Sciences **105:**17730-17735.
228. **Ishige K, Zhang H, Kornberg A.** 2002. Polyphosphate kinase (PPK2), a potent, polyphosphate-driven generator of GTP. Proceedings of the National Academy of Sciences **99:**16684-16688.
229. **Whitehead MP, Eagles L, Hooley P, Brown MR.** 2014. Most bacteria synthesize polyphosphate by unknown mechanisms. Microbiology **160:**829-831.
230. **Batten Laura E, Parnell Alice E, Wells Neil J, Murch Amber L, Oyston PCF, Roach Peter L.** 2016. Biochemical and structural characterization of polyphosphate kinase 2 from the intracellular pathogen *Francisella tularensis*. Bioscience Reports **36**.
231. **Peng L, Luo W-Y, Zhao T, Wan C-S, Jiang Y, Chi F, Zhao W, Cao H, Huang S-H.** 2012. Polyphosphate kinase 1 is required for the pathogenesis process of meningitic *Escherichia coli* K1 (RS218). Future Microbiology **7:**411-423.
232. **Kristensen O, Ross B, Gajhede M.** 2008. Structure of the PPX/GPPA Phosphatase from *Aquifex aeolicus* in Complex with the Alarmone ppGpp. Journal of Molecular Biology **375:**1469-1476.
233. **Kristensen O, Laurberg M, Liljas A, Kastrup JS, Gajhede M.** 2004. Structural Characterization of the Stringent Response Related Exopolyphosphatase/Guanosine Pentaphosphate Phosphohydrolase Protein Family. Biochemistry **43:**8894-8900.
234. **Malde A, Gangaiah D, Chandrashekhar K, Pina-Mimbela R, Torrelles JB, Rajashekara G.** 2014. Functional characterization of exopolyphosphatase/guanosine pentaphosphate phosphohydrolase (PPX/GPPA) of *Campylobacter jejuni*. Virulence **5:**521-533.
235. **Sy J, Lipmann F.** 1973. Identification of the Synthesis of Guanosine Tetraphosphate (MS I) as Insertion of a Pyrophosphoryl Group into the 3′-Position in Guanosine 5′-Diphosphate. Proceedings of the National Academy of Sciences **70:**306-309.
236. **Haseltine WA, Block R.** 1973. Synthesis of Guanosine Tetra- and Pentaphosphate Requires the Presence of a Codon-Specific, Uncharged Transfer Ribonucleic Acid in the Acceptor Site of Ribosomes. Proceedings of the National Academy of Sciences **70:**1564-1568.
237. **Haseltine WA, Block R.** 1972. MSI and MSII made on ribosome in idling step of protein synthesis. Nature **238:**381-384.
238. **Cashel M, Gentry DR, Hernandez VJ, Vinella D.** 1996. *Escherichia coli* and *Salmonella*: cellular and molecular biology. Escherichia coli and Salmonella: cellular and molecular biology **1:**1458-1496.
239. **Charity JC, Costante-Hamm MM, Balon EL, Boyd DH, Rubin EJ, Dove SL.** 2007. Twin RNA Polymerase–Associated Proteins Control Virulence Gene Expression in *Francisella tularensis*. PLoS Pathog **3:**e84.
240. **Sharma AK, Payne SM.** 2006. Induction of expression of hfq by DksA is essential for *Shigella flexneri* virulence. Molecular Microbiology **62:**469-479.
241. **He H, Cooper JN, Mishra A, Raskin DM.** 2012. Stringent Response Regulation of Biofilm Formation in *Vibrio cholerae*. Journal of Bacteriology **194:**2962-2972.
242. **Godfrey HP, Bugrysheva JV, Cabello FC.** 2002. The role of the stringent response in the pathogenesis of bacterial infections. Trends in Microbiology **10:**349-351.
243. **Pizarro-Cerdá J, Tedin K.** 2004. The bacterial signal molecule, ppGpp, regulates *Salmonella* virulence gene expression. Molecular Microbiology **52:**1827-1844.

244. **Erickson DL, Lines JL, Pesci EC, Venturi V, Storey DG.** 2004. *Pseudomonas aeruginosa relA* Contributes to Virulence in *Drosophila melanogaster*. Infection and Immunity **72:**5638-5645.
245. **Jain V, Kumar M, Chatterji D.** 2006. ppGpp: stringent response and survival. Journal of microbiology (Seoul, Korea) **44:**1-10.
246. **Nano FE, Zhang N, Cowley SíC, Klose KE, Cheung KKM, Roberts MJ, Ludu JS, Letendre GW, Meierovics AI, Stephens G, Elkins KL.** 2004. A *Francisella tularensis* Pathogenicity Island Required for Intramacrophage Growth. Journal of Bacteriology **186:**6430-6436.
247. **Nano FE, SCHMERK CRYS.** 2007. The *Francisella* Pathogenicity Island. Annals of the New York Academy of Sciences **1105:**122-137.
248. **Guina T, Radulovic D, Bahrami AJ, Bolton DL, Rohmer L, Jones-Isaac KA, Chen J, Gallagher LA, Gallis B, Ryu S, Taylor GK, Brittnacher MJ, Manoil C, Goodlett DR.** 2007. MglA Regulates *Francisella tularensis* subsp. *novicida* (*Francisella novicida*) Response to Starvation and Oxidative Stress. Journal of Bacteriology **189:**6580-6586.
249. **Lauriano CM, Barker JR, Yoon SS, Nano FE, Arulanandam BP, Hassett DJ, Klose KE.** 2004. MglA regulates transcription of virulence factors necessary for *Francisella tularensis* intraamoebae and intramacrophage survival. Proceedings of the National Academy of Sciences **101:**4246-4249.
250. **Hansen A-M, Gu Y, Li M, Andrykovitch M, Waugh DS, Jin DJ, Ji X.** 2005. Structural Basis for the Function of Stringent Starvation Protein A as a Transcription Factor. Journal of Biological Chemistry **280:**17380-17391.
251. **Wolfson JS, Hooper DC, McHugh GL, Bozza MA, Swartz MN.** 1990. Mutants of *Escherichia coli* K-12 exhibiting reduced killing by both quinolone and beta-lactam antimicrobial agents. Antimicrobial Agents and Chemotherapy **34:**1938-1943.
252. **Maisonneuve E, Castro-Camargo M, Gerdes K.** 2013. (p)ppGpp Controls Bacterial Persistence by Stochastic Induction of Toxin-Antitoxin Activity. Cell **154:**1140-1150.
253. **Wang X, Wood TK.** 2011. Toxin-Antitoxin Systems Influence Biofilm and Persister Cell Formation and the General Stress Response. Applied and Environmental Microbiology **77:**5577-5583.
254. **Bokinsky G, Baidoo EEKA, Swetha Burd, Helcio Weaver DL, Soon T, Keasling, D. J.** 2013. HipA-Triggered Growth Arrest and Lactam Tolerance in *Escherichia coli* Are Mediated by RelA-Dependent ppGpp Synthesis. Journal of Bacteriology **195:**3173-3182.
255. **Yamaguchi Y, Inouye M.** 2011. Regulation of growth and death in Escherichia coli by toxin–antitoxin systems. Nat Rev Micro **9:**779-790.
256. **Kuroda A.** 2006. A Polyphosphate-Lon Protease Complex in the Adaptation of *Escherichia coli* to Amino Acid Starvation. Bioscience, Biotechnology, and Biochemistry **70:**325-331.
257. **Malone JH, Oliver B.** 2011. Microarrays, deep sequencing and the true measure of the transcriptome. BMC Biology **9:**1-9.
258. **Trost B, Moir CA, Gillespie ZE, Kusalik A, Mitchell JA, Eskiw CH.** 2015. Concordance between RNA-sequencing data and DNA microarray data in transcriptome analysis of proliferative and quiescent fibroblasts. Royal Society Open Science **2**.
259. **Venter JC.** 2001. The Sequence of the Human Genome. Science **291:**1304-1351.
260. **Venter JC.** 2010. Multiple personal genomes await. Nature **464:**676-677.
261. **Loman NJ, Misra RV, Dallman TJ, Constantinidou C, Gharbia SE, Wain J, Pallen MJ.** 2012. Performance comparison of benchtop high-throughput sequencing platforms. Nat Biotech **30:**434-439.
262. **Wang Z, Gerstein M, Snyder M.** 2009. RNA-Seq: a revolutionary tool for transcriptomics. Nat Rev Genet **10:**57-63.

263. **Picker LJ, Hansen SG, Lifson JD.** 2012. New Paradigms for HIV/AIDS Vaccine Development. Annual Review of Medicine **63:**95-111.
264. **Chang ST, Sova P, Peng X, Weiss J, Law GL, Palermo RE, Katze MG.** 2011. Next-Generation Sequencing Reveals HIV-1-Mediated Suppression of T Cell Activation and RNA Processing and Regulation of Noncoding RNA Expression in a CD4+ T Cell Line. mBio **2**.
265. **Fehniger TA, Wylie T, Germino E, Leong JW, Magrini VJ, Koul S, Keppel CR, Schneider SE, Koboldt DC, Sullivan RP, Heinz ME, Crosby SD, Nagarajan R, Ramsingh G, Link DC, Ley TJ, Mardis ER.** 2010. Next-generation sequencing identifies the natural killer cell microRNA transcriptome. Genome Research **20:**1590-1604.
266. **Yang Z, Bruno DP, Martens CA, Porcella SF, Moss B.** 2010. Simultaneous high-resolution analysis of vaccinia virus and host cell transcriptomes by deep RNA sequencing. Proceedings of the National Academy of Sciences **107:**11513-11518.
267. **Zhao H, Dahlö M, Isaksson A, Syvänen A-C, Pettersson U.** 2012. The transcriptome of the adenovirus infected cell. Virology **424:**115-128.
268. **Chen Z, Duan X.** 2011. Ribosomal RNA Depletion for Massively Parallel Bacterial RNA-Sequencing Applications, p. 93-103. *In* Kwon MY, Ricke CS (ed.), High-Throughput Next Generation Sequencing: Methods and Applications. Humana Press, Totowa, NJ.
269. **Ku CS, Roukos DH.** 2013. From next-generation sequencing to nanopore sequencing technology: paving the way to personalized genomic medicine. Expert Review of Medical Devices **10:**1-6.
270. **Luciani F, Bull RA, Lloyd AR.** 2012. Next generation deep sequencing and vaccine design: today and tomorrow. Trends in Biotechnology **30:**443-452.
271. **Maxson ME, Darwin AJ.** 2004. Identification of Inducers of the *Yersinia enterocolitica* Phage Shock Protein System and Comparison to the Regulation of the RpoE and Cpx Extracytoplasmic Stress Responses. Journal of Bacteriology **186:**4199-4208.
272. **Kakoschke T, Kakoschke S, Magistro G, Schubert S, Borath M, Heesemann J, Rossier O.** 2014. The RNA Chaperone Hfq Impacts Growth, Metabolism and Production of Virulence Factors in *Yersinia enterocolitica*. PLoS ONE **9:**e86113.
273. **Darwin AJ, Miller VL.** 1999. Identification of *Yersinia enterocolitica* genes affecting survival in an animal host using signature-tagged transposon mutagenesis. Molecular Microbiology **32:**51-62.
274. **Titball RW, Williamson ED.** 2004. *Yersinia pestis* (plague) vaccines. Expert Opinion on Biological Therapy **4:**965-973.
275. **Eyles JE, Sharp GJE, Diane Williamson E, Spiers ID, Oya Alpar H.** 1998. Intra nasal administration of poly-lactic acid microsphere co-encapsulated *Yersinia pestis* subunits confers protection from pneumonic plague in the mouse. Vaccine **16:**698-707.
276. **Elvin SJ, Williamson ED.** 2000. The F1 and V subunit vaccine protects against plague in the absence of IL-4 driven immune responses. Microbial Pathogenesis **29:**223-230.
277. **Fleming DM, Crovari P, Wahn U, Klemola T, Schlesinger Y, Langussis A, Øymar K, Garcia ML, Krygier A, Costa H, Heininger U, Pregaldien J-L, Cheng S-M, Skinner J, Razmpour A, Saville M, Gruber WC, Forrest B, Group ftC-TAS.** 2006. Comparison of the Efficacy and Safety of Live Attenuated Cold-Adapted Influenza Vaccine, Trivalent, With Trivalent Inactivated Influenza Virus Vaccine in Children and Adolescents With Asthma. The Pediatric Infectious Disease Journal **25:**860-869.
278. **Argaman L, Elgrably-Weiss M, Hershko T, Vogel J, Altuvia S.** 2012. RelA protein stimulates the activity of RyhB small RNA by acting on RNA-binding protein Hfq. Proceedings of the National Academy of Sciences **109:**4621-4626.
279. **Geng J, Song Y, Yang L, Feng Y, Qiu Y, Li G, Guo J, Bi Y, Qu Y, Wang W, Wang X, Guo Z, Yang R, Han Y.** 2009. Involvement of the Post-Transcriptional Regulator Hfq in *Yersinia pestis* Virulence. PLoS ONE **4:**e6213.

280. **Bai G, Golubov A, Smith EA, McDonough KA.** 2010. The Importance of the Small RNA Chaperone Hfq for Growth of Epidemic *Yersinia pestis*, but Not *Yersinia pseudotuberculosis*, with Implications for Plague Biology. Journal of Bacteriology **192:**4239-4245.
281. **Bellows LE, Koestler BJ, Karaba SM, Waters CM, Lathem WW.** 2012. Hfq-dependent, co-ordinate control of cyclic diguanylate synthesis and catabolism in the plague pathogen *Yersinia pestis*. Molecular Microbiology **86:**661-674.
282. **Rempe KA, Hinz AK, Vadyvaloo V.** 2012. Hfq Regulates Biofilm Gut Blockage That Facilitates Flea-Borne Transmission of *Yersinia pestis*. Journal of Bacteriology **194:**2036-2040.
283. **Deng Z, Meng X, Su S, Liu Z, Ji X, Zhang Y, Zhao X, Wang X, Yang R, Han Y.** 2012. Two sRNA RyhB homologs from *Yersinia pestis* biovar microtus expressed in vivo have differential Hfq-dependent stability. Research in Microbiology **163:**413-418.
284. **Stanley NR, Lazazzera BA.** 2004. Environmental signals and regulatory pathways that influence biofilm formation. Molecular Microbiology **52:**917-924.
285. **Dewanti R, Wong ACL.** 1995. Influence of culture conditions on biofilm formation by *Escherichia coli* O157:H7. International Journal of Food Microbiology **26:**147-164.
286. **Balzer GJ, McLean RJC.** 2002. NoteThe stringent response genes *relA* and *spoT* are important for *Escherichia coli* biofilms under slow-growth conditions. Canadian Journal of Microbiology **48:**675-680.
287. **Kulesus RR, Diaz-Perez K, Slechta ES, Eto DS, Mulvey MA.** 2008. Impact of the RNA Chaperone Hfq on the Fitness and Virulence Potential of Uropathogenic Escherichia coli. Infection and Immunity **76:**3019-3026.
288. **Robinson VL, Oyston PCF, Titball RW.** 2005. A dam mutant of *Yersinia pestis* is attenuated and induces protection against plague. FEMS Microbiology Letters **252:**251-256.
289. **Taylor VL, Titball RW, Oyston PCF.** 2005. Oral immunization with a dam mutant of *Yersinia pseudotuberculosis* protects against plague. Microbiology **151:**1919-1926.
290. **Oyston PCF, Mellado-Sanchez G, Pasetti MF, Nataro JP, Titball RW, Atkins HS.** 2010. A *Yersinia pestis guaBA* mutant is attenuated in virulence and provides protection against plague in a mouse model of infection. Microbial Pathogenesis **48:**191-195.
291. **Milton DL, O'Toole R, Horstedt P, Wolf-Watz H.** 1996. Flagellin A is essential for the virulence of *Vibrio anguillarum*. Journal of Bacteriology **178:**1310-1319.
292. **Ford DC, Ireland PM, Bullifent HL, Saint RJ, McAlister EV, Sarkar-Tyson M, Oyston PCF.** 2014. Construction of an inducible system for the analysis of essential genes in *Yersinia pestis*. Journal of Microbiological Methods **100:**1-7.
293. **Sun W, Wang S, Curtiss R.** 2008. Highly Efficient Method for Introducing Successive Multiple Scarless Gene Deletions and Markerless Gene Insertions into the *Yersinia pestis* Chromosome. Applied and Environmental Microbiology **74:**4241-4245.
294. **Handa N, Morimatsu K, Lovett ST, Kowalczykowski SC.** 2009. Reconstitution of initial steps of dsDNA break repair by the RecF pathway of *E. coli*. Genes & Development **23:**1234-1245.
295. **West SC.** 1996. The RuvABC proteins and Holliday junction processing in *Escherichia coli*. Journal of Bacteriology **178:**1237-1241.
296. **Sharples GJ, Ingleston SM, Lloyd RG.** 1999. Holliday Junction Processing in Bacteria: Insights from the Evolutionary Conservation of RuvABC, RecG, and RusA. Journal of Bacteriology **181:**5543-5550.
297. **Sharan SK, Thomason LC, Kuznetsov SG, Court DL.** 2009. Recombineering: a homologous recombination-based method of genetic engineering. Nat. Protocols **4:**206-223.

298. **Nilles ML, Williams AW, Skrzypek E, Straley SC.** 1997. *Yersinia pestis* LcrV forms a stable complex with LcrG and may have a secretion-related regulatory role in the low-Ca2+ response. Journal of Bacteriology **179:**1307.
299. **Perry RD, Pendrak ML, Schuetze P.** 1990. Identification and cloning of a hemin storage locus involved in the pigmentation phenotype of *Yersinia pestis*. Journal of Bacteriology **172:**5929-5937.
300. **Buchrieser C, Prentice M, Carniel E.** 1998. The 102-Kilobase Unstable Region of *Yersinia pestis* Comprises a High-Pathogenicity Island Linked to a Pigmentation Segment Which Undergoes Internal Rearrangement. Journal of Bacteriology **180:**2321-2329.
301. **Qadri F, Hossain SA, Ciznár I, Haider K, Ljungh A, Wadstrom T, Sack DA.** 1988. Congo red binding and salt aggregation as indicators of virulence in *Shigella* species. Journal of Clinical Microbiology **26:**1343-1348.
302. **Daskaleros PA, Payne SM.** 1987. Congo red binding phenotype is associated with hemin binding and increased infectivity of *Shigella flexneri* in the HeLa cell model. Infection and Immunity **55:**1393-1398.
303. **Stugard CE, Daskaleros PA, Payne SM.** 1989. A 101-kilodalton heme-binding protein associated with congo red binding and virulence of *Shigella flexneri* and enteroinvasive *Escherichia coli* strains. Infection and Immunity **57:**3534-3539.
304. **Pansegrau W, Lanka E, Barth PT, Figurski DH, Guiney DG, Haas D, Helinski DR, Schwab H, Stanisich VA, Thomas CM.** 1994. Complete Nucleotide Sequence of Birmingham IncPα Plasmids. Journal of Molecular Biology **239:**623-663.
305. **Grahn AM, Haase J, Bamford DH, Lanka E.** 2000. Components of the RP4 Conjugative Transfer Apparatus Form an Envelope Structure Bridging Inner and Outer Membranes of Donor Cells: Implications for Related Macromolecule Transport Systems. Journal of Bacteriology **182:**1564-1574.
306. **Bates S, Cashmore AM, Wilkins BM.** 1998. IncP Plasmids Are Unusually Effective in Mediating Conjugation of *Escherichia coli* and *Saccharomyces cerevisiae*: Involvement of the Tra2 Mating System. Journal of Bacteriology **180:**6538-6543.
307. **Simon R, Priefer U, Puhler A.** 1983. A broad host range mobilization system for *in vivo* genetic engineering: transposon mutagenesis in gram negative bacteria. Nature Biotechnology **1:**784-791.
308. **Guilfoyle A, Maher MJ, Rapp M, Clarke R, Harrop S, Jormakka M.** 2009. Structural basis of GDP release and gating in G protein coupled Fe2+ transport. The EMBO journal **28:**2677-2685.
309. **Ghorbel S, Smirnov A, Chouayekh H, Sperandio B, Esnault C, Kormanec J, Virolle MJ.** 2006. Regulation of ppk Expression and *In Vivo* Function of Ppk in *Streptomyces lividans* TK24. Journal of Bacteriology **188:**6269-6276.
310. **Baykov AA, Evtushenko OA, Avaeva SM.** 1988. A malachite green procedure for orthophosphate determination and its use in alkaline phosphatase-based enzyme immunoassay. Analytical Biochemistry **171:**266-270.
311. **Feng J, Chen Y, Pu J, Yang X, Zhang C, Zhu S, Zhao Y, Yuan Y, Yuan H, Liao F.** 2011. An improved malachite green assay of phosphate: Mechanism and application. Analytical Biochemistry **409:**144-149.
312. **Sherwood AR, Paasch BC, Worby CA, Gentry MS.** 2013. A malachite green-based assay to assess glucan phosphatase activity. Analytical Biochemistry **435:**54-56.
313. **Wrench AP, Gardner CL, Siegel SD, Pagliai FA, Malekiha M, Gonzalez CF, Lorca GL.** 2013. MglA/SspA Complex Interactions Are Modulated by Inorganic Polyphosphate. PLoS ONE **8:**e76428.

314. **Fung DKC, Chan EWC, Chin ML, Chan RCY.** 2010. Delineation of a Bacterial Starvation Stress Response Network Which Can Mediate Antibiotic Tolerance Development. Antimicrobial Agents and Chemotherapy **54:**1082-1093.
315. **Ortiz-Severín J, Varas M, Bravo-Toncio C, Guiliani N, Chávez FP.** 2015. Multiple antibiotic susceptibility of polyphosphate kinase mutants (*ppk1* and *ppk2*) from *Pseudomonas aeruginosa* PAO1 as revealed by global phenotypic analysis. Biological Research **48:**1-6.
316. **Schatz A, Bugle E, Waksman SA.** 1944. Streptomycin, a Substance Exhibiting Antibiotic Activity Against Gram-Positive and Gram-Negative Bacteria. Experimental Biology and Medicine **55:**66-69.
317. **Yoshizawa S, Fourmy D, Puglisi JD.** 1998. Structural origins of gentamicin antibiotic action. The EMBO Journal **17:**6437-6448.
318. **Karimi R, Ehrenberg M.** 1994. Dissociation Rate of Cognate Peptidyl-tRNA from the A-Site of Hyper-Accurate and Error-Prone Ribosomes. European Journal of Biochemistry **226:**355-360.
319. **Chopra I, Roberts M.** 2001. Tetracycline Antibiotics: Mode of Action, Applications, Molecular Biology, and Epidemiology of Bacterial Resistance. Microbiology and Molecular Biology Reviews **65:**232-260.
320. **Rasmussen B, Noller HF, Daubresse G, Oliva B, Misulovin Z, Rothstein DM, Ellestad GA, Gluzman Y, Tally FP, Chopra I.** 1991. Molecular basis of tetracycline action: identification of analogs whose primary target is not the bacterial ribosome. Antimicrobial Agents and Chemotherapy **35:**2306-2311.
321. **Maaland MG, Papich MG, Turnidge J, Guardabassi L.** 2013. Pharmacodynamics of Doxycycline and Tetracycline against *Staphylococcus pseudintermedius*: Proposal of Canine-Specific Breakpoints for Doxycycline. Journal of Clinical Microbiology **51:**3547-3554.
322. **Guerra W, Silva IR, Azevedo EA, Monteiro ARdS, Bucciarelli-Rodriguez M, Chartone-Souza E, Silveira JN, Fontes APS, Pereira-Maia EC.** 2006. Three new complexes of platinum(II) with doxycycline, oxytetracycline and chlortetracycline and their antimicrobial activity. Journal of the Brazilian Chemical Society **17:**1627-1633.
323. **Hooper DC, Wolfson JS, Ng EY, Swartz MN.** 1987. Mechanisms of action of and resistance to ciprofloxacin. The American journal of medicine **82:**12-20.
324. **Shapiro AB, Andrews B.** 2012. Allosteric inhibition of the DNA-dependent ATPase activity of *Escherichia coli* DNA gyrase by a representative of a novel class of inhibitors. Biochemical Pharmacology **84:**900-904.
325. **Morrison DC, Jacobs DM.** 1976. Binding of polymyxin B to the lipid A portion of bacterial lipopolysaccharides. Immunochemistry **13:**813-818.
326. **Cabiscol E, Tamarit J, Ros J.** 2010. Oxidative stress in bacteria and protein damage by reactive oxygen species. International Microbiology **3:**3-8.
327. **Farr SB, Kogoma T.** 1991. Oxidative stress responses in *Escherichia coli* and *Salmonella typhimurium*. Microbiological Reviews **55:**561-585.
328. **Gao R, Yuan Z, Zhao Z, Gao X.** 1998. Mechanism of pyrogallol autoxidation and determination of superoxide dismutase enzyme activity. Bioelectrochemistry and Bioenergetics **45:**41-45.
329. **Bakshi CS, Malik M, Regan K, Melendez JA, Metzger DW, Pavlov VM, Sellati TJ.** 2006. Superoxide Dismutase B Gene (*sodB*)-Deficient Mutants of *Francisella tularensis* Demonstrate Hypersensitivity to Oxidative Stress and Attenuated Virulence. Journal of Bacteriology **188:**6443-6448.
330. **Fee JA.** 1991. Regulation of sod genes in *Escherichia coli*: relevance to superoxide dismutase function. Molecular Microbiology **5:**2599-2610.

331. **Tardat B, Touati D.** 1993. Iron and oxygen regulation of *Escherichia coli* MnSOD expression: competition between the global regulators Fur and ArcA for binding to DNA. Molecular Microbiology **9:**53-63.
332. **Niederhoffer EC, Naranjo CM, Bradley KL, Fee JA.** 1990. Control of *Escherichia coli* superoxide dismutase (*sodA* and *sodB*) genes by the ferric uptake regulation (*fur*) locus. Journal of Bacteriology **172:**1930-1938.
333. **Dubrac S, Touati D.** 2000. Fur Positive Regulation of Iron Superoxide Dismutase in *Escherichia coli*: Functional Analysis of the *sodB* Promoter. Journal of Bacteriology **182:**3802-3808.
334. **Demple B.** 1991. Regulation of Bacterial Oxidative Stress Genes. Annual Review of Genetics **25:**315-337.
335. **Ochsner UA, Vasil ML, Alsabbagh E, Parvatiyar K, Hassett DJ.** 2000. Role of the *Pseudomonas aeruginosa oxyR-recG* Operon in Oxidative Stress Defense and DNA Repair: OxyR-Dependent Regulation of *katB-ankB, ahpB,* and *ahpC-ahpF*. Journal of Bacteriology **182:**4533-4544.
336. **Hishinuma S, Yuki M, Fujimura M, Fukumori F.** 2006. OxyR regulated the expression of two major catalases, KatA and KatB, along with peroxiredoxin, AhpC in *Pseudomonas putida*. Environmental Microbiology **8:**2115-2124.
337. **Deuerling E, Mogk A, Richter C, Purucker M, Schumann W.** 1997. The *ftsH* gene of *Bacillus subtilis* is involved in major cellular processes such as sporulation, stress adaptation and secretion. Molecular Microbiology **23:**921-933.
338. **Fux CA, Costerton JW, Stewart PS, Stoodley P.** 2005. Survival strategies of infectious biofilms. Trends in Microbiology **13:**34-40.
339. **Lombardo M-J, Aponyi I, Rosenberg SM.** 2004. General Stress Response Regulator RpoS in Adaptive Mutation and Amplification in *Escherichia coli*. Genetics **166:**669-680.
340. **Bjedov I, Tenaillon O, Gérard B, Souza V, Denamur E, Radman M, Taddei F, Matic I.** 2003. Stress-Induced Mutagenesis in Bacteria. Science **300:**1404-1409.
341. **Korch SB, Hill TM.** 2006. Ectopic Overexpression of Wild-Type and Mutant *hipA* Genes in *Escherichia coli*: Effects on Macromolecular Synthesis and Persister Formation. Journal of Bacteriology **188:**3826-3836.
342. **Gerdes K, Maisonneuve E.** 2012. Bacterial Persistence and Toxin-Antitoxin Loci. Annual Review of Microbiology **66:**103-123.
343. **Mylonakis E, Casadevall A, Ausubel FM.** 2007. Exploiting Amoeboid and Non-Vertebrate Animal Model Systems to Study the Virulence of Human Pathogenic Fungi. PLoS Pathog **3:**e101.
344. **Steinert M, Leippe M, Roeder T.** 2003. Surrogate hosts: protozoa and invertebrates as models for studying pathogen-host interactions. International Journal of Medical Microbiology **293:**321-332.
345. **Tan MW.** 2002. Cross-Species Infections and Their Analysis, p. 539-565, Annual Review of Microbiology, vol. 56. Annual Reviews.
346. **Garcia-Lara J, Needham AJ, Foster SJ.** 2005. Invertebrates as animal models for *Staphylococcus aureus* pathogenesis: a window into host-pathogen interaction. FEMS Immunology & Medical Microbiology **43:**311-323.
347. **Champion OL, Cooper IAM, James SL, Ford D, Karlyshev A, Wren BW, Duffield M, Oyston PCF, Titball RW.** 2009. *Galleria mellonella* as an alternative infection model for *Yersinia pseudotuberculosis*. Microbiology **155:**1516-1522.
348. **Bergin D, Reeves EP, Renwick J, Wientjes FB, Kavanagh K.** 2005. Superoxide Production in *Galleria mellonella* Hemocytes: Identification of Proteins Homologous to the NADPH Oxidase Complex of Human Neutrophils. Infection and Immunity **73:**4161-4170.

349. **Lavine MD, Strand MR.** 2002. Insect hemocytes and their role in immunity. Insect Biochemistry and Molecular Biology **32:**1295-1309.
350. **Nappi AJ.** 1973. The role of melanization in the immune reaction of larvae of *Drosophila algonquin* against *Pseudeucoila bochei*. Parasitology **66:**23-32.
351. **Aperis G, Burgwyn Fuchs B, Anderson CA, Warner JE, Calderwood SB, Mylonakis E.** 2007. *Galleria mellonella* as a model host to study infection by the *Francisella tularensis* live vaccine strain, p. 729-734, Microbes and Infection. Forum on Rational vaccine development against malaria, vol. 9.
352. **Schell MA, Lipscomb L, DeShazer D.** 2008. Comparative Genomics and an Insect Model Rapidly Identify Novel Virulence Genes of *Burkholderia mallei*. Journal of Bacteriology **190:**2306-2313.
353. **Erickson DL, Russell CW, Johnson KL, Hileman T, Stewart RM.** 2011. PhoP and OxyR transcriptional regulators contribute to *Yersinia pestis* virulence and survival within *Galleria mellonella*. Microbial Pathogenesis **51:**389-395.
354. **Harding CR, Schroeder GN, Collins JW, Frankel G.** 2013. Use of *Galleria mellonella* as a Model Organism to Study *Legionella pneumophila* Infection. Journal of Visualized Experiments : JoVE**:**50964.
355. **Senior NJ, Bagnall MC, Champion OL, Reynolds SE, La Ragione RM, Woodward MJ, Salguero FJ, Titball RW.** 2011. *Galleria mellonella* as an infection model for *Campylobacter jejuni* virulence. Journal of Medical Microbiology **60:**661-669.
356. **Russell P, Eley SM, Hibbs SE, Manchee RJ, Stagg AJ, Titball RW.** 1995. A comparison of Plague vaccine, USP and EV76 vaccine induced protection against *Yersinia pestis* in a murine model. Vaccine **13:**1551-1556.
357. **Guzman LM, Belin D, Carson MJ, Beckwith J.** 1995. Tight regulation, modulation, and high-level expression by vectors containing the arabinose PBAD promoter. Journal of Bacteriology **177:**4121-4130.
358. **Van Acker H, Gielis J, Acke M, Cools F, Cos P, Coenye T.** 2016. The Role of Reactive Oxygen Species in Antibiotic-Induced Cell Death in *Burkholderia cepacia* Complex Bacteria. PLoS ONE **11:**e0159837.
359. **Kohanski MA, Dwyer DJ, Hayete B, Lawrence CA, Collins JJ.** 2007. A common mechanism of cellular death induced by bactericidal antibiotics. Cell **130:**797-810.
360. **Liu Y, Imlay JA.** 2013. Cell Death from Antibiotics Without the Involvement of Reactive Oxygen Species. Science **339:**1210-1213.
361. **Fang FC.** 2013. Antibiotic and ROS linkage questioned. Nat Biotech **31:**415-416.
362. **Wright GD, Hung DT, Helmann JD.** 2013. How antibiotics kill bacteria: new models needed? Nature medicine **19:**544-545.
363. **Maisonneuve E, Castro-Camargo M, Gerdes K.** 2013. (p)ppGpp controls bacterial persistence by stochastic induction of toxin-antitoxin activity. Cell **154**.
364. **Gerdes K, Maisonneuve E.** 2015. Remarkable Functional Convergence: Alarmone ppGpp Mediates Persistence by Activating Type I and II Toxin-Antitoxins. Molecular Cell **59:**1-3.
365. **Jones BD, Faron M, Rasmussen JA, Fletcher JR.** 2014. Uncovering the components of the *Francisella tularensis* virulence stealth strategy. Frontiers in cellular and infection microbiology **4**.
366. **Kadzhaev K, Zingmark C, Golovliov I, Bolanowski M, Shen H, Conlan W, Sj+Âstedt A.** 2009. Identification of Genes Contributing to the Virulence of *Francisella tularensis* SCHU S4 in a Mouse Intradermal Infection Model. PLoS ONE **4:**e5463.
367. **Kingry LC, Cummings JE, Brookman KW, Bommineni GR, Tonge PJ, Slayden RA.** 2013. The *Francisella tularensis* FabI Enoyl-Acyl Carrier Protein Reductase Gene Is Essential to Bacterial Viability and Is Expressed during Infection. Journal of Bacteriology **195:**351-358.

368. **Lai XH, Golovliov I, Sj+Âstedt A.** 2004. Expression of IglC is necessary for intracellular growth and induction of apoptosis in murine macrophages by *Francisella tularensis*. Microbial Pathogenesis **37:**225-230.
369. **Faron M, Fletcher JD, Rasmussen JA, Long ME, Allen LA, Jones BD.** 2013. The Francisella tularensis migR, trmE, and cphA genes contribute to FPI gene regulation and intracellular growth by modulation of the stress alarmone ppGpp. Infection and Immunity.
370. **Ludu JS, de Bruin OM, Duplantis BN, Schmerk CL, Chou AY, Elkins KL, Nano FE.** 2008. The *Francisella* Pathogenicity Island Protein PdpD Is Required for Full Virulence and Associates with Homologues of the Type VI Secretion System. Journal of Bacteriology **190:**4584-4595.
371. **Meibom KL, Dubail I, Dupuis M, Barel M, Lenco J, Stulik J, Golovliov I, Sjöstedt A, Charbit A.** 2008. The heat-shock protein ClpB of *Francisella tularensis* is involved in stress tolerance and is required for multiplication in target organs of infected mice. Molecular Microbiology **67:**1384-1401.
372. **Milne TS, Michell SL, Diaper H, WikstrÂm P, Svensson K, Oyston PCF, Titball RW.** 2007. A 55 kDa hypothetical membrane protein is an iron-regulated virulence factor of *Francisella tularensis* subsp. *novicida* U112. Journal of Medical Microbiology **56:**1268-1276.
373. **Barker JR, Chong A, Wehrly TD, Yu JJ, Rodriguez SA, Liu J, Celli J, Arulanandam BP, Klose KE.** 2009. The *Francisella tularensis* pathogenicity island encodes a secretion system that is required for phagosome escape and virulence. Molecular Microbiology **74:**1459-1470.
374. **Schmerk CL, Duplantis BN, Wang D, Burke RD, Chou AY, Elkins KL, Ludu JS, Nano FE.** 2009. Characterization of the pathogenicity island protein PdpA and its role in the virulence of *Francisella novicida*. Microbiology **155:**1489-1497.
375. **Santic M, Molmeret M, Klose KE, Jones S, Kwaik YA.** 2005. The *Francisella tularensis* pathogenicity island protein IglC and its regulator MglA are essential for modulating phagosome biogenesis and subsequent bacterial escape into the cytoplasm. Cellular Microbiology **7:**969-979.
376. **Law HT, Sriram A, Fevang C, Nix EB, Nano FE, Guttman JA.** 2014. IglC and PdpA Are Important for Promoting *Francisella* Invasion and Intracellular Growth in Epithelial Cells. PLoS ONE **9:**e104881.
377. **Eng RH, Padberg FT, Smith SM, Tan EN, Cherubin CE.** 1991. Bactericidal effects of antibiotics on slowly growing and nongrowing bacteria. Antimicrobial Agents and Chemotherapy **35:**1824-1828.
378. **Chuang YM, Belchis DA, Karakousis PC.** 2013. The Polyphosphate Kinase Gene ppk2 Is Required for *Mycobacterium tuberculosis* Inorganic Polyphosphate Regulation and Virulence. mBio **4**.
379. **Candon HL, Allan BJ, Fraley CD, Gaynor EC.** 2007. Polyphosphate Kinase 1 Is a Pathogenesis Determinant in *Campylobacter jejuni*. Journal of Bacteriology **189:**8099-8108.
380. **McMeechan A, Lovell MA, Cogan TA, Marston KL, Humphrey TJ, Barrow PA.** 2007. Inactivation of ppk differentially affects virulence and disrupts ATP homeostasis in *Salmonella enterica serovars Typhimurium* and *Gallinarum*. Research in Microbiology **158:**79-85.
381. **Rashid MH, Rumbaugh K, Passador L, Davies DG, Hamood AN, Iglewski BH.** 2000. Polyphosphate kinase is essential for biofilm development, quorum sensing, and virulence of *Pseudomonas aeruginosa*. Proc Natl Acad Sci U S A **97**.
382. **Gunn JS.** 2001. Bacterial modification of LPS and resistance to antimicrobial peptides. Journal of Endotoxin Research **7:**57-62.

383. **Phillips NJ, Schilling B, McLendon MK, Apicella MA, Gibson BW.** 2004. Novel Modification of Lipid A of *Francisella tularensis*. Infection and Immunity **72:**5340-5348.
384. **Gangaiah D, Liu Z, Arcos Js, Kassem II, Sanad Y, Torrelles JB, Rajashekara G.** 2010. Polyphosphate Kinase 2: A Novel Determinant of Stress Responses and Pathogenesis in *Campylobacter jejuni*. PLoS ONE **5:**e12142.
385. **Kim K-S, Rao NN, Fraley CD, Kornberg A.** 2002. Inorganic polyphosphate is essential for long-term survival and virulence factors in *Shigella* and *Salmonella* spp. Proc Natl Acad Sci U S A **99**.
386. **Korbsrisate S, Vanaporn M, Kerdsuk P, Kespichayawattana W, Vattanaviboon P, Kiatpapan P, Lertmemongkolchai G.** 2005. The *Burkholderia pseudomallei* RpoE (AlgU) operon is involved in environmental stress tolerance and biofilm formation. FEMS Microbiology Letters **252:**243-249.
387. **Osiriphun Y, Wongtrakoongate P, Sanongkiet S, Suriyaphol P, Thongboonkerd V, Tungpradabkul S.** 2009. Identification and Characterization of RpoS Regulon and RpoS-Dependent Promoters in *Burkholderia pseudomallei*. Journal of Proteome Research **8:**3118-3131.
388. **Chirakul S, Bartpho T, Wongsurawat T, Taweechaisupapong S, Karoonutaisiri N, Talaat AM, Wongratanacheewin S, Ernst RK, Sermswan RW.** 2014. Characterization of BPSS1521 *bprD*, a Regulator of *Burkholderia pseudomallei* Virulence Gene Expression in the Mouse Model. PLoS ONE **9:**e104313.
389. **Loprasert S, Whangsuk W, Sallabhan R, Mongkolsuk S.** 2003. Regulation of the *katG-dpsA* operon and the importance of KatG in survival of *Burkholderia pseudomallei* exposed to oxidative stress. FEBS Letters **542:**17-21.
390. **Logue CA, Peak IRA, Beacham IR.** 2009. Facile construction of unmarked deletion mutants in *Burkholderia pseudomallei* using *sacB* counter-selection in sucrose-resistant and sucrose-sensitive isolates. Journal of Microbiological Methods **76:**320-323.
391. **Wrench AP, Gardner CL, Gonzalez CF, Lorca GL.** 2013. Identification of a small molecule that modifies MglA/SspA interaction and impairs intramacrophage survival of *Francisella tularensis*. PloS one **8:**e54498.
392. **Ramsey KM, Dove SL.** 2016. A response regulator promotes *Francisella tularensis* intramacrophage growth by repressing an anti-virulence factor. Molecular Microbiology **101:**688-700.
393. **Vogt SL, Green C, Stevens KM, Day B, Erickson DL, Woods DE, Storey DG.** 2011. The Stringent Response Is Essential for *Pseudomonas aeruginosa* Virulence in the Rat Lung Agar Bead and Drosophila melanogaster Feeding Models of Infection. Infection and Immunity **79:**4094-4104.
394. **Abbott A, Butler H, Redhead N, Ragoussis J.** Evaluation of TITANIUM™ Taq DNA Polymerase for High-Throughput Genotyping Using the MassARRAY System.
395. **Team RC.** 2005. R: A language and environment for statistical computing. R foundation for Statistical Computing.
396. **Warnes GR, Bolker B, Bonebakker L, Gentleman R, Huber W, Liaw A, Lumley T, Maechler M, Magnusson A, Moeller S.** 2009. gplots: Various R programming tools for plotting data. R package version **2**.
397. **Twine SM, Mykytczuk NCS, Petit MD, Shen H, Sjöstedt A, Wayne Conlan J, Kelly JF.** 2006. *In vivo* proteomic analysis of the intracellular bacterial pathogen, *Francisella tularensis*, isolated from mouse spleen. Biochemical and Biophysical Research Communications **345:**1621-1633.
398. **Brown MJ, Russo BC, O'Dee DM, Schmitt DM, Nau GJ.** 2014. The contribution of the glycine cleavage system to the pathogenesis of *Francisella tularensis*. Microbes and Infection **16:**300-309.

399. **Sjostedt A, Flieger A.** 2010. *Francisella tularensis* metabolism and its relation to virulence. Francisella tularensis and tularemi**:**7.
400. **Mohapatra NP, Soni S, Bell BL, Warren R, Ernst RK, Muszynski A, Carlson RW, Gunn JS.** 2007. Identification of an Orphan Response Regulator Required for the Virulence of *Francisella* spp. and Transcription of Pathogenicity Island Genes. Infection and Immunity **75:**3305-3314.
401. **Jozefczuk S, Klie S, Catchpole G, Szymanski J, Cuadros-Inostroza A, Steinhauser D, Selbig J, Willmitzer L.** 2010. Metabolomic and transcriptomic stress response of *Escherichia coli*. Mol Syst Biol **6**.
402. **Li W, Choi H, Bouveret E, Zhang Y, Weisshaar J.** 2014. Single Molecule Study of Rela During the Stringent Response in Live *E. Coli* Cells. Biophysical Journal **106:**462a-463a.
403. **Brown DR, Barton G, Pan Z, Buck M, Wigneshweraraj S.** 2014. Nitrogen stress response and stringent response are coupled in *Escherichia coli*. Nat Commun **5**.
404. **Gallant JA.** 1979. Stringent control in *E. coli*. Annual review of genetics **13:**393-415.
405. **Durfee T, Hansen A-M, Zhi H, Blattner FR, Jin DJ.** 2008. Transcription Profiling of the Stringent Response in *Escherichia coli*. Journal of Bacteriology **190:**1084-1096.
406. **O'Farrell PH.** 1978. The suppression of defective translation by ppGpp and its role in the stringent response. Cell **14:**545-557.
407. **Vital M, Chai B, Ostman B, Cole J, Konstantinidis KT, Tiedje JM.** 2015. Gene expression analysis of *E. coli* strains provides insights into the role of gene regulation in diversification. ISME J **9:**1130-1140.
408. **Sebbane F, Lema+«tre N, Sturdevant DE, Rebeil R, Virtaneva K, Porcella SF, Hinnebusch BJ.** 2006. Adaptive response of *Yersinia pestis* to extracellular effectors of innate immunity during bubonic plague. Proceedings of the National Academy of Sciences **103:**11766-11771.
409. **Rosqvist R, Magnusson KE, Wolf-Watz H.** 1994. Target cell contact triggers expression and polarized transfer of Yersinia YopE cytotoxin into mammalian cells. The EMBO journal **13:**964-972.
410. **Fukuto HS, Svetlanov A, Palmer LE, Karzai AW, Bliska JB.** 2010. Global Gene Expression Profiling of *Yersinia pestis* Replicating inside Macrophages Reveals the Roles of a Putative Stress-Induced Operon in Regulating Type III Secretion and Intracellular Cell Division. Infection and Immunity **78:**3700-3715.
411. **Mojib N, Andersen DT, Bej AK.** 2011. Structure and function of a cold shock domain fold protein, CspD, in *Janthinobacterium* sp. Ant5-2 from East Antarctica. FEMS Microbiology Letters **319:**106-114.
412. **Law RJ, Hamlin JNR, Sivro A, McCorrister SJ, Cardama GA, Cardona ST.** 2008. A Functional Phenylacetic Acid Catabolic Pathway Is Required for Full Pathogenicity of *Burkholderia cenocepacia* in the Caenorhabditis elegans Host Model. Journal of Bacteriology **190:**7209-7218.
413. **Yudistira H, McClarty L, Bloodworth RAM, Hammond SA, Butcher H, Mark BL, Cardona ST.** 2011. Phenylalanine induces *Burkholderia cenocepacia* phenylacetic acid catabolism through degradation to phenylacetyl-CoA in synthetic cystic fibrosis sputum medium. Microbial Pathogenesis **51:**186-193.
414. **Berlutti F, Morea C, Battistoni A, Superti F, Ammendolia MG, Valenti P.** 2005. Iron Availability Influences Aggregation, Biofilm, Adhesion and Invasion of *Pseudomonas Aeruginosa* and *Burkholderia Cenocepacia*. International Journal of Immunopathology and Pharmacology **18:**661-670.
415. **Tuanyok A, Kim HS, Nierman WC, Yu Y, Dunbar J, Moore RA, Baker P, Tom M, Ling JML, Woods DE.** 2005. Genome-wide expression analysis of iron regulation in *Burkholderia pseudomallei* and *Burkholderia mallei* using DNA microarrays. FEMS Microbiology Letters **252:**327-335.

416. **Alice AF, López CS, Lowe CA, Ledesma MA, Crosa JH.** 2006. Genetic and Transcriptional Analysis of the Siderophore Malleobactin Biosynthesis and Transport Genes in the Human Pathogen *Burkholderia pseudomallei* K96243. Journal of Bacteriology **188:**1551-1566.
417. **Ulett GC, Currie BJ, Clair TW, Mayo M, Ketheesan N, Labrooy J, Gal D, Norton R, Smith CA, Barnes J, Warner J, Hirst RG.** 2001. *Burkholderia pseudomallei* virulence: definition, stability and association with clonality. Microbes and Infection **3:**621-631.
418. **Thomas MS.** 2007. Iron acquisition mechanisms of the *Burkholderia cepacia* complex. BioMetals **20:**431-452.
419. **Franke J, Ishida K, Ishida-Ito M, Hertweck C.** 2013. Nitro versus Hydroxamate in Siderophores of Pathogenic Bacteria: Effect of Missing Hydroxylamine Protection in Malleobactin Biosynthesis. Angewandte Chemie International Edition **52:**8271-8275.
420. **Louden BC, Haarmann D, Lynne AM.** 2011. Use of Blue Agar CAS Assay for Siderophore Detection. Journal of Microbiology & Biology Education : JMBE **12:**51-53.
421. **Miethke M, Westers H, Blom E-J, Kuipers OP, Marahiel MA.** 2006. Iron Starvation Triggers the Stringent Response and Induces Amino Acid Biosynthesis for Bacillibactin Production in *Bacillus subtilis*. Journal of Bacteriology **188:**8655-8657.
422. **Earhart C.** 1996. Uptake and metabolism of iron and molybdenum. Escherichia coli and Salmonella: cellular and molecular biology, 2nd ed. ASM Press, Washington, DC**:**1075-1090.
423. **Seto E, Shi Y, Shenk T, Chang L, Shenk T, Courey A, Tiian R.** 1993. Crystal structure of the DsbA protein required for disulphide bond formation *in vivo*. Nature **365**.
424. **Kobayashi T, Kishigami S, Sone M, Inokuchi H, Mogi T, Ito K.** 1997. Respiratory chain is required to maintain oxidized states of the DsbA-DsbB disulfide bond formation system in aerobically growing *Escherichia coli cells*. Proceedings of the National Academy of Sciences **94:**11857-11862.
425. **Takahashi Y-h, Inaba K, Ito K.** 2004. Characterization of the Menaquinone-dependent Disulfide Bond Formation Pathway of *Escherichia coli*. Journal of Biological Chemistry **279:**47057-47065.
426. **Inaba K, Ito K.** 2008. Structure and mechanisms of the DsbB–DsbA disulfide bond generation machine. Biochimica et Biophysica Acta (BBA) - Molecular Cell Research **1783:**520-529.
427. **Thomas RM, Twine SM, Fulton KM, Tessier L, Kilmury SLN, Ding W, Harmer N, Michell SL, Oyston PCF, Titball RW, Prior JL.** 2011. Glycosylation of DsbA in *Francisella tularensis* subsp. *tularensis*. Journal of Bacteriology **193:**5498-5509.
428. **Price AC, Zhang Y-M, Rock CO, White SW.** 2001. Structure of β-Ketoacyl-[acyl carrier protein] Reductase from *Escherichia coli*: Negative Cooperativity and Its Structural Basis. Biochemistry **40:**12772-12781.
429. **Waller RF, Ralph SA, Reed MB, Su V, Douglas JD, Minnikin DE, Cowman AF, Besra GS, McFadden GI.** 2003. A Type II Pathway for Fatty Acid Biosynthesis Presents Drug Targets in *Plasmodium falciparum*. Antimicrobial Agents and Chemotherapy **47:**297-301.
430. **Tasdemir D, Lack G, Brun R, Rüedi P, Scapozza L, Perozzo R.** 2006. Inhibition of *Plasmodium falciparum* Fatty Acid Biosynthesis: Evaluation of FabG, FabZ, and FabI as Drug Targets for Flavonoids. Journal of Medicinal Chemistry **49:**3345-3353.
431. **Lu H, Tonge PJ.** 2008. Inhibitors of FabI, an Enzyme Drug Target in the Bacterial Fatty Acid Biosynthesis Pathway. Accounts of Chemical Research **41:**11-20.
432. **Kammler M, Schön C, Hantke K.** 1993. Characterization of the ferrous iron uptake system of *Escherichia coli*. Journal of Bacteriology **175:**6212-6219.
433. **Hantke K.** 1987. Ferrous iron transport mutants in *Escherichia coli* K12. FEMS Microbiology Letters **44:**53-57.

434. **Perry RD, Mier I, Fetherston JD.** 2007. Roles of the Yfe and Feo transporters of *Yersinia pestis* in iron uptake and intracellular growth. BioMetals **20:**699-703.
435. **Volk K, Breunig SD, Rid R, Herzog J, Brauer M, Hundsberger H, Klein C, Muller N, Onder K.** 2016. Structural analysis and interaction studies of acyl carrier protein (*acpP*) of *Staphylococcus aureus*, an extraordinarily thermally stable protein. Biological chemistry.
436. **Therisod H, Weissborn AC, Kennedy EP.** 1986. An essential function for acyl carrier protein in the biosynthesis of membrane-derived oligosaccharides of *Escherichia coli*. Proceedings of the National Academy of Sciences **83:**7236-7240.
437. **Rawlings M, Cronan JE.** 1992. The gene encoding *Escherichia coli* acyl carrier protein lies within a cluster of fatty acid biosynthetic genes. Journal of Biological Chemistry **267:**5751-5754.
438. **Mikolajczyk S, Brody S.** 1990. De novo fatty acid synthesis mediated by acyl-carrier protein in *Neurospora crassa* mitochondria. European Journal of Biochemistry **187:**431-437.
439. **Lai C-Y, Cronan JE.** 2004. Isolation and Characterization of β-Ketoacyl-Acyl Carrier Protein Reductase (*fabG*) Mutants of *Escherichia coli* and *Salmonella enterica* Serovar *Typhimurium*. Journal of Bacteriology **186:**1869-1878.
440. **Mogk A, Deuerling E, Vorderwülbecke S, Vierling E, Bukau B.** 2003. Small heat shock proteins, ClpB and the DnaK system form a functional triade in reversing protein aggregation. Molecular Microbiology **50:**585-595.
441. **Perry R, Mier I, Jr., Fetherston J.** 2007. Roles of the Yfe and Feo transporters of *Yersinia pestis* in iron uptake and intracellular growth. Biometals **20:**699-703.
442. **Mathy N, Pellegrini O, Serganov A, Patel DJ, Ehresmann C, Portier C.** 2004. Specific recognition of rpsO mRNA and 16S rRNA by *Escherichia coli* ribosomal protein S15 relies on both mimicry and site differentiation. Molecular Microbiology **52:**661-675.
443. **Batey RT, Williamson JR.** 1996. Interaction of the *Bacillus stearothermophilus* ribosomal protein S15 with 16 S rRNA: I. Defining the minimal RNA site. Journal of molecular biology **261:**536-549.
444. **Schnier J, Kimura M, Foulaki K, Subramanian AR, Isono K, Wittmann-Liebold B.** 1982. Primary structure of *Escherichia coli* ribosomal protein S1 and of its gene *rpsA*. Proceedings of the National Academy of Sciences **79:**1008-1011.
445. **Van Dieijen G, Van Knippenberg PH, Van Duin J.** 1976. The Specific Role of Ribosomal Protein S1 in the Recognition of Native Phage RNA. European Journal of Biochemistry **64:**511-518.
446. **Szer W, Hermoso JM, Leffler S.** 1975. Ribosomal protein S1 and polypeptide chain initiation in bacteria. Proceedings of the National Academy of Sciences **72:**2325-2329.
447. **Zurawski G, Zurawski SM.** 1985. Structure of the *Escherichia coli* S10 ribosomal protein operon. Nucleic Acids Research **13:**4521-4526.
448. **Apirion D.** 1967. Three Genes that affect *Escherichia coli* Ribosomes. Journal of molecular biology **30:**255-275.
449. **Chittum HS, Champney WS.** 1994. Ribosomal protein gene sequence changes in erythromycin-resistant mutants of *Escherichia coli*. Journal of Bacteriology **176:**6192-6198.
450. **Golovliov I, Twine SM, Shen H, Sjostedt A, Conlan W.** 2013. A Δ*clpB* Mutant of *Francisella tularensis* Subspecies holarctica Strain, FSC200, Is a More Effective Live Vaccine than *F. tularensis* LVS in a Mouse Respiratory Challenge Model of Tularemia. PLoS ONE **8:**e78671.
451. **Motin VL, Georgescu AM, Fitch JP, Gu PP, Nelson DO, Mabery SL, Garnham JB, Sokhansanj BA, Ott LL, Coleman MA, Elliott JM, Kegelmeyer LM, Wyrobek AJ, Slezak**

TR, Brubaker RR, Garcia E. 2004. Temporal Global Changes in Gene Expression during Temperature Transition in *Yersinia pestis*. Journal of Bacteriology **186:**6298-6305.

452. **Straskova A, Pavkova I, Link M, Forslund A-L, Kuoppa K, Noppa L, Kroca M, Fucikova A, Klimentova J, Krocova Z, Forsberg Å, Stulik J.** 2009. Proteome Analysis of an Attenuated *Francisella tularensis dsbA* Mutant: Identification of Potential DsbA Substrate Proteins. Journal of Proteome Research **8:**5336-5346.
453. **Jackson MW, Plano GV.** 1999. DsbA Is Required for Stable Expression of Outer Membrane Protein YscC and for Efficient Yop Secretion in *Yersinia pestis*. Journal of Bacteriology **181:**5126-5130.
454. **Mehboob S, Hevener KE, Truong K, Boci T, Santarsiero BD, Johnson ME.** 2012. Structural and Enzymatic Analyses Reveal the Binding Mode of a Novel Series of *Francisella tularensis* Enoyl Reductase (FabI) Inhibitors. Journal of Medicinal Chemistry **55:**5933-5941.
455. **Lindgren H, Honn M, Salomonsson E, Kuoppa K, Forsberg Å, Sjöstedt A.** 2011. Iron Content Differs between *Francisella tularensis* Subspecies *tularensis* and Subspecies *holarctica* Strains and Correlates to Their Susceptibility to H2O2-Induced Killing. Infection and Immunity **79:**1218-1224.
456. **Hamlin JN, Bloodworth RA, Cardona ST.** 2009. Regulation of phenylacetic acid degradation genes of *Burkholderia cenocepacia* K56-2. BMC Microbiology **9:**1-10.
457. **Neilands J.** 1981. Iron absorption and transport in microorganisms. Annual review of nutrition **1:**27-46.
458. **Wexselblatt E, Oppenheimer-Shaanan Y, Kaspy I, London N, Schueler-Furman O, Yavin E, Glaser G, Katzhendler J, Ben-Yehuda S.** 2012. Relacin, a Novel Antibacterial Agent Targeting the Stringent Response. PLoS Pathog **8:**e1002925.
459. **Maisonneuve E, Gerdes K.** 2014. Molecular Mechanisms Underlying Bacterial Persisters. Cell **157:**539-548.
460. **Maeda T, Mazzulli JR, Farrance IK, Stewart AF.** 2002. Mouse DTEF-1 (ETFR-1, TEF-5) is a transcriptional activator in alpha 1-adrenergic agonist-stimulated cardiac myocytes. The Journal of biological chemistry **277:**24346-24352.
461. **Donnenberg MS, Kaper JB.** 1991. Construction of an eae deletion mutant of enteropathogenic *Escherichia coli* by using a positive-selection suicide vector. Infection and Immunity **59:**4310-4317.
462. **Kumar P, Sweeney TR, Skabkin MA, Skabkina OV, Hellen CUT, Pestova TV.** 2013. Inhibition of translation by IFIT family members is determined by their ability to interact selectively with the 5'-terminal regions of cap0-, cap1- and 5'ppp- mRNAs. Nucleic Acids Research.
463. **Anders S, Pyl PT, Huber W.** 2014. HTSeq - A Python framework to work with high-throughput sequencing data.